# Integration of anaerobic digestion and hydrothermal liquefaction for sewage sludge management

by

Harveen Kaur Tatla

A thesis submitted in partial fulfilment of the requirements for the degree of

Master of Science

in

Process Control

Department of Chemical and Materials Engineering

University of Alberta

# Abstract

Given the volume of sewage sludge produced worldwide, efficient waste management and energy recovery techniques are essential. Anaerobic digestion (AD) and hydrothermal liquefaction (HTL) are viable avenues for the valorization of sewage sludge. Their combination produces a synergistic framework that reduces intrinsic constraints, leading to improved productivity and all-encompassing sludge usage. Energy recovery from either standalone AD followed by HTL or standalone HTL followed by AD has been the subject of numerous research; however, a systematic comparison of energy recovery from both integrated sequences under the same operating circumstances and feedstock has not yet been comprehensively examined. This research gap hinders the thorough understanding of the optimal approach for sewage sludge valorization processes and their advancement in a circular bioeconomy. In order to close this gap, this thesis includes a comparative analysis of energy recovery from both integrated schemes under identical operating conditions using sewage sludge as a feedstock. Additionally, it also explores the techno-economic assessment (TEA) for a large-scale integrated AD-HTL system to evaluate economic feasibility and viability of this integrated approach.

Firstly, the energy recovery efficiency of two sequencing configurations: HTL followed by AD and AD followed by HTL, at varying HTL operating conditions of 250, 300, and 350 °C for 30 and 60 minutes each was systemically evaluated. Our results demonstrated that the HTL-AD sequence yields higher energy recovery in the form of biocrude, with a concentration of fatty acids due to the high lipid content in primary sludge. On the other hand, the AD-HTL sequence recovers more energy in the form of biomethane, due to the easily degradable nature of primary sludge in regard to lower nitrogen content. Energy recovery for the HTL-AD sequence ranges from 47.2% to 84.5%, while the AD-HTL sequence ranges from 57.2% to 77.3%. The HTL-AD system recovers the highest energy at 300 °C for 60 minutes, whereas at other operating conditions, the AD-HTL system achieves higher energy recovery than the HTL-AD system.

Secondly, a techno-economic assessment aimed at identifying the performance targets necessary for achieving economic viability was conducted. Three proposed configurations with a processing capacity of 1.1 million tons of primary sludge annually were assessed. Our results concluded that AD- HTL system computed the lowest LCOE of \$11.4/ GJ, due to additional revenue stream generated from biocrude and hydrochar. The integration of HTL process for the degradation of digestate emphasis on importance of generation of additional revenue streams for achieving economic viability. Sensitivity analysis showcased that the incorporation of low- cost electricity or adoption of renewable energy sources, is crucial for achieving economic and environmental goals. Additionally, optimizing the AD and HTL process can be beneficial to achieve economic targets.

# Preface

Chapter 1 of the thesis introduces the anaerobic digestion, hydrothermal liquefaction, and significance of their integration. Additionally, it provides the scope and objectives of this thesis, specifying the aims and research gap that needs to be addressed. This chapter also includes a structured outline of the thesis.

Chapter 2 of this thesis has been published as Tatla, H. K., Ismail, S., Khan, M. A., Dhar, B. R., & Gupta, R., 2024. *"Coupling Hydrothermal Liquefaction and Anaerobic Digestion for Waste Biomass Valorization: A Review in Context of Circular Economy"* in *Chemosphere*, vol 136, 142419. Tatla, H.K. was responsible for writing the original draft, conceptualization, review, and editing. Ismail, S. assisted with writing the original draft. Khan, M.A., Dhar, B.R., and Gupta, R. were responsible for the review, editing, project administration, and supervising this work.

Chapter 3 of this thesis has been submitted as Tatla, H.K., Niknejad, P., Ismail, S., Khan, M. A., Dhar, B. R., & Gupta, R., 2024. *"A Comprehensive Assessment of Integrating Anaerobic Digestion and Hydrothermal Liquefaction Processes: Harnessing Energy from Sewage Sludge"* in Energy Conversion and Management. Tatla, H.K. was responsible for experimental design, experiment and data collection, writing original draft, review, and editing. Niknejad, P. assisted with conducting the experiments. Ismail, S. assisted with writing the original draft. Khan, M.A., Dhar, B.R., and Gupta, R. were responsible for the review, editing, project administration, and supervising this work.

Chapter 4 of this thesis includes a comprehensive techno- economic analysis of an integrated AD- HTL system for sewage sludge management. A plant with a processing capacity of 1.1million tonnes of primary sludge annually was assessed to achieved economic performance targets for three proposed cases. Sensitivity analysis was conducted to identify the parameters crucial to achieve economic viability. Preliminary greenhouse gas emissions were calculated to improve long-term sustainability of the integrated systems.

# Dedication

First and foremost, I dedicate this work to God, the Almighty, who have been my guiding light on this path. It is by His strength that I am able to overcome every setback in my path. His divine presence has provided me a courage to remain focused and keep- going mindset. I dedicate my every accomplishment to him, and I am incredibly appreciative of His unwavering support and direction.

Secondly, I am really grateful for the love and support that I have received from my family. Your unwavering belief in me has been the foundation upon which I built this work. Mom and Dad, I owe everything in my life to you. Your constant support has been the cornerstone of my academic journey. Your sacrifices, hard work, and love have always inspired me to be a better person. Mom and Dad, I owe everything in my life to you.

Finally, I would especially like to thank my sister. You have always been my pillar of support during good times and bad. I will always be appreciative of your love and support. You have been my confidante and my source of laughter through both the good and challenging times.

With all deep respect, love, and gratitude, I dedicate this thesis to all of you.

# Acknowledgements

I would like to acknowledge and give my warmest thanks to my supervisors, Dr. Bipro Ranjan Dhar, Dr. Rajender Gupta, and Dr. Mohd. Adnan Khan. I am grateful to them for providing me an opportunity to grow within the research field. Throughout my research journey, they have provided crucial guidance, feedback, and support. Their dedication to fostering a dynamic and collaborative research environment has also had a significant influence on the success and direction of my work.

I am sincerely grateful to the members of my MSc defense committee for their time and effort in evaluating my thesis. Their insightful comments of my work have helped me to refine my research and deepen my understanding of this topic.

Special thanks to members of my research group, in particular Tejaswini Eagalapati, Sherif Ismail, Sohrab Hejazi, and Parisa Niknejad, for inspiration through guidance, encouragement, cooperation, and support.

I would like to gratefully acknowledge the Natural Sciences and Engineering Research Council of Canada financial support through the Discovery Grants. The opportunities that have been created by this funding are greatly appreciated.

# Table of Contents

# List of Tables

# List of Figures

# Abbreviations and Units

| | |
|---|---|
| AC | Alternating Current |
| $NH_4^+$ | Ammonium Ion |
| Amps | Ampere (Electric current unit) |
| AD | Anarobic digestion |
| AD-HTL | Anaerobic digestion followed by hydrothermal liquefaction |
| $i$ | Annual interest rate |
| HTL-AP | Aqueous phase generated by hydrothermal liquefaction |
| BMP | Biomethane Production |
| CAPEX | Capital expenditure |
| CRF | Capital Recovery Factor |
| Ch | Carbohydrates |
| C | Carbon |
| $CO_2$ | Carbon dioxide |
| CMS | Carbon Molecular Sieves |
| CO | Carbon monoxide |
| C/N | Carbon per Nitrogen |
| cm | Centimeter |
| °C | Celsius |
| COD | Chemical Oxygen Demand |
| CEC | Commission for Environmental Cooperation. |
| CSTR | Continuous Stirred Tank Reactor |

| | |
|---|---|
| $Cost_{Desulphurization}$ | Cost of desulphurization unit |
| $m^3$ | Cubic meters |
| DCM | Dichloromethane |
| DC | Direct Current |
| DCF | Discounted Cash Flow |
| DOM | Dissolved Organic Matter |
| $ | Dollars |
| db | Dry basis |
| BoP | Electrical balance of plant |
| e- | Electron |
| EF | Emission Factor |
| $C_2H_6$ | Ethane |
| € | Euros |
| ER | Exchange Ratio |
| F/M | Feedstock to microorganism |
| $Nm^3/h$ | Flowrate at standard conditions |
| FTIR | Fourier transform infrared spectroscopy |
| FCI | Fixed Capital Investment |
| GC | Gas chromatography |
| GC-MS | Gas Chromatography-Mass Spectrometry |
| GHSV | Gas Hourly Space Velocity |
| GJ | Gigajoules |
| GWP | Global warming potential |
| g | Gram |

| | |
|---|---|
| g/L | Gram per liter |
| GAC | Granular Activated Carbon |
| GHG | Greenhouse gas emissions |
| HRAD | High- Rate Anaerobic Digestion |
| HHV | Higher heating value |
| h | Hours |
| HRT | Hydraulic Retention Time |
| H | Hydrogen element |
| $H_2$ | Hydrogen gas |
| $H_2O_2$ | Hydrogen peroxide |
| $H_2S$ | Hydrogen sulfide |
| HTL | Hydrothermal liquefaction |
| HTL-AD | Hydrothermal liquefaction followed by anaerobic digestion |
| HMF | Hydroxymethyl furfural |
| IRR | Internal Rate of Return |
| Kg | Kilogram |
| KW | Kilowatts |
| kWh | Kilowatt- hour |
| LCOE | Levelized Cost of Energy |
| LCA | Life Cycle Assessment |
| Li | Lipids |
| L | Liters |
| LCFS | Low Carbon Fuel Standard |
| LHV | Lower Heating Value |

| | |
|---|---|
| MF | Maintenance Factor |
| MPa | Mega pascal |
| MJ | Megajoules |
| MJ/kg | Megajoules per kilogeram |
| MW | Megawatts |
| m | Meter |
| $CH_4$ | Methane |
| MER | Methane Emission Rate |
| µL | Microliter |
| µm | Micrometer |
| mbar | Millibar (pressure’s unit) |
| mg/L | Milligrams per liter |
| mL | Milliliter |
| mm | Millimeter |
| mmol | Millimole |
| min | Minutes |
| NPV | Net Present Value |
| N | Nitrogen element |
| $N_2$ | Nitrogen gas |
| Ω | Ohm |
| O&M | Operating & Maintenance costs |
| OPEX | Operational expenditure |
| O | Oxygen element |
| $O_2$ | Oxygen gas |

| | |
|---|---|
| O/C | Oxygen per carbon |
| *n* | Plant lifetime (years) |
| PM | Polyurethane Matrixes |
| HTL-WW | Post-HTL wastewater |
| psi | Pound per square inch (Pressure's unit) |
| PAC | Powdered Activated Carbon |
| PtG | Power-to-Gas |
| PSA | Pressure Swing Adsorption unit |
| PS | Primary sludge |
| $C_3H_8$ | Propane |
| Pr | Proteins |
| PEM | Proton Exchange Membrane system |
| PEC | Purchased Equipment Cost |
| RPAs | Relative Peak Areas |
| RFS | Renewable Fuel Standard |
| RNG | Renewable Natural Gas |
| R&D | Research and development |
| rpm | Revolutions per minute |
| sec | Seconds (time) |
| NaOH | Sodium hydroxide |
| SRT | Solid Retention Time |
| $SO_4$ | Sulfate |
| S | Sulfur |
| A | Surface area |

| | |
|---|---|
| SNG | Synthetic Natural Gas |
| TEA | Techno- Economic Analysis |
| TSA | Temperature Swing Adsorption |
| TCD | Thermal conductivity detection |
| t | Tonnes (mass unit) |
| TAN | Total Ammonia Nitrogen |
| TOC | Total Organic Carbon |
| TS | Total solids |
| VFAs | Volatile fatty acids |
| VS | Volatile solids |
| V | Volume |
| $V_{AD}$ | Volume of anaerobic digester |
| $V_{gst}$ | Volume of gas storage tank |
| $V_{st}$ | Volume of storage tank |
| WWTFs | Wastewater treatment facilities |
| WWTPs | Wastewater treatment plants |
| $H_2O$ | Water |
| wt.% | Weight percentage |
| $W_p$ | Work done by pump |
| yr | Year |
| $Y_i$ | Yield of product (i) |

# Chapter 1

# Introduction

## 1.1 Background

Wastewater treatment facilities (WTFs) treat the wastewater generated from households, industries and commercialized sectors worldwide. A vast quantity of sludge is produced as waste product during this treatment in order to ensure clean water supply as per health and environmental regulations (Sikosana et al., 2019). Nearly 380 billion cubic meters ($m^3$) of wastewater was produced worldwide in 2020. This volume is expected to increase by 24% in 2030 and 51% in 2050 (Qadir et al., 2020). As a result, this will lead to generation of an enormous amount of sludge. For example, approximately 7.1 million and 660,000 tons of dry sewage sludge is generated by United States and Canada, respectively every year (Canadian Council of Ministers of the Environment, 2012; Krause & Bronstein, 2024). Production of sludge in such a vast quantity can pose severe challenges for its efficient and sustainable disposal.

There are several issues in the way of traditional sludge management techniques such as landfilling, incineration, and land application. Landfilling was earlier a common strategy for sludge disposal. However, it is facing restrictions due to limited space availability because of the growing population. Moreover, leachate formation can cause several environmental risks due to contamination of groundwater (Gavrilescu & Schiopu, 2010). Incineration is a useful method for the volume reduction of waste but due to its high energy demand, its economic viability is a big issue (Beyene et al., 2018). Land application method is facing restrictions from government due to its variable characteristics and presence of heavy metals in it (Wang et al., 2008). Additionally, transportation of sludge is still a financial burden for WWTFs. Therefore, advanced treatment techniques like Hydrothermal Liquefaction (HTL) and Anaerobic Digestion (AD) are emerging as a promising solution for sludge valorization to address these limitations (Chen et al., 2020a; Di Capua et al., 2020).

AD is a well- established commercialized technology that has been implemented from several years worldwide (Awasthi et al., 2021; Sawatdeenarunat et al., 2015). One of the biggest advantages of AD is its ability to generate biogas and reduce the waste volume. The biogas can be used for the production of electricity and thermal energy or upgraded into renewable natural gas, hence providing a source of clean fuel (Sawatdeenarunat et al., 2015). Moreover, the resulting digestate holds a potential to be utilized as fertilizer in farmlands (Awasthi et al., 2021). However, there are some drawbacks of this technology. Presence of heavy metals and pathogen restricts the use of digestate as a fertilizer (Kamali et al., 2016; Nkoa, 2013; Samoraj et al., 2022). Therefore, in such a scenario, post treatments like HTL seems to be viable option for valorizing the digestate and enhancing the overall sustainability of the process (Angenent et al., 2018).

HTL is a thermochemical technology used to convert biomass into valuable products like biocrude, hydrochar, gases, and aqueous phase at high temperature and pressure (Grande et al., 2021). HTL can process high moisture content feedstocks making this process well- suited for sludge management (Zhang et al., 2020). The aqueous stream produced from this process is called HTL-AP. It contains a fraction of organic carbon and mineral depending on the process operating conditions and feedstock characteristics (SundarRajan et al., 2021). A key challenge of HTL process is handling and disposal of HTL-AP. In this regard, adding AD as a post-treatment method would have an added advantage as HTL-AP can act as a substrate for biogas production. This would avoid any potential environmental risk related to its disposal (Gerber Van Doren et al., 2017; Gu et al., 2019).

Integrating HTL and AD offers a synergistic approach to sewage sludge treatment, overcoming the inherent limitations of each process and enabling a more comprehensive utilization of resources, thereby advancing the circular economy (Rezaee et al., 2020; Okolie et al., 2022). Thus, this incorporation improves the overall efficacy of the process. Numerous research studies have evaluated energy recovery from either HTL followed by AD or vice versa (Cabrera et al., 2023; Li et al., 2019; Posmanik et al., 2017b; Vardon et al., 2011). However, comparison of energy recovery from integration of AD and HTL under identical operating conditions and feedstock have not been studied yet. Moreover, the techno-economic analysis (TEA) of a large-scale integrated AD-HTL system for sewage sludge management has not yet been fully investigated, leaving a significant research gap in capturing the true value proposition of this approach.

## 1.2 Scope and Objective

The purpose of this study is to examine two integrated schemes for sewage sludge management: Hydrothermal Liquefaction (HTL) followed by Anaerobic Digestion (AD), and vice versa, using identical operating conditions and feedstock. Furthermore, the study presents a preliminary techno- economic assessment (TEA) of a large-scale integrated AD-HTL system, paving the way for its wider application in the wastewater treatment sector.

Two specific objectives of this thesis were:

a) To perform a comparative analysis of the energy recovery from the two integrated processes—HTL followed by AD and vice versa—for sewage sludge.

b) To conduct a TEA aimed at identifying performance targets required to achieve economic viability for a large- scale integrated AD-HTL system.

## 1.3 Thesis Outline

This thesis includes five chapters. Chapter 1 provides the introduction to anaerobic digestion, hydrothermal liquefaction, and their integration topic. It also emphasizes the research gap and objective of the study conducted. Chapter 2 provides a review article based on the integration of anaerobic digestion and hydrothermal liquefaction for biomass valorization. Chapter 3 includes the experimental work conducted and its findings in the form of a research paper. Chapter 4 includes a detailed techno- economic assessment study of a large- scale integrated plant. It evaluated the key performance indicators to achieve economic profitability and sustainability. Finally, Chapter 5 summarizes the key findings of an experimental investigation and techno-economic analysis and provides recommendations for future research work.

# Chapter 2

# Coupling hydrothermal liquefaction and anaerobic digestion for waste biomass valorization: A review in the context of circular economy

*A version of this chapter was published in Chemosphere; 361 (2024) 142419.*

## 2.1 Introduction

The shift towards a circular economy is essential for attaining sustainability and tackling the challenges of resource depletion, waste generation, environmental degradation, and climate change (Antar et al., 2021; Awasthi et al., 2021). To this end, biomass waste, comprising agricultural residues, food waste, forestry by-products, organic fractions of municipal solid waste, municipal sewage sludge, and other organic materials, presents both an environmental challenge and an untapped resource (Awasthi et al., 2021). For instance, North America generates nearly 265 million tonnes of organic waste, as reported by the CEC in 2017. Out of this total, around 75 million tonnes are directed towards composting and anaerobic digestion facilities, leaving approximately 190 million tonnes to be disposed of (CEC, 2017). These statistics underscore the significant challenge posed by the scale of waste generation in North America.

Globally, 70% of the waste generated is disposed of in landfills (ESWET, 2020). The sheer volume of waste being dumped poses significant environmental and health risks, as it can release harmful substances and chemicals, polluting groundwater and surface water (Chavan et al., 2022). Consuming polluted water can lead to gastrointestinal illnesses, skin problems, and long-term health complications (Siddiqua et al., 2022). Addressing this problem requires urgent and comprehensive efforts to promote sustainable waste management practices and reduce reliance on landfilling. To address the challenges with waste disposal, various technologies are being developed to transform waste biomass into valuable products while addressing waste disposal, energy generation, and resource recovery challenges. Research in waste valorization primarily focuses on two major areas: biochemical conversion processes and thermal conversion processes (Awasthi et al., 2021).

Among biochemical processes, anaerobic digestion (AD) is considered as a commercial and matured bioprocess for biogas generation from waste biomass and has been globally implemented for several years (Awasthi et al., 2021; Sawatdeenarunat et al., 2015). AD is defined as a biological degradation process without oxygen, producing methane-rich biogas and nutrient-rich digestate. AD relies on naturally occurring microorganisms to facilitate the breakdown of organic matter, and wet biowastes serve as the most desirable feedstock for this process (Awasthi et al., 2021; Xu et al., 2018b). In the process of AD, carbonaceous organic waste—primarily made up of proteins, lipids, and carbohydrates—is transformed into biogas through four distinct reaction stages: hydrolysis, acidogenesis, acetogenesis, and methanogenesis (see **Figure 2.1**). During hydrolysis, complex organic biopolymers with high molecular weights are broken down into simpler organic compounds with lower molecular weights by enzymes called hydrolytic enzymes (Ren et al., 2018). These enzymes break down proteins into amino acids, lipids into fatty acids, and carbohydrates into simple sugars like glucose. In the subsequent acidogenesis stage, acidogenic bacteria metabolize the hydrolyzed monomers, converting them into volatile fatty acids (VFAs), hydrogen gas, ammonium ions, and reduced sulfur. Acetogenesis is the stage where acetogenic bacteria further metabolize the VFAs into acetate, hydrogen ($H_2$), and carbon dioxide ($CO_2$). Finally, methanogenic archaea, a group of microorganisms, metabolize acetate, hydrogen, and carbon dioxide to produce methane. Methanogenesis is a slow process compared to the preceding stages and requires strict anaerobic conditions for optimal performance (Morales-Polo et al., 2018).

The AD process presents distinct advantages for treating waste biomass, including energy recovery in the form of methane, volume reduction, and nutrient recycling (Sawatdeenarunat et al., 2015). Despite its numerous advantages, the AD process still has various limitations, such as fluctuations in methane yield if the feedstock contains inhibitory and non-biodegradable compounds like plastics, heavy metals, and halogenated compounds (Kamali et al., 2016). Additionally, the proper handling and disposal of anaerobic digestate poses challenges. Due to its elevated pH and ammonia content, the anaerobic digestate has the potential to release ammonia and nitrous oxide (Nkoa, 2013). Nitrous oxide, in particular, has a global warming potential (GWP) that is 273 times higher than $CO_2$ (US EPA, 2023). Furthermore, when animal slurries are used as feedstock for AD, the resulting digestate tends to contain elevated levels of metal elements such as copper, zinc, and manganese (Nkoa, 2013; Samoraj et al., 2022). Therefore, ensuring sustainability requires the employment of appropriate treatment methods for digestate. AD is suggested to be integrated with other thermochemical processes to reduce environmental impacts (Angenent et al., 2022).

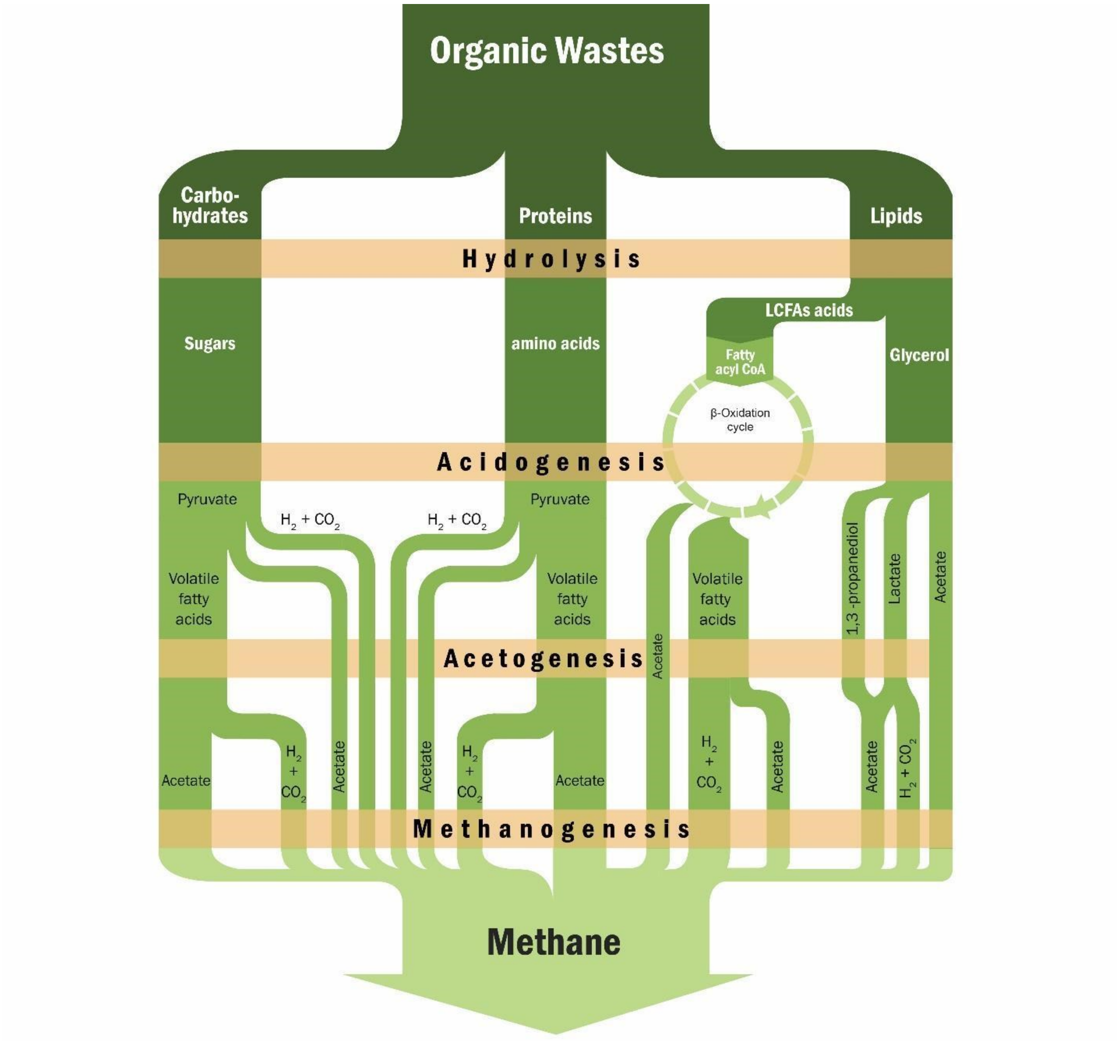

**Figure 2.1:** Methane production routes from different organic waste fractions (carbohydrates, proteins, and lipids).

On the other hand, various thermochemical processes, such as pyrolysis, gasification, and hydrothermal liquefaction (HTL), have garnered attention for converting waste biomass into bio-oil, syngas, and hydrochar as the main products. HTL, in particular, has garnered significant attention owing to its promising ability to produce energy-dense intermediate products, referred to as biocrude. Current research endeavors aim to enhance biocrude yield through the addition of catalysts and manipulation of process parameters tailored to the characteristics of the feedstock.

HTL process offers distinct advantages, such as shorter reaction times and a broader range of feedstock compatibility, enhancing its potential as a viable and versatile energy generation method (Grande et al., 2021). HTL has the capability to manage feedstock with elevated levels of moisture, eliminating the need for dewatering (Zhang et al., 2020).

Operating at temperatures ranging from 250 to 374 °C and pressures between 2 and 25 MPa, HTL can transform a wide variety of waste feedstock into valuable products (Mathankar et al., 2021; Kumar et al., 2018). The elevated operating conditions of the HTL process leads to a reduction in water dielectric constant, which further facilitates the degradation of lipids, proteins, and carbohydrates, resulting in the formation of biocrude, HTL-AP, gasses, and hydrochar. **Figure 2.2** outlines the detailed conversion pathways of these three components. Lipids, the main contributor to biocrude formation, undergo hydrolysis to form fatty acids and glycerol. Glycerol is further degraded and condensed to form water- soluble compounds and gaseous products. Meanwhile, fatty acids are converted to long-chain alkanes through decarboxylation and hydrogenation, and to alcohols through deoxygenation. These alcohols are then esterified with fatty acids to form fatty acid esters (Fan et al., 2022; Hao et al., 2021). Proteins, the primary contributor of nitrogenous compounds, undergo hydrolysis to form amino acids. These amino acids then catalyze the production of carboxylic acids, ammonia, amides and carbon dioxide through parallel deamination and decarboxylation reactions. Additionally, some fatty acids might react with ammonia to form fatty acid amides (Wei et al., 2024). In the carbohydrate, the non-cellulose component undergoes hydrolysis to form glucose and fructose. Glucose can also isomerize to fructose, albeit at a low rate. Due to this low isomerization rate, glucose is primarily degraded to phenols and furans through ring openings and cyclization. Additionally, it also produces nitrogenous heterocyclic compounds through Maillard reactions with amino acids. Fructose is generally degraded into 5-hydroxymethyl furfural (5-HMF). The cellulose component of carbohydrate includes cellulose, hemicellulose, and lignin. Celluloses and hemicelluloses are initially decomposed into glucose, pentose, and hexose in reactions. These monosaccharides are further decomposed, condensed, and hydrogenated to form aldehydes, ketones and 5-HMF. Lignins are hydrolysed to form different phenolic compounds and methoxybenzene. Some of these compounds undergo further hydrolysis to form aromatic hydrocarbons and aromatic polymers, while others re-polymerize to form hydrochar (Xu & Li, 2021). The biocrude oil produced as the primary product of the HTL process is a complex mixture of various chemical compounds. This diverse composition makes it a suitable and valuable feedstock for the production of biofuels or bio-based platform chemicals (Beims et al., 2020).

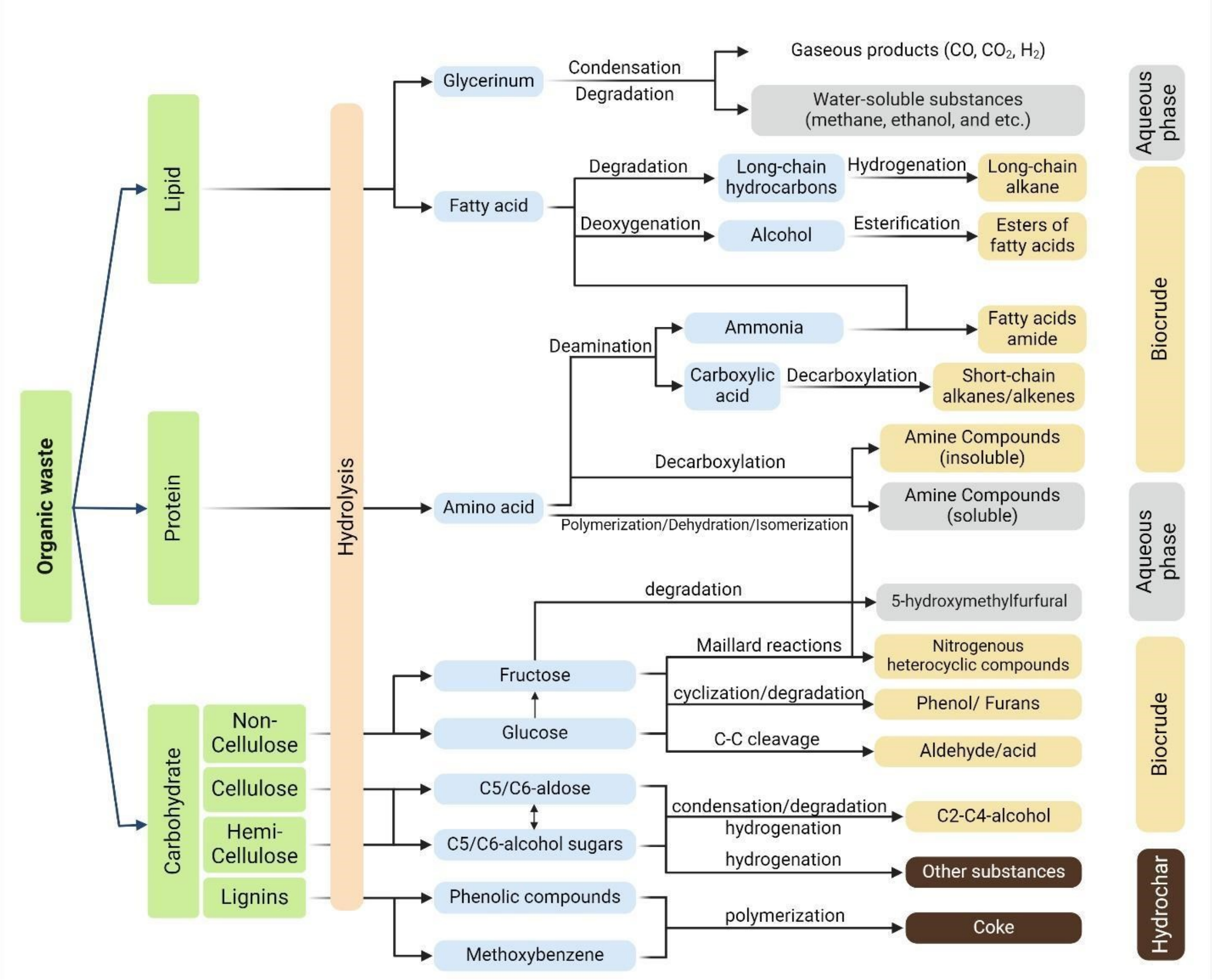

**Figure 2.2**: Conversion pathways of different organic waste components (carbohydrates, proteins, and lipids) during the HTL process.

Despite its numerous advantages, the disposal of the aqueous stream generated during the HTL process remains a significant concern. The aqueous stream produced during HTL, commonly referred to as post-HTL wastewater (HTL-WW) or hydrothermal liquefaction aqueous phase (HTL-AP), contains significant amounts of organic carbon and nutrients derived from the feedstock (SundarRajan et al., 2021). However, discharging HTL-AP into the environment without adequate treatment can pose substantial health and environmental risks, primarily due to the presence of toxic chemicals and high levels of ammonium. Therefore, ensuring the safe handling, utilization, and disposal of HTL-AP remains a critical challenge, which hinders the widespread adoption of HTL for waste biomass valorization (Rout et al., 2023). Introducing an additional process to valorize the HTL-AP could potentially enhance its overall economic feasibility and help mitigate environmental concerns (Gerber Van Doren et al., 2017; Gu et al., 2019). AD is emerging as a suitable technology for integration with HTL to efficiently utilize residual carbon (Gerber Van Doren et al., 2017).

Coupling HTL and AD offers a synergistic approach to the treatment of waste biomass. By coupling these two processes, the inherent limitations of each can be overcome, leading to enhanced overall efficiency, improved product quality, and a more comprehensive utilization of biomass feedstock (Rezaee et al., 2020; Okolie et al., 2022). By critically evaluating existing literature and case studies, this review paper aims to enhance our understanding of the potential of combining HTL and AD as a sustainable and integrated solution for waste biomass treatment. Ultimately, this knowledge will support the development and optimization of this hybrid technology, fostering a circular economy approach and advancing towards a more efficient and environmentally friendly waste management paradigm, aligning with UN Sustainable Development Goals.

Numerous reviews have extensively addressed waste biomass valorization using AD and HTL as separate processes (Capson-Tojo et al., 2016; Fan et al., 2023; Lytras et al., 2020; Paul et al., 2021). However, these reviews did not explicitly highlight the potential synergies that arise from integrating AD and HTL. To the best of our knowledge, a comprehensive review focusing on integrating HTL and AD for more effective waste valorization has yet to be conducted. Thus, this review paper aims to bridge this gap by showcasing how integrating AD and HTL using various sequencing techniques presents a complementary approach to organic waste valorization in line with circular economy principles. Distinguishing itself from existing literature, this review strategically unfolds across distinct sections to illuminate the intricate integration of AD and HTL. **Section 2.1** establishes the significance of integration by providing an insightful overview of AD and HTL, including their limitations. **Sections 2.2 and 2.3** intricately detail the integration of HTL followed by AD procedures and vice versa, delving into influencing factors, procedural intricacies, and exhaustive product characterization. **Section 2.4** shifts focus to articulate the integration of AD and HTL within the circular bioeconomy context, elucidating its implications. **Section 2.5** systematically assesses the environmental impact and outlines effective toxicity management strategies. In **Section 2.6**, navigation through prospects and challenges provides a balanced perspective on the integration's potential benefits and hurdles. The conclusive **Section 2.7** synthesizes insights into the pros and cons of each configuration, providing a comprehensive understanding of the integrated AD and HTL landscape.

## 2.2 Performing Hydrothermal Liquefaction followed by Anaerobic Digestion

### *2.2.1 Process Operation*

This section offers a detailed overview of the procedural steps involved in the HTL followed by AD sequence. The HTL process followed by AD is being pursued by various research groups, and ongoing R&D is still underway. Briefly, in the first step, the feedstock is introduced into an HTL reactor. After sealing and purging with nitrogen, the reactor operating temperature is then raised to a specific level and maintained for a determined hydraulic retention time, which varies depending on the feedstock type. Upon the completion of the reaction, the reactor is cooled down to room temperature using a water bath, and the reactor is depressurized by collecting the generated gas in an airbag. Finally, the reactor is opened to collect the solid-liquid products. The HTL-AP obtained after the separation process serves as the feed for the subsequent anaerobic reactor (Li et al., 2022; Zheng et al., 2017).

The AD experiments are often conducted in batch reactors using serum bottles, utilizing granular sludge as the inoculum. Different quantities of HTL-AP are added to each bottle, and water is used to attain the desired working volume. Before sealing the bottles with caps connected to airbags, the headspace of each bottle is purged with nitrogen for 3-5 minutes. Following this, the bottles are placed in a water bath and incubated at a specified temperature, either mesophilic or thermophilic, depending on the experimental conditions (Chen et al., 2016; Wang et al., 2021; Cabrera et al., 2023). The volume of biogas produced is measured using a syringe, and the methane content is determined by gas chromatography (GC). Typically, experiments are conducted in triplicate to ensure reliability and consistency (Li et al., 2019; Si et al., 2019). After reviewing the detailed procedure of HTL followed by AD, it becomes essential to explore various extraction techniques for biocrude, gases, hydrochar, and HTL-AP. This overview will enable a deeper analysis of their respective applications.

### *2.2.2 Extraction of Hydrothermal Liquefaction Products*

The HTL process involves sequential reactions that convert organic matter in the feedstock into multiple distinct products, namely biocrude, HTL-AP, a solid residue commonly referred to as hydrochar, and gaseous byproducts (Beims et al., 2020). In the context of the previous section, this section reviews various extraction methods documented in existing literature to recover these products for their further applications. The extraction of HTL products follows the subsequent procedure:  Upon the completion of the HTL process, the reactor undergoes a cooling phase until it reaches room temperature. Subsequently, the reactor is depressurized, and the resulting gas is carefully captured within a Tedlar bag to enable subsequent composition analysis (Mathankar et al., 2021). The gaseous phase exhibits a yield ranging from 7 to 33% by weight of the initial solids present in the feedstock (Cabrera and Labatut, 2021). The primary constituent of this gas is carbon dioxide, which remains relatively stable in quantity between 250 and 350°C (Mathankar et al., 2021. However, beyond this temperature range, the carbon dioxide content starts to diminish while there is a simultaneous increase in the presence of small hydrocarbons such as methane ($CH_4$), ethane ($C_2H_6$), propane ($C_3H_8$), and hydrogen ($H_2$) (Cabrera and Labatut, 2021).

For the solid-liquid mixture, various separation methods are utilized to isolate the constituents within it, comprising hydrochar, aqueous phase, and solvent. Filtration is commonly employed to separate solids from a solid-liquid mixture. The resulting filtrate is called HTL-AP (Chen et al., 2016; Mathankar et al., 2021). **Table 2.1** presents an overview of the methodologies employed for the separation of hydrochar.

**Table 2.1:** A comprehensive examination of techniques utilized for the separation of hydrochar.

| Feedstock of HTL | Method used to separate hydrochar | References |
|---|---|---|
| Cornstalk | Centrifugation at 10000 rpm for 10 min | (Chen et al., 2020a) |
| Rice straw | Filtration by 300-mesh screen | (Chen et al., 2016; Chen et al., 2015) |
| Dry sewage sludge | Filtration by Buchner funnel | (Li et al., 2022) |
| *Spirulina* powder | Filtration by 1.0 $\mu$m pore size glass | (Zheng et al., 2017) |

| | | |
|---|---|---|
| | fiber filter | |
| Sewage sludge | Vacuum filtration by Buchner funnel | (Hao et al., 2020) |
| Four feedstocks: (a) Ch-Pr; (b) Ch-Li; (c) Pr-Li; and (d) Ch-Pr-Li | Gravimetric filtration | (Posmanik et al., 2017a) |
| Swine manure | Filtration by 0.45 µm filters | (Si et al., 2019; Yang et al., 2018) |
| Sewage sludge & its digestate | Vacuum filtration with GF-1 glass fiber filter paper | (Cabrera et al., 2023) |
| Barley straw | Vacuum filtration | (Zhu et al., 2015) |
| Swine manure | Vacuum filtration using a Whatman filter paper with a pore size of 11 µm | (Minarick et al., 2011) |
| HTL, hydrothermal liquefaction; Ch, carbohydrates; Pr, proteins; Li, lipids | | |

The HTL-AP has the potential to contain a substantial proportion of organics, typically ranging from 20% to 40%, along with 60–80% of the nutrients derived from the feedstock (Silva Thomsen et al., 2022). The exact fraction of organic carbon in HTL-AP is influenced by process conditions and the lipid content of the feedstock (Gerber Van Doren et al., 2017).

The reactor undergoes a thorough rinsing process utilizing solvent, typically performed at least three times, to facilitate the recovery of the oil phase. This process yields a solution known as the solvent phase. Acetone and dichloromethane (DCM) are the commonly employed solvents for this purpose (Cabrera et al., 2023; Zhu et al., 2015). Furthermore, the solid residue remaining on the filter paper obtained after getting HTL-AP as filtrate is also rinsed with solvent to extract the oil phase entrapped within it. The resulting solution is subsequently mixed with the solvent phase. The solid product is subjected to a drying process in an oven for 24 hours and is referred to as hydrochar (Cabrera et al., 2023; Li et al., 2022; Zhu et al., 2015). A comprehensive analysis of hydrochar typically involves diverse tests, such as elemental analysis to ascertain its composition, Fourier transform infrared spectroscopy (FTIR) to identify functional groups on its surface, and a morphology study (Mathankar et al., 2021). Depending on its nitrogen, phosphorus, and potassium levels, hydrochar can serve as both a soil amendment and a fertilizer (Cabrera et al., 2021).

To facilitate biocrude extraction, the solvent phase mixture undergoes treatment in a rotary evaporator. Alternatively, centrifugation can be employed as another method to eliminate the solvent from the solvent phase mixture (Li et al., 2022; Cabrera et al., 2023; Zhu et al., 2015). Additional methodologies for extracting biocrude from the solvent-phase mixture encompass glass fiber filtration and solid-phase extraction techniques (Posmanik et al., 2017a; Zheng et al., 2017). Following the separation process, a dark brown, highly viscous mixture remains, commonly referred to as biocrude (Mathankar et al., 2021). The HTL process typically converts over 50% of the biomass, on a dry and ash-free basis, into biocrude (Ghadge et al., 2022). Biocrude is composed of a diverse array of chemical compounds, including aromatics, aldehydes, ketones, alcohols, carboxylic acids, and straight and cyclic hydrocarbons (Beims et al., 2020). Biocrude can serve as a viable transportation fuel after undergoing upgrades to its chemical and physical properties to meet fuel standards. This shift provides important benefits, moving us away from relying on fossil fuels towards renewable biofuels (Ramirez et al., 2015). The yield and characteristics of biocrude are influenced by both the feedstock and the operating conditions employed in the HTL process. For instance, biocrude from feedstocks like algae, municipal solid waste, or food waste typically has higher levels of ash, moisture, and heteroatoms (Ghadge et al., 2022).

In conclusion, a diverse array of extraction techniques plays a pivotal role in effectively recovering valuable products from the solid-liquid mixture resulting from HTL processing. These methods not only underscore the versatility of the HTL process but also offer opportunities for optimizing product yields and qualities across a spectrum of applications. Additionally, variations in process parameters significantly affect product yield and quality. Therefore, the next section will focus on analyzing the impact of critical process parameters on product quality and yield.

### *2.2.3 Critical Process Parameters*

This section analyzes the impact of critical process parameters, such as variations in operation temperature and retention time, on the subsequent AD process. Operating temperature and retention time often influence the chemical constituents of the HTL-AP obtained. For instance, the feedstock utilized in the HTL process consists of a diverse array of proteins as its biochemical constituents (Rout et al., 2023). When exposed to the HTL process, the proteinaceous substances undergo a transformation attributable to their elevated concentration of ammonia and nitrogenous compounds (Rout et al., 2023). Therefore, HTL-AP is often characterized by elevated levels of total organic carbon (TOC), chemical oxygen demand (COD), ammonium, and nitrogenous compounds existing in the form of emerging heterocyclic rings or chemicals containing heteroatoms such as carbon and sulfur (Khoshnevisan et al., 2021; Silva Thomsen et al., 2022). These ammonia and nitrogenous compounds within the aqueous phase exhibit inhibitory properties on microbial biodegradation processes occurring during AD, thereby directly influencing methane production (Gu et al., 2019). The HTL-AP of cornstalks was found to contain inhibitory compounds, namely phenyl and N-containing compounds. Interestingly, during the AD process, instead of undergoing degradation, the proportion of these compounds actually increased (Chen et al., 2020a). In the case of rice straw as feedstock, the methane production through HTL-AP was observed to be significantly lower than the theoretical yield. This disparity indicates the presence of recalcitrant compounds, specifically furans, ketones, and phenols, which were identified during the analysis (Chen et al., 2016). Therefore, the operating temperature and retention time become critical factors in the HTL process, significantly influencing the composition of the HTL-AP (Angenent et al., 2018; Mao et al., 2021). **Table 2.2** shows a concise overview of key studies that have investigated the effect of various process parameters on AD outcomes.

**Table 2.2:** Summary of studies that highlight the influence of HTL operating temperature and retention time on HTL-AP and the subsequent AD process.

| Feedstock | HTL Conditions | AD Conditions | Key Findings | References |
|---|---|---|---|---|
| Cornstalk | 300 °C; 60 min | Batch; 35 & 55 °C | 1. Due to elevated temperature, the fraction of production of biodegradable organics in AP was reduced.<br>2. The percentage of Phenolic compounds derived from the lignin component of Cornstalk in AP was 43%.<br>3. Phenolic compounds were identified as significant contributors to the aromaticity of the HTL-AP, potentially acting as inhibitors during the AD process. | (Chen et al., 2020a) |
| Dry Sewage Sludge | 300 – 375 °C; 15 min | Batch; 38 °C | 1. The HTL-AP exhibited a higher concentration of refractory compounds derived from temperatures 320 °C and above.<br>2. These toxic compounds impede the degradation of organic compounds and hinder the conversion of VFAs, sugars, etc. | (Li et al., 2022) |

| | | | | |
|---|---|---|---|---|
| *Spirulina* powder | 300 °C; 30 min | Batch; 37 °C | 1. Elevated operating temperatures during the HTL process resulted in decreased RPAs related to N and O heterocyclic compounds and higher cumulative methane production and vice-versa. | (Zheng et al., 2017) |
| Sewage Sludge | 320 °C; 60 min | Batch; 37 °C | 1. Elevated temperatures during the HTL process promote increased degradation of sewage sludge, resulting in the formation of smaller molecules (such as CHON) characterized by high aromaticity and low polarity.<br>2. Inhibitory compounds were detected in the DOM at both temperatures, with a higher percentage of CHO compounds found at 320 °C. | (Hao et al., 2020) |
| Four feedstocks: (a) Ch-Pr; (b) Ch-Li; (c) Pr-Li; and (d) Ch-Pr-Li | 250, 300, and 350 °C; 20 min | Batch; 37 °C | 1. At elevated HTL temperatures, the composition of biodegradable organics is diminished, hence leading to a decrease in biomethane yield from the aqueous phase.<br>2. As the HTL process temperature increases, the rate of biomethane | (Posmanik et al., 2017a) |

| | | | | |
|---|---|---|---|---|
| | | | production decreases. | |
| Rice Straw | 250 – 320 ℃; 0.5 – 4 h | Batch; 37 ℃ | 1. As the HTL process temperature rises, the amount of easily biodegradable organics decreases.<br>2. As the residence time was extended from 0.5 hours to 1, 2, and 4 hours, a corresponding decrease in methane yield was observed. | (Chen et al., 2017) |
| HTL, hydrothermal liquefaction; AP, aqueous phase; AD, anaerobic digestion; VFAs, volatile fatty acids; RPAs, relative peak areas; TAN, total ammonia nitrogen, DOM, dissolved organic matter; Ch, carbohydrates; Pr, proteins; Li, lipids | | | | |

Li et al. (2022) conducted temperature variations ranging from 300 to 375 °C to examine the impact on the composition of the aqueous phase derived from sewage sludge. It was observed that as the temperature increased, there was a notable rise in the percentage of volatile solids converted to biocrude. Despite the high COD concentration observed in HTL-AP within temperature variations ranging from 300 to 375 °C, the relative COD concentration decreases with increasing temperature. The identified inhibitory compounds included benzene, phenol, and pyridine. When subjected to HTL at a temperature of 300 °C for 30 minutes, *spirulina* powder yields HTL-AP characterized by a substantial concentration of COD. Despite elevated COD concentration, an extended lag phase occurs due to release of nitrogen in HTL-AP in the form of ammonia which hampers the biodegradation process. Furthermore, the presence of recalcitrant compounds such as phenol, benzene, N and O heterocyclic compounds, and straight amides further impacts the biodegradation process efficiency (Zheng et al., 2017). Hao et al. (2020) conducted an experiment utilizing HTL on sewage sludge, employing 320 °C temperature. The results indicate that HTL-AP sample obtained at 320 °C temperature contains CHON compounds. Notably, the HTL-AP exhibited a higher relative area percentage of CHO compounds. These compounds have inhibitory effects on the AD process. During the HTL process of rice straw, conducted within a temperature range of 250 to 320 °C and with retention times ranging from 0.5 to 4 hours, it was observed that higher temperatures resulted in an increased production of specific compounds, such as phenols and ketones, contributing to inhibiting AD when compared to lower temperature conditions (Chen et al., 2017).

During the AD process of the aqueous phase obtained from swine manure, a distinct lag phase was observed as the concentration of HTL-AP increased from 6.7% to 13.3%. Furthermore, for concentrations exceeding 33.3%, complete inhibition of the AD process was observed. The primary factor contributing to both the lag phase and inhibition was the presence of ammonia, primarily resulting from the high TAN content in the aqueous phase (Zhou et al., 2015).

The studies mentioned above indicate that the release of nitrogen in the form of ammonia in the aqueous phase can lead to inhibition and impact the biodegradability of organic compounds during the AD process. Therefore, pretreatments are deemed necessary and are often pursued to mitigate the presence of recalcitrant substances in wastewater resulting from HTL. These pretreatment techniques play a crucial role in partially or completely eliminating these recalcitrant compounds, thereby enhancing anaerobic digestion performance (Leng et al., 2020). Zheng et al. (2017) employed adsorption methods to treat the wastewater derived from *Spirulina* powder through HTL. The effectiveness of two absorbents, namely zeolite and granular activated carbon (GAC), as well as polyurethane matrixes (PM), for biofilm formation was evaluated. The results indicated that GAC and PM exhibited higher efficiency in removing COD compared to the control and zeolite, resulting in a reduction in the lag phase. GAC and PM demonstrated effective adsorption of recalcitrant compounds such as nitrogenous compounds present in the HTL-AP, consequently leading to increased biogas production. Additionally, the ammonia concentration remained below the threshold value for inhibition, i.e., $NH_4^+$-N above 4920 mg/L, indicating that zeolite did not play a significant role in reducing toxic compounds and resulted in lower methane production compared to GAC and PM. In another study, Mao et al. (2021) conducted struvite precipitation on the aqueous phase derived from a mixture of dewatered sewage sludge during HTL. The findings revealed that the precipitation process effectively recovered nitrogen and other nutrients, which are known to cause inhibition. This recovery of nutrients through precipitation resulted in an enhanced methane yield. Wang et al. (2021) conducted a comprehensive study involving both struvite precipitation and biochar detoxification techniques on the wastewater generated from HTL of sewage sludge. Struvite precipitation was employed to eliminate ammonia, while biochar detoxification aimed to remove phenolic compounds. The results indicated that implementing both techniques yielded significant improvements, reducing the lag phase and enhancing methane yield compared to using either technique alone. However, it was observed that ammonia removal exhibited a higher level of effectiveness compared to the removal of phenolic compounds.

To address the high concentration of N-heterocyclic compounds in swine manure HTL-AP, Si et al. (2019) implemented ozone pretreatment and GAC addition. Ozone pretreatment was employed to partially oxidize the N-heterocyclic compounds, while GAC was utilized to adsorb the recalcitrant compounds present in the aqueous phase. When ozone pretreatment was conducted alone or in combination with GAC, it resulted in an extended lag phase compared to the control group. Conversely, adding GAC alone reduced the lag phase by adsorbing toxic compounds. However, the highest methane yield was achieved when both pre-treatment methods were employed simultaneously. Li et al. (2019) conducted a study to evaluate the efficacy of zeolite in adsorbing toxic compounds in HTL-AP derived from *Chlorella* 1067. The findings revealed that an increase in zeolite size and adsorption temperature resulted in a decrease in TAN adsorption, while a higher dosage of zeolite led to an increase in TAN adsorption. Zeolite demonstrated effectiveness in removing recalcitrant compounds such as ammonia and sulfate, thereby promoting increased methane yield and reducing the lag phase. The inclusion of powdered activated carbon (PAC) in swine manure HTL-AP was investigated by Zhou et al. (2015) to alleviate the presence of toxic compounds. The findings revealed that the addition of PAC effectively enhanced methane production and reduced the lag phase in the AD process. This enhancement is likely due to PAC's ability to adsorb inhibitory compounds, creating a more favorable environment for biodegradation.

In conclusion, operating temperature and retention time play crucial roles in determining the characteristics of HTL-AP. While an increase in temperature may lead to higher COD concentrations, it also results in elevated release of nitrogen in the form of ammonia in the aqueous phase, thereby hindering HTL-AP biodegradability during the AD process. Additionally, the importance of pretreatments is underscored, with different methods highlighted to enhance biomethane yield from the AD process. The efficacy of these pretreatments depends on the characteristics of the feedstock and HTL operating conditions. These insights emphasize the significance of pretreatments in maximizing the benefits of the HTL followed by AD sequence across diverse feedstock sources. Researchers continue to explore innovative pretreatment methods to further enhance the biodegradability of HTL-AP.

To further optimize the benefits of the HTL followed by AD sequence, it is essential to discuss energy recovery from different products to assess the efficacy of this sequence, as well as digestate quality to analyze its potential applications. Therefore, the focus will shift in the next section towards characterizing biomethane yield, digestate characteristics, and energy recovered from this integrated sequence.

### *2.2.4 Characterization of Biomethane Yield, Energy Efficiency, and Digestate Quality*

This section emphasizes the efficacy of the HTL followed by AD process by evaluating biomethane yield, digestate quality, and energy recovered from this integration, primarily through biomethane and biocrude production. Cabrera et al. (2023) documented that, through Monte Carlo uncertainty analyses employing sewage sludge as a feedstock, the energy recovery from the HTL-AD and AD alone falls within the ranges of 54.6-91.2% and 33.2-71.1%, respectively.

Accurate quantification of methane produced from the aqueous phase is of significant importance for assessing the ease of organic matter degradation and identifying the presence of inhibitory compounds. Meticulous measurement and assessment of the biomethane yield under diverse conditions and varying feedstock compositions allow for the effective evaluation of the robustness of the HTL followed by the AD process. This quantitative analysis enables optimization of system performance by identifying potential limitations and implementing targeted improvements.

Additionally, energy recovery efficiency represents a pivotal dimension that necessitates careful consideration, as it quantifies the energy derived from the integration of HTL and AD. The higher levels of COD and TOC in the HTL-AP serve as indicators of increased potential for energy recovery (Rout et al., 2023). The formula employed for computing energy recovery from each product is expressed by using equation (2.1) as follows:

$$ER_i = \frac{Y_i \times HHV_i}{HHV_{feedstock}} \tag{2.1}$$

where $ER_i$ is the energy recovery, i is the energy product (biocrude or methane), $Y_i$ is the yield for each energy product, $HHV_i$ is the higher heating value of each energy product (MJ/kg), and $HHV_{feedstock}$ is the higher heating value of the feedstock (MJ/kg) (Posmanik et al., 2017a; Cabrera et al., 2023).

The Higher heating value (HHV) is calculated by modified Dulong's formula based on elemental composition, as shown in equation (2.2):

$$\text{HHV (MJ/kg)} = 0.338 \times \text{C} + 1.428(\text{H} - \text{O}/8) \tag{2.2}$$

where C, H, and O are the mass percentage of carbon, hydrogen, and oxygen (%, w/w), respectively (Posmanik et al., 2017a; Cabrera et al., 2023).

Moreover, the characterization of digestate properties plays a crucial role in evaluating the environmental impact and potential nutrient recycling of HTL-AP. While AD is unable to remove certain nutrients, such as nitrogen and phosphorus, from the digestate, it is important to assess and understand the properties of the digestate due to its nutrient-rich nature (Leng et al., 2020). **Table 2.3** presents a comprehensive analysis of the biomethane yield, energy recovery, and digestate characterization as documented in the literature.

The synergistic application of HTL and AD demonstrates a superior energetic output by converting the feedstock into valuable bioproducts such as biocrude oil and biomethane, surpassing the individual energy yields achievable through either process alone (Angenent et al., 2018). The biomethane yield, digestate characteristics, and energy recovery of the HTL followed by AD process are largely influenced by the characteristics of the feedstock and the operating conditions of the integrated process. For example, Li et al. (2020) reported that the HTL-AD system recovered 52.09% of the energy in the form of biocrude when using dry sewage sludge as feedstock, operating at 350°C for 15 minutes. Additionally, they found that 2.38%, 2.95%, and 1.49% of the energy is recovered for organic loadings of 2, 4, and 6 g COD/L, respectively, using HTL-AP as feedstock in the AD process. Conversely, Cabrera et al. (2023) observed that the HTL followed by AD process recovered 77.9 ± 1.9% of total energy, with 60.2 ± 2.6% of energy recovered in the form of biocrude when using sewage sludge as feedstock and operating the HTL process at 350°C for 30 minutes. Additionally, it was reported that pretreatments enhance the energy recovery of the HTL followed by AD process as energy recovery for the biomethane yield improves. In order to address the inhibitory compounds present in HTL-AP and enhance biomethane yield for improved energy recovery, Li et al. (2019) conducted zeolite adsorption on *Chlorella* 1067 HTL-AP, performed at 300 °C for 30 minutes. The outcomes of the study revealed that zeolite adsorption effectively removed recalcitrant compounds, resulting in increased methane production. Consequently, the energy recovery of the HTL-AD system witnessed a notable increase from 64.1% to 70.5%.

In summary, **Table 2.3** provides an overview of the various feedstocks used in the HTL-AD system and how different operating conditions influence biomethane yield, digestate characteristics, and energy recovery. The outcomes of HTL followed by the AD process reveal a predominant recovery of energy in the form of biocrude, with minimal energy retrieval in the form of methane. This highlights an energy trade-off between biocrude and biomethane production, where optimization of this exchange maximizes overall energy recovery. Incorporating pretreatment methods into HTL-AP improves the energy recovery of the HTL-AD system. The carbon content of digestate demonstrates its potential as a soil amendment. Researchers are actively investigating methods to optimize the HTL followed by the AD process and maximize total energy recovery from this integrated system.

**Table 2.3:** The intricate details of the study's examination encompass biomethane yield, energy recovery, and the characterization of digestate.

| HTL-AP Source & Operating Conditions | Pre-treatment method | Conditions for AD in batch reactor | Organic loading (g COD/L) | Biomethane yield | COD removed (%) | Energy recovered | Digestate properties | References |
|---|---|---|---|---|---|---|---|---|
| Dry Sewage Sludge; 350 °C for 15 min | - | 38 °C | 2 | 309.4 mL $CH_4$/g COD | 72.5 | From Biocrude: 52.09%<br>From HTL-AP in the form of biomethane: 2.38% | pH: 7.88; No VFAs conc.; TAN conc.: 0.4 g/L | (Li et al., 2022) |
| Dry Sewage Sludge; 350 °C for 15 min | - | 38 °C | 4 | 226.6 mL $CH_4$/g COD | 62.9 | From Biocrude: 52.09%<br>From HTL-AP in the form of biomethane: 2.95% | pH: 7.9; Minimal VFAs conc.; TAN conc.: 0.99 g/L | (Li et al., 2022) |
| Dry Sewage Sludge; 350 °C for 15 min | - | 38 °C | 6 | 127.3 mL $CH_4$/g COD | 38 | From Biocrude: 52.09%<br>From HTL-AP in the form of biomethane: 1.49% | pH: 8.2; VFAs conc.: 1.2 g/L; TAN conc.: 1.2 g/L | (Li et al., 2022) |

| | | | | | | | | |
|---|---|---|---|---|---|---|---|---|
| Ch-Pr-Li; 250 °C for 20 min | - | 37 °C | 4 | 175 mL $CH_4$/g COD | 40 | Total energy recovered 〜 54% | - | (Posmanik et al., 2017a) |
| Ch-Pr-Li; 300 °C for 20 min | - | 37 °C | 4 | 170 mL $CH_4$/g COD | 36.17 | Total energy recovered 〜 60% | - | (Posmanik et al., 2017a) |
| Ch-Pr-Li; 350 °C for 20 min | - | 37 °C | 4 | 150 mL $CH_4$/g COD | 31.43 | Total energy recovered 〜 70% | - | (Posmanik et al., 2017a) |
| Wastewater sludge; 325 °C for 30 min (maintained pH at 7.0) | Struvite precipitation and biochar detoxification | 35 °C | - | 225 mL $CH_4$/g COD | 48 | - | Change in TN composition: -12% & Acetate composition: -30% | (Wang et al., 2021) |
| Sewage Sludge; 350 °C for 30 min | - | 37 °C | 1 | 274.6 mL $CH_4$/g COD | 79.47 | Total energy recovered: 77.9 ± 1.9%; Energy recovered from biocrude: 60.2 ± 2.6% | Increase in TAN conc.: 145 %; VFAs conc: 16 mg COD\ L | (Cabrera et al., 2023) |
| Swine Manure; 270 °C for 1 hr | GAC adsorption | 37 °C | 10 | 228 mL $CH_4$/g COD | 97.3 | - | pH: 7.33; Total nitrogen: 375 mg/l & Phosphorus: 17.5 mg/l | (Yang et al., 2018) |

| | | | | | | | | |
|---|---|---|---|---|---|---|---|---|
| Swine Manure; 270 ℃ for 1 hr | Ozone pre-treatment | 37 ℃ | 10 | 187 mL $CH_4$/g COD | 65.6 | - | pH: 7.61; Total nitrogen: 500 mg/l & Phosphorus: 18.5 mg/l | (Yang et al., 2018) |
| *Chlorella* 1067; 300 ℃ for 30 min | - | 35 ℃ | 4 | 10.95 mmol/g COD | 49.49 | Total energy recovered: 64.1% | - | (Li et al., 2019) |
| *Chlorella* 1067; 300 ℃ for 30 min | Zeolite adsorption | 35 ℃ | 4 | 14.79 mmol/g COD | 60.33 | Total energy recovered: 70.5% | Total carbon: 9.74 % of the feedstock & Total nitrogen: 14.8% of the feedstock | (Li et al., 2019) |

HTL, hydrothermal liquefaction; AP, aqueous product; AD, anaerobic digestion; VFAs, volatile fatty acids; TAN, total ammonia nitrogen; Ch, carbohydrates; Pr, proteins; Li, lipids; GAC, granular activated carbon; COD, chemical oxygen demand

## 2.3 Anaerobic Digestion followed by Hydrothermal Liquefaction

### *2.3.1 Process Operation*

In the context of the review paper, this forthcoming section will examine the operational process of another sequencing method: AD followed by HTL. This exploration will offer detailed insights into the procedural intricacies of this sequencing approach.

The AD coupled with HTL is being pursued by various research groups, and ongoing R&D is still underway. Below is a summary of the steps followed in laboratory settings: AD experiments are conducted within cylindrical digesters, wherein dried feedstock, if applicable, is mixed with deionized water to achieve a desired solid content by weight. The resulting feedstock slurry is then blended with inoculum in a prescribed food-to-microorganism ratio within each digester. Subsequently, the cylindrical digesters are sealed with stoppers, and the headspace is purged with nitrogen for 3-5 minutes. The stoppers are connected to tubing equipped with control mechanisms and attached to an airbag for gas collection. The sealed bottles are immersed in a water bath and subjected to specific temperatures, either mesophilic or thermophilic, based on the experimental requirements. The experiments are typically carried out for a designated hydraulic retention time (HRT) to enable biogas production. To ensure reliability and consistency, all experiments are performed in triplicate. The volume of generated biogas is measured using a gas meter or syringe, while the methane content is determined using gas chromatography (Forster-Carneiro et al., 2008; Raposo et al.,2012).

After the AD experiment, the resulting digestate serves as a feedstock for the HTL. After sealing and purging with nitrogen, the HTL reactor is heated to a specified temperature and maintained for a designated HRT, which varies depending on the feedstock. To ensure optimal mixing, a dedicated magnetic drive impeller agitation device is employed, typically operating at 300 rpm throughout all experimental runs. The reaction time commences once the reactor reaches the predefined temperature set point. Upon completion of the reaction, the reactor is deactivated and gradually cooled to ambient temperature using a water bath. The reactor is depressurized by collecting the generated gas in an airbag. Next, the reactor is opened to collect the solid and liquid products. A separation process is then carried out to isolate the various components of the HTL process. The product separation procedures employed for extraction are consistent with those described in the preceding section. The resulting products include biocrude, gasses, hydrochar, and an aqueous phase (HTL-AP) (Eboibi et al., 2015; Niknejad et al., 2023).

Ongoing research aims to optimize the AD followed by HTL process, extending the capabilities of existing AD plants. To conclude, streamlining and optimizing this process procedure and extraction methods directly influence methane and biocrude yields. Moreover, the AD process parameters can significantly affect HTL product yields due to feedstock characteristics. Subsequent sections will explore the impact of these process parameters on digestate characteristics, which in turn affects the HTL process.

### *2.3.2 Critical Process Parameters*

Digestate characteristics are shaped by AD hydraulic retention time, while HTL product yields are primarily influenced by the feedstock characteristics. This section will discuss the impact of AD process parameters, specifically variations in hydraulic retention time on subsequent HTL process product yields.

AD primarily relies on naturally occurring microorganisms to facilitate the breakdown of organic matter, and wet bio-wastes serve as the most desirable substrates for this process (Awasthi et al., 2021). During the AD of biomass, the majority of the readily biodegradable material is transformed into biogas. However, the residual material, known as digestate, exhibits reduced biodegradability (Somers et al., 2018). Digestate typically exhibits lower concentrations of carbon and hydrogen, along with an elevated pH. The content of $NH_4^+$-N in the digestate is influenced by the total nitrogen content present in the initial feedstock. Through the application of HTL to the digestate derived from AD, the remaining organic compounds can be effectively converted into valuable products, including biocrude (Möller & Müller, 2012).

As stated earlier, AD operating conditions would influence the digestate quality as well as subsequent HTL performance. For instance, the residence times applied during AD plays a pivotal role in determining the biocrude yield attained during the subsequent HTL process. Eboibi et al. (2015) conducted a study to assess the influence of hydraulic retention time (HRT) on biocrude yield using cow manure with 8% dry solids content as the feedstock. The AD experiments were carried out at temperatures of 29°C for varying HRTs: 10, 18, 28, 38, 50, and 60 days. The results indicated a positive correlation between HRT and biomethane yield, with higher yields observed as the HRT increased. Although the carbon content of the digestate remained relatively consistent across most HRTs, the digestate obtained after 60 days exhibited the lowest carbon content. Following the AD process, HTL experiments were conducted at 350°C for 30 minutes, with sodium carbonate serving as a catalyst. The biocrude yield exhibited a distinct trend corresponding to the HRT durations, with maximum and minimum yields obtained at 38 and 60 days, respectively. This decrease in biocrude yield at 60 days HRT can be attributed to the lower carbon and hydrogen content in the digestate. The observed increase in biocrude yield from 28 to 38 days HRT is attributed to the accumulation of microbial biomass material during the AD process. However, a subsequent decrease at 50- & 60-days HRT suggests the conversion of this accumulated material into methane during the initial stages of AD. Overall, the study underscores the importance of maximizing biogas yield to enhance biocrude production, highlighting the potential for improved resource recovery in waste management systems. Vardon et al. (2011) conducted an HTL experiment utilizing anaerobic sewage sludge obtained from wastewater treatment facilities. The findings revealed that the anaerobically digested sewage sludge exhibited diminished levels of protein and lipid content while displaying a higher carbohydrate content. This outcome can be attributed to the prior consumption of the easily biodegradable fraction during biogas formation. As a result of the comparatively lower conversion efficiency of carbohydrates, the yield of biocrude was notably reduced. Furthermore, the resulting biocrude exhibited elevated levels of oxygen and nitrogen content, posing a significant challenge for the biofuel industry in terms of upgrading and refining processes.

In the HTL process, researchers frequently use catalysts to enhance the degradation mechanism and increase the yield of biocrude. Additionally, strategic catalyst incorporation not only boosts biocrude or gas production but also inhibits the formation of hydrochar (Zhang et al., 2020). In a research study conducted by Posmanik et al. (2017b), acidic and base catalysts were employed during the HTL process to assess their influence on product yield and quality. Phosphoric acid and sodium hydroxide served as the acidic and base catalysts, respectively. The feedstock was cow manure digestate. The use of the acidic catalyst resulted in a remarkable 59% increase in biocrude yield, while the base catalyst contributed to a 15% increase. This substantial improvement in yield observed with the acidic catalyst can be attributed to the initial highly alkaline pH of the manure (i.e., 9.1), primarily due to its elevated ammonia content. Furthermore, the presence of both acid and base catalysts facilitated the decarboxylation reaction, contributing to improved product formation. Conversely, the utilization of acidic and base catalysts led to a reduction in hydrochar yield by 10% and 25%, respectively. Additionally, when the acidic catalyst was employed, the yield of the aqueous phase decreased to 35%, whereas the base catalyst resulted in an increase to 39% for the aqueous phase yield. Motavaf et al. (2021) investigated the impact of supported metals, bulk metal oxides, and a range of salt, acid, and base additives on the HTL process of food waste. The findings indicated that supported metals and the aforementioned additives had no discernible influence on the biocrude yield. However, the utilization of additives proved effective in enhancing the Higher Heating Value (HHV) of biocrude by diminishing the oxygen and nitrogen content while improving the hydrogen content. Metal oxides such as $CeO_2$, $La_2O_3$ and $SiO_2$ demonstrated a positive influence on both biocrude yield and elemental composition. Notably, $SiO_2$ exhibited the most substantial impact, resulting in a 9 wt.% increase in biocrude production, followed by $La_2O_3$ then $CeO_2$. The energy recovery in the form of biocrude saw a significant rise of 90%, 80%, and 80% with the application of $SiO_2$, $La_2O_3$ and $CeO_2$, respectively. Hence, this study can be beneficial for the energy recovery in the form of biocrude when implementing AD followed by HTL.

To conclude, the hydraulic retention time significantly influences digestate characteristics, ultimately affecting the biocrude yield. Longer retention times increase biogas production but reduce carbon content in the digestate, leading to decreased biocrude yield. Thus, hydraulic retention time negatively impacts biocrude yield. Additionally, the strategic use of catalysts during the HTL process is crucial for enhancing biocrude production. Metal oxides, acidic catalysts, and base catalysts show positive results for the yield of the biocrude; the results can vary depending on the characteristics of the feedstock. These insights emphasize the importance of catalyst utilization during the HTL process to maximize the benefits from AD-HTL configuration.

In order to enhance the efficacy of the AD followed by HTL sequence, it is essential to expand this study to include an analysis of energy recovery from this sequential configuration, as well as the characterization of the biocrude and aqueous phase generated, to evaluate their potential applications. Consequently, the next section will focus on biocrude yield, aqueous phase characteristics, and energy recovery from the AD-HTL system.

### *2.3.3 Characterization of Biocrude Yield, Energy Recovery, and Aqueous Phase*

This section will deal with the characterization of biocrude yield, HTL-AP, and energy recovered as it is a fundamental aspect of the study of AD followed by the HTL process. The characterization of biocrude yield, energy recovered, and the HTL-AP is a fundamental aspect of the study of AD followed by the HTL process. Understanding the properties and composition of these components is essential for assessing the efficiency and possible uses of biocrude and the aqueous phase. The determination of biocrude yield and the characterization of its composition are essential aspects influenced by various parameters, including feedstock properties, operating conditions such as temperature and residence time, and the use of catalysts (Dimitriadis & Bezergianni, 2017). Thus, a comprehensive understanding of biocrude yield and its composition is crucial for HTL process optimization, assessing product quality, guiding downstream processing, evaluating environmental impact, and facilitating comparative analysis. This knowledge supports the development of efficient and sustainable biocrude production and utilization, advancing the utilization of renewable biomass resources as an alternative to fossil fuels (Mishra et al., 2022).

The overall efficiency of the integrated AD and HTL processes can be assessed by determining the energy recovered by using equations 1 and 2 as stated in **Section 2.2.4**. It provides insights into the amount of energy harnessed from biomass feedstock and how effectively it has been converted into useful forms, such as biogas and biocrude. Monitoring and optimizing energy recovery helps identify areas for improvement, maximize energy utilization, and enhance overall process efficiency (Yadav et al., 2021).

Thoroughly characterizing the aqueous phase, a valuable byproduct of HTL, is of significant importance in understanding its composition, quality, potential applications, and environmental implications. The aqueous phase contains a range of nutrients that can be effectively utilized in high-rate AD (HRAD) to produce biomethane, ultimately increasing energy recovery and promoting resource recycling (Kassem et al., 2020a; Kassem et al., 2020b). However, the presence of N-containing compounds can have an inhibitory effect on AD (Cabrera et al., 2023). Therefore, a comprehensive examination of these aspects enhances understanding of the quality and potential uses of biocrude, maximizes energy recovery, and facilitates nutrient recycling from the aqueous phase, ultimately contributing to a more environmentally conscious and resource-efficient approach to biomass conversion.

Eboibi et al. (2015) conducted an investigation by manipulating the HRT during AD and analyzing its impact on the yield and quality of biocrude obtained through subsequent HTL using cow manure as the feedstock. The energy recovery from the biocrude was 52.3%, 82.9%, 62.12%, 72.0%, 60.7%, and 51.6% for the digestate obtained from hydraulic retention times (HRT) of 10, 18, 28, 38, 50, and 60 days, respectively, with the utilization of sodium carbonate as a catalyst. The observed variation in yield can be attributed to the proliferation of microbial mass during the AD process. Vardon et al. (2011) also conducted the HTL experiment using digested anaerobic sludge with a 26% dry solid content as the feedstock. The HTL process was conducted at a temperature of 300°C for a duration of 30 minutes. Given the low lipid content and high carbohydrate content in the feedstock, the biocrude yield obtained was measured at only 9.4%. The resulting biocrude exhibited a significant composition of ester, phenolic, and nitrogenous compounds, attributed to the higher percentage of protein and carbohydrate content in the feedstock. These findings underscore the critical importance of considering the composition of the HTL feedstock, as they directly influence the chemical composition of the biocrude. Moreover, the study emphasizes the necessity for a deeper understanding of biocrude characteristics when assessing potential biocrude applications and refining requirements.

To underscore the significance of catalysts in the HTL process within the integrated AD-HTL system, Posmanik et al. (2017b) conducted an HTL experiment using digested cattle manure with 8% dry solid content. The HTL experiment was conducted at 300 °C for 60 minutes. Two catalysts, phosphoric acid and sodium hydroxide, were selected to assess their impact on biocrude yield. Both catalysts demonstrated a positive effect on biocrude yield. With phosphoric acid, the biocrude yield increased from 36.48 to 58 wt.%, while with sodium hydroxide, it increased from 36.48 to 42 wt.%.

In summary, **Table 2.4** presents a thorough evaluation of biomethane yield, energy recovery, and aqueous phase characterization across various studies encompassing diverse feedstocks. These findings shed light on the complex relationship between AD retention time and biocrude energy recovery, underscoring the need for optimization strategies in integrated AD-HTL systems. Moreover, the elemental composition analysis of digestate underscores the potential of HTL as a carbon recovery mechanism post-AD. Furthermore, the study underscores the pivotal role of catalyst incorporation during HTL to bolster biocrude yield and enhance overall energy recovery. Additionally, the examination of carbon and nitrogen content in the aqueous phase reveals promising prospects for nutrient recovery, adding an additional dimension to the sustainability profile of the AD-HTL system. Looking ahead, researchers will focus on refining the AD-HTL process to overcome challenges and maximize efficiency. This research makes a substantial contribution to our understanding of renewable energy and waste management, paving the way for advancements in sustainable energy production and resource recovery. In essence, the study not only enriches our knowledge of AD-HTL systems but also holds promise for their practical implementation, offering innovative solutions to address pressing environmental and energy challenges.

**Table 2.4:** The intricate details of biocrude yield, energy recovery, and the characterization of the aqueous phase (AP).

| Feedstock | Dry solids content in feedstock (% w/w) | AD Operating Temperature (℃) | AD Retention time (days) | Biomethane yield | Digestate chemical composition (%) | HTL Operating Conditions | Addition of Catalyst | Energy recovered | Aqueous phase properties | References |
|---|---|---|---|---|---|---|---|---|---|---|
| Cow manure | 8 | 29 | 10 | 3.9 $m^3$/ (kg VS added) | C: 34.1; H: 5.1; N: 1.5; S: 0.4 & O: 43.9 (w/w dry basis) | 350 ℃ for 30 min | Sodium carbonate | 52.3 % in the form of biocrude | C: 16.3; H: 3.0; N: 3.1; S: 1.8 & O: 75.8 (% w/w) | (Eboibi et al., 2015) |
| Cow manure | 8 | 29 | 18 | 19.1 $m^3$/ (kg VS added) | C: 31.2; H: 3.9; N: 1.2; S: 0.2 & O: 48.5 (w/w dry basis) | 350 ℃ for 30 min | Sodium carbonate | 82.9 % in the form of biocrude | C: 23.9; H: 2.7; N: 0.8; S: 0.3 & O: 72.3 (% w/w) | (Eboibi et al., 2015) |
| Cow manure | 8 | 29 | 28 | 19.9 $m^3$/ (kg VS added) | C: 33.9; H: 5.2; N: 1.8; S: 0.5 & O: 43.6 (w/w dry basis) | 350 ℃ for 30 min | Sodium carbonate | 62.12 % in the form of biocrude | C: 24.3; H: 3.6; N: 1.5; S: 0.4 & O: 70.2 (% w/w) | (Eboibi et al., 2015)] |
| Cow manure | 8 | 29 | 38 | 20.2 $m^3$/ (kg VS added) | C: 31.8; H: 3.7; N: 1.6; S: 0.4 & O: 47.3 (w/w dry basis) | 350 ℃ for 30 min | Sodium carbonate | 72.0 % in the form of biocrude | C: 24.6; H: 2.9; N: 1.8; S: 0.4 & O: 70.3 (% w/w) | (Eboibi et al., 2015) |
| Cow manure | 8 | 29 | 50 | 20.6 $m^3$/ (kg VS | C: 32.3; H: 3.7; N: 1.8; | 350 ℃ for 30 min | Sodium carbonate | 60.7 % in the form of | C: 22.9; H: 2.7; N: 0.9; | (Eboibi et al., 2015) |

| | | | | | | | | | | |
|---|---|---|---|---|---|---|---|---|---|---|
| | | | | added) | S: 0.3 & O: 46.8 (w/w dry basis) | | | biocrude | S: 0.3 & O: 73.2 (% w/w) | |
| Cow manure | 8 | 29 | 60 | 22.6 $m^3$/ (kg VS added) | C: 19.9; H: 2.8; N: 0.8; S: 0.7 & O: 60.8 (w/w dry basis) | 350 °C for 30 min | Sodium carbonate | 51.6 % in the form of biocrude | C: 19.1; H: 3.1; N: 1.9; S: 0.7 & O: 75.2 (% w/w) | (Eboibi et al., 2015) |
| Digested Anaerobic Sludge | 26 | - | - | - | Crude protein: 15; Crude lipid: <1; Total carbohydrates: 54; NDF: 51; ADF: 36; Lignin: 10 & Ash: 31 | 300 °C for 30 min | - | Biocrude yield: 9.4% & HHV: 32.0 MJ/kg | - | (Vardon et al., 2011) |
| Digested cattle manure | 8 | - | - | - | C: 34.3; H: 3.7; N: 2.3 & O: 25.9 | 300 °C for 60 min | - | Biocrude yield ≈36.48 wt.% (on a carbon basis) & HHV: 33.4 MJ/kg | Lactic acid: 26 ± 4 mg C per g of C in feed & Acetic acid: 38 ±4 mg C per g of C in feed | (Posmanik et al., 2017b) |
| Digested cattle manure | 8 | - | - | - | C: 34.3; H: 3.7; N: 2.3 & O: 25.9 | 300 °C for 60 min | Phosphoric acid | Biocrude yield: 58 wt. % (on a carbon | Recovery of Lactic acid | (Posmanik et al., 2017b) |

|  |  |  |  |  |  |  |  |  |  |  |
|---|---|---|---|---|---|---|---|---|---|---|
|  |  |  |  |  |  |  |  | basis) & HHV: 34.8 MJ/kg | & Acetic acid decreased by 85% & 44% respectively (based on carbon recovery) |  |
| Digested cattle manure | 8 | - | - | - | C: 34.3; H: 3.7; N: 2.3 & O: 25.9 | 300 ℃ for 60 min | Sodium hydroxide | Biocrude yield: 42 wt. % (on a carbon basis) & HHV: 34.0 MJ/kg | Recovery of Lactic acid & Acetic acid increased by 88% & 176% respectively (based on carbon recovery) | (Posmanik et al., 2017b) |

## 2.4 Integrating Anaerobic Digestion with Hydrothermal Liquefaction in a Circular Bioeconomy Context

This section will discuss the integration of AD and HTL in a circular bioeconomy context as the transition from a linear to a circular economy is paramount to mitigate the effects of human activities on human health and the natural environment. A circular economy promotes continuous use, reuse, refurbishing, and recycling of materials, decreasing environmental impact, preserving natural resources, and supporting sustainability. Within the framework of a circular bioeconomy, sustainability is linked to the responsible management of bio-based renewable resources, creating a regenerative economic cycle (Tan and Lamers, 2021). The integration of AD and HTL represents a promising pathway towards achieving the principles of a circular bioeconomy in the context of organic waste valorization. This integration not only maximizes energy recovery but also transforms the diverse components of biomass into high-value products (Kassem et al., 2020a; Kassem et al., 2020b).

In the scenario when AD is followed by HTL, AD of organic waste produces biogas and digestate. Biogas is a renewable energy source, and digestate, which is nutrient-rich, is an excellent precursor for the subsequent HTL process. The HTL converts the digestate into valuable biocrude while also producing hydrochar and gases. The enriched digestate and the diverse valuable byproducts contribute to a circular system by closing material and energy loops (Eboibi et al., 2015; Posmanik et al., 2017b; Vardon et al., 2011). The second integration scenario includes HTL followed by AD, which offers distinct advantages. HTL transforms biowastes into biocrude, hydrochar, and gases, and the aqueous phase (HTL-AP) becomes a nutrient-rich solution. This HTL-AP, when integrated into the AD system, augments biogas production, thereby maximizing energy recovery from the entire organic feedstock. This closed-loop system not only minimizes waste but also enhances the sustainability credentials of organic waste treatment (Chen et al., 2020a; Chen et al., 2016; Li et al., 2022). Thus, the integration of AD and HTL emerges as a key strategy in realizing the full potential of organic feedstocks within the circular bioeconomy framework as we move towards a more sustainable future. In addition, this integrated system is closely aligned with the water, food, and energy nexus, recognizing the interdependence of these essential resources (**Figure 2.3**). In terms of the water system, integration ensures the judicious use of water resources. Both the AD and HTL processes operate with water-rich organic feedstocks. HTL-AP creates a closed-loop system when returned to AD. This integrated approach optimizes energy recovery from organic waste, generating biogas from AD and biocrude from HTL. This recovered energy is essential not only for sustaining the integrated system but also for energy consumption in food production and other related processes. As for the food system, nutrient-rich byproducts contribute to the circularity within the food system, treated water from the integrated system is used in food production, and the fertilizers produced are utilized to enhance soil fertility and crop productivity.

In summary, whether AD precedes HTL or vice versa, the integration of these two systems plays a crucial role in the circular bioeconomy paradigm. It improves resource efficiency, reduces waste, and establishes a circular system that aligns with the complex dynamics of water, food, and energy, representing a tangible step towards a more sustainable and circular future. To assess the effectiveness of this integration, environmental impact and toxicity management should also be considered.

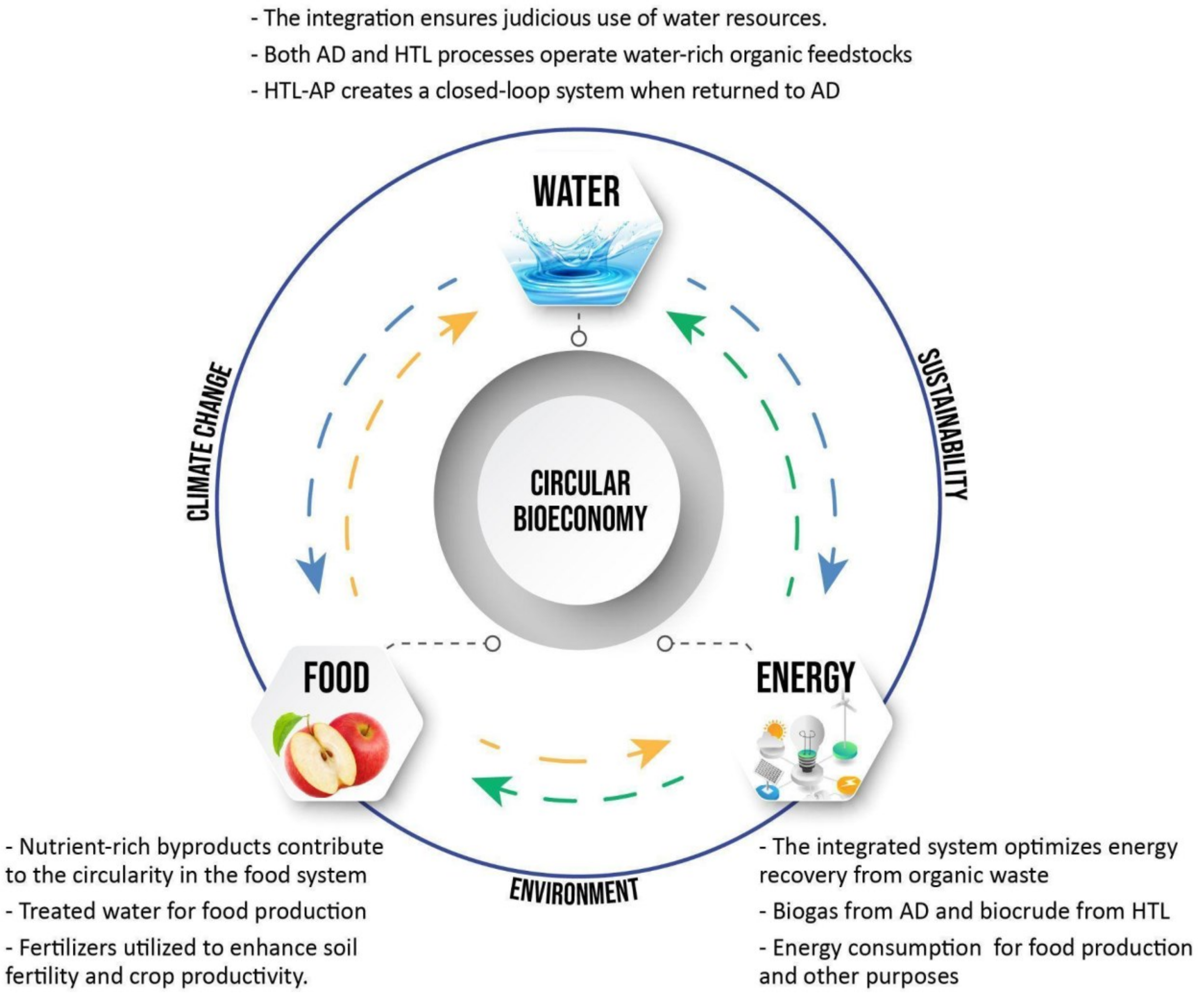

- The integration ensures judicious use of water resources.
- Both AD and HTL processes operate water-rich organic feedstocks
- HTL-AP creates a closed-loop system when returned to AD

- Nutrient-rich byproducts contribute to the circularity in the food system
- Treated water for food production
- Fertilizers utilized to enhance soil fertility and crop productivity.

- The integrated system optimizes energy recovery from organic waste
- Biogas from AD and biocrude from HTL
- Energy consumption for food production and other purposes

**Figure 2.3:** Integration of HTL and AD in the context of the Water-Energy-Food nexus, aiming to achieve sustainability and contribute to the development of a circular bioeconomy.

## 2.5 Environmental Impact and Toxicity Management

This section addresses the management of toxins generated during the HTL-AD and vice versa process, as well as its environmental impact. The integrated AD and HTL have immense potential for sustainable biomass management, thereby contributing to the circular bioeconomy. However, the complex interaction of various components in these processes may result in the introduction of potentially toxic compounds that influence system efficiency and environmental sustainability. To ensure a circular bioeconomy, the environmental effects and toxicity must be carefully considered. Here, toxicity assessment and strategies for minimization within the integrated AD and HTL systems were explored. The conversion of organic feedstocks in AD and HTL systems can lead to the formation of various toxic compounds, which could affect the microbial communities and process performance. HTL produces recalcitrant and highly toxic compounds within the HTL-AP, including organic acids, phenols, amides, esters, alcohols, ketones, *N*-heterocyclic compounds, and cyclic hydrocarbons (Xu et al., 2022). These compounds present in the HTL-AP constitute an estimated 20-50% of the organic content of the feedstock, which harms soil, water, and human health. In addition, the toxicity of HTL-AP hinders the subsequent processes, e.g., AD. For instance, Zheng et al. (2017) observed approximately 50% inhibition occurring at an inclusion ratio of 6% HTL-AP, while nearly complete inhibition was observed at inclusion ratios higher than 24%. The inhibitory effect of HTL-AP on anaerobes is primarily attributed to its high ammonia concentrations and recalcitrant organic compounds (e.g., phenol and benzene), which limit the digestibility and biogas production in the AD stage.

Additionally, hydrochar, a by-product of the HTL process, holds immense potential as a versatile carbonaceous material with applications ranging from soil amendment to energy storage. Its composition, enriched with elements like nitrogen, phosphorus, and potassium, makes hydrochar an attractive alternative to chemical fertilizers. Nonetheless, certain studies have emphasized the importance of considering potential toxicity when using hydrochar as a soil amendment. For example, Hao et al. (2018) investigated the toxicity of dissolved organic matter (DOM) associated with hydrochar. The results concluded that the high operating temperature of HTL leads to increased toxicity of hydrochar-based DOM. This heightened toxicity is attributed to the production of highly aromatic and low molecular weight compounds at elevated temperatures, as the increment in temperature facilitates decarboxylation, dehydration, and condensation reactions. Furthermore, the hydrophobic nature of these compounds causes them to adhere to the surface of hydrochar, thereby contributing to its associated toxicity. This increase in toxicity further inhibits cyanobacterial growth, posing potential harm to the aquatic environment. Fregolente et al. (2021) investigated the utilization of hydrochar derived from sugarcane residues as a soil conditioner for maize production. The findings revealed that applying hydrochar at higher rates in the field adversely affected plant development by reducing water availability in the soil system. Similarly, Cervera-Mata et al. (2021) examined the use of hydrochar derived from spent coffee grounds in lettuce cultivation (Lactuca sativa var. longifolia). Their results indicated that the resulting hydrochar inhibited plant growth. However, it was observed that the concentration of both macro elements (Ca, Na, and Mg) and microelements (Cu and Fe) increased. Researchers have been exploring various techniques, such as washing with organic solvents, natural aging of hydrochar, and heavy metal immobilization, depending on the structure and porosity, to mitigate the effects of toxins (Karatas et al., 2022).

Furthermore, the toxicity of AD effluent and digestate is vital to assess the environmental impact of the integrated AD and HTL systems. The AD effluent, the liquid phase of the AD process byproduct, may contain compounds with potentially toxic properties. These compounds include ammonia, sulfide, and volatile fatty acids, which can have a negative impact on the environment and pose challenges for the subsequent utilization of the effluent (Tawfik et al., 2022). Additionally, the digestate, the solid phase of the AD process byproduct, may contain potentially toxic compounds, including heavy metals and recalcitrant organic compounds, which necessitate careful assessment to ensure their safe disposal or beneficial reuse (O'Connor et al., 2022). The type and concentration of these compounds in the AD effluent or digestate primarily depend on the feedstock and the addition of chemicals used in the process. Thus, mitigating and reducing the impact of these toxic compounds is crucial for the successful implementation of the integrated system, ensuring sustainability within the circular bioeconomy framework.

Innovative toxicity-reduction methods for HTL-AP have been critical in promoting the sustainability and environmental compatibility of combined AD and HTL systems. Table 5 summarizes studies exploring the toxicity mitigation methods for HTL-AP derived from various feedstocks under different HTL conditions and their subsequent impact on the AD process. Researchers investigated various approaches, including biological treatments such as algal bioreactors, $H_2O_2$ addition, and adsorption process using granular activated carbon (GAC) and zeolite (Pham et al., 2013 and Zheng et al., 2017). Quispe-Arpasi et al. (2018) conducted a study to explore the impact of adding $H_2O_2$ on toxic compounds within *Spirulina* HTL-AP. The introduction of $H_2O_2$ led to increased methane production. This enhancement is attributed to the decomposition of $H_2O_2$, which generates highly reactive radicals. These radicals, in turn, oxidize inhibitory compounds, transforming them into easily biodegradable low-molecular-weight compounds. As a result, 66.7% of the energy is effectively recovered. Pham et al. (2013) explored the detoxification of HTL-AP using algal bioreactor treatment followed by GAC adsorption. The cytotoxicity index of HTL-AP decreased by 30% following algal bioreactor treatment and 92.5% after subsequent GAC treatment with a 20-minute empty bed contact time (EBCT). In a study conducted by Zheng et al. (2017), three distinct methods were examined to alleviate the toxicity of HTL-AP on AD performance. The utilization of zeolite, GAC, and polyurethane matrices (PM) resulted in total methane yields of 136 mL/g COD, 169 mL/g COD, and 168 mL/g COD, respectively. These values represented increases of 11%, 37%, and 36% compared to the control. Zeolite adsorption was employed to mitigate the inhibition of toxic compounds (i.e., ammonia, N-heterocyclic compounds, etc.) found in HTL-AP on the methane production and energy recovery of the AD process. The methane production increased by 32–117% compared with that without zeolite adsorption (Li et al., 2019). To summarize, the main objectives of these strategies are to minimize cytotoxicity, improve biogas production efficiency, and ensure the safe and environmentally responsible management of HTL-AP. Furthermore, research has explored optimizing operational conditions and employing diverse feedstocks to adjust the composition of HTL-AP, thereby reducing its negative impact on subsequent biological processes (SundarRajan et al., 2021; Watson et al., 2020). These innovative methods progress the integrated AD and HTL systems toward achieving a more sustainable and circular bioeconomy (Li et al., 2019; Quispe-Arpasi et al., 2018; Zheng et al., 2017). To assess the feasibility of integrating AD and HTL, it is essential to consider both the prospects and challenges of the integrated schemes.

**Table 2.5:** An overview of studies investigating the different pretreatment methods of HTL-AP and their impact on the subsequent AD process.

| Feedstock for HTL | HTL Conditions | Pre-treatment of HTL-AP | Anaerobic digestion conditions | Methane yield (mL/g COD) | Outcomes | Reference |
|---|---|---|---|---|---|---|
| *Spirulina* | 300 °C; 30 min | Zeolite adsorption: 2 g/L | 37 °C; Load: 5 g/L; Dilution: 15x | 227 | Increased methane production rate | (Zheng et al., 2017) |
| *Chlorella* | - | - | 37 °C; Co-digestion; Dilution: 5x | 14-244 | 30% of HTL-AP can be digested but chloride salts and nitrogen compounds exhibit inhibition effects | (Fernandez et al., 2018) |
| *Testraselmis* | - | - | 37 °C; Co-digestion; Dilution: 1.67-5x | 31–133 | 30% of HTL-AP can be digested but chloride salts and nitrogen compounds exhibit inhibition effects | (Fernandez et al., 2018) |
| *Nannochloropsis* | 320 °C; 30 min | Struvite recovery | 37 °C; Load: 1 g/L; Dilution: 97x | 182 | Greater methane yield with less lag phase | (Shakya et al., 2017) |
| *Nannochloropsis* | 320 °C; 30 min | Glacial acetic acid: 30% | 37 °C; Load: 1 g/L; Dilution: 97x | 84 | Greater methane yield with less lag phase | (Shanmugam et al., 2017) |
| Corn straw | 260 °C; 10 min | - | 37 °C; Load: 8 g/L; Dilution: 5x | 156 | Degradation of furan and nitrogen compounds to a greater extent | (Si et al., 2018) |

| | | | | | | |
|---|---|---|---|---|---|---|
| Sewage sludge | 170-320 °C; 30 min | - | 37 °C; Load: 0.75 g/L | 136-286 | HTL-AP retention time inversely proportional to methane yield | (Chen et al., 2019c) |
| Swine manure | 270 °C; 60 min | Glacial acetic acid: 20 g/L | 37 °C; Load: 20 g/L; Dilution: 2x | 212 | Increase in methane production rate and yield with less lag phase | (Si et al., 2019) |
| Swine manure | - | Acetic acid: 2 g/L | 37 °C; Load: 13 g/L; Dilution: 30x | 150–175 | Increased methane production rate with a lower lag phase | (Zhou et al., 2015) |
| Dewatered sewage sludge mixture | 220 °C; 3h | Struvite precipitation | 36 °C | 2247 | Methane yield increased by 38% | (Mao et al., 2021) |
| Wastewater sludge | 325 °C; 30 min | Struvite precipitation and biochar detoxification | 35 °C; maintained pH at 7.0 | 225 | Methane production rate increased by 90% | (Wang et al., 2021) |
| *Chlorella* 1067 | 300 °C; 30 min | Zeolite adsorption | 35 °C; Load: 2-5 g/L | 10.70–14.79 mmol/(g COD) | The lag phase shortened, and methane yield increased by 32–117% | (Li et al., 2019) |
| Rice straw | 270 °C; 30 min | Adsorption by modified commercially purchased resin | - | - | Adsorption of phenolic compounds increased by 1.5 times | (Chen et al., 2015) |
| Swine manure | 270 °C; 60 min | GAC adsorption: 20 g/L GAC | 37 °C; Load: 10 g/L | 228 | Shorter lag phase and method production increased by 67.7% | (Yang et al., 2018) |

| | | | | | | |
|---|---|---|---|---|---|---|
| Swine manure | 270 °C; 60 min | Ozone pre-treatment: 2.1 mg O3/ mL HTL-AP | 37 °C; Load: 10 g/L | 187 | Methane yield increased by 37.5% | (Yang et al., 2018) |
| *Spirulina* | 300 °C; 30 min | Oxidation pre-treatment | 37 °C | 4.60-5.31 mmol/(g COD) | Reduction in N-heterocyclic compounds led to an increase in higher methane yield | (Quispe-Arpasi et al., 2018) |

HTL-AP, hydrothermal liquefaction aqueous phase; GAC, granular activated carbon

## 2.6 Prospects and Challenges

This section examines the benefits, challenges, and meta-analysis of integrated AD-HTL and HTL-AD systems. The integration of AD with HTL using different sequencing methods holds great promise in addressing the challenges of waste management, energy sustainability, and resource recovery. Each sequential configuration, such as AD followed by HTL or HTL followed by AD, has shown distinct and noteworthy benefits that contribute to the overall efficiency and performance of the integrated process.

The sequential combination of HTL followed by AD offers several advantages. Firstly, HTL is particularly beneficial for challenging biomass feedstocks like lignocellulosic biomass, which can be difficult to effectively digest in AD due to its agglomerated structure. HTL acts as a pre-treatment method, breaking down the complex structure of these materials and making them more accessible for microbial degradation in AD. This enhances the overall digestibility and efficiency of the process (Mao et al., 2021). Secondly, HTL has the capability to convert a larger portion of biomass into biocrude oil, which serves as an energy-dense fuel. The production of biocrude oil through HTL provides an additional energy stream that can be utilized effectively, reducing reliance on traditional fossil fuels and promoting sustainability (Baloch et al., 2018). Furthermore, the subsequent AD stage in the sequence allows for the efficient utilization of residual organic matter present in the aqueous phase (Watson et al., 2020).

On the other hand, AD followed by HTL also offers several advantages in the biomass-to-energy conversion process. Firstly, the HTL stage in this sequence plays a crucial role in maximizing the energy yield by converting the remaining organic fraction into biocrude. This biocrude serves as a valuable energy resource, enhancing overall energy recovery and contributing to waste valorization (Kassem et al., 2020b). Secondly, the management and disposal of digestate resulting from organic waste can pose significant challenges. However, integrating HTL as a post-treatment step effectively mitigates this issue. HTL helps divert organic waste from landfills, thereby reducing nitrous oxide emissions and land pollution. Additionally, it transforms digestate into valuable products, providing a viable solution for its handling and disposal (Cabrera et al., 2021; Eboibi et al., 2015). Furthermore, employing HTL as a post-treatment provides an opportunity to recover additional nutrients from the digestate. This process enables the production of biocrude and other valuable byproducts, promoting resource recovery and enhancing the overall sustainability of the system (Kassem et al., 2020a; Kassem et al., 2020b). Moreover, a notable advantage of this process lies in the potential for retrofitting numerous existing commercial AD plants to incorporate HTL. In contrast, the HTL followed by the AD process is characterized by new technologies.

In a study conducted by Cabrera et al. (2023), the focus was on energy recovery from sequential configurations for sewage sludge management. The anaerobic digestion (AD) process occurred under mesophilic conditions, while HTL was conducted at 350°C for 30 minutes. The feedstock utilized was waste activated sludge, recognized for its recalcitrant compounds. By conducting energy calculations based on biomethane and biocrude, it was determined that the HTL-AD configuration achieved a remarkable 78% energy recovery, surpassing the 69% achieved by the AD-HTL system. These findings underscore the superior energy recovery potential of the HTL-AD system compared to its AD-HTL counterpart. The observed discrepancy in energy recovery between the two configurations can be attributed to the presence of inhibitory compounds in the feedstock, leading to reduced methane yield during the AD process. This highlights the importance of considering process sequencing and feedstock characteristics in optimizing energy recovery from sewage sludge management systems.

While the sequential configurations of HTL and AD present promising opportunities for waste treatment, energy generation, and resource recovery, there are certain challenges that need to be addressed in order to fully harness their potential in various waste management applications. One of the key concerns is the application of HTL products, particularly the biocrude oil obtained from the HTL process of biomass. Although biocrude oil is a highly desirable product, it contains higher concentrations of nitrogen (N) and oxygen (O) elements as well as water in comparison to petroleum crude oil. As a result, the upgradation of biocrude oil is essential to making it suitable for use as a transportation fuel. However, developing a cost-effective upgradation process for biocrude oil poses several hurdles, starting with the significant capital investment required for the HTL process itself. Addressing these challenges and finding efficient upgradation methods for biocrude oil are crucial steps in realizing its full potential as a viable transportation fuel (Baloch et al., 2018; Ramirez et al., 2015; Zhang et al., 2019a).

Furthermore, hydrochar, a valuable byproduct of HTL, offers the potential to enhance soil quality and support sustainable agriculture practices. As a soil amendment, hydrochar releases nutrients gradually, facilitating optimal plant growth and contributing to carbon sequestration efforts (Dieguez-Alonso et al., 2018; Islam et al., 2021). However, it is crucial to consider the potential toxicity associated with dissolved organic matter (DOM) derived from hydrochar. Studies have revealed inhibitory effects on bacterial growth, indicating the need for cautious handling and application of hydrochar. Notably, the toxicity of hydrochar is influenced by the operating temperature during HTL, with higher temperatures correlating to increased toxicity (Hao et al., 2018). Therefore, careful evaluation, monitoring, and potential detoxification techniques are necessary to ensure the environmentally responsible use of hydrochar in various applications. However, a few studies suggested that hydrochar can be effectively utilized as a conductive additive for enhancing AD, where hydrochar can provide a pathway for direct electron exchange between bacteria and methanogens (Ren et al., 2020; Usman et al., 2020). Furthermore, hydrochar can be used as solid fuel or as low-cost adsorbents for various environmental applications (Fang et al., 2018).

The strategic approach for optimizing organic waste valorization is depicted in **Figure 2.4**. In the HTL-AD configuration, the produced biocrude can be refined into transportation fuel through hydrotreating and distillation, while the resulting hydrochar finds utility as a soil amendment, adsorbent, and/or conductive additive for AD. Furthermore, struvite precipitation in HTL-AP allows for the recovery of struvite, serving as a valuable biofertilizer. Prior to AD, pretreatment steps are implemented to eliminate inhibitory compounds. Upgrading the biogas generated from AD to renewable natural gas (RNG) enhances its applicability for heat or electricity generation. The digestate obtained from AD serves dual purposes as a soil amendment and a feedstock for HTL. In the AD-HTL configuration, the utilization of biocrude, hydrochar, and biogas aligns with the previously outlined configuration. The HTL-AP, post struvite precipitation and toxic removal, can be amalgamated with the AD feedstock, providing a streamlined approach for maximizing organic waste valorization.

Techno-economic analysis (TEA) and life cycle assessment (LCA) of the integration of AD and HTL are crucial tools for evaluating the economic feasibility, environmental impacts, and overall sustainability of such integrated processes. TEA and LCA for this integrated system depend on several factors, including process efficiency, capital and operating costs, economic viability, product quality, market dynamics, regulatory compliance, and, most importantly, technological risks.

To date, there has been limited research published on the TEA and LCA of integrated AD and HTL systems. The proposed AD-HTL system, an extension of existing AD plants, has attracted significant interest among researchers, particularly regarding its TEA and LCA implications. In a recent study by Kassem et al. (2020), the TEA of AD-HTL systems for cow manure waste management was investigated. The experimental conditions chosen for AD are mesophilic with an HRT of 20 days, while HTL conditions were set at 300°C for 60 minutes. The study also examined the incorporation of a biomethanation unit aimed at converting carbon dioxide generated during both processes into renewable natural gas using hydrogen generated from renewable sources. Notably, the findings emphasized the critical role of the electricity selling price in determining the economic viability of this system. Furthermore, HTL operation and maintenance costs account for 23% of the total operation and maintenance costs due to the high temperature, pressure operating conditions, and residence time. Additionally, it was suggested that co-digestion with other waste streams could further enhance the system's economic incentives, potentially bolstered by government support. The integration of AD and HTL technologies presents promising avenues for managing waste sustainably and producing renewable energy. Further research and analysis in the TEA and LCA domains are essential for elucidating the full potential and feasibility of such integrated systems.

Kassem et al. (2020b) also conducted another study on the AD-HTL system, integrating the High-Rate Anaerobic Digestion (HRAD) system for the biological degradation of HTL-AP in cow manure waste management. The operating conditions for AD included mesophilic conditions with a solid retention time (SRT) of 15-25 days, while HTL was conducted at 300°C for 60 minutes. For HRAD, an SRT of 8 days was selected. The study highlights the dependence of economic feasibility on various factors, including electricity and co-product selling prices, system scale, project lifetime, and financial parameters. Notably, the electricity selling price and discount rate emerge as the primary determinants of economic viability. Increasing the electricity selling price significantly improves the project's net present value (NPV), while factors such as system scale and government support moderately enhance project economics.

Considering process efficiency and product quality is crucial because both processes of the integrated system depend on feedstock and operating conditions. Assessing the efficiency and yield of processes to convert feedstock into products like biogas, biocrude, and other valuable products is essential for economic performance. Furthermore, evaluating the quality of these products is important, as biogas and biocrude need upgrading to be used as renewable natural gas and biofuel, respectively. The cost of upgrading becomes a major factor in considering process feasibility, accounting for both capital and operating costs.

Moreover, the energy required for the HTL process, including heating and pressurization, can be a significant component of operating costs. Rising energy prices or process inefficiencies may increase operating expenses. Additionally, new or innovative technologies, such as HTL, may carry uncertainties and technical risks. If the technology does not perform as expected or encounters unforeseen challenges during implementation, it can lead to cost overruns and delays.

Skilled personnel will be required to operate and maintain the HTL facility. Also, market conditions for bio-based products, like bio-oil produced through HTL, can be unpredictable. Fluctuations in market demand and product prices can affect the economic viability of this integrated system. Lastly, meeting environmental and safety regulations may necessitate additional investments in monitoring equipment, emissions control systems, and compliance measures, contributing to both capital and operating expenses.

**Figure 2.5** summarizes the factors influencing the integration of AD and HTL in both sequential configurations. The figure highlights key variables such as process efficiency, resource utilization, and technological compatibility. Understanding these factors is crucial for optimizing the integration process and achieving maximum synergies between AD and HTL technologies. This figure also highlights which configuration (AD-HTL or HTL-AD system) may yield superior results depending on various contextual factors. Understanding these nuances is pivotal for selecting the most suitable integration approach for optimal performance. By discerning the advantages and limitations of each configuration, stakeholders can make informed decisions to enhance overall process efficiency and resource utilization. Such insights pave the way for more effective implementation strategies and sustainable outcomes.

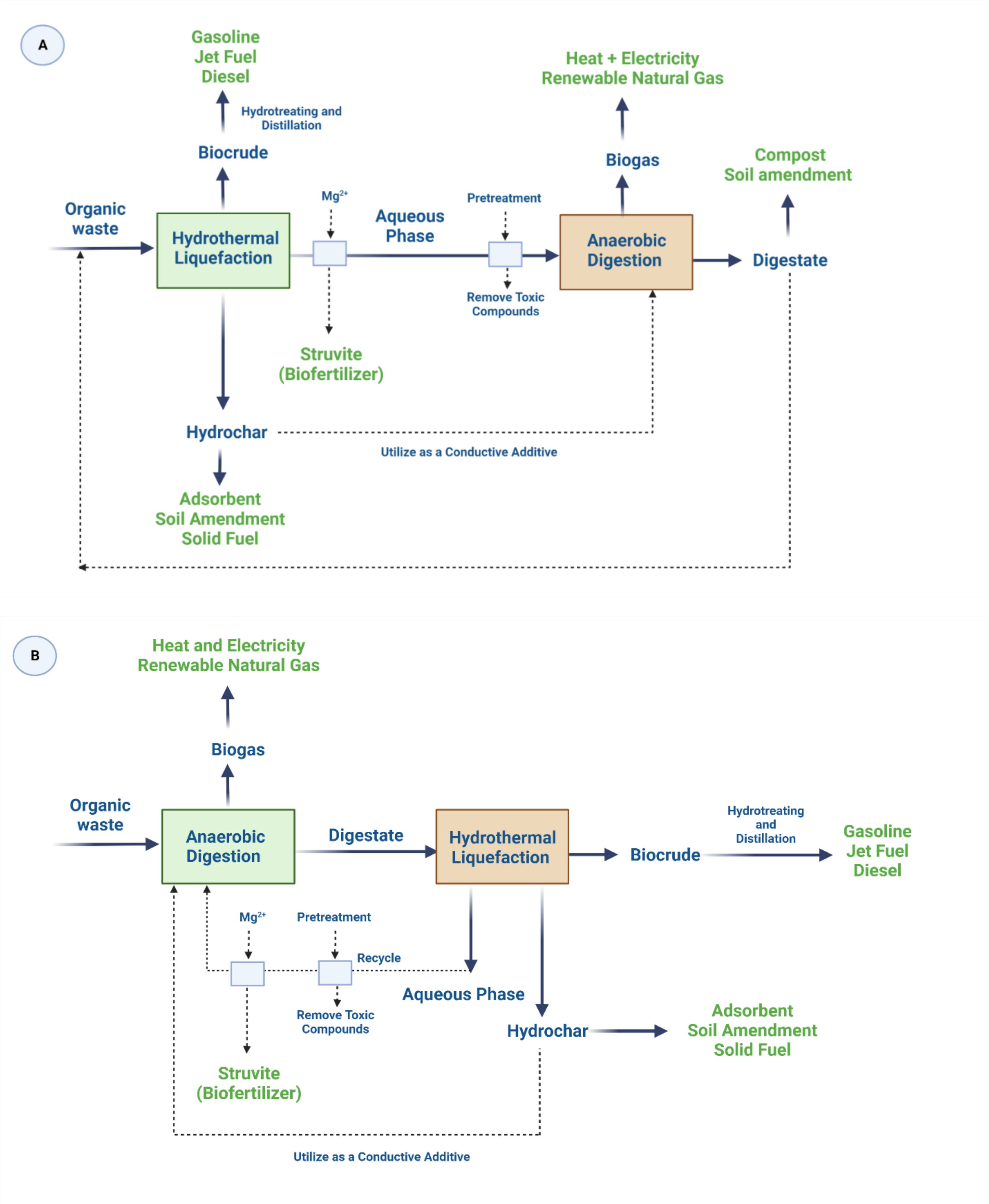

**Figure 2.4:** Strategies for maximizing organic waste valorization in (A) HTL followed by AD, and (B) AD followed by HTL.

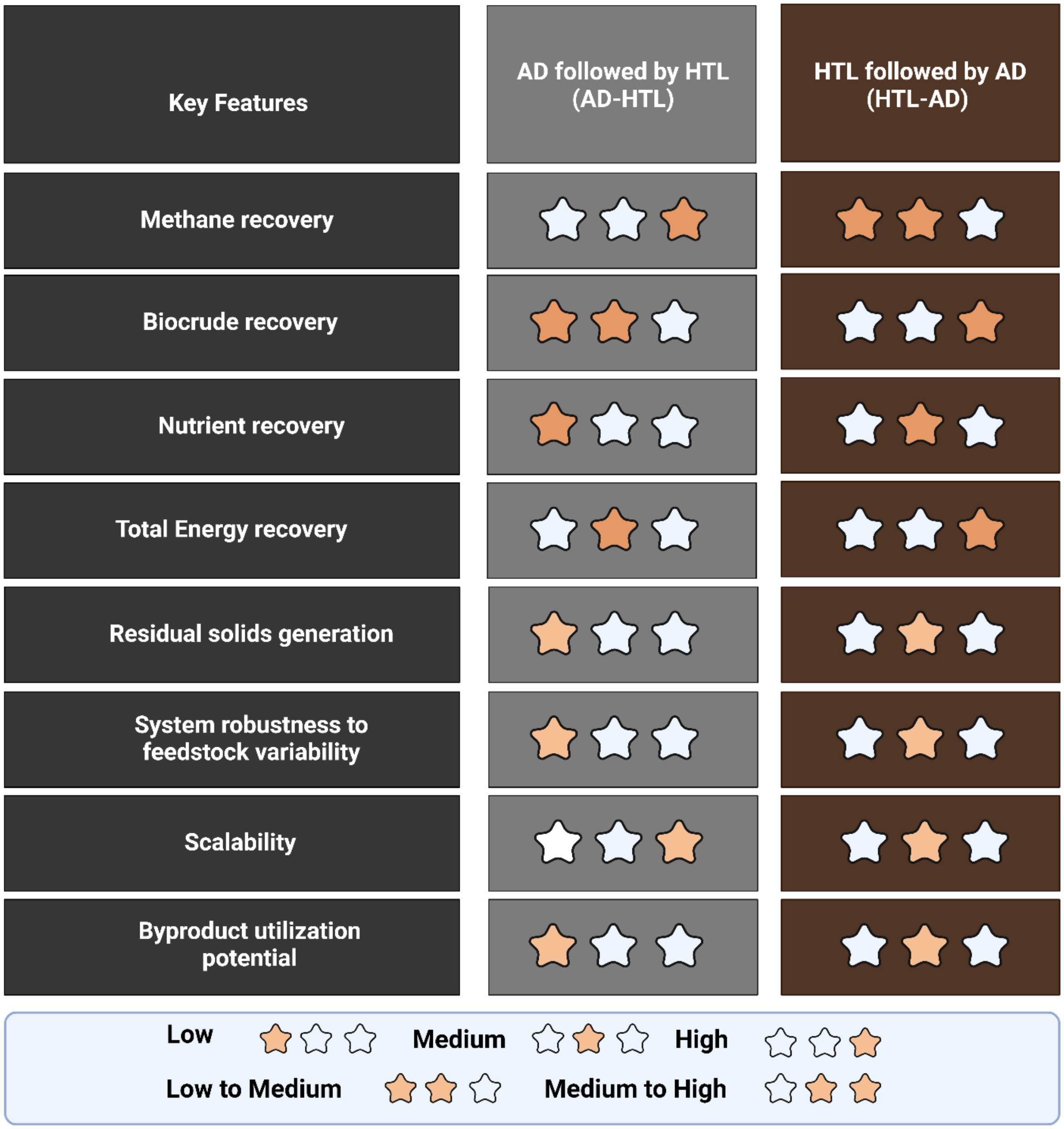

| Key Features | AD followed by HTL (AD-HTL) | HTL followed by AD (HTL-AD) |
|---|---|---|
| Methane recovery | ☆☆★ | ★★☆ |
| Biocrude recovery | ★★☆ | ☆☆★ |
| Nutrient recovery | ★☆☆ | ☆★☆ |
| Total Energy recovery | ☆★☆ | ☆☆★ |
| Residual solids generation | ★☆☆ | ☆★☆ |
| System robustness to feedstock variability | ★☆☆ | ☆★☆ |
| Scalability | ☆☆★ | ☆★☆ |
| Byproduct utilization potential | ★☆☆ | ☆★☆ |

Low ★☆☆ Medium ☆★☆ High ☆☆★

Low to Medium ★★☆ Medium to High ☆★★

**Figure 2.5:** Summary of impact of crucial factors on AD followed by HTL and HTL followed by AD configurations.

## 2.7 Conclusion

The integration of AD and HTL with different sequencing holds the promise of significantly enhancing sustainability and promoting circular economy practices within the realm of waste management. Throughout this comprehensive review, in the sequencing of HTL followed by AD, the introduction of a pre-treatment on HTL-AP has been identified as a key factor in unleashing the untapped potential of recalcitrant compounds, accentuating the efficacy of this approach. Conversely, the alternative strategy of AD followed by HTL, with a focus on applying HTL to AD- derived digestate and integrating catalysts to stimulate biocrude production, unveils a promising avenue for resource recovery and valorization. Numerous studies have underscored the superior performance of the HTL-AD system in terms of energy and resource recovery. Concurrently, researchers have recognized the scalability advantage of the AD-HTL system, which seamlessly integrates HTL technology into existing AD plants. However, despite these acknowledgments, a critical gap persists in identifying the optimal system configuration tailored to specific operating conditions and feedstock characteristics. This underscored gap underscores the imperative for further research to precisely delineate the most effective system configuration. Therefore, conducting comparative analyses (HTL followed by AD vs. AD followed by HTL) is essential to provide the necessary guidance for optimizing these systems. Looking ahead, future research should prioritize the execution of comprehensive life cycle assessments and techno-economic analyses of these integrated systems. This approach will allow for a systematic evaluation of their feasibility and environmental impacts. The implications extend far beyond waste management, potentially reducing the carbon footprint and driving sustainable practices. The outcomes of such research are poised to influence policy decisions and industry practices for years to come.

# Chapter 3

# A Comprehensive Assessment of Integrating Anaerobic Digestion and Hydrothermal Liquefaction Processes: Harnessing Energy from Sewage Sludge

*A version of this chapter is submitted in a journal for peer-review and publication.*

## 3.1 Introduction

Fossil fuels have powered modern society, but at the same time, they also contribute to several environmental challenges. Continued dominance by fossil fuels would only imply severe environmental consequences, raising a dire need to explore sustainable alternatives. Currently, much attention has been focused on renewable and sustainable energy sources, and organic waste streams receive considerable attention because of their promising conversion potential into energy carriers. Sewage sludge is one of the most promising organically rich semi-solid waste generated in the wastewater treatment process. (Crini & Lichtfouse, 2018).

So far, various promising technologies that might convert the organic fractions of sewage sludge into various renewable fuels through biochemical and thermochemical methods are being developed (Cieślik et al., 2015). These techniques bring about a comprehensive view of dealing with sludge in a very workable manner: changing what was considered waste into a resource (Piadeh et al., 2024). For instance, anaerobic digestion (AD) is an established biochemical process in which organic matter is subjected to microbial activities in absence of oxygen to produce biogas, a methane-rich biofuel (Awasthi et al., 2021; Xu et al., 2018b). In terms of waste management, there is a whole list of AD's advantages. First of all, it minimizes the amount of organic waste by a greater extent and reduces reliance on landfills. Biogas can be utilized for combined heat and power generation or upgraded to renewable natural gas, hence offering a clean source of energy (Awasthi et al., 2021; Sawatdeenarunat et al., 2015). The process also produces a nutrient-rich digestate consisting of solid-liquid fraction of the biomass that can be used as an excellent fertilizer further reducing reliance on chemical fertilizers (Kiyasudeen S et al., 2016). There are, however, some disadvantages to AD. One of the main challenges is digestate management and disposal. While this might be highly valued as fertilizer, the actual composition depends on the feedstock used in the AD process. This variability within the digestate therefore calls for careful analysis and possibly treatment of the digestate prior to agricultural application to avoid the introduction of contaminants or pathogens to the soil (Kamali et al., 2016; Nkoa, 2013; Samoraj et al., 2022). In addition, the large volumes of digestate may pose logistics difficulties in transportation and storage and hence require some management strategies (Jasińska et al., 2023).

Present research and development works focus on optimization of more efficient digestate management practices. Thermochemical methods further utilize the residual organic carbon in the digestate. At the forefront of thermochemical processes, hydrothermal liquefaction (HTL) has yielded such great interest in recent research on its huge potential to convert wet organic feedstock into biocrude and other co-products (Tatla et al., 2024). HTL operates at temperature range of 250 to 375 °C and pressurized to 4-25 MPa. The obtained biocrude can be further upgraded to either biofuels or chemicals, and hence can constitute a very promising source of renewable energy (Elliott et al., 2015). Besides the biocrude, the hydrothermal liquefaction process generates an aqueous phase, HTL-AP, containing organic carbon and dissolved minerals. Its composition depends on operating conditions and feedstock characteristics. The presence of organic compounds in the HTL-AP makes it a suitable substrate for the AD process. Therefore, the integration of AD into thermochemical processes can be optimized for organic waste resource potential, minimizing waste generation while providing more added sustainability to waste management systems (Eboibi et al., 2015; Vardon et al., 2011).

The integration of AD with HTL thus provides a complementary waste management system in which the limitation of one process is overcome by the other. Though AD is very efficient in degrading easily biodegradable matter, it faces problems concerning the management of complex feedstocks and their digestate. These are quite effectively complemented by HTL, as it easily converts complex materials and digestate into biocrude. The aqueous phase that remains after HTL becomes an excellent feedstock for AD, allowing for maximum biomethane production. This integrated valorization of waste into valuable biocrude and biogas is accompanied by the production of potentially fertilizable digestate and hydrochar. This helps diminish landfills and chemical fertilizers. Finally, it closes a loop within a waste management system with more circularity and sustainability (Li et al., 2019; Li et al., 2022; Posmanik et al., 2017b). Most of the research has been done on energy recovery from either standalone AD followed by HTL or standalone HTL followed by AD (Cabrera et al., 2023; Li et al., 2019; Posmanik et al., 2017b; Vardon et al., 2011). However, there is no systematic comparison done for the energy recoveries under identical operating conditions and using the same feedstock for both integrated sequences. This tends to be one of the research gaps that will impede carrying out such a study in the quest of maximizing energy recovery from sewage sludge. Therefore, the current work has comprehensively analyzed an integrated scheme focusing on HTL products distribution and its characteristics, biomethane production, digestate quality, and energy recovery. The present study is expected to perform a systematic comparison of the two approaches with the purpose of informing the development of a more robust and efficient strategy related to energy recovery from sewage sludge treatment.

## 3.2 Materials and Methods

### *3.2.1 Feedstock and inoculum characterization*

The feedstock, primary sludge (PS), was collected from a local Edmonton wastewater treatment plant in Alberta, Canada. The PS was stored in a cold room at 4°C until it was needed to perform the experimental procedures. On the other hand, the inoculum (anaerobic digested sludge) was also collected from the same treatment plant before the start of the AD experiments and kept in a cold room at 4°C. The composition of the inoculum is described in **Table S1**. The inoculum was first acclimated at 37°C for 7 days to activate the microbial communities and reduce possible biogas production from the degradation of residual organics prior to the AD experiment. The proximate analysis of the PS showed that total solids (TS), volatile solids (VS), and ash contents were 1.749 ± 0.02%, 1.166 ± 0.01%, and 33.334 ± 0.11%, respectively on a dry basis. The ultimate analysis provided the elemental composition of PS, namely nitrogen at 3.477 ± 0.09%, carbon at 36.511 ± 1.25%, hydrogen at 5.156 ± 0.20%, sulfur at 0.562 ± 0.01%, and oxygen at 20.960 ± 1.55% on a dry basis. The calculated higher heating value (HHV) for PS was 16.02 ± 0.99 MJ/kg, which reflected its energy content and continued to give support for it being used as a feedstock for such processes.

### *3.2.2 Experimental procedures*

This work presents two experimental scenarios that will contribute to the optimized treatment of PS, which is the feedstock for both HTL and AD. The two sequencing scenarios are: HTL followed by AD, depicted as Scheme 1 and AD followed by HTL, depicted as Scheme 2. In Scheme 1, PS is first treated via the HTL process to produce biocrude and hydrochar. Then, HTL-AP generated through the HTL process is fed into the AD system for processing. In contrast, Scheme 2 presents the direct feeding of PS into the AD process; the resulting digestate will be fed to the HTL system.

#### *3.2.2.1 Hydrothermal liquefaction*

For the HTL operation, a 250 mL batch hydrothermal reactor (Parr 4843, T-316 SS, Max. pressure: 5000 psi, Max. temperature: 500 °C, Parr Instruments Company, Moline, IL, USA) was utilized. The reactor was equipped with a thermocouple for temperature monitoring, a gas inlet for nitrogen purging, a gas outlet, a pressure gauge, and a cooling water system. A volume of 150 mL of feedstock was used in each HTL experiment. A flexible graphite gasket with a silver goop (an oil-based thread lubricant) was utilized for reactor sealing, and compression bolts on the Parr high-pressure vessel were then securely tightened using a socket wrench. It is nitrogen-purged three times at an exact pressure of 150 psi to attain an inert environment. There is leak checking through nitrogen purging at 200 psi, maintaining that pressure for 10 minutes. Mechanical stirring attached to an electric motor was used to ensure proper stirring of the feedstock. The reactor vessel was capped with a heater vessel to assure that the operational temperature could be reached (Chen et al., 2016; Li et al., 2022; Zheng et al., 2017). The experiments were carried out for two different feedstocks, i.e., PS presented in Scheme 1 and digestate obtained after AD in Scheme 2, in the temperature range of 250, 300, and 350 °C for each residence time of 30 and 60 min. Once the experiment was finished, the heating was switched off and the heating jacket was removed. Cold water was circulated in order to bring the reactor down to room temperature.

Then, after the experiment, the gas outlet of the reactor was connected to the gas bag to collect the gases produced for composition analysis. After opening the reactor, the solid–liquid mixture was vacuum filtered with the help of Whatman filter paper (Grade 2, diameter: 55 mm, pore size: 8 μm). The filtration process was done to separate the solid residue and the filtrate. The filtrate was named HTL-AP, refrigerated at 4 °C, and later analyzed. The entrapped oil is extracted from the solid residue by washing with acetone. This provides the acetone phase of this operation.

The reactor needs to be washed at least three times with acetone to extract the sticky materials adhered to its base. The obtained solid residue of such washing is recovered by vacuum filtration and the resulting solution was combined with the solvent phase. The obtained dried solid product was kept at 105 °C for 24 hours to be considered as hydrochar. Rotary evaporations were carried out under vacuum conditions to extract the biocrude in an acetone phase maintaining high pressure at about 556 mbar and 72 mbar at 40 °C to remove both acetone and water, respectively (Niknejad et al., 2023).

#### *3.2.2.2 Anaerobic digestion*

PS and HTL-AP, which is derived from the HTL of PS, were used as feedstock in the AD experiment. The batch reactor for the AD experiment was a 500 mL serum bottle with a working volume of 250 mL. The food-to-microorganism ratio (F/M) was maintained at 2 for both sets of AD experiments based on VS content. The bottles were fitted with a mechanical mixer and an electrical motor which allowed the continuous stirring of the solution at 200 rpm throughout the experiment.

Before initiating the experiments, nitrogen was purged into each reactor for about 3–5 minutes to maintain anaerobic conditions within the serum bottles. Subsequently, these digesters were placed in a water bath (20 L General Purpose Water Bath, PolyScience, Illinois, USA) set at a mesophilic temperature (37±2 °C). The stoppers were fitted with tubing, connecting them to individual bottles containing an absorption solution of 3 M NaOH solution with the addition of a pH indicator, thymolphthalein, to capture the acidic gases such as carbon dioxide and hydrogen sulfide present within the biogas. Each of the outlet pipes for the absorption solution bottles was connected to a 1 L gas bag via the tubing, through which biomethane gas could be collected. Daily measurements of methane gas volume were recorded using a glass syringe. Concurrently, blank bottles containing only inoculum underwent incubation to quantify the endogenous biogas generated (Hao et al., 2020; Mao et al., 2021; Zheng et al., 2017). This value was essential for subsequent subtraction from the experimental data at the conclusion of the experiment. Each AD test for each feedstock persisted until the cumulative biomethane yield curve reached a plateau. All experiments were conducted in triplicate. The digestate samples obtained after completing experiments were refrigerated at 4 °C until further analysis and experiments.

### *3.2.3 Calculations*

The yields of the products: biocrude, HTL-AP, or hydrochar, were determined on the basis of the weight of TS in each product in relation to the weight of TS, dry basis, in feedstock fed into the reactor. This was calculated by equation (3.1):

$$Y_i\,(\%) = \frac{TS_i}{TS_{Feedstock}} \times 100 \tag{3.1}$$

where $Y_i$ is the product yield (wt.%); $TS_i$ and $TS_{Feedstock}$ represents the total solids (g) of the product and feedstock fed into the HTL reactor, respectively (Cabrera et al., 2023).

The biomethane yield from PS and HTL-AP is calculated by using the following equation (3.2):

$$Y_{Methane}(\%) = \frac{Experimental\ methane\ production}{Theoretical\ methane\ production} \times 100 \tag{3.2}$$

The yield of gasses and volatiles produced during the HTL process under different operating conditions was determined by complementing the sum of the yields of the three other products yields (i.e., biocrude, HTL-AP, and hydrochar) to 100% (Cabrera et al., 2023; Li et al., 2022). The yield of volatiles was considered to account for compounds lost during the separation of HTL products, the drying process of biocrude and hydrochar, as well as losses occurring during sample transfers.

The elemental composition of PS, digestate, hydrochar, and biocrude was analyzed to determine the HHV. HHV was estimated using Dulong's formula with the equation (3.3):

$$HHV\left(\frac{MJ}{Kg}\right) = 0.338 \times C + 1.428\left(H - \frac{O}{8}\right) + 0.095 \times S \tag{3.3}$$

where C, H, O and S are the mass percentages of carbon, hydrogen, oxygen, and sulfur (% w/w), respectively (Niknejad et al., 2023).

The energy recovery from each product (i.e., biocrude, biomethane, and hydrochar) was computed using equation (3.4):

$$ER_i(\%) = \frac{Y_i \times HHV_i}{HHV_{Primary\ sludge}} \times 100 \tag{3.4}$$

where $ER_i$ represents the energy recovery, i donates the energy product (biocrude, biomethane, or hydrochar), $Y_i$ is the yield for each energy product ($wt_{Product}/\ wt_{PS}$), $HHV_i$ is the higher heating value of each energy product (MJ/kg), and $HHV_{Primary\ Sludge}$ is the higher heating value of the PS on a dry ash-free basis (MJ/kg). The HHV of biomethane is taken as 55.5 MJ/kg (Posmanik et al., 2017a; Cabrera et al., 2023).

### *3.2.4 Analytical methods*

TS, VS and ash content were measured using the standard methods. Chemical oxygen demand (COD) and total ammonia nitrogen (TAN) concentrations were determined using HACH reagent kits (HACH, Loveland, CO, USA) (Federation and Association, 2005). The CHNS analysis was made by Flash 2000 Organic Elemental Analyzer (Thermo Fisher, Cambridge, UK) for dried samples of PS, digestate, biocrude and hydrochar. The oxygen content was calculated by complementing the carbon, hydrogen, nitrogen, sulfur, and ash content to 100%. All the analyses were done in duplicates, and the mean values are reported here (Cabrera et al., 2023).

The chemical constituents of the biocrude were identified by GC-MS using an Agilent 6890 GC (Agilent, USA) coupled to a 5973-network mass spectrometer (Agilent, USA) and a HP-5MS (30 m x 0.25 mm, df = 0.25 microns) column. The samples were prepared using dichloromethane as a solvent. Subsequently, the mixture underwent micro-centrifugation, and the supernatant was filtered through a 0.2 μm PTFE filter. For GC analysis, 1 μL of the sample was injected in split mode (50:1) with a carrier gas (helium). The GC column heating was initiated at 40 °C for 2 minutes, and then, with a heating ramp of 10 °C/min, it reached up to 280 °C and was heated for 10 minutes. The NIST library for mass spectra was employed to identify probable compounds in each sample. FTIR spectroscopy (Nicolet 8700 FTIR spectrometer, Thermo Fisher, USA) was performed for each sample (i.e., PS, digestate, biocrude, aqueous phase, and hydrochar). Different functional groups associated with each sample were identified based on the wavenumber, referring to relevant literature. Gas chromatography (7890B, Agilent Technologies, Santa Clara, USA) equipped with a thermal conductivity detector (TCD) and two columns (Molsieve 5A 60/80 mesh and Hayesep N 80–100 mesh) was employed to analyze the composition of gasses generated during the HTL process (Niknejad et al., 2023).

### *3.2.5 Statistical analysis*

All the statistics are computed using the Microsoft Excel program. A paired Student's t-test was performed in Microsoft Excel to test for significant differences between experimental results.

For this study, a 95% confidence interval was used as the level of significance, represented as $p < 0.05$.

## 3.3 Results and Discussion

### *3.3.1 Hydrothermal liquefaction*

Results from HTL tests in Scheme 1 and Scheme 2 are discussed in detail in this section. In Scheme 1, PS is the feedstock for HTL, followed by AD, while in Scheme 2, HTL is applied to digestate, the product of the initial step of AD.

### *3.3.1.1 Product distribution*

**Figure 3.1** shows the distribution of different products produced during the HTL of PS and digestate (derived after AD of PS) under different operating conditions. The bio-crude yield, obtained during HTL of PS, lay in the range 18.9 to 40.7 wt.%, which is within the yield range reported in literature from 14.8 to 40 wt.%. (Cheikhwafa et al., 2024; Huang et al., 2013; Inoue et al., 1997; Malins et al., 2015; Prestigiacomo et al., 2021; Qian et al., 2017). In Scheme 2, biocrude yields from the HTL of digestate varied from 10.7 to 21.3 wt.%. Yields of biocrude from digestate varied across the literature from a minimum of 9.4 to a maximum of 44 wt.% (Vardon et al., 2011; Eboibi et al., 2015). The reason for these yield differences may relate to feedstock characteristics, operating conditions, and differences in the biocrude extraction methods (Dimitriadis & Bezergianni, 2017; Mathanker et al., 2021; Watson et al., 2019). The trend of the biocrude yield in both schemes significantly increased ($p < 0.05$) with increasing operating temperature and retention time, reaching its maximum at 300 °C for 60 minutes with yields of 40.7 wt.% (Scheme 1) and 21.3 wt.% (Scheme 2). A higher temperature increases the yield of biocrude due to the availability of more energy for bond breaking. Thus, the reaction rate of biomass hydrolysis and decomposition of volatile matter into biocrude was increased (Cheikhwafa et al., 2024). Beyond an optimum of 300 °C for the two schemes, further increases in temperature depressed the yield of biocrude due to thermal degradation that favored the formation of more gaseous products (Li et al., 2018). For example, in Scheme 1, increasing the temperature from 300 to 350 °C at a retention time of 30 minutes raised the gaseous yield from 46.5% to 56.6%, and at 60 minutes, from 28.5% to 47.9%. While in Scheme 2, increasing the temperature from 300 to 350 °C increased the gaseous yields from 30.0 to 43.6% at 30 minutes and from 26.4 to 45.5% within 60 minutes. Besides, there was an increase in the yield of biocrude with an increase in retention time, which means longer the retention time, higher the yields, as depicted in **Figure 3.1**. This finding may be attributed to the further degradation and hydrolysis of organics (Eboibi et al., 2014). In both schemes, the decline in HTL-AP yield with increased temperature and prolonged retention times at higher temperatures (>300 °C) can be ascribed to the direct transformation of dissolved organics within the aqueous phase into biocrude (Eboibi et al., 2014).

The hydrochar yield within Scheme 1 ranges between 24.4 and 32.4 wt.%, while in the case of Scheme 2, this ranged from 35.3 to 42.8 wt.%. For both schemes, increasing operating temperatures reduced the yield of hydrochar. This is due to the fact that increased temperatures will lead to higher rates of hydrolysis and decomposition reactions (Nakason et al., 2018). Variations in the effect of retention time on hydrochar yield in both schemes are illustrated in **Figure 3.1**. This could be due to the continuous polymerization of dissolved fragments in the aqueous phase, ultimately forming insoluble solids (Zhang et al., 2019b).

Yields of HTL-AP decreased, as the operating temperature was raised from 250 °C to 350 °C coupled with an increased retention time, due to the conversion of dissolved organics into biocrude or gases. On the other hand, gas yield increased with increased temperature in the range of 250 °C to 350 °C in both schemes because of the conversion of lighter hydrocarbons into gaseous products. However, changes in retention time did not have much impact on gas yield.

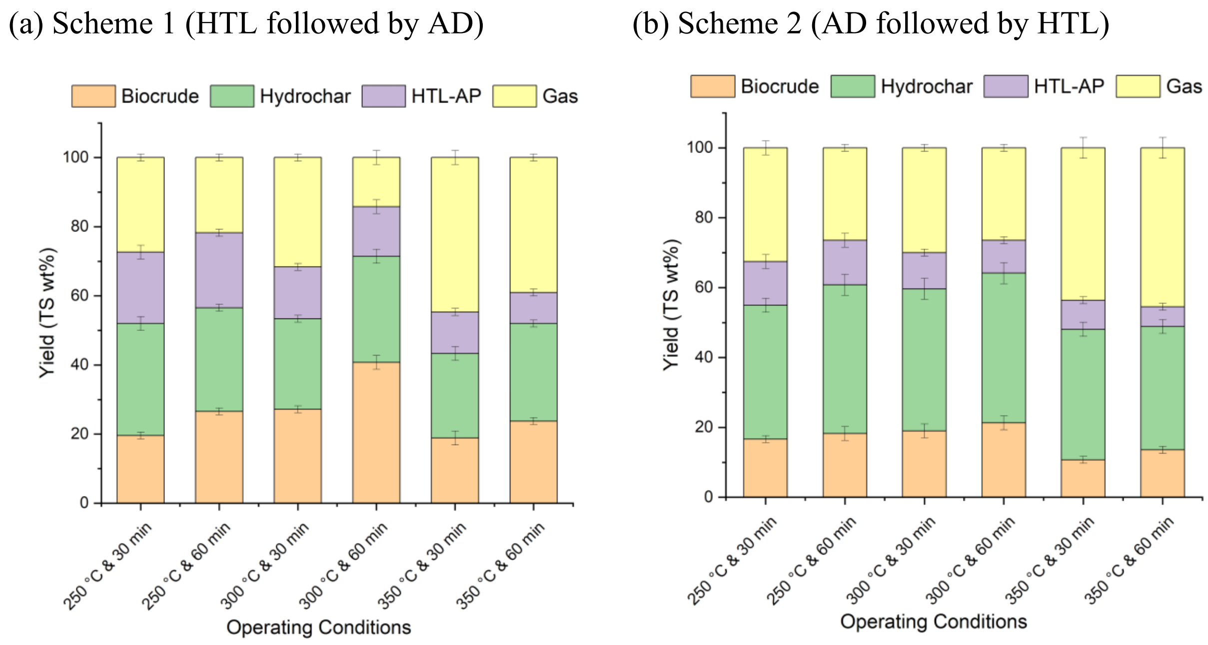

**Figure 3.1:** Variations in the yields of HTL byproducts at different operating temperatures and retention times for (a) Scheme 1 (HTL followed by AD) and (b) Scheme 2 (AD followed by HTL).

### *3.3.1.2 Biocrude characterization*

The HHV of the PS-derived biocrude was between 30.2-35.3 MJ/kg, while that of digestate was between 30.7 and 36.0 MJ/kg. The difference in values of HHV is due to the different operating conditions. The calculated HHV values of biocrude are consistent with values reported in literature (Anastasakis et al., 2018; Prestigiacomo et al., 2021; Vardon et al., 2011; Cabrera et al. 2023). It is observed that the biocrude from both schemes had higher energy density compared to their feedstock materials. However, there was no significant variation in the HHVs of the two schemes. This is mainly because the ash content was filtered off effectively under vacuum; thus, a higher carbon content resulted in relatively similar ranges of HHV values in both schemes (Cabrera et al., 2023). **Table 3.1** presents elemental composition of feedstocks and biocrudes obtained for both schemes under different operating conditions.

**Table 3.1:** Detailed characteristics of feedstocks and resulting biocrudes obtained from HTL under various operating conditions in both schemes.

| HTL Operating | Elemental Analysis (wt. %, dry basis) | Atomic Ratio | HHV (MJ/kg) |
|---|---|---|---|

| Conditions | N | C | H | S | O | H/C | O/C | |
|---|---|---|---|---|---|---|---|---|
| Scheme 1 (HTL followed by AD) | | | | | | | | |
| PS | 3.48 ± 0.09 | 36.51 ± 1.25 | 5.16 ± 0.20 | 0.56 ± 0.01 | 20.96 ± 1.55 | 1.7 ± 0.01 | 0.4 ± 0.05 | 16.02 ± 0.99 |
| 250°C & 30 min | 3.18 ± 0.09 | 65.62 ± 1.27 | 9.40 ± 0.02 | 0.55 ± 0.06 | 21.24 ± 1.21 | 1.7 ± 0.03 | 0.2 ± 0.02 | 31.9 ± 0.65 |
| 250°C & 60 min | 2.25 ± 0.04 | 67.01 ± 0.37 | 10.30 ± 0.05 | 0.87 ± 0.15 | 19.56 ± 0.31 | 1.8 ± 0.02 | 0.2 ± 0.01 | 33.9 ± 0.11 |
| 300°C & 30 min | 2.22 ± 0.07 | 65.87 ± 1.80 | 10.37 ± 0.12 | 0.62 ± 0.07 | 20.91 ± 1.81 | 1.9 ± 0.04 | 0.2 ± 0.03 | 33.4 ± 1.06 |
| 300°C & 60 min | 2.08 ± 0.02 | 59.96 ± 0.43 | 10.33 ± 0.06 | 0.51 ± 0.02 | 27.12 ± 0.44 | 2.1 ± 0.01 | 0.3 ± 0.01 | 30.2 ± 0.28 |
| 350°C & 30 min | 2.47 ± 0.03 | 71.85 ± 0.65 | 9.61 ± 0.05 | 0.58 ± 0.01 | 15.49 ± 0.66 | 1.6 ± 0.02 | 0.2 ± 0.01 | 35.3 ± 0.32 |
| 350°C & 60 min | 2.08 ± 0.01 | 68.59 ± 0.69 | 10.11 ± 0.05 | 0.66 ± 0.09 | 18.56 ± 0.72 | 1.8 ± 0.02 | 0.2 ± 0.01 | 34.4 ± 0.39 |
| Scheme 2 (AD followed by HTL) | | | | | | | | |
| Digestate | 3.40 ± 0.05 | 27.8 ± 0.57 | 3.80 ± 0.10 | 0.75 ± 0.05 | 14.48 ± 0.62 | 1.6 ± 0.02 | 0.4 ± 0.02 | 12.2 ± 0.44 |
| 250°C & 30 min | 3.78 ± 0.06 | 62.80 ± 1.86 | 9.35 ± 0.16 | 1.43 ± 0.09 | 22.65 ± 2.04 | 1.8 ± 0.02 | 0.3 ± 0.03 | 30.7 ± 1.22 |
| 250°C & 60 min | 5.06 ± 0.14 | 65.04 ± 1.05 | 9.41 ± 0.08 | 1.72 ± 0.20 | 18.78 ± 1.24 | 1.7 ± 0.01 | 0.2 ± 0.02 | 32.2 ± 0.70 |
| 300°C & 30 min | 3.78 ± 0.11 | 69.30 ± 0.37 | 9.38 ± 0.14 | 2.13 ± 0.02 | 15.42 ± 0.52 | 1.6 ± 0.02 | 0.2 ± 0.01 | 34.3 ± 0.35 |

| | | | | | | | | |
|---|---|---|---|---|---|---|---|---|
| 300°C & 60 min | 3.94 ± 0.02 | 71.66 ± 0.63 | 9.58 ± 0.06 | 1.57 ± 0.03 | 13.24 ± 0.67 | 1.6 ± 0.01 | 0.1 ± 0.01 | 35.7 ± 0.39 |
| 350°C & 30 min | 3.78 ± 0.17 | 73.34 ± 0.43 | 8.70 ± 0.06 | 1.58 ± 0.07 | 12.60 ± 0.49 | 1.4 ± 0.02 | 0.1 ± 0.01 | 35.1 ± 0.19 |
| 350°C & 60 min | 3.73 ± 0.07 | 75.72 ± 0.40 | 8.49 ± 0.08 | 1.40 ± 0.01 | 10.66 ± 0.41 | 1.3 ± 0.02 | 0.1 ± 0.01 | 36.0 ± 0.31 |

HTL: hydrothermal liquefaction; HHV: higher heating value; PS: primary sludge.

In Schemes 1 & 2, at a 30-minute retention time, the increase in temperature increased the carbon composition of the biocrude. This phenomenon occurred because of the breakdown of organic matter, with temperatures exceeding 250 °C required for the degradation of proteins and carbohydrates, while temperatures above 300 °C are necessary for lipid degradation (Fan et al., 2022). In Scheme 1, which utilized PS as a feedstock, extending the retention time at elevated temperatures (>300 °C) reduced carbon content within the resulting biocrude. This phenomenon may be attributed to thermal cracking processes within the biocrude, converting PS, known for its high content of easily degradable crude fat, into the gaseous phase during hydrothermal liquefaction (Akhtar & Amin, 2011). In Scheme 2, where digestate was the feedstock, a prolonged retention time at temperatures exceeding 300 °C exhibited the opposite effect, increasing the carbon content in the derived biocrude. This can be attributed to the higher content of less degradable organics in digestate than PS (SUZUKI et al., 1988).

The oxygen content of the biocrude from Scheme 1 ranged from 15.49 to 27.12%, while in Scheme 2, it varied from 10.66 to 22.65%. This result indicates that more intensive deoxygenation reactions were achieved through the HTL processing of Scheme 2 as compared with that of Scheme 1. Carbon dioxide and water as co-products of the HTL process facilitate the removal of oxygen. Both decarboxylation and dehydration reactions form carbon dioxide and water, respectively (Cabrera et al., 2023). In Scheme 1, at the initial stages, the H/C ratio was greater compared to feedstock and then started decreasing when the temperature reached up to 350 °C. Increasing retention time resulted in increasing the H/C ratio. In contrast, Scheme 2 showed a higher H/C ratio than that in the feedstock, but such a ratio was decreased with increasing temperature and longer retention time. The increase in the H/C ratio of biocrude, compared to the feedstock, could be attributed to the highly paraffinic nature of the biocrude formed from the HTL process (Castello et al., 2019). In Scheme 1, the increase in either temperature or retention time did not greatly affect the O/C ratio. For Scheme 2, increases in temperature and extension of the retention time resulted in a decreased O/C ratio. The reduction of the O/C ratio was greater than that of the H/C ratio, indicating that decarboxylation is the dominant oxygen removal route. This, therefore, gave rise to the improved H/C ratio of biocrude in Scheme 2.

In Scheme 1, the nitrogen content of the biocrude was within the range 2.08-3.18%, while for Scheme 2, the range of nitrogen content was within 3.73 and 5.06%. While there are minor differences, all the trends observed show relatively small magnitudes of discrepancy in nitrogen content in the biocrude samples derived under different operating conditions. This is because PS has a low protein composition, which results in a lower nitrogen content in the biocrude. On the other hand, digestate is richer in nitrogen than PS; this would explain the differences between the two schemes in terms of nitrogen content. In Scheme 1, retention time positively affected the biocrude composition: longer retention times increased the nitrogen concentration. For shorter retention times, the increase in temperature first lowered the nitrogen content and then continued to increase it from 350 °C. In Scheme 2, increasing the temperature at a 30-minute retention time has no significant effect on nitrogen composition. However, at a 60-minute retention time, the nitrogen content decreased with increasing operating temperature. The variations in nitrogen composition in biocrude are primarily due to isomerization, defragmentation/depolymerization, and condensation reactions of proteins during the hydrothermal liquefaction process (Jena et al., 2011). On the other hand, sulfur levels in the biocrude from Scheme 1 varied between 0.51 and 0.87%, whereas in Scheme 2, these levels were between 1.40 and 2.13%. These differences in sulfur content can be linked to varying sulfur concentrations in the feedstock and changes in operating conditions (Obeid et al., 2019). Typically, organic sulfur is predominantly recovered in the biocrude, whereas inorganic sulfur is recovered in the aqueous phase and hydrochar (Neveux et al., 2014).

While the elemental analyses provided a good overview of the energy content and quality of the biocrude, the GC-MS analyses enabled an exact insight into the chemical compounds present. These data are important to develop an interpretation of the biocrude in terms of its technical appropriateness for upgrading into transportation fuel. The identified chemical compounds by using GC-MS are listed in **Table S2** with their retention time and peak area percentage. In the analysis, all the compounds with less than 0.75% peak areas were excluded (Niknejad et al., 2023). Further, the identified compounds were characterized into their functional groups. **Figure 3.2** is a representation of the functional groups of the biocrude produced from the various feedstocks under different operating conditions.

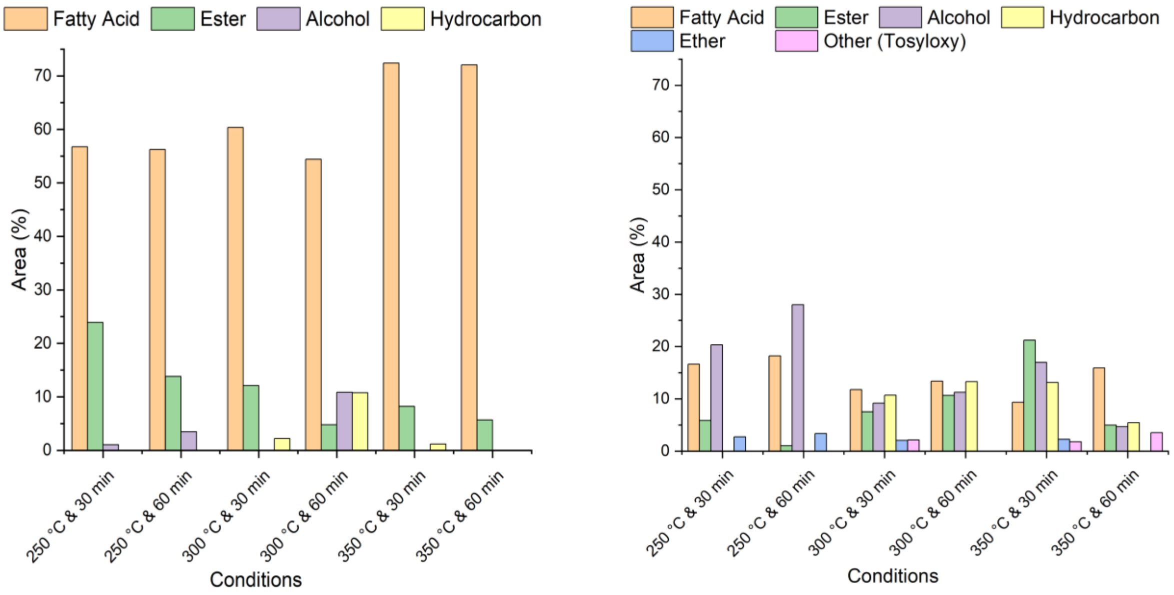

(a) Scheme 1 (HTL followed by AD)

(b) Scheme 2 (AD followed by HTL)

**Figure 3.2:** GC-MS analysis results for biocrude derived from (a) Scheme 1 (HTL followed by AD) and (b) Scheme 2 (AD followed by HTL).

PS is rich in total lipids, free fatty acids, and wax/gum besides having a high proportion of cellular lipids. This feature makes PS an appropriate raw material for the production of biofuel (Zhu et al., 2017). Thus, biocrude from both Scheme 1 and Scheme 2 had a high amount of fatty acids and its derivatives. Especially, biocrude obtained in Scheme 1, where PS was the direct feedstock for the HTL process, contained more fatty acids and derivatives than that from Scheme 2. Fatty acids, such as n-hexadecanoic acid, octadecanoic acid, oleic acid, and cis-vaccenic acid, result from the hydrolysis of lipids, which in turn allows a portion of these acids to be converted into long-chain alkanes via decarboxylation and hydrogenation processes (Wei et al., 2024). Some of the fatty acids are converted to alcohols by deoxygenation and then these alcohols are esterified with other fatty acids to form esters such as octadecyl hexadecanoate, hexadecyl hexadecanoate, tetradecyl hexadecanoate, and L-(+)-ascorbic acid 2,6-dihexadecanoate (Wei et al., 2024; Zhang & Zhang, 2014). The lignin fraction of the feedstock is used to produce ethers such as cholestane, 3-ethoxy-, (3.beta., 5.alpha.)- (Singh et al., 2014). Amides, such as hexadecanamide, pentanamide, and nonanamide, result from the condensation of fatty acids with amines, derived from proteins that undergo rapid decomposition via decarboxylation and deamination during the HTL process (Chiaberge et al., 2013; Palardy et al., 2017). The N-containing heterocyclic compounds, such as 4-(Methylthio)canthin-6-one, are prepared through the Maillard reaction. It is in this process that amino acids provided by proteins undergo a chemical reaction with reducing sugars from carbohydrates (Chen et al., 2014; Zhang et al., 2016).

In Scheme 1, the percentage of peak area of fatty acids with the increase in temperature from 56.8% to 72.4% while changing retention time did not have any significant effect on the proportion of peak area of the fatty acids. On the contrary, at 300 °C, percentage of peak area of fatty acids decreased from 60.4% to 54.4% as the retention time increased from 30 min to 60 min. This was followed by a sharp increase in the area percentage of alcohols from 0 to 10.9% and hydrocarbons from 2.2 to 10.8%, with retention time extended to 60 minutes. As the low nitrogen content was calculated in the elemental analysis, the expectation is that the peak area percentage of nitrogen-containing compounds is likely below 0.75%. Consequently, nitrogen-containing compounds were not detected in the biocrude derived from PS, except under operating conditions of 350 °C and 60 minutes. In scheme 2, the peak area percentage of fatty acids decreased from 16.7% to 9.4% as the temperature increased at a retention time of 30 minutes. Conversely, at a retention time of 60 minutes, there was an increase in the yield of fatty acids at each specific temperature. In line with Scheme 1, nitrogen-containing compounds were absent in the biocrude derived from digestate, except under an operating temperature of 250 °C and retention times of 30 and 60 minutes. At the operating conditions of 250 °C and 30 min, the peak area percentage of amides reached 16.3%. Under the same operating conditions, the N-containing heterocyclic compounds amounted to 3.9%. On the whole, GC-MS results illustrated that biocrude from both schemes had dominating contents of fatty acids and their derivatives, which implied the necessity of upgrading through further deoxygenation and denitrogenation processes (Castello et al., 2019).

The FTIR analysis of biocrude offers a more thorough comparison of functional group characteristics compared to GC-MS, providing spectral band assignments and interpretations based on prior research studies (Duan & Savage, 2010; Francioso et al., 2010; Lievens et al., 2011). **Figure S1** shows the FTIR results for biocrude of different HTL operating conditions for both schemes. In scheme 1, as evident from the GC - MS analysis, due to high percentage presence of fatty acids, a strong C=O stretch (1720 - 1700 cm-1) was observed (Vardon et al., 2011). **Table S3** represents a detailed breakdown of the identified functional groups for each FTIR spectrum. When analyzing the FTIR graphs, there was a consistent trend where increasing operating temperatures and retention times resulted in increasing peak intensities. The consistency of the trend observed indeed confirms the fact that with increasing temperature and retention period, more degradation is facilitated for volatile content in feedstocks. While at 250 °C, the variations of peak intensities were negligible over different retention times, at 300 °C, the variations became better and were even further amplified at 350 °C. Specifically, the peak intensities at temperatures between 300 °C and 350°C are much wider at 30 minutes as compared to those observed at a retention time of 60 minutes.

The peaks of functional groups as noted in the FTIR graphs of Scheme 2 were similar when compared with those that had been identified in the FTIR graphs of Scheme 1. However, the intensity of these peaks was very different whereby these were more intense in Scheme 2 than those which had been recorded in Scheme 1. This discrepancy may be attributed to the prior biological degradation of chemical compounds in Scheme 2, resulting in an accelerated rate of reaction during the HTL process, in contrast to the feedstock in Scheme 1. At temperatures of 250 °C and 300 °C, an increase in retention time from 30 to 60 minutes corresponded to a rise in peak intensities. On the other hand, at a temperature of 350 °C, increasing the retention time from 30 to 60 minutes reduced the peak intensities, which may be due to increased degradation of functional groups into the formation of other co-products at longer retention times. Moreover, for a retention time of 30 minutes, peak intensities have not varied much upon increasing the temperature from 250 °C to 300 °C. However, with a temperature increase up to 350 °C, the peak intensities had an obvious increase. At the retention time of 60 minutes, the peak intensities for 300 °C were much higher compared with 250 °C, while on further increasing the temperature up to 350 °C, the peak intensities decreased down to values even below those for 250 °C.

#### *3.3.1.3 Characterization of aqueous phase*

The COD of the aqueous phase, as obtained from the HTL process of PS (Scheme 1) and digestate (Scheme 2), is presented in **Table 3.2**. For Scheme 1, the COD range within different operating conditions of HTL was from 12,299 to 14,728 mg/L. On the contrary, for Scheme 2, different HTL operating conditions showed COD range between 7,650 and 9,161 mg/L. Indeed, for temperatures greater than 250 °C, the COD of the aqueous phase in both schemes has fallen substantially with time, indicating further conversion of water-soluble organics to gaseous products, biocrude, and/or hydrochar (Gai et al., 2015). It is further reflected in the increase in the yield of biocrude and gaseous products with increasing temperature. However, in both schemes, no significant variation was seen in COD with respect to changes in retention time.

Protein hydrolysis releases amino acids, which could be deaminated and decarboxylated further. Ammonia is formed from deamination, while water-soluble amino acid derivatives are formed from decarboxylation (Fan et al., 2022). All these nitrogenous compounds contribute together to total ammonia- nitrogen (TAN) content. In addition, TAN concentration profiles exhibited the same trends for both schemes. TAN concentration increased with the increase in temperature up to 300 °C, beyond which it decreased at higher temperatures. With the lower temperatures, like 250 °C and 300 °C, long retention times gave rise to higher TAN concentrations. This probably took place owing to the enhancement effect on the deamination reactions, which, in turn, would convert amine and amide compounds involved in the biocrude to ammonia that dissolved in the HTL-AP (Shakya et al., 2015). However, an increase in temperatures up to 350 °C was followed by a decrease in TAN concentration with increasing retention times. This suggests that, under high-temperature conditions, nitrogen may be preferably retained within the biocrude, resulting in reduced TAN levels in HTL-AP (Gai et al., 2015).

**Table 3.2:** COD and TAN concentrations of HTL-AP generated from (a) Scheme 1 (HTL followed by AD) and (b) Scheme 2 (AD followed by HTL).

| Experimental Conditions | Primary Sludge (Scheme 1) | | Digestate (Scheme 2) | |
|---|---|---|---|---|
| | COD (mg/L) | TAN (mg/L) | COD (mg/L) | TAN (mg/L) |

| | | | | |
|---|---|---|---|---|
| 250 °C & 30 min | 14510 ± 14 | 427 ± 5 | 9025 ± 10 | 862 ± 11 |
| 250 °C & 60 min | 14728 ± 13 | 470 ± 4 | 9161 ± 19 | 886 ± 10 |
| 300 °C & 30 min | 13567 ± 25 | 560 ± 3 | 8439 ± 13 | 911 ± 9 |
| 300 °C & 60 min | 13253 ± 35 | 564 ± 12 | 8244 ± 23 | 927 ± 2 |
| 350 °C & 30 min | 12532 ± 28 | 473 ± 10 | 7795 ± 21 | 836 ± 1 |
| 350 °C & 60 min | 12299 ± 11 | 454 ± 8 | 7650 ± 16 | 827 ± 3 |

FTIR analysis was performed on HTL-AP samples to have a comprehensive insight into the molecular behavior in water by understanding the nature of solute-solvent interactions and the structural dynamics of the molecules in the aqueous phase. **Figure S2** presents the FTIR spectra for the HTL-AP of different HTL operating conditions for both schemes. Organic acids, which are the major components of the produced aqueous phase, were generated through various paths. First, high temperature and pressure during HTL make proteins break into their constituent amino acids by hydrolysis reactions. The amino acids undergo subsequent deamination reactions where an amine group is removed; thus organic acids are released along with ammonia (Watson et al., 2019). HTL facilitates the hydrolysis of lipids, among which the most common one is triglycerides in biomass feedstock. The hydrolysis reaction of triglycerides gives glycerol and free fatty acids. These organic acids add to the general pool of organic acids present in the HTL-AP product (SundarRajan et al., 2021). The organic acid formation also originates from carbohydrates within the feedstock. These carbohydrates are hydrolyzed into their monosaccharides under the harsh operating conditions of HTL. These monosaccharides further fragment, may undergo rearrangement, and might react with other components in the feedstock. Some products of these complex reactions can be precursors that are easily transformed to acetic acid (Chen et al., 2014). The aqueous phase generated by means of HTL was enriched in nitrogenous compounds like amines. These can be generated through decarboxylation of amino acids, thereby releasing CO2. Another path toward cyclic amides includes cyclization reactions of amino acids (Leng & Zhou, 2018). Heterocyclic compounds with a ring structure including nitrogen atoms were also present in the aqueous phase. These products most likely originate from the decomposition of melanoidins. The formation of melanoidins themselves is a result of the Maillard reactions, which occur between amino acids and saccharides at high temperatures during HTL (Aierzhati et al., 2019). Degradation of saccharides during HTL may cause the formation of various oxygenated compounds in the aqueous phase. These can further degrade into ketones and alcohols. Besides this, dehydration of saccharide may result in furfural derivatives, probably further converted to cyclic oxygenated compounds (Leng & Zhou, 2018; Xu et al., 2018a). Another type of oxygenated compound is a phenol derivative. Their mechanism of formation may include mainly two ways: 1) aldol splitting with further cyclization of the saccharide and 2) oligomers' dehydration with further cyclization - the oligomers are shorter saccharide chains. The aqueous phase also contains dissolved inorganic salts originating from the ash content of the biomass (Aierzhati et al., 2019; Hu et al., 2019).

**Table S3** presents a detailed description of the functional groups identified in the FTIR analysis. Scheme 1 demonstrated that at 250 °C with an extended residence time, the intensity of peaks corresponding to bonded or non-bonded hydroxyl groups and saturated aliphatic groups increased (**Figure S2**). It tends to indicate that the reactions responsible for these functional groups were favored through longer retention times. In addition, peaks corresponding to N-containing compounds also increased in intensity, as observed from TAN data. It was, therefore, indicated that longer residence times favored the formation of amines and heterocyclic compounds. Besides, Scheme 1 gave an indication of the decrease in intensity of the peaks from unsaturated aldehydes, ketones, alcohols, esters, ethers, alkanes, alkenes, and aromatic stretching. This would tend to indicate the conversion of these compounds into biocrude during the process. At 300 °C, the intensities in peaks within the product spectrum increased with increased residence time from 30 to 60 minutes. This trend was just about similar to that observed at the residence time of 30 minutes where increasing temperature starting from 250 °C up to 350 °C also tended to increase peak intensities. These observations indicate further degradation of organic compounds and likely contribute to the aqueous-phase formation. On the other hand, at the higher temperature of 350 °C, peaks of lower intensities with increased residence time from 30 to 60 minutes were observed. This would suggest that further rearrangement and polymerization of compounds occurred, which favored the formation of biocrude and other co-products. Curiously, this trend of peak intensity decreasing with the increase in residence time also continues when the temperature is varied from 250 °C to 350 °C, while the residence time was kept constant at 60 minutes. One deviation regarding these data was observed at 300 °C. During this temperature, a residence time of 60 minutes increased the peak intensity instead of decreasing it, especially in functional groups within the wavenumber range of 500-1610 cm$^{-1}$. It implies that at 300 °C, there is further degradation of biomass compared to the higher temperature, which might be leading to smaller molecules with these functional groups.

Scheme 2 showed that at the lower temperatures (250 °C), increased residence time from 30 to 60 minutes generally reduced peak intensity (**Figure S2**), except for the peak for C=C ring aromatics with various substitutions, whose intensity remained stable or even grew stronger. The pattern repeats in all three temperatures (250 °C, 300 °C, and 350 °C). At a constant residence time of 30 minutes, raising the temperature from 250 °C to 350 °C generally resulted in a peak intensity loss. However, the peak due to C=C ring aromatics at 350 °C exhibited some fluctuations, which ran contrary to the general rule. An intriguing observation in this respect was that at a residence time of 60 minutes. In this case, the increased temperature from 250 °C to 300 °C originally produced the effect of decreasing peak intensity. With further rises up to 350 °C, this trend was reversed by an increase in peak intensity.

#### *3.3.1.4 Hydrochar*

The HHV of hydrochar from PS as presented in Scheme 1 ranged from 4.1 to 7.4 MJ/kg, while the HHV of hydrochar obtained from digestate according to Scheme 2 was from 2.2 to 5.8 MJ/kg. The hydrochar of both schemes had a low energy density coupled with a high ash content compared to their feedstock samples. The energy content of hydrochar from PS was higher compared to that from digestate. This difference occurred because PS contained more available carbon for HTL than digestate, which had already consumed part of its carbon for biomethane production. **Table S4** presents the elemental composition of hydrochar produced under different operational conditions. The increase in temperature had a negative effect on the carbon content of hydrochar in both schemes. This reduction in carbon content with increased HTL operating temperatures may be because the carbon is mainly used for the formation of biocrude and gases. In Scheme 1, the extension of retention time favored the carbon content of hydrochar. However, in Scheme 2, there was no marked change in the carbon content with the increased retention time. Probably, this was so because in Scheme 2, digestate was used as feedstock for HTL, which was much less degradable as compared to the PS used in Scheme 1. Therefore, an increase in retention time from 30 to 60 minutes in Scheme 2 was not sufficient to degrade more organic matter present in digestate.

The increase in operating temperature for both 30- and 60-minutes retention times in both schemes led to increased ash content for the hydrochar (**Table S4**). Increased temperature favored the polymerization and condensation of chemical compounds to higher degrees, leading to increased ash formation (Kumar et al., 2018). In Scheme 1, the increase in retention time did not strongly influence the ash content of the hydrochar. However, under Scheme 2, the decrease of ash content was observed with the increased retention time at the lower temperatures, that is, at 250°C due to the rearrangement of the chemical compounds for the production of biocrude. On the other hand, no such variation has been observed in cases of high temperatures.

FTIR analysis was also performed to provide basic understanding of the chemical nature of hydrochar, which is important for optimizing its production processes and in seeking its many potential applications in various fields, including soil amendment. **Figure S3** presents the FTIR results for hydrochar of different HTL operating conditions for both schemes. Further elaboration on the functional groups observed in the FTIR spectra can be found in **Table S3**. **Figure S3** shows that in Scheme 1, at 250 °C, 300 °C, and 350 °C, the intensity of peaks increased as the retention time was extended from 30 to 60 minutes. This indicated that longer retention times facilitated the conversion of biomass into solid products through hydrolysis, dehydration, decarboxylation, and aromatization reactions, as well as through the polymerization and condensation of reaction intermediates released into the liquid phase (Rivas-Arrieta et al., 2024). At a 30-minute retention time, as the temperature increased from 250 °C to 300 °C and then to 350 °C, the peak intensity decreased. This reduction in intensity could be due to the water in the feedstock acting as a reaction medium, preventing the polymerization of intermediate products (Ponnusamy et al., 2020). This decreased the yield of hydrochar but increased the yield of biocrude, as confirmed by elemental analysis showing a decrease in carbon content with rising temperatures. However, there was no significant difference in peak intensities when the temperature increased from 300 °C to 350 °C. A similar trend was followed at a 60-minute retention time as temperature increased from 250 °C to 300 °C and finally to 350 °C. Interestingly, peak intensities at 350 °C were different, matching the intensity of 250 °C, which was reasoned to be due to the complexity of PS.

Scheme 2 also depicted the same trends of FTIR peaks as Scheme 1. In contrast, at 250 °C, peaks at 3200-3570 $cm^{-1}$ (characteristic for O-H stretching) and at 1000 $cm^{-1}$ (characteristic for inorganic ions and oxycompounds) had strongly diminished in intensities with the increase in retention time from 30 to 60 minutes. It therefore meant that the longer retention time favored the full decomposition of biomass in the digestate toward increased production of biocrude and suppression of hydrochar formation with its associated polymerization reactions (Ponnusamy et al., 2020). At 300 °C and 350 °C, a similar trend occurred with increasing retention time, but the difference in peak intensity weakened accordingly. The peak observed at 30 min retention time increased with increasing operating temperature from 250 to 300 °C. Increased conversion of biomass to products, such as hydrochar, owing to higher reaction rates at elevated temperatures may explain such an increase. At 350 °C, the intensity decreased, probably because of increased decomposition of these products into smaller molecules or volatile components (Zheng et al., 2015). In contrast to this, the peak intensities for the 60-minute retention time continuously increased from 250 °C to 300 °C and further to 350 °C. This continuous rise indicated that longer retention times allowed more conversion and condensation reactions; thus, larger molecules were formed, which reflected in stronger peaks at higher temperatures.

### *3.3.2 Anaerobic digestion*

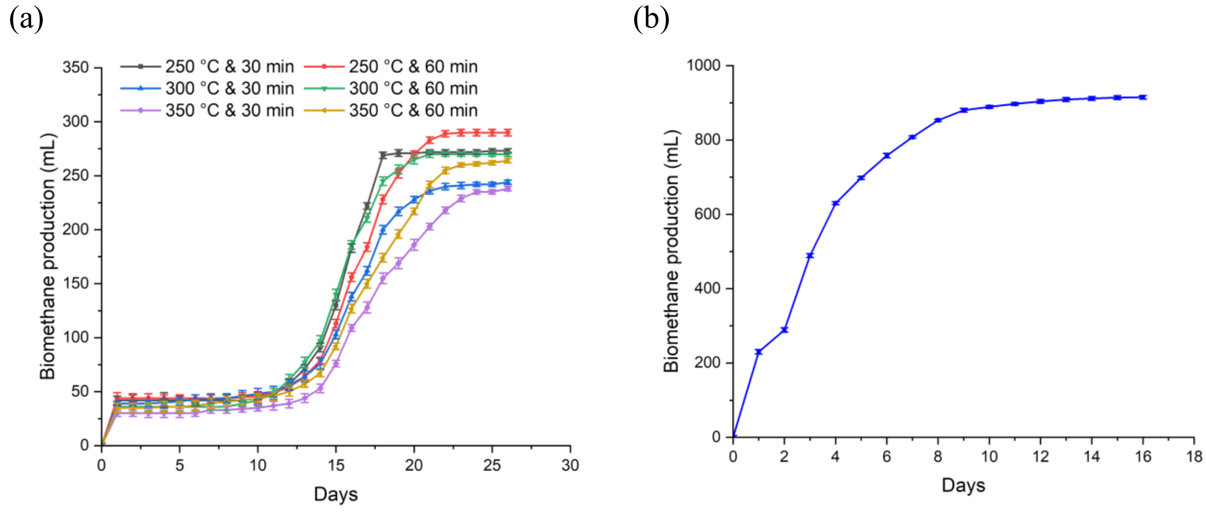

**Figure 3.3:** Cumulative biomethane production from feedstock of: (a) Scheme 1 (HTL followed by AD) and (b) Scheme 2 (AD followed by HTL).

The biomethane production for Scheme 1 indicated a temporary lag-phase between day 2-7 (**Figure 3.3 (a)**). This is perhaps due to adaptation time taken by the anaerobic microbiota to probably inhibitory compounds presented in HTL-AP (Cabrera et al., 2023). This can be explained by the inhibition given to the N-containing compounds, as evidenced in the FTIR analysis of the AD process. The cumulative biomethane production varied regarding operating conditions from HTL aqueous phase. The obtained cumulative methane production was 290 ± 4 ml at 250 °C & 60 min, 273 ± 10 ml at 250 °C & 30 min, 270 ± 9 ml at 300 °C & 60 min, 264 ± 11 ml at 350 °C & 60 min, 244 ± 8 ml at 300 °C & 30 min, and 238 ml ± 6 at 350 °C & 30 min. The highest cumulative biomethane production (290 ± 4 ml) was obtained from the aqueous phase generated under HTL operating conditions of 250 °C and 60 minutes. Conversely, the lowest production (238 ± 6 ml) was observed at 350 °C and 30 minutes. This trend could be related to the influence of the temperature in HTL on the aqueous phase characteristics; higher temperatures favor a conversion into bio-oil, which would leave fewer available readily biodegradable organic matter for methanogenesis in the aqueous phase (Posmanik et al., 2017a). Therefore, a higher TOC concentration from the 250 °C 60-minute condition resulted in a higher biomethane yield. Moreover, at 250 °C more complex volatile organic matter was probably degraded for a longer residence time into simpler forms which also enhanced biodegradability. The TAN concentration can inhibit the AD process by suppressing enzyme activities responsible for biomethane generation in a wide range of concentrations from 1700 to 14,000 mg/L (Li et al., 2019). In this work, biomethane produced shows no significant influence caused by the TAN concentration. It was believed to be because of the low range recorded in the study against those concentrations reported in the literature. Scheme 2 achieved a cumulative biomethane production of 915 mL after 19 days (Figure 3.3 (b)); this may have resulted because of the easy biodegradability nature of the PS substrate. PS obtained directly from the primary clarifier of the wastewater treatment plants is generally low in protein content and never before underwent any biological degradation (Demirbas et al., 2017). These properties made it readily amenable to bioconversion in the AD process.

### *3.3.2.1 Digestate characteristics*

The elemental composition of the feedstock significantly impacts the resulting digestate characteristics. **Table 3.3** presents the detailed elemental analysis of digestates from both schemes. Scheme 1 demonstrated a noteworthy contrast: while biomethane production from the HTL-AP varied depending on the HTL operating conditions, the elemental composition of the digestate remained relatively constant when using HTL-AP as a feedstock in the AD process. Compared to the PS (the original feedstock), the digestate from Scheme 1 exhibited a decrease in carbon and hydrogen content. This reduction was attributed to their consumption during methane (CH4) formation, leading to a lower overall energy content in the digestate (Möller & Müller, 2012). Contrarily, the nitrogen content increased in the digestate. This is due to the "N concentration effect," which results from the fact that carbon degrades preferably to form $CO_2$ and $CH_4$ during the AD process, while nitrogen is preserved (Tambone et al., 2010). In the same way, the ash content was higher (43.3–47.9%) in the digestate than in PS at 33.3%. Scheme 2 also followed a similar trend to that of Scheme 1. In the digestate of PS feedstock, carbon content reduced from 36.5% to 27.8% and hydrogen from 5.2% to 3.8%. In contrast, ash increased from 33.3% to 49.8%. Nitrogen did not show any significant difference.

**Table 3.3:** Elemental analysis of the resulting digestate from both schemes.

| Digestate Characteristics | Elemental Analysis (wt. %, dry basis) | | | | | | HHV (MJ/kg) |
|---|---|---|---|---|---|---|---|
| | N | C | H | S | O | Ash content | |
| Scheme 1 (HTL followed by AD) | | | | | | | |
| HTL-AP: 250°C & 30 min | 4.01 ± 0.01 | 30.3 ± 0.01 | 4.0 ± 0.01 | 0.83 ± 0.01 | 17.58 ± 0.04 | 43.3 ± 0.05 | 12.9 ± 0.03 |
| HTL-AP: 250°C & 60 min | 3.69 ± 0.02 | 28.3 ± 0.02 | 3.7 ± 0.10 | 0.77 ± 0.02 | 17.13 ± 0.28 | 46.5 ± 0.13 | 11.8 ± 0.20 |
| HTL-AP: 300°C & 30 min | 3.54 ± 0.01 | 28.3 ± 0.01 | 3.7 ± 0.01 | 0.81 ± 0.02 | 17.85 ± 0.02 | 45.8 ± 0.02 | 11.7 ± 0.01 |

| | | | | | | | |
|---|---|---|---|---|---|---|---|
| HTL-AP: 300°C & 60 min | 3.65 ± 0.01 | 28.8 ± 0.01 | 3.8 ± 0.01 | 0.77 ± 0.04 | 17.39 ± 0.04 | 45.6 ± 0.01 | 12.1 ± 0.02 |
| HTL-AP: 350°C & 30 min | 3.66 ± 0.05 | 29.2 ± 0.04 | 3.8 ± 0.10 | 0.77 ± 0.06 | 16.13 ± 0.48 | 46.5 ± 0.09 | 12.5 ± 0.33 |
| HTL-AP: 350°C & 60 min | 3.50 ± 0.04 | 28.3 ± 0.01 | 3.7 ± 0.01 | 0.75 ± 0.03 | 15.85 ± 0.15 | 47.9 ± 0.11 | 12.1 ± 0.06 |
| Scheme 2 (AD followed by HTL) | | | | | | | |
| PS Digestate | 3.40 ± 0.05 | 27.8 ± 0.57 | 3.80 ± 0.10 | 0.75 ± 0.05 | 14.48 ± 0.62 | 49.8 ± 0.30 | 12.2 ± 0.44 |

HTL-AP: aqueous phase generated from hydrothermal liquefaction process; HHV: higher heating value; PS: primary sludge.

FTIR spectra obtained for the digestate from Scheme 1 and Scheme 2 are presented in **Figure S4**. Functional groups detected in the wavenumber range agreed with those detected in the biocrude, HTL-AP, and hydrochar samples. Details of the identification of the functional groups present within the samples using the FTIR analysis were found in **Table S3**. Scheme 1 displayed an intensity decrease of the peak between 2500 and 4000 $cm^{-1}$, indicating the breakdown of alcohol, amino groups, and saturated aliphatic groups (Chen et al., 2019b; Pipitone et al., 2020). In addition, the peak between 1500 and 1580 $cm^{-1}$, the intensity level of which also decreased, represented aromatics with various substitutions (Lievens et al., 2011). The observed loss in intensity in this case may be due to the degradation of soluble organics, present in the PS for biomethane formation. The increased intensity of the peak in the 1750–1590 $cm^{-1}$ region indicated larger macromolecules degrading to ketones, aldehydes, amino acids, and amides. The increase in intensity of the peak near 1000 $cm^{-1}$ wavenumber region suggests the increment of inorganic ion concentration. This could be because most of the organic fraction was utilized in the AD process for biomethane formation.

Scheme 2 shows intensities of peaks in the digestate significantly higher compared to the initial HTL-AP coming from HTL. Surprisingly, the most active spike occurred at 3400-4000 cm⁻¹; this is generally associated with the stretching vibration of O-H bonds in hydroxyl groups. It should be indicated, though, that in this region, one also takes into consideration the contribution of water molecules. The increase in the peak intensities observed can be due to two possible interpretations. One possibility is that complex organic molecules were partially degraded into simpler parts during HTL, and then AD further processed these compounds into its parts; yet some of the functional groups could still exist or concentrate because overall organic content was lower in the digestate than the initial HTL-AP. It is this concentration effect that leads to stronger peaks in the FTIR. In this, the water content in digestate was lower compared to HTL-AP. While a hydroxyl peak (3400-4000 cm⁻¹) can contribute to the increase in intensity of some peaks, a decrease in water content normally affects the baseline of FTIR spectra. This could be one of many reasons for the rest of the peaks seeming more pronounced (Guan et al., 2010). The wavenumber region between 500 and 2500 cm⁻¹ for the HTL-AP derived from higher operating temperatures was stronger in intensity than that of the digestate; this is possibly because the higher temperature HTL-AP feedstock contained more of these functional groups.

### *3.3.3 Evaluation of energy recovery efficiencies*

**Table 3.4:** Detailed energy recovery from biocrude and biomethane from (a) Scheme 1 (HTL followed by AD) and (b) Scheme 2 (AD followed by HTL).

| Operating conditions | Scheme 1 (HTL followed by AD) | | | Scheme 2 (AD followed by HTL) | | |
|---|---|---|---|---|---|---|
| | Energy recovery from | | Total energy recovered (%) | Energy recovery from | | Total energy recovered (%) |
| | Biocrude (%) | Biomethane (%) | | Biomethane (%) | Biocrude (%) | |
| 250°C for 30 min | 39.0 | 10.86 | 49.8 | 37.70 | 26.4 | 64.1 |
| 250°C for 60 min | 56.3 | 11.87 | 68.1 | 37.70 | 30.3 | 68.0 |

| | | | | | | |
|---|---|---|---|---|---|---|
| 300°C for 30 min | 56.7 | 7.04 | 63.7 | 37.70 | 34.1 | 71.8 |
| 300°C for 60 min | 76.9 | 7.65 | 84.5 | 37.70 | 39.6 | 77.3 |
| 350°C for 30 min | 41.6 | 5.63 | 47.2 | 37.70 | 19.5 | 57.2 |
| 350°C for 60 min | 51.0 | 4.83 | 55.8 | 37.70 | 25.2 | 62.9 |

Energy recovery efficiency was considered as the basis of evaluating both schemes' performance. **Table 3.4** summarizes the calculated percentages of energy recovered via AD and HTL, and through the overall system for both configurations at different operating conditions. Total energy recovery refers to the total energy content recovered combined from biocrude and biomethane. These results provide indications on the optimum performance conditions necessary for maximization of energy yield with the aim of increasing the sustainability of PS valorization processes. Hydrochar was excluded from the end analysis in this study because it has less energy content and economic value compared to other by-products like biocrude and methane. Previous works have indicated that hydrochar has limited applicability and is in lower demand in the market, regarding its use as fuel or soil amendment (Cervera-Mata et al., 2021; Fregolente et al., 2021). Moreover, energy recovery from hydrochar is much lower, which justifies its exclusion in the context of optimization of overall energy efficiency of the system (Cabrera et al., 2023).

Under the operating conditions of 250°C for 30 minutes, Scheme 1 attained a total energy recovery of 49.8%, wherein 39.0% was biocrude and 10.86% biomethane. When the reaction time was prolonged up to 60 minutes at the same temperature, the total energy recovery increased to 68.1%, in which the contribution to biocrude and biomethane was 56.3% and 11.87%, respectively. In this respect, increasing the reaction temperature to 300°C for 30 minutes could account for 63.7% of total energy recovery because of high energy recovery from biocrude at 56.7% and biomethane at 7.04%. Increasing the reaction time to 60 minutes at this temperature yielded the highest recovery of total energy in Scheme 1, at 84.5%, while biocrude and biomethane contributions were 76.9% and 7.65%, respectively. However, the overall energy recovery at 350°C was 47.2% for 30 minutes and 55.8% for 60 minutes of reaction time with the contributions of biocrude and biomethane estimated to be 41.6% and 5.63% and 51.0% and 4.83%, respectively.

Scheme 2 showed a different energy recovery behavior from Scheme 1. Here, keeping the temperature at 250°C for 30 minutes gave a holistic energy recovery of 64.1%, wherein biomethane recovery was 37.70% and biocrude recovery was 26.4%. It kept a similar trend when prolonging to 60 minutes at the same temperature, giving an overall energy recovery of 68.0% with increased biocrude recovery of 30.3%. Scheme 2 at 300°C for 30 minutes attained about 71.8% total energy recovery, wherein biomethane and biocrude contributed about 37.70% and 34.1%, respectively. The prolongation of the reaction time to 60 minutes at this temperature increased the total energy recovery to 77.3%, wherein biomethane and biocrude had contributions of 37.70% and 39.6%, respectively. The total energy recovery at 350°C for 30 minutes was 57.2%, biomethane contributing 37.70% and biocrude 19.5%. Further increasing the reaction time to 60 minutes resulted in an overall energy recovery of 62.9% of biomethane and biocrude at 37.70% and 25.2%, respectively.

The comparative analysis of the two schemes therefore follows that, in general, Scheme 2 gives higher total energy recovery than Scheme 1, especially because of the consistent biomethane production. Scheme 1, however, does show great potential under optimal conditions, meaning 300°C for 60 minutes, reaching the highest total energy recovery. The reasons for this outcome lie in the fact that at this condition the maximum yield of biocrude was attained as high as 40.7 wt.%, which is considered optimum for the production of biocrude. From the results obtained from this work, it can be established that operation conditions are very vital for the maximization of energy recovery, and the integration scheme to be used will be based on various process needs and outcome.

At the lower temperature of 250°C, Scheme 2 always showed higher total energy recovery compared to Scheme 1, irrespective of reaction time. This trend continued at the higher temperature, which was 300°C, and hence Scheme 2 achieved better energy recovery for the reaction times of 30 minutes and 60 minutes. While Scheme 1 obviously decreased in energy recovery at the highest temperature of 350°C, Scheme 2 was still able to obtain the relatively higher total energy recovery. This may indicate that Scheme 2, AD followed by HTL, can be more robust and flexible; it can therefore provide more reliable performance in a wide temperature range. These results clearly indicate that the operating conditions of HTL would need to be optimized in an integrated system for PS treatment. While there may be certain advantages to the HTL-AD configuration under specific conditions, the AD-HTL configuration provides a more flexible approach that could achieve higher energy recovery across a wide range of HTL operating parameters.

## 3.4 Conclusion

Different sequences of AD and HTL integration offer good prospects for sewage sludge management. This combined system will provide several advantages, including energy recovery, as well as overcome some drawbacks from both individual processes. Results from the current study showed that the two schemes offer different characteristics in energy recovery and product characterization at different temperatures and reaction times. The comparative analysis of the two schemes reveals a trade-off between production of biocrude and biomethane. Scheme 1 is superior in yield for the production of biocrude, which is essential in applications requiring liquid fuels, while at the same time, Scheme 2, where AD precedes HTL, can be viewed as more balanced in yield with higher biomethane production that can be quite useful in direct energy applications like heating and electricity generation. Especially, Scheme 2 reached up to 77.3%, with biomethane content of 39.6% and biocrude of 37.7%. These results point out that the optimal integration of AD and HTL is actually based on specific energy needs and end products. Moreover, the reaction time and temperature are identified as factors that have an important role in reaching maximum energy recovery. Both schemes improved energy recovery at longer reaction times at lower temperatures, whereas higher temperatures did not always provide better results, showing an optimization of operation conditions. Further research should focus on the further optimization of these parameters and on scalability and economic viability of these integrated processes for better applicability in practice for waste management and energy production.

# Chapter 4

# Integrating Anaerobic Digestion and Hydrothermal Liquefaction for Sewage Sludge Management: A Techno- Economic Analysis

## 4.1 Introduction

Municipal wastewater treatment plants (WWTPs) are among the most valuable facilities that have grown globally, sustaining the clean water supply of the public. These plants treat the wastewater that comes out from residential, commercial, and business sectors to give supply to the communities with clean and safe water (Sikosana et al., 2019). The volume of wastewater to be generated worldwide in 2020 is estimated to be about 380 billion cubic meters ($m^3$). Moreover, this is forecasted to increase by 24% in 2030 and further by 51% in 2050 (Qadir et al., 2020). It therefore implies that the quantity of sewage sludge to be produced worldwide as a result of the wastewater treatment process would be immense. For example, it is estimated that sewage sludge produced annually in the United States is around 7.1 million dry tons (Krause & Bronstein, 2024). Similarly, Canada produces an estimated volume of about 660,000 dry tons of sludge annually (Canadian Council of Ministers of the Environment, 2012). This enormous amount of sludge makes its efficient and ecological disposal very difficult.

Sludge arises at many stages of the wastewater treatment process in WWTPs. These phases do have a great impact on the properties and composition of sludge. The whole treatment consists of three phases: primary, secondary, and tertiary (Janaszek et al., 2024). Primary sludge is thus produced during primary treatment, when organic matter, sand, grit, and settleable materials are removed by physical processes, including sedimentation (Li et al., 2024). Next comes the biological process of secondary treatment in which organic waste is decomposed with the help of microorganisms, thus producing secondary sludge that consists of these microorganisms along with organic material settled down (Demirbas et al., 2017). Finally, chemical precipitation or filtering practices utilized in removing further impurities like nutrients in an optional tertiary treatment step for polishing the effluent treated would produce tertiary sludge (Zagklis & Bampos, 2022). The structure of the sewage sludge, normally a mixture of organic and inorganic components such as heavy metals, pathogens, and various chemical pollutants, including nutrients like phosphorus and nitrogen, is usually affected by this multistage treatment process (Ramzanipour et al., 2023). This complexity in composition requires comprehensive measures of treatment and management in an effort to minimize potential risks to the environment and public health. In case of high contamination with heavy metals and pathogens, sludge cannot be used safely in agriculture, which requires more processing to meet safety criteria (Chung et al., 2012).

There are several obstacles associated with each of the conventional sludge disposal techniques, including land application, incineration, and landfilling. Once a common practice, landfilling is becoming less popular because of land unavailability due to growing population and increasing pressure from governmental bodies. Environmental concerns are also raised by the possibility of landfill leachate that can contaminate groundwater (Gavrilescu & Schiopu, 2010). Incineration is an energy intensive method and produces air pollutants, which makes it an expensive and less environmentally friendly method (Beyene et al., 2018). Strict rules to prevent soil and water contamination limit the use of sludge as land application, which uses treated sludge as fertilizer. Moreover, the public's opinion on the use of biosolids on farms can further limit this option, as the sludge quality and the presence of pollutants in it are unpredictable (Wang et al., 2008). Besides, transportation and storage of sludge require extra monetary and logistical barriers. For better sludge management, research into advanced treatments like hydrothermal liquefaction (HTL) and anaerobic digestion (AD) goes on as a means to solve such difficulties (Chen et al., 2020; Di Capua et al., 2020).

As presented in previous chapters, integration of AD followed by HTL holds great potential for sewage sludge management as it eradicates the problem of disposal of generated digestate and also leads to the formation of biocrude, biogas, and other valuable co-products, enhancing the overall energy recovery of the integrated system. This combined strategy plays a crucial role to maximize resource recovery: While AD efficiently decreases the volume of sludge and generates biogas, HTL transforms the digestate into bio-crude and other high-value products (Eboibi et al., 2015). Additionally, as compared to traditional sludge disposal techniques, the synergy of AD and HTL helps to minimize greenhouse gas emissions and leads to a more environmentally friendly &

sustainable waste management system. By converting garbage into useful resources, this all-encompassing strategy not only solves waste management issues but also advances the circular economy (Cabrera et al., 2023).

In the previous chapter, we presented a systematic comparison of energy recovery from AD- HTL to obtain a comprehensive understanding of energy recovery from sewage sludge. In this chapter we present the economic viability of this approach. The commercialization of integrated AD-HTL systems for sludge management represents a transformative advancement in sustainable wastewater treatment. Although numerous techno-economic assessments (TEAs) have been conducted for standalone AD and HTL processes, the economic feasibility of the integrated AD-HTL system is not fully captured. These new integrated plans must be economically viable since environmental sustainability and economic factors go hand in hand. Although environmental sustainability for integrated AD-HTL systems has been effectively assessed experimentally before, the present work expands the analysis by performing a TEA aimed at setting performance targets necessary to attain economic viability. In addition, the given study investigated cost-cutting means such as the methanation process that converts carbon dioxide to methane gas with a reduced emission of greenhouse gases while at the same time providing a closed-loop resource management system. These are: stand-alone AD with PSA unit for methane separation; stand-alone AD with PSA and methanation unit; and integrated AD-HTL system with PSA and methanation unit. The main aim of this study is to provide an early assessment of large-scale integrated AD-HTL system and to pave a wider route to its adoption in the wastewater treatment industry. The model identifies the relevant cost variables, uncertainty in production cost, and potential economic benefit determinants that may help develop a robust, economically viable, and sustainable sludge management system.

## 4.2 Literature Review

An extensive overview of TEA studies based on biomass valorization is reviewed in this section, including an assessment of the integrated approach's scalability, energy efficiency, cost-effectiveness, and environmental impact.

Tian et al. (2020) conducted the TEA study on integrating the AD-HTL-AD system for sewage sludge management. The mixed sludge of waste activated sludge, and PS was used as feedstock in this research. Thickened sludge was first fed as feedstock into the AD unit, and the digestate derived was then fed as feedstock into the HTL unit. In order to maximize resource recovery, the HTL-AP was fed into a secondary AD unit. The TEA concluded that HTL (15.5%) and AD (16.6%) were the highest contributors to the total equipment cost. Moreover, maintenance costs had the highest share (47%) of the capital expenditure (CAPEX). For the assessment of its profitability, Net Present Value (NPV) was calculated for this integrated process. The NPV was assumed to be $177.36 million in the estimation for this study. Sensitivity analysis identified that feedstock input rate and discount rate were the critical parameters through which the economic performance of the system would be affected. Moreover, the introduction of economic incentives together with the production of "green" by-products-biochar and biocrude-was pointed out as an element that is required for the real implementation of these retrofitting designs into WWTFs. This study, however, had numerous drawbacks: A lack in the purification of biogas for the generation of electricity and off-gas release during the HTL process will reduce overall environmental benefits for the system. Also, the integrated approaches for sewage sludge management are rarely centered on any TEA study, which further gives it a significant scope for research.

Kaseem et al. (2020b) performed TEA on an integrated system that coupled HTL with AD for the management of dairy waste, anchored on valorization from cow manure. The system consisted of cow-dung digestion in the AD unit and using the obtained digestate as feedstock for HTL. The study clearly outlines the importance of economies of scale and the selling price of electricity for the process financial viability. The profitability of the approach was dependent on the revenue generated from hydrochar and biocrude. In a similar study, Kaseem et al. (2020a) evaluated an AD-HTL system by incorporating a biomethanation unit and an electrolyzer to enhance methane recovery and reduce greenhouse gas (GHG) emissions. The study concludes that capital cost of electrolyzer and its electricity contribution was the main contributor to the CAPEX and operational expenditure (OPEX). Carbon credit systems improved the project's financial viability, highlighting the importance of financial incentives in a large-scale system. Both studies emphasize the economic and environmental potential of integrated AD-HTL systems but also highlight the critical role of economies of scale, market prices, and financial incentives in achieving profitability.

These studies underline the importance of process optimization-integrating methanation units and applying the HTL products-to increase profitability while reducing GHG emissions. The scale of the project and financial incentives therefore play an important role in rendering large-scale integrated plants financially viable. Besides, through the sensitivity analyses, parameters of interest include electricity costs and discount rates for the overall financial performance of the system. Additionally, the previous studies conducted largely depend on assumptions rather than experimental data; hence, there is a big gap in research. This study links the TEA with experimental findings, offering a stronger and more solid test of the economic feasibility of the integrated approach.

## 4.3 Scope and Process Description

### *4.3.1 Scope of study and system boundary*

A plant with a processing capacity of 1.1 million tonnes per annum of PS was considered for this study. **Figure 4.1** illustrates the three proposed system configurations. **Figure 4.1(a)** presents a baseline scenario (Case 1) comprising an anaerobic digester integrated with bio-desulfurization and PSA units. **Figure 4.1(b)** integrates a methanation unit and an electrolyzer to the baseline configuration to mitigate carbon dioxide ($CO_2$) emissions (Case 2) and increase methane yield. **Figure 4.1(c)** incorporates the HTL unit to manage digestate while generating additional revenue streams from hydrochar and biocrude (Case 3).

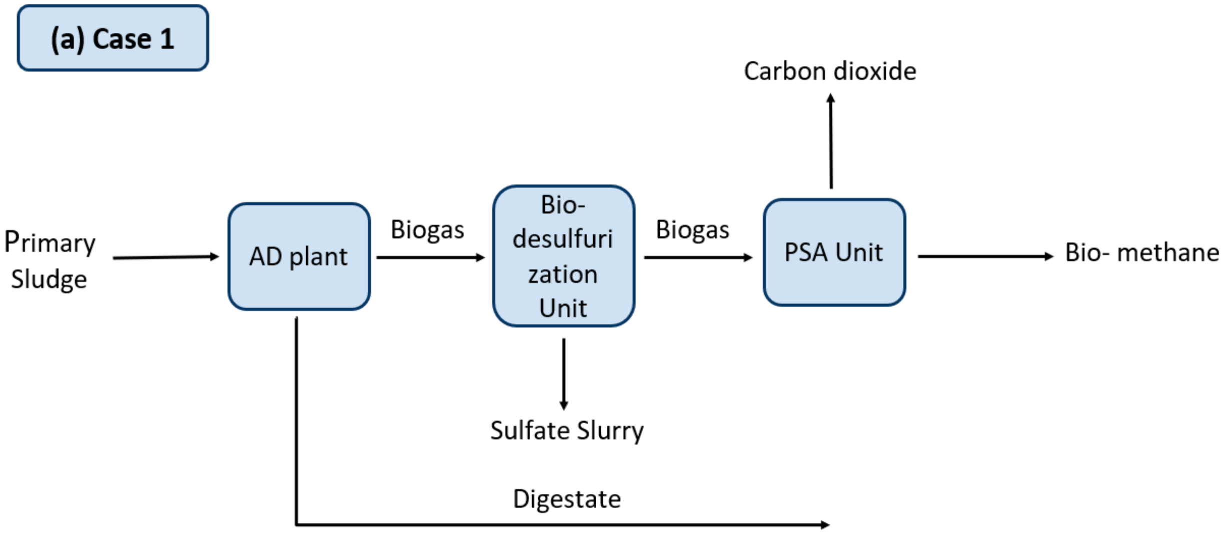

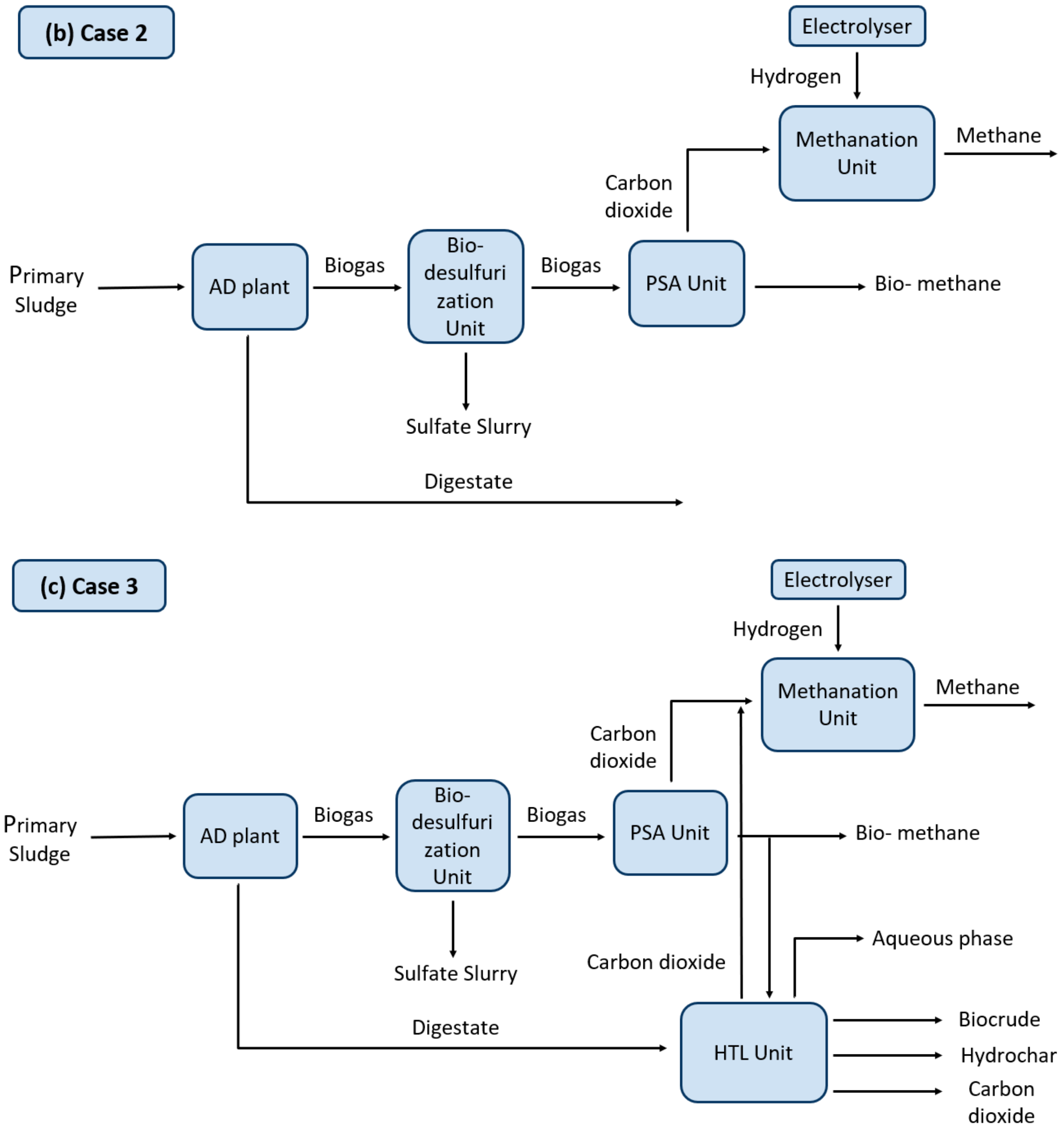

**Figure 4.1:** Process flow diagrams for (a) Case 1, (b) Case 2, and (c) Case 3.

### *4.3.2 Feedstock characteristics*

The PS used as feedstock in this study was collected from the Local WWTP, Edmonton, Alberta, Canada. Proximate analysis was performed for determining characteristics of the PS. The TS content of PS was measured as 3.00 ± 0.02% and the content of VS was calculated as 2.50 ±

0.01%. The calculated values are in close proximity to literature values (Dereli et al., 2009; Markis et al., 2016). These kinds of compositional parameters are of prime importance for understanding sludge behavior in the subsequent AD and HTL since they directly affect their respective biochemical and thermochemical conversions in terms of efficiency and yield (Meegoda et al., 2018; Mishra et al., 2022).

### *4.3.3 Process description, operating conditions, and assumptions*

#### *4.3.3.1 AD Unit*

**Figure 4.2** illustrates the schematic flow diagram of the AD unit in the base case scenario. PS was first kept in a feedstock holding tank that had capacity to contain a day's worth of sludge at room temperature (20°C). Prior to entering the digester, the feedstock was mixed with recirculated effluent for effective mixing, increasing the feedstock temperature to 31°C. This helped to optimize the digestion process. The mixture was then run through a heat exchanger, which raised the temperature even higher to 40°C in order to preserve the ideal operating conditions required for the AD process. A single-stage Continuous Stirred Tank Reactor (CSTR) was considered as an anaerobic digester that was intended to run in a mesophilic environment, namely in the 35–37°C temperature range, which is ideal for mesophilic bacterial activity (O'Connor et al., 2021). Thermophilic conditions, which operate at higher temperatures between 50 and 60°C, are another method of running the AD process. Mesophilic conditions were chosen for this investigation because they are stable and required less energy than other conditions, which makes them a dependable and affordable option even if this method can speed up the digestive process (Kim et al., 2002).

The hydraulic retention time (HRT) for the process was set to 15 days, considering the fact that PS is highly degradable sludge (Elefsiniotis & Oldham, 1994; Li et al., 2024). Mainly, methane and $CO_2$ make up the composition of biogas, and the chemical composition of feedstock determines the composition; hence, optimization of the characteristics of feedstock should be considered along with maximization of the biogas yields (Chew et al., 2021). The digestate after AD was stored in a digestate storage tank for further utilization. The data in **Table 4.1** present the composition of the biogas, obtained from a wide review of related literature (Sanaye & Yazdani, 2022). Therefore, the composition will include components such as methane ($CH_4$), $CO_2$, water ($H_2O$), and trace amounts of other gases.

**Table 4.1:** Detailed volumetric composition of biogas.

| Biogas composition | $CH_4$ | $CO_2$ | $H_2$ | $H_2O$ | $H_2S$ | $N_2$ |
|---|---|---|---|---|---|---|
| Volumetric percentage (%) | 65.00 | 27.80 | 0.01 | 6.29 | 0.30 | 0.60 |

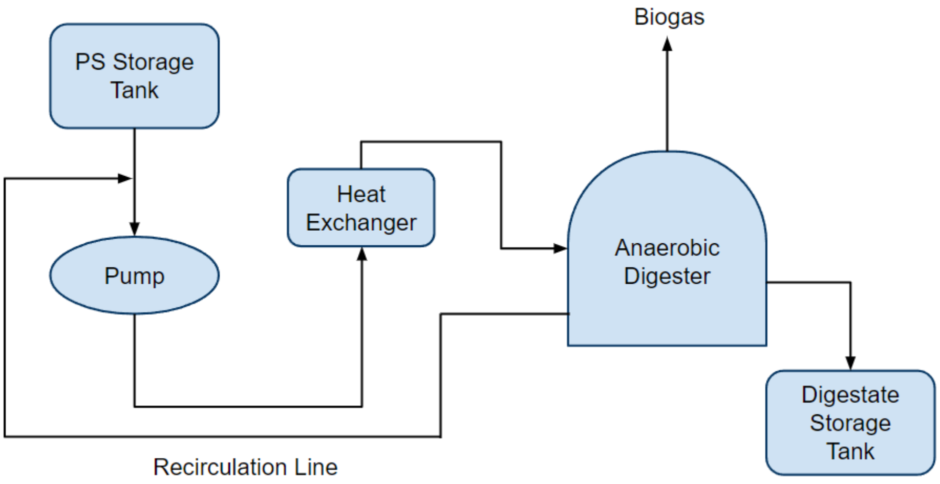

**Figure 4.2:** Schematic representation of the AD unit.

### *4.3.3.2 Bio- desulfurization Unit*

First, raw biogas is passed through a filtration step that includes a coarse gravel filter. This removes large solid particulates and protects downstream equipment, cleaning the biogas. Additionally, this filtration step functions like an in-line condensate trap, removing water vapor condensed out of the biogas stream. A water loading efficiency for the water traps of 33% was used (Sanaye & Yazdani, 2022). The biogas then goes through bio-desulfurization unit to remove hydrogen sulfide ($H_2S$). One such corrosive gas produced within the digester is $H_2S$-from the degradation of sulfur-containing organic matter, including protein and amino acids. Its removal is of significance not only for preventing equipment corrosion but also for ensuring subsequent steps in the biogas upgrading process operate optimally (Becker et al., 2022).

The bio-desulfurization unit, also known as a bio-trickling filter, is a class of packed bed systems that are containing $H_2S$-oxidizing microorganisms. A schematic diagram of a bio-trickling filter is presented in **Figure 4.3**. It finds an application due to its cost-effectiveness and lesser energy input compared to other chemical-based methods. These active microorganisms in this packing material inside the unit are immobilized and require oxygen to oxidize the $H_2S$ in the biogas into either elemental sulfur or sulfate, depending upon whether there is partial or complete oxidation (Khoshnevisan et al., 2017). It is so designed that a controlled amount of air introduces oxygen that supports microbial activity without increasing the oxygen content in the biogas that exits the bio-desulfurization unit beyond 1-2%. It was assumed that the $H_2S$ in the bio-desulfurization unit would be converted into sulfate, described by equation (4.1), with a conversion efficiency of 98% (Haosagul et al., 2020a; Zhuo et al., 2022):

$$H_2S + \frac{5}{2} O_2 \rightarrow SO_4 + H_2O \tag{4.1}$$

The elemental sulfur is hydrophilic and, as it is oxidized into sulfate, forms ionic bonds and attaches itself to microorganisms (Tichý et al., 1994). To counteract this and prevent the accumulation of the sulfur from occurring and affecting the efficiency of the process, there must be a countercurrent water flow in the packed bed system (Haosagul et al., 2020b). The resulting sulfate concentration in the water was assumed to be 2100 mg/L (Sposob et al., 2021). The biogas exiting the bio-desulfurization unit is subsequently stored in a six-hour capacity holding tank to mitigate flow fluctuations and ensure a steady feed to the downstream PSA unit. A water trap with water loading efficiency of 33% within the tank removes condensate formed as the biogas undergoes a heat loss (Sanaye & Yazdani, 2022). To facilitate the biogas upgrading process, the gas is compressed and heated via a blower before entering the PSA unit.

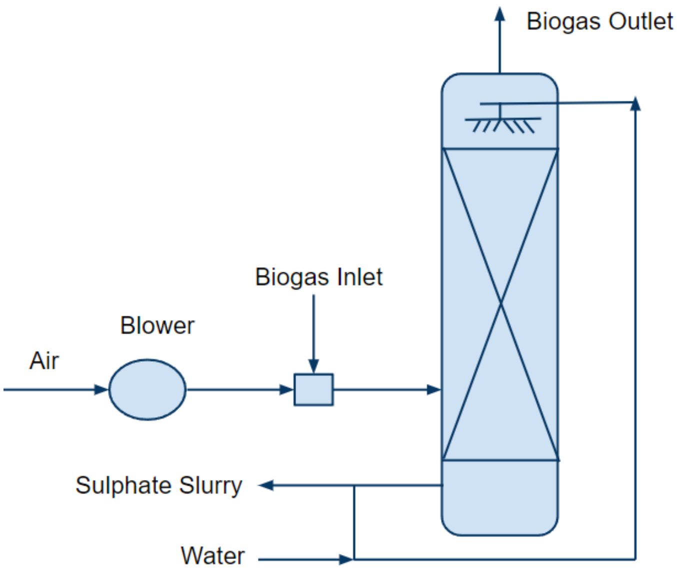

**Figure 4.3:** Schematic representation of a bio-trickling filter.

### *4.3.3.3 PSA Unit*

After the removal of $H_2S$ from the biogas, the gas stream is processed through a PSA unit for the separation of carbon dioxide and methane, thereby recovering high-purity methane, also referred to as bio-methane. For the purposes of modeling, it was assumed that complete separation of carbon dioxide within the PSA unit was achieved.

PSA is a dry separation technique making use of the physical properties of gases. The process generally includes compressing the raw biogas to high pressure before passing into an adsorption column where carbon dioxide would be selectively adsorbed, and methane passed through. When the column is saturated with carbon dioxide, the adsorbent material decreases in pressure to allow the carbon dioxide to desorb and is sent into an off-gas stream. To maintain a continuous production, several columns are done in series; each column then follows a series of adsorption and desorption phases. The key characteristics of a PSA system include the feeding and purging pressures, the type of adsorbent used, cycle time, and the interconnection between columns, among other factors (De Hullu et al., 2008). A simplified process diagram of a PSA upgrading unit is illustrated in **Figure 4.4**.

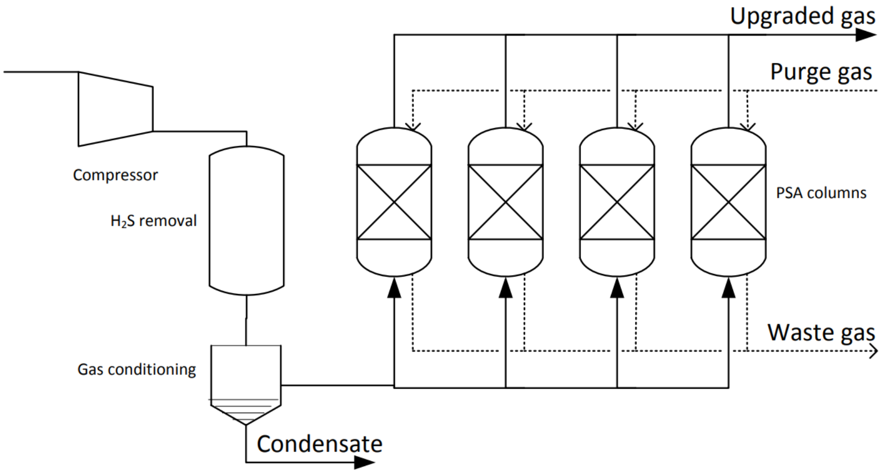

**Figure 4.4:** Process diagram for upgrading of biogas with PSA. **Source:** Adapted from (De Hullu et al., 2008).

The four main stages of a PSA column cycle, also called the Skarstrom cycle, are pressurization (1), feed (2), blowdown (3), and purge (4). **Figure 4.5** shows these stages as well as the pressure profiles that correspond to them. Raw biogas is fed into the column during the feed phase, where methane passes through, and carbon dioxide is adsorbed onto the bed material. The blowdown phase begins when the bed material is saturated with carbon dioxide and the feed phase comes to an end. At the start of the blowdown phase, the column still contains some raw biogas, resulting in a small loss of methane along with the desorbed carbon dioxide. The carbon dioxide-rich gas is released from the column during this phase, which is indicated by reduction in pressure that allows the carbon dioxide to desorb from the adsorbent. When the column reaches its lowest pressure, the purge phase begins. Upgraded gas is circulated through the column during this stage to clear the bed material of any residual desorbed carbon dioxide. When the column has completely been cleared, it becomes regenerated and can be re-pressurized with either raw biogas or upgraded gas, starting the cycle anew (Grande, 2011).

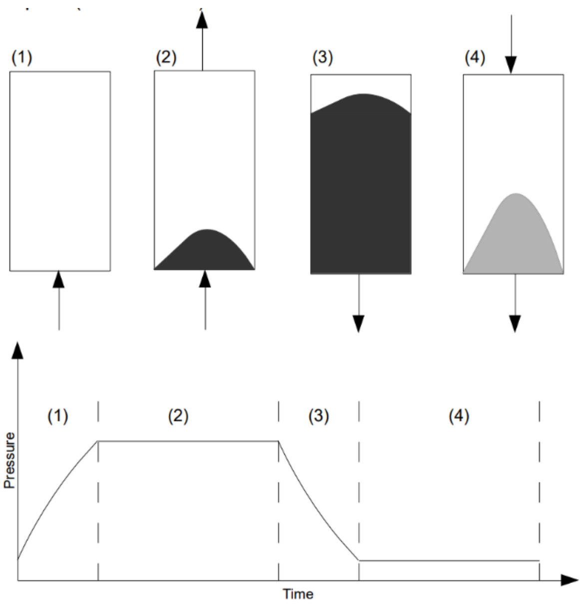

**Figure 4.5:** Schematics of the four phases in the Skarstrom cycle and a pressure profile of the cycle. **Source:** Adapted from (Rege et al., 2001).

Most PSA units have four towers since the PSA cycle itself usually involves four steps. This way, at any one time, one is sure that one column is on adsorption while the other three are undergoing various stages of regeneration. Columns are often paired such that the gas leaving one column during the blowdown step pressurizes another during the pressure equalization step to minimize methane losses. This link decreases the energy use by the process as a whole besides reducing methane loss. The cycle on the PSA column usually takes two to ten minutes (Grande et al., 2011; Spoorthi et al., 2011).

Using multiple columns in a PSA unit can reduce methane losses and improve energy efficiency. For example, the recirculation of the gas flow can increase the methane yield by five percent. Simulations suggest that a four-column PSA unit produced upgraded gas with 98% methane purity, achieving higher yield and lower energy consumption (Santos et al., 2011).

Expanding the number of columns increases the design complexity and installation costs. Hence, this complex design enables optimization in terms of energy required. Ongoing research in PSA technology is focused on several areas, including minimizing the size of PSA units, optimizing the technology for small-scale applications, reducing energy consumption, combining different adsorbents to enhance their properties, and integrating the separation of $H_2S$ and $CO_2$ into a single column (Grande et al., 2011; Maheshwary et al., 2012; Spoorthi et al., 2010).

The choice of adsorbent material is crucial for the performance of a PSA unit. The adsorbent is a porous solid material which has a high specific surface area. Commonly used adsorbents include activated carbons, natural and synthetic zeolites, silica gels, and carbon molecular sieves (CMS) (Alonso-Vicario et al., 2010; Grande et al., 2011). Adsorbents are generally classified into categories: equilibrium adsorbents and kinetic adsorbents. Equilibrium adsorbents have a much higher capacity for adsorbing $CO_2$ than methane like activated carbons and zeolites. In contrast, kinetic adsorbents have micropores that have adsorbed hydrocarbons smaller than the carbon dioxide molecules (Grande et al., 2011).

Adsorption isotherm diagrams include the relation of gas adsorption, as related to pressure, for a specific adsorbent. **Figure 4.6** shows adsorption isotherms of two generic adsorbents, I (1) and II (2). These isotherms indicate an equilibrium level of adsorption at certain pressures. During PSA operation, raw biogas is introduced into the column at the feed pressure, $P_{feed}$, where the adsorbents can retain certain amounts of carbon dioxide, $q_{feed,1}$ and $q_{feed,2}$. When equilibrium is reached, meaning the adsorbent is saturated with carbon dioxide, the pressure is reduced to $P_r$ to regenerate the adsorbent. Pressure drops through -desorption of carbon dioxide from the surface of the adsorbent to a new equilibrium at $q_{reg,1}$ and $q_{reg,2}$. The difference, $\Delta q$, is the amount of carbon dioxide separated during the cycle from the raw gas stream. Though adsorbent (2) has higher capacity for carbon dioxide adsorption at $P_f$, it is quite evident that adsorbent (1) will be the better choice for this process since $\Delta q_1$ is a lot larger than $\Delta q_2$. This indicates that an effective adsorbent should have a nearly linear isotherm. A steep initial curve requires the carbon dioxide to be desorbed at very low pressures to achieve efficient separation, which in turn increases the power consumption of the process (Grande et al., 2011).

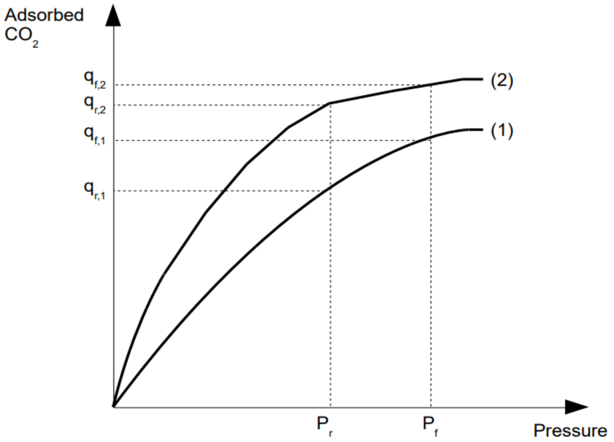

**Figure 4.6:** Two generic adsorbent isotherms. **Source:** Adapted from (Grande et al., 2011).

#### *4.3.3.4 Electrolyzer*

The $CO_2$ separated from the PSA unit undergoes a reaction with hydrogen to produce methane, thus reducing emissions. This phase of the study focuses on the production of hydrogen and its subsequent utilization to convert carbon dioxide generated from both the AD and HTL units into additional methane. This approach provides increased methane production and reduced greenhouse gas emissions, thereby increasing the sustainability of the integrated process.

These include the alkaline electrolysis and proton exchange membrane (PEM) system that have been commercialized. Alkaline electrolysis is rather an established technology in use since the 1920s in the production of hydrogen for fertilizer and chlorine industries (IEA, 2019). Alkaline electrolyzers with capacities of up to 165 MW were constructed during the last century. Most of them are out of operation, as steam methane reforming (SMR) became the leading technology in hydrogen production. Among the evident advantages of the use of alkaline electrolyzers is their relatively lower capital cost compared to PEM systems, since they do not require expensive metal catalysts (Li et al., 2016; Schmidt et al., 2017). Despite these merits, alkaline electrolysis also has a number of drawbacks, such as low current density-less than 0.45 $A/cm^2$-, low operating pressure-below 30 bar-, relatively larger system size, and expensive hydrogen production cost (Zeng & Zhang 2010). Furthermore, alkaline electrolyzers also face some problems under variable operation conditions, such as frequent start-ups or fluctuating power inputs. Additionally, operating outside a load range of 25 to 100% of their nominal capacity can adversely affect both system efficiency and the purity of the hydrogen and oxygen gases produced (Buttler & Spliethoff, 2018). Therefore, these shortcomings make alkaline electrolyzers less favorable where renewable energy sources, like solar and wind, are used, which often require the electrolyzer to adapt to changing power inputs.

On the contrary, PEM water electrolysis was developed to overcome the short comings of alkaline electrolysis (IEA, 2019). Unlike alkaline systems, these electrolyzers use pure water as an electrolyte. Hence, the recovery and recycling of corrosive potassium hydroxide required in alkaline electrolyzers are not required in the electrolyzers.

Industries are increasingly favoring PEM systems due to several advantages, including their compact design, high system efficiency (ranging from 52% to 69% LHV) even at high current densities (1–2 A/cm²), and their ability to respond quickly to changing power inputs. PEM electrolyzers can operate dynamically across a wide range (0–160% of nominal load) and function at low temperatures (20–80ºC), while also producing ultrapure hydrogen at elevated pressures (30–80 bar) (Buttler & Spliethoff, 2018; Carmo et al., 2013; Schmidt et al., 2017).

In the last years, there has been significant cost reduction in the stacks of PEM electrolyzers, thereby enabling much greater diffusion of this technology. Given its very good performance characteristics and competitive costs, PEM electrolysis will likely represent the main route for the production of sustainable hydrogen by 2030 (IEA, 2019; Schmidt et al., 2017).

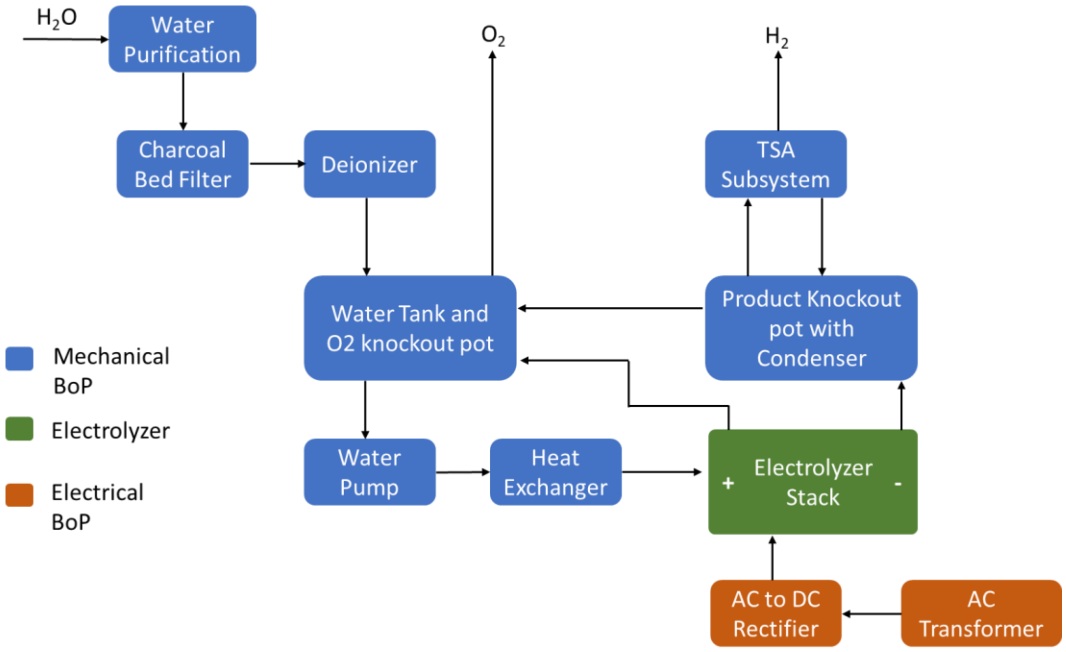

**Figure 4.7:** Block flow diagram of a PEM water electrolysis plant. **Source:** Adapted from (Peterson et al., 2020).

In our process, we considered the use of a large-scale PEM electrolysis plant consisting of electrolyzer stacks and mechanical and electrical balance of plant (BoP) components, as illustrated in **Figure 4.7**. The mechanical BoP comprises auxiliary components such as water purification systems, deionizers, pumps, heat exchangers, and the temperature swing adsorption (TSA) system. Knockout pots or liquid-vapor separators are also used to achieve high-purity separation of hydrogen and oxygen, typically higher than 99.9% (ISPT, 2022). The electrical BoP will also include the AC to DC rectifier, control systems, sensors, circuit breakers, and all other components needed.

At the moment, plants of large-scale water electrolysis are operational or under commissioning with scale capacities of up to 20 MW. Most importantly, a number of plants for PEM electrolyzers in the multi-megawatt scale are considered under various European programs such as the Haeolus program (Hydrogenics, 2.5 MW), H2Future (6 MW), and REFHYNE (ITM, 10 MW initially, with scale-up to 100 MW in phase 2). In addition, a 20 MW PEM electrolyser by Hydrogenics was also commissioned in Canada in January 2021 (Fuel Cells Bulletin, 2019). Several planned projects for the 2020-2025 period are awaiting final financing decisions at values of 50 MW to over 250 MW.

### *4.3.3.5 Methanation Unit*

The methanation process can be carried out in two types of reactors: biological and catalytic reactors. The methanation process involves several reactions. Most important reactions are the one that includes $CO_2$ hydrogenation (Equation (4.3)) and CO hydrogenation (Equation (4.4)). Several reactions took place during the process apart from the major one, like the reverse water-gas shift reaction (Equation (4.5)) and the Boudouard reaction (Equation (4.6)). The $CO_2$ hydrogenation process can be viewed as a combination of CO hydrogenation and the reverse water-gas shift reaction. Both of these reactions contribute to the overall conversion of $CO_2$ into methane.

$$CO_2\,(g) + 4\,H_2\,(g) \rightleftharpoons CH_4(g) + 2\,H_2O(g) \quad \Delta H_r^0 = -165.1\;kJ/mol \tag{4.3}$$

$$CO\,(g) + 3\,H_2\,(g) \rightleftharpoons CH_4(g) + \,H_2O(g) \quad \Delta H_r^0 = -206.3\;kJ/mol \tag{4.4}$$

$$CO_2\ (g) +\ H_2\ (g) \rightleftharpoons CO\ (g) +\ H_2O(g) \quad \Delta H_r^0 = +\,41.2\ kJ/mol \tag{4.5}$$

$$2\ CO\ (g) \rightleftharpoons C\ (s) + CO_2(g) \quad \Delta H_r^0 = -172.5\ kJ/mol \tag{4.6}$$

Both CO and $CO_2$ hydrogenation are highly exothermic reactions, which means that high temperatures can limit their conversion rates, particularly for $CO_2$.

Catalytic methanation reactors typically operate at 200–550°C and pressures of 1–100 bar. Metals such as Ni, Ru, Rh, and Co can serve as catalysts, but nickel is preferred for its high activity, $CH_4$ selectivity, and low cost (Mills & Steffgen, 1974; Vannice, 1976). However, nickel-based catalysts require high-purity feed gas, free from halogen and sulfur compounds (Barbarossa & Vanga, 2011; Bartholomew, 2001). The highly exothermic methanation reaction generates approximately 2 MW of heat per cubic meter of catalyst bed (compared to 0.6 $MW/m^3$ in methanol synthesis) at a GHSV of 5000 $h^{-1}$ and full $CO_2$ conversion. It is only possible to effectively operate temperature control in order to avoid thermodynamic limits and to prevent catalyst sintering. A number of reactor designs were developed, for example: fixed-bed, fluidized-bed, three-phase, and structured reactors. Fixed- and fluidized-bed reactors have already gained established technology status, but other designs are still under development.

Adiabatic fixed-bed reactors typically operate in series, with 2 to 5 reactors using intercooling and sometimes gas recirculation (Kiendl et al., 2014; Schaaf et al., 2014). In adiabatic operation, catalysts must withstand a wide temperature range (250–700°C), with key concerns being cracking and sintering (Bartholomew, 2001). Alternatively, cooled fixed-bed reactors can be used, featuring cooling tube bundles or plates (Kopyscinski et al., 2010; Buxbaum, 2013; Sterner & Stadler, 2014). While cooling simplifies the process setup compared to adiabatic systems, it increases reactor costs.

The mixing of solids in fluidized-bed reactors produces near-isothermal conditions that assist in operational control and allow effective heat removal, making the reactor design easier (Kopyscinski et al., 2011; Rönsch & Ortwein, 2011; Seemann et al., 2010). However, the intense mechanical load due to fluidization causes significant attrition to both catalyst and reactor walls, leading eventually to deactivation of the catalyst (Bartholomew, 2001). Also, $CO_2$ conversion might not be entirely due to bubbling. The reactor is also bounded by the superficial gas velocity; it should be high enough to fluidize but not so high that the catalysts are lost.

Three-phase reactors, such as slurry reactors, are another methanation approach (Götz et al., 2013a; Götz et al., 2013b; Lefebvre et al., 2015; Meng et al., 2015; Zhang et al., 2014). These reactors contain a liquid phase, typically heat transfer oils like Dibenzyltoluene, in which fine catalyst particles are suspended by the gas flow. Consequently, the liquid phase has a high heat capacity, which provides effective temperature control and almost isothermal operations, hence simplifying the design of the process. However, the challenges arise from gas-liquid mass transfer limitations and probable decomposition or evaporation of the suspension liquid (Götz et al., 2013a; Gotz, 2014; Götz et al., 2015; Lefebvre et al., 2015).

Structured reactors, like monolith reactors, have been developed to address the issues of temperature hot spots and high pressure drops in adiabatic fixed-bed reactors. Their internal metallic structure significantly improves radial heat transport, enhancing it by two to three orders of magnitude (Janke et al., 2014). Micro-structured reactors are the form of structured reactors that depict high compactness, offering high surface-area-to-volume ratios to make them more efficient in heat transfer and a low pressure drop too (Brooks et al., 2007 Görke et al., 2005 Liu et al., 2012 Müller et al., 2013). In the case of catalyst deposition on the metallic surface, challenges are faced. Replacing deactivated catalysts requires re-coating of the entire reactor.

An advanced development in structured reactors is the sorption-enhanced methanation concept. In this process, water generated during methanation is absorbed by the catalyst carrier, which has adsorbent properties. This reduces the thermodynamic limitations on the conversion rate. For removing the absorbed water, temperature swing and/or pressure swing, with or without purge gas, can be employed. A further innovation by Zurich University of Applied Sciences integrates water removal with a regeneration step, allowing the catalytic materials and microstructure to be renewed (Borgschulte et al., 2013; Walspurger et al., 2014).

#### *4.3.3.6 HTL Unit*

The digestate, a byproduct of the AD process, is fed as the feedstock for the HTL unit. The HTL system includes a batch reactor, heat exchangers, pumps, and a product separation unit. HTL unit was designed to convert the organic fraction of the digestate into biocrude, hydrochar, aqueous phase, and $CO_2$ gas (Van Doren et al., 2017).

The HTL section of the plant, illustrated in **Figure 4.8**, can process 2,963 tonnes of digestate per day for the base case scenario. Initially, the feedstock was pressurized to 2,900-3,000 psia and preheated to 288°C using a series of two double-pipe heat exchangers that recover heat from the liquid product mixture of biocrude and HTL-AP (Knorr et al., 2013). Following this, the digestate was further heated to the operating temperature of 300°C for 60 minutes using electricity and natural gas. The operating conditions of HTL unit were selected to maximize biocrude yield (Snowden-Swan et al., 2017). The gaseous product consists of primarily $CO_2$ and $C_1$-$C_5$ gases. The gaseous product may require scrubbing depending on local environmental regulations (Jones et al., 2014). The chemical mechanism involved in HTL process is in-depth discussed in **Chapter 2**. Post-reaction, the reactor effluent is directed to a hot filter where solids are removed. These solids comprise of 60-70% water, ash, char, and trace organics. Biocrude tends to become entrapped in these solids. The extent of loss of biocrude is dependent on the ash content of the feedstock. After the solids are separated, the remaining biocrude-aqueous-gas mixture is cooled to 60°C, depressurized to 30 psia, and separated in a three-phase separator (Snowden-Swan et al., 2017). The biocrude is collected, stored and sent to an upgrading facility for further refinement into a usable transportation fuel (Xu et al., 2018). Aqueous phase, which contains soluble organics, ammonia and metal salts, can undergo struvite precipitation to recover ammonia and may also be utilized as a substrate in the AD process (Watson et al., 2020).

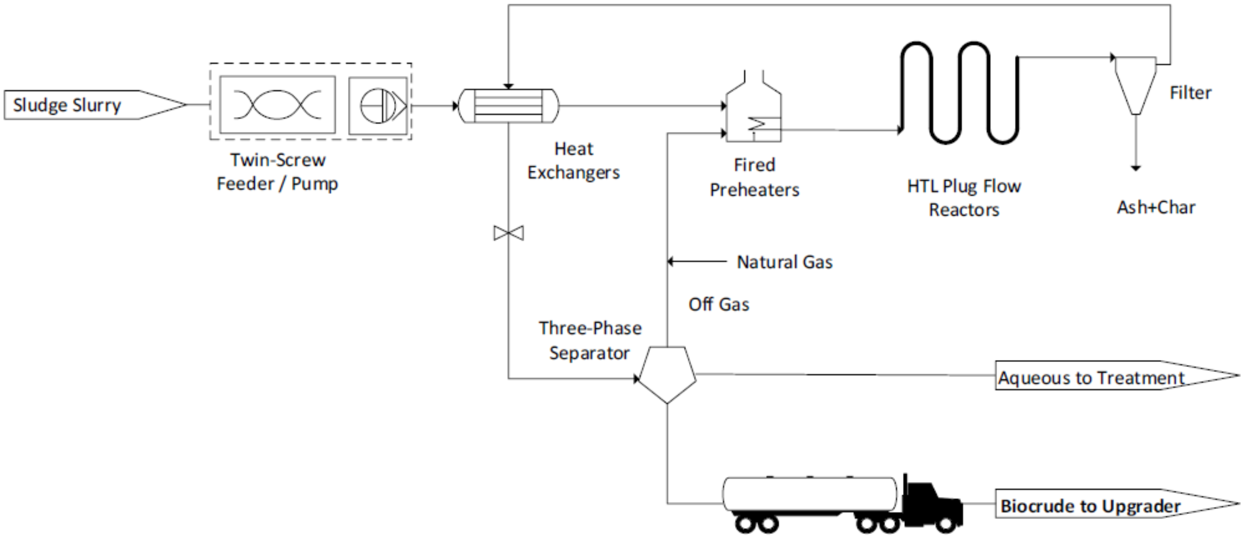

**Figure 4.8:** Process flow diagram of the HTL unit. **Source:** Adapted from (Snowden-Swan et al., 2017).

## 4.4 Process Inputs

The performance and product yields from AD and HTL product yields were derived from experimental results presented in Chapter 3. The experimental data yields a methane production rate of 562 L/kg of volatile solids fed (**Figure 4.9(a)**), which is consistent with the typical methane yield range of 300-600 L/kg-VS reported in the literature (Jenicek et al., 2012).

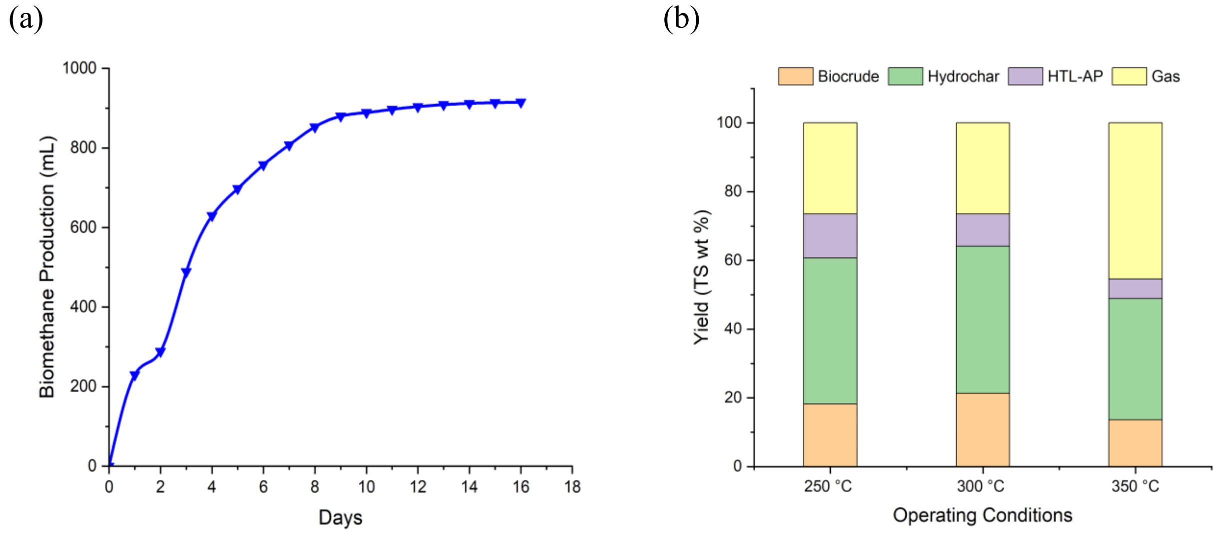

**Figure 4.9:** Experimental yield results of (a) AD, and (b) HTL process.

The yield assessment of biocrude, hydrochar, aqueous phase, and gaseous products (primarily $CO_2$) from HTL was experimentally determined using digestate as the feedstock. Product yields were expressed as a percentage of the total solids in the HTL feedstock. The resulting product distribution is depicted in **Figure 4.9(b)** with varying operating temperature. The retention time of these operating conditions was kept 60 minutes. As illustrated in **Figure 4.9(b)**, the biocrude yield reaches its peak at an operating temperature of 300°C. As a result, the operating conditions of 300°C for 60 minutes were chosen for HTL unit. Elemental analysis was done to determine the higher heating value (HHV) of biocrude. From that, the HHV for the biocrude was calculated at 0.0357 GJ/kg (Tatla et al., 2024).

Extensive sensitivity analysis was done to establish the project's sensitivity in respect of economic fluctuations. This was done by changing various input parameters such as the discount rate, PS feedstock input, biogas yield, volatile content in PS feedstock, selling price of electricity and water, transport logistics, biocrude yield and selling price, hydrochar yield and selling price, and taxes/credits on carbon dioxide. The values used as input parameters for the best-case and worst-case scenarios were tabulated in **Table 4.2**.

**Table 4.2:** Detailed input parameters for the best and worst-case scenarios for all three cases.

| Parameters | Base Scenario | Best Scenario | Worst Scenario |
|---|---|---|---|
| PS feed rate (tonnes/yr) | 1100000 | 1650000 | 550000 |
| Biogas yield (L/kg-VS fed) | 562 | 843 | 261 |
| Electricity price ($/kWh) | 0.05 | 0.03 | 0.08 |
| Water price ($/m3) | 1.54 | 0.77 | 2.31 |
| Discount rate (%) | 8 | 4 | 12 |
| Transportation distance (km) | 5 | 2.5 | 7.5 |
| Transportation cost ($/km) | 4.02 | 2.01 | 6.03 |
| Volatile Content in PS (%) | 2.5 | 3.75 | 1.25 |
| Biocrude yield (%) | 21.3 | 31.95 | 10.65 |
| Biocrude selling price ($/GJ) | 51.00 | 76.50 | 25.50 |
| Hydrochar yield (%) | 42.80 | 64.20 | 21.40 |
| Hydrochar selling price ($/kg) | 0.09 | 0.13 | 0.04 |
| CO2 taxes ($/t-CO2) | 80 | 40 | 120 |

Based on literature review, electricity and water prices were anchored at \$0.05/kWh and \$1.54/m³, respectively (Fang & Xu, 2014; Herter & Wayland, 2010).

## 4.5 Economic Input Parameters and TEA Methodology

### *4.5.1 Capital expenditure (CAPEX)*

The Purchased Equipment Cost (PEC) of the AD system and bio-desulfurization unit components was estimated based on cost correlations given in **Table 4.3**. Suitable exchange ratio (ER) adjustments were accordingly made to the reference year 2020 for inflation. ER is calculated by taking the ratio of the equipment cost index over the reference cost index (Sanaye et al., 2020). To account against the installation and other incidental expenses, 30% of the PEC was added to calculate the total fixed capital investment (FCI) (Amigun & Von Blottnitz, 2009).

**Table 4.3:** Cost equations and exchange ratios of various equipment in the AD unit.

| Equipment Title | Reference year | Cost equation (\$) | Capacity unit | Reference |
|---|---|---|---|---|
| Feed storage tank | 2003 | $10^{[4.8509-0.3973\,Vst\ +0.1445\,(Vst)^{2}]}$ | $m^3$ | (Turton et al., 2008) |
| Feed heat exchanger | 2005 | $32800 \times \frac{(A}{80)}^{0.68} \times \frac{(661.7}{370.6)} \times 6.4$ | $m^2$ | (Sanaye et al., 2020) |
| Feed pump | 2011 | $3540 \times W_p^{0.71}$ | KW | (Mirmasoumi et al., 2018) |
| Anaerobic digester | 2016 | $840221.55 \times \frac{(V_{AD}}{3000)}^{0.8}$ | $m^3$ | (Mirmasoumi et al., 2018) |
| Digestate storage tank | 2003 | $10^{[4.8509-0.3973\,Vst\ +0.1445\,(Vst)^{2}]}$ | $m^3$ | (Turton et al., 2008) |
| Gravel filter | 2011 | $0.01 \times Cost_{Desulphurization}$ | \$ | (Sanaye & Yazdani, 2022) |
| Desulfurization unit | 2011 | $\frac{(1}{1.12) \times 15974.13 \times V_{biogas}^{0.3555}}$ | $m^3/h$ | (Allegue & Hinge, 2014) |
| Flare stack | 2013 | $4600 \times V_{biogas}^{0.61}$ | $ft^3/min$ | Anon (2017) |

| | | | | |
|---|---|---|---|---|
| Gas storage tank | 2012 | $\frac{(1}{1.12)\times V_{gst}}$ | $m^3$ | (Petrollese & Cocco, 2020) |
| $V_{st}$: Volume of storage tank; $A$: surface area; $W_p$: Work done by pump; $V_{AD}$: Volume of anaerobic digester; $Cost_{Desulphurization}$: Cost of desulphurization unit; $V_{biogas}$: Biogas flow rate; $V_{gst}$: Volume of gas storage tank. | | | | |

The capital investment for the PSA unit was determined using a biogas capacity-specific investment cost curve depicted in **Figure 4.10**. The capital investment cost includes equipment cost and its installation (Bauer et al., 2013).

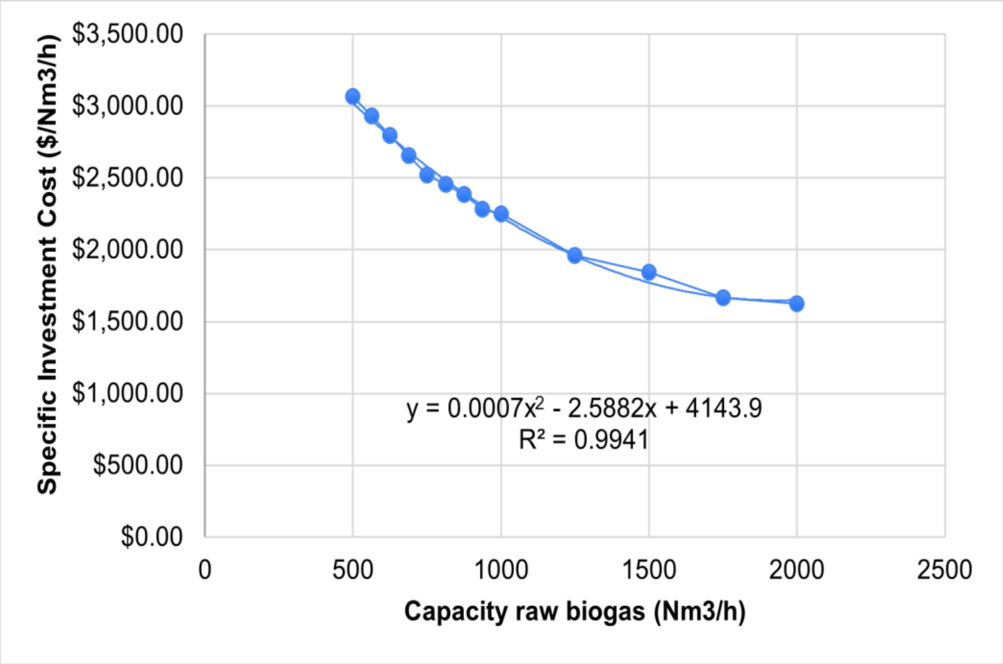

**Figure 4.10:** Specific investment cost for PSA upgrading units. **Source:** Adapted from (Urban et al., 2009).

There have been various TEA studies based on the cost of PEM water electrolysis process. The hydrogen production cost was determined by various factors like capital cost of the electrolyzer, its conversion efficiency (kWh/$kg_{H2}$), electricity costs, and annual operating hours (Bellotti et al., 2022). The capital cost of electrolyzer was based on bottom-up cost estimates or quotes/inquiries from electrolyzer manufacturers (Reksten et. al, 2022). The resulting plant cost (in $/kW) for PEM electrolyzers is shown in **Figure 4.11** and was based on the following co-relation:

$$C = \left(k + \frac{k}{Q} Q^{\alpha}\right)\left(\frac{V}{V^{0}}\right)^{\beta} \tag{4.7}$$

where, C is the electrolyzer plant cost per kW, $k_0$ and k are fitting constants, Q is the electrolyzer plant capacity and V and $V_0$ are plant installation year and reference year, respectively. α and β are fitting constants and are usually referred to as a scaling factor and learning factor, respectively. For PEM electrolyzers, $\alpha = 0.622$, $\beta = -158.9$, $k = 9458.2$, $k_0 = 585.85$ and $V_0 = 2020$ (Reksten et al., 2022). **Figure 4.11** provides CAPEX estimates for different electrolyzer sizes, indicating that scaling the electrolyzer size leads to CAPEX reductions.

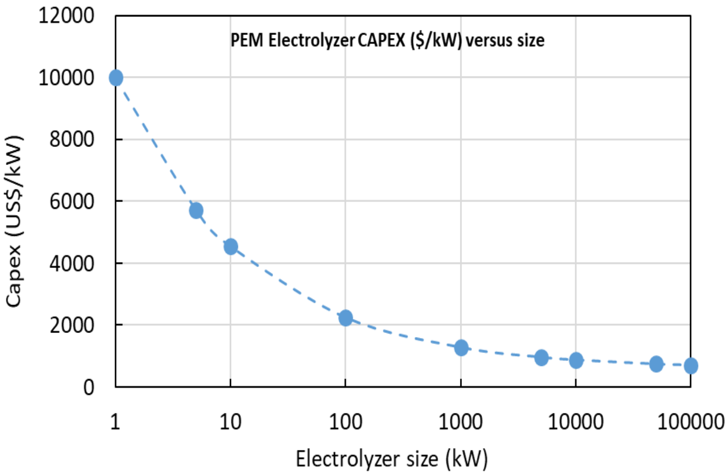

**Figure 4.11:** CAPEX versus size of the electrolyzer. **Source:** Adapted from (Reksten et al., 2022).

The most accurate capital investment for catalytic methanation was provided by Outotec GmbH. A correlation between methane output power and capital costs was provided by them. The base capital cost of the methanation unit was estimated at €2,000,000 for a methane production capacity of 5 MW (Graf et al., 2014; Van Leeuwen & Zauner, 2018). A non-linear cost function was utilized to estimate the capital expenditure of the methanation unit (**Equation (4.8)**). A scaling factor of 0.7 was incorporated in the equation. Furthermore, inflation adjustments were included to refine cost estimates.

$$\frac{Capital\ cost\ (Methanation\ Unit)_x}{Capital\ cost\ (Methanation\ Unit)_5} = \left(\frac{x}{5}\right)^{0.7} \times ER \tag{4.8}$$

where, $x$ represents the methane production (MW) from the methanation unit and ER accounts for the exchange ratio.

HTL process has been researched for bench- and pilot-scale. It has not been subjected to full-scale commercialization. The capital cost was estimated by a correlation with dry feed rate (Snowden-Swan et al., 2017). The base capital cost of the HTL unit for a dry feed rate of 8299 kg/h was determined to be \$11,340,000 (Knorr et al., 2013; Snowden-Swan et al., 2017). A non-linear cost function was utilized to estimate the capital expenditure of the HTL unit (**Equation (4.9)**). A scaling factor of 0.6 was incorporated in the equation. Furthermore, inflation adjustments factor known as the exchange ratio (ER) was applied to the estimated capital cost.

$$\frac{Capital\ cost\ (HTL\ Unit)_x}{Capital\ cost\ (HTL\ Unit)_{8299}} = \left(\frac{x}{8299}\right)^{0.6} \times ER \tag{4.9}$$

where, $x$ represents the dry feed rate (kg/h) entering the HTL unit and ER accounts for the exchange ratio.

### *4.5.2 Operating & Maintenance (O & M) costs*

AD is a well-established and mature technology. The annual O&M costs were estimated at 2% of the FCI. The O&M expenses are generally lower due to the reduced need for frequent maintenance and consistent performance (Aui & Wright, 2014).

The operating costs for the PSA and methanation units were computed from their respective electricity requirements. The total electricity consumption was reported in between 0.15 and 0.3 kWh/Nm³ (Bauer et al., 2013). The electricity consumption for the upgrading process for raw biogas was around 0.2 kWh/Nm³. The cost for drying and final compression was estimated to be 0.17 kWh/Nm³ (Pertl et al., 2010). The Swedish PSA units indicated an energy demand between 0.25 and 0.3 kWh/Nm³. The lowest energy consumption values are due to utilization of external cooling water. In contrast, slightly higher values are due to cooling machines. Additionally, incorporation of a catalytic oxidizer can increase energy demand to 0.3 kWh/Nm³ (Bauer et al., 2013).

However, the literature does not document much on operational costs for methanation reactors. Guilera et al. (2021) have provided an estimate for the electricity consumption of methanation reactors. The O&M cost of the methanation reactor amounts to 0.111 kWh per kWh methane produced.

A capital recovery factor-based methodology was used to calculate annual maintenance costs for the bio-desulfurization, PSA, and methanation units. This approach involved firstly calculating the equivalent annual investment cost. Then, it is subsequently multiplied by a maintenance factor (MF) to estimate annual expenditures. **Equations (4.10-4.12)** were employed for these computations:

$$Capital\ recovery\ factor\ (CRF) = \frac{i(1+i)^n}{(1+i)^n - 1} \tag{4.10}$$

$$Equivalent\ annual\ investment\ cost\ \left(\frac{\$}{year}\right) = PEC\ \times CRF \tag{4.11}$$

$$Annual\ maintenance\ cost\ \left(\frac{\$}{year}\right) = Equivalent\ annual\ investment\ cost\ \times MF \tag{4.12}$$

where, i denotes the annual interest rate of 8% for base case scenario, n represents the plant lifetime (years), PEC signifies the purchased equipment cost ($), CRF is the capital recovery factor, and MF is the maintenance factor (Sanaye et al., 2020). A maintenance factor of 0.06 was applied to estimate maintenance and repair costs (Fang & Xu, 2014).

A detailed energy balance was performed for the PEM electrolyzer to assess both its energy and water requirements. The OPEX of the electrolyzer includes several cost components: electricity costs for the stack and balance of the plant, stack replacement costs, water costs, and annual operation and maintenance costs (labor, maintenance, insurance, taxes) (Reksten et al., 2022). The total OPEX for the electrolyzer was estimated by calculating these key components. Stack replacement was estimated at 15% of installed capital cost. Additionally, O&M costs were estimated at 3% of uninstalled capital costs (Buttler & Spliethoff, 2018; Peterson et al., 2020).

Annual O&M costs for the HTL unit included electricity use, external heat addition, labor needs and component maintenance. The base case O&M cost for the HTL unit was estimated at $2,760,000 at a dry feed rate of 8299 kg/h.

### *4.5.3 Transportation costs*

PS transportation from the WWTF to the three proposed plants was included in the overall cost analysis. For the base case scenario, a transportation distance of 5.0 km between the WWTF and the plant was assumed. The associated transportation costs, encompassing both fixed and variable components, were estimated at $ 4.02 per kilometer for a 30-ton PS load (Tesfamariam et al., 2020). Annual truck trips were determined by dividing the annual sludge feed rate by the truck capacity.

### *4.5.4 TEA Methodology*

A discounted cash flow (DCF) model was developed in Microsoft Excel to evaluate the financial viability of the project. Contingency was accounted to cover unexpected expenses and uncertainties during project execution. It was estimated to be 20% of the FCI (James et al., 2009). Additionally, working capital was allocated to finance day-to-day operational expenses to ensure smooth and continuous operations. Working capital is typically set at 15% of the FCI, (James et al., 2009).

This analysis includes estimation of levelized cost of energy (LCOE). LCOE is a key indicator of the project's economic feasibility. It represents the breakeven selling price of methane for which the project becomes viable. It was estimated by setting the NPV to zero in the DCF model. Thus, LCOE ($/GJ) represents the minimum methane selling price to recover the fixed infrastructure investment. Case 3 was a computation of its LCOE, with revenues accounted for from both biocrude and hydrochar.

The discount rate is a critical parameter that reflects time value of money and risk profile of the project in DCF modeling. It is used as a benchmark for comparing future cash flows to their present value. It was varied in the sensitivity analysis to compute varying risk scenarios. A base case discount rate of 8% was applied for present value calculations in the economic analysis (Jouny et al., 2018). The parameters listed in **Table 4.4** were kept constant throughout the economic analysis for three different cases.

**Table 4.4:** Economic parameters for techno economic analysis.

| Economic parameters | Value unit | Value | Reference |
|---|---|---|---|
| Plant lifetime | years | 20 | (Matute et al., 2019) |

|  |  |  |  |
|---|---|---|---|
| Annual working days | days | 350 | (Jouny et al., 2018) |
| Depreciation lifetime | years | 10 | (Steward et al., 2012) |
| Tax rate | % | 35.0 | (Dodge, 2024) |
| Contingency | % of FCI | 20 | (James et al., 2009) |
| Salvage value | % of FCI | 12 | (Jouny et al., 2018) |
| Working/startup capital | % of FCI | 15 | (James et al., 2009) |
| Number of plant staff | - | 10 | (James et al., 2009) |
| Staff salary cost | $/hour | 25.00 | - |

## 4.6 Environmental Impact

Calculations of GHG emissions were performed in order to track the effect of each proposed case on the environment. In this regard, all emissions due to the consumption of electricity, on-site $CO_2$, and on-site fugitive methane are considered. The amount of $CO_2$ emitted related to the use of grid electricity is calculated using an emission factor (EF) of 0.110 kg $CO_2$/kWh. These are the average emissions from the Canadian grid (C.E.R., 2024). Fugitive emissions were also added due to the production and use of natural gas in the plant. For this, a methane leak rate of 2% was assumed to calculate these emissions. **Equations (4.14 – 4.16)** were used to evaluate these emissions. The total GHG emissions were calculated by summing all these emissions.

$$Electricity\ emissions\ \left(\frac{kg\ CO_2}{GJ\ CH_4}\right) = Electricity\ consumption\ (kWh) \times EF \tag{4.14}$$

$$On-site\ CO_2\ emissions\ \left(\frac{kg\ CO_2}{GJ\ CH_4}\right) = \frac{Annual\ CO_2\ emissions\ (kg)}{Annual\ Methane\ production\ (GJ)} \tag{4.15}$$

$$On-site\ fugitive\ CH_4\ emissions\ \left(\frac{kg\ CO_2}{GJ\ CH_4}\right) = \frac{CH_4\ production\ \left(\frac{kg}{yr}\right) \times MER\ \times GWP}{Annual\ Methane\ production\ (GJ)} \tag{4.16}$$

where, *EF* denotes the grid electricity emission factor in kg CO2 emissions per kWh, MER depicts methane emission rate (%), and GWP represents global warming potential, which accounts for 28 g $CO_2$-eq/ g $CH_4$) (Canada, E. and C. C., 2024).

## 4.7 $CO_2$ taxes/ credits

In order to bring down the level of emission and reduce pollution, the carbon pricing policies, otherwise known as output-based-pricing systems, have been adopted by the government. The threshold value for $CO_2$ emission has been set to 10.6 tonnes -$CO_2$ per 100,000 $m^3$ of $CH_4$ produced (*Consolidated federal laws of Canada*, 2024). If the emissions are less than this threshold value, the difference would be considered as credits and if vice- versa, the difference would be counted as $CO_2$ taxes. The carbon pricing of $ 80/ tonne is considered to calculate these taxes/credits (Dion & Linden-Fraser, 2024).

## 4.8 Results & Discussion

### *4.8.1 Product recovery and electricity requirement for base case scenario*

For each of the three suggested base case scenarios, a thorough mass and energy balance was performed. These calculations were used to quantify inputs, outputs, and electricity consumption of each equipment. The whole process efficiency was evaluated by analyzing the electricity requirements and product recovery. As mentioned in **section 4.3.3.1**, the composition of the biogas produced from sludge was derived from Sanaye & Yazdani (2022). The accompanying **tables** provide in- depth detail of the mass flow rates entering, exiting, distribution of products in each unit. **Table 4.5** outlines the comprehensive mass balance of the equipment involved in the Case 1 scenario.

**Table 4.5:** Detailed material balance for the proposed Case 1 base scenario.

1. AD Unit

| AD unit | | | Reference/ Notes |
|---|---|---|---|
| Primary sludge feed input rate | 1100000 | tonnes/year | Assumption |
| Volatile content in primary sludge | 2.5 | % | (Dereli et al., 2009; Markis et al., 2016) |
| | 0.872 | kg/sec | |
| Biogas production | 562 | L/kg-Vs fed | |

|  |  |  |  |
|---|---|---|---|
|  | 490.07 | Litre/sec | Experimental results & density of biogas calculated at T = 36°C & P = 1.013 bar (Sanaye & Yazdani, 2022) |
|  | 0.59 | kg/sec |  |
| Digestate production | 34.29 | kg/sec |  |

| **Biogas exiting the AD unit** |  |  |  |
|---|---|---|---|
| Composition | Mass (kg/sec) | Weight (%) | Weight fraction |
| $CH_4$ | 0.255 | 43.325 | 0.43325 |
| $CO_2$ | 0.300 | 50.841 | 0.50841 |
| $H_2$ | 0.000 | 0.001 | 0.00001 |
| $H_2O$ | 0.028 | 4.710 | 0.04710 |
| $H_2S$ | 0.003 | 0.425 | 0.00425 |
| $N_2$ | 0.004 | 0.698 | 0.00628 |
| $O_2$ | 0 | 0 | 0 |
| Average molecular weight |  | 30.514 | g/mol |

## 2. Gravel filter

| **Gravel filter** |  |  | **Reference/ Notes** |
|---|---|---|---|
| Biogas inlet | 0.589 | kg/sec |  |
| Water loading efficiency | 33 | % | (Sanaye & Yazdani, 2022) |
| Water trap outlet | 0.009 | kg/sec |  |
| Biogas outlet | 0.580 | kg/sec |  |

| **Biogas exiting the gravel filter** |  |  |  |
|---|---|---|---|
| Composition | Mass (kg/sec) | Weight (%) | Weight fraction |

| | | | |
|---|---|---|---|
| $CH_4$ | 0.255 | 44.009 | 0.44009 |
| $CO_2$ | 0.300 | 51.644 | 0.51644 |
| $H_2$ | 0.000 | 0.001 | 0.00001 |
| $H_2O$ | 0.019 | 3.206 | 0.03206 |
| $H_2S$ | 0.003 | 0.432 | 0.00432 |
| $N_2$ | 0.004 | 0.709 | 0.00709 |
| $O_2$ | 0 | 0 | 0 |
| Average molecular weight | | 30.711 | g/mol |

## 3. Bio- desulfurization Unit

| **Bio- desulphurization unit** | | | **Reference/ Notes** |
|---|---|---|---|
| $H_2S + \frac{5}{2} O_2 \rightarrow SO_4 + H_2O$ | | | (Zhuo et al., 2022) |
| Biogas inlet | 0.580 | kg/sec | |
| $H_2S$ in biogas | 0.003 | kg/sec | |
| Oxygen required for reaction | 0.006 | kg/sec | |
| Excess oxygen added | 2 | Times | (Khoshnevisan et al., 2017) |
| Total oxygen added | 0.018 | kg/sec | |
| Air required | 0.077 | kg/sec | Weight distribution of air: Oxygen= 23%; Nitrogen= 76%; & Other gases: 1% |
| $H_2S$ removal efficiency | 98 | % | (Haosagul et al., 2020a; Zhuo et al., 2022) |
| $SO_4$ formation | 0.0069 | kg/sec | |
| $H_2O$ formation | 0.0013 | kg/sec | |
| Sulfur tank concentration | 2100 | mg/l | (Sposob et al., 2021) |
| 1 kg of $SO_4$ = | 476.19 | kg of $H_2O$ | |

| | | | |
|---|---|---|---|
| Water required | 3.2936 | kg/sec | |
| Make up water/ input | 3.2923 | kg/sec | (Sposob et al., 2021) |
| Slurry output | 3.3006 | kg/sec | |
| Bio- desulfurization gas outlet | 0.649 | kg/sec | |

| **Biogas exiting the bio- desulphurization unit** | | | |
|---|---|---|---|
| Composition | Mass (kg/sec) | Weight (%) | Weight fraction |
| $CH_4$ | 0.255 | 39.418 | 0.39418 |
| $CO_2$ | 0.300 | 46.257 | 0.46257 |
| $H_2$ | 0.000 | 0.001 | 0.00001 |
| $H_2O$ | 0.019 | 2.871 | 0.02871 |
| $H_2S$ | 0.000 | 0.008 | 0.00008 |
| $N_2$ | 0.062 | 9.630 | 0.09630 |
| $O_2$ | 0.012 | 1.815 | 0.01815 |
| Average molecular weight | | 30.479 | g/mol |

## 4. Gas storage

| **Gas storage** | | | **Reference/ Notes** |
|---|---|---|---|
| Biogas inlet | 0.649 | kg/sec | |
| Water loading efficiency | 33 | % | (Sanaye & Yazdani, 2022) |
| Water trap outlet | 0.006 | kg/sec | |
| Biogas outlet | 0.642 | kg/sec | |

| **Biogas exiting the gas storage** | | | |
|---|---|---|---|
| Composition | Mass (kg/sec) | Weight (%) | Weight fraction |

| | | | |
|---|---|---|---|
| $CH_4$ | 0.255 | 39.80 | 0.39796 |
| $CO_2$ | 0.300 | 46.70 | 0.46700 |
| $H_2$ | 0.000 | 0.001 | 0.00001 |
| $H_2O$ | 0.012 | 1.94 | 0.01941 |
| $H_2S$ | 0.000 | 0.008 | 0.00008 |
| $N_2$ | 0.062 | 9.72 | 0.09723 |
| $O_2$ | 0.012 | 1.83 | 0.01832 |
| Average molecular weight | | 30.598 | g/mol |

5. PSA Unit

| **PSA unit** | | | **Reference/ Notes** |
|---|---|---|---|
| Biogas inlet | 0.642 | kg/sec | |
| Methane outlet | 0.256 | kg/sec | Assumption (100% separation) |
| $CO_2$ outlet | 0.300 | kg/sec | Assumption (100% separation) |
| Other gases outlet | 0.087 | kg/sec | Assumption (100% separation) |

A comprehensive mass balance of the equipment of Case 2 is shown in Table **4.6**. The case 2 involves integration of methanation unit to the Case 1 configuration. The mass balance for other equipment remains consistent with that of Case 1.

**Table 4.6:** Detailed material balance of methanation unit of Case 2 configuration.

| **Methanation unit** | | | **Reference/ Notes** |
|---|---|---|---|
| $CO_2$ input | 0.300 | kg/sec | Assumption (100% conversion) |
| $H_2$ input | 0.055 | kg/sec | |
| $CH_4$ produced | 0.109 | kg/sec | |

|  |  |  |  |
|---|---|---|---|
| $H_2O$ produced | 0.246 | kg/sec |  |

An in- detailed mass balance of all equipment involved in Case 3 is presented in **Table 4.7**. Case 3 includes incorporation of a HTL unit to proposed Case 2 process. The mass flow rate in methanation and HTL unit is discussed thoroughly in this section. However, the mass flow rate of other equipment remains consistent with that of Case 1.

**Table 4.7:** Detailed material balance of methanation and HTL unit of Case 3 configuration.

6. Methanation Unit

| **Methanation unit** |  |  | **Reference/ Notes** |
|---|---|---|---|
| $CO_2$ input | 0.641 | kg/sec | Assumption (100% conversion) |
| $H_2$ input | 0.118 | kg/sec |  |
| $CH_4$ produced | 0.234 | kg/sec |  |
| $H_2O$ produced | 0.525 | kg/sec |  |

7. HTL Unit

| **HTL unit** |  |  |  | **Reference/ Notes** |
|---|---|---|---|---|
| Digestate input |  | 34.29 | kg/sec |  |
| Total solid content in digestate |  | 3.75 | % | (Dereli et al., 2009; Markis et al., 2016) |
|  |  | 1.286 | kg/sec |  |
| Output | Yield (TS wt. %) |  |  |  |
| Biocrude | 21.3 | 0.274 | kg/sec | Experimental results (**Figure 4.9 (b)**) |
| Hydrochar | 42.80 | 0.550 | kg/sec |  |
| Gases | 26.50 | 0.341 | kg/sec |  |
| HTL- AP | 0.121 | 0.121 | kg/sec |  |
| $H_2O$ |  | 33.005 | kg/sec |  |
| Total HTL-AP |  | 33.126 | kg/sec |  |

Extended energy balance was performed for each equipment against three proposed configurations to judge the electricity demand. In the **Tables** below, careful analysis of the energy dynamics for each unit is performed, with the aim of depicting aspects that can still be optimized for further overall energy efficiency in integrated operations. The general electricity consumption of equipment in Case 1 is provided in **Table 4.8**.

**Table 4.8:** Detailed electricity consumption of the equipment in the Case 1 configuration.

a) Sludge pump

| **Electricity consumption of sludge pump** | | | **Reference/ Notes** |
|---|---|---|---|
| Change in pressure across pump | 1.8 | Bar | (Sanaye & Yazdani, 2022) |
| Primary sludge feed input rate | 34.88 | kg/sec | |
| Recirculation line flow rate | 69.76 | kg/sec | (Meister et al., 2018) |
| Total flow rate | 104.64 | kg/sec | |
| Density of primary sludge | 1020.8 | kg/m$^3$ | Experimental results |
| Power required | 18.45 | KW | |
| Electricity consumption | 442.84 | kWh/day | |

b) Anaerobic Digester

| **Electricity consumption of anaerobic digester** | | | **Reference/ Notes** |
|---|---|---|---|
| Primary sludge inlet flow rate | 125.57 | tonnes/hour | |
| Power requirement | 0.85 | kWh/tonnes | (Ranieri et al., 2021) |
| | 106.7 | KW | |
| Electricity consumption | 2561.64 | kWh/day | |

c) Bio- desulfurization blower

| **Electricity consumption of bio- desulfurization blower** | | | **Reference/ Notes** |
|---|---|---|---|
| Pressure at inlet | 1.01 | Bar | (Sanaye & Yazdani, 2022) |
| Pressure at outlet | 1.04 | Bar | (Sanaye & Yazdani, 2022) |
| Air flow rate | 0.077 | kg/sec | Based on mass balance calculations |
| Required air power | 2300.02 | Watt | Air power (Watts) = Flow rate (kg/sec) * Pressure difference (Pascals) |
| Electrical efficiency | 87.5 | % | (Li et al., 2024) |
| Mechanical power required | 2.629 | KW | Mechanical power = Air power/ electrical efficiency |
| Electricity consumption | 63.09 | kWh/day | |

d) Bio- desulfurization unit pump and heat exchanger

| **Electricity consumption of bio- desulfurization unit pump and heat exchanger** | | | **Reference/ Notes** |
|---|---|---|---|
| Biogas inlet flow rate | 0.580 | kg/sec | |
| Air inlet flow rate | 0.077 | kg/sec | |
| Density of biogas & air mixture | 1.2178 | kg/$m^3$ | Based on mass balance calculations |
| Power requirement | 0.01 | kWh/N $m^3$ | (Sanaye & Yazdani, 2022) |
| | 19.4 | KW | |
| Electricity consumption | 466.05 | kWh/day | |

e) PSA blower

| **Electricity consumption of PSA blower** | **Reference/ Notes** |
|---|---|

| | | | |
|---|---|---|---|
| Pressure at inlet | 1.03 | Bar | (Liu et al., 2011) |
| Pressure at outlet | 1.1 | Bar | (Liu et al., 2011) |
| Biogas flow rate | 0.642 | kg/sec | |
| Required power | 44967.87 | Watt | Air power (Watts) = Flow rate (kg/sec) * Pressure difference (Pascals) |
| Electrical efficiency | 87.5 | % | (Li et al., 2024) |
| Mechanical power required | 51.392 | KW | Mechanical power = Air power/ electrical efficiency |
| Electricity consumption | 1233.40 | kWh/day | |

f) PSA Unit

| **Electricity consumption of PSA unit** | | | **Reference/ Notes** |
|---|---|---|---|
| Biogas inlet flow rate | 0.642 | kg/sec | |
| Density of biogas | 1.2059 | kg/m$^3$ | Based on mass balance calculations |
| Power requirement | 0.3 | kWh/N m$^3$ | (Bauer et al., 2013) |
| | 575.3 | KW | |
| Electricity consumption | 13807.58 | kWh/day | |

**Table 4.9** presents a detailed energy balance of the equipment specific to Case 2, integrated within the baseline Case 1, with particular emphasis on the electrolyzer and methanation unit. The energy balance for other equipment remains consistent with that of Case 1.

**Table 4.9:** Detailed electricity consumption of the equipment in the Case 2 configuration.

g) Electrolyzer

| **Electricity consumption of electrolyzer** | | | **Reference/ Notes** |
|---|---|---|---|
| Operating current density | 2 | A/cm$^2$ | (Badgett et al., 2024) |
| Operating voltage | 1.9 | V | (Badgett et al., 2024) |
| Moles e-/day | 4.76E+06 | | |

| | | | |
|---|---|---|---|
| Total electrons in system per day | 2.8662E+30 | e-/day | |
| Total charge per day | 4.5859E+11 | Coulomb/day | |
| Charge per second | 5.3078E+06 | Total Amps | |
| Area of electrolyzer | 2653890.5 | cm$^2$ | |
| | 265.4 | m$^2$ | |
| Total land area | 1326.95 | m$^2$ | |
| Cell active area | 700 | cm$^2$ | (Peterson et al., 2020) |
| Number of cells | 3791 | | |
| BoP electrical usage | 5.4 | kWh/kg | (Peterson et al., 2020) |
| | 1070.7 | KW | |
| Stack capacity | 10084.8 | KW | |
| Power requirement | 11155.5 | KW | |
| Electricity consumption | 267732.1 | kWh/day | |

h) Methanation Unit

| **Electricity consumption of methanation unit** | | | **Reference/ Notes** |
|---|---|---|---|
| Higher heating value of methane | 0.0555 | GJ/kg | (Kassem et al., 2020b) |
| Methane production | 0.365 | kg/sec | |
| | 486161 | kWh/day | |
| Electricity consumption | 0.111 | kWh/kWh of $CH_4$ produced | (Guilera et al., 2021) |
| | 53964 | kWh/day | |

**Table 4.10** presents a detailed energy balance of the equipment specific to Case 3, integrated within the baseline Case 1 scenario, with particular emphasis on the electrolyzer, methanation, and HTL unit. The energy balance for other equipment remains consistent with that of Case 1.

**Table 4.10:** Detailed electricity consumption of the equipment in the Case 3 configuration.

a) Electrolyzer

| Electricity consumption of electrolyzer | | | Reference/ Notes |
|---|---|---|---|
| Operating current density | 2 | A/cm$^2$ | (Badgett et al., 2024) |
| Operating voltage | 1.9 | V | (Badgett et al., 2024) |
| Moles e-/day | 1.02E+07 | | |
| Total electrons in system per day | 6.1219E+30 | e-/day | |
| Total charge per day | 9.7951E+11 | Coulomb/day | |
| Charge per second | 1.1337E+07 | Total Amps | |
| Area of electrolyzer | 5668459.6 | cm$^2$ | |
| | 566.8 | m$^2$ | |
| Total land area | 2834.23 | m$^2$ | |
| Cell active area | 700 | cm$^2$ | (Peterson et al., 2020) |
| Number of cells | 8098 | | |
| BoP electrical usage | 5.4 | kWh/kg | (Peterson et al., 2020) |
| | 2287.0 | KW | |
| Stack capacity | 21540.1 | KW | |
| Power requirement | 23827.1 | KW | |
| Electricity consumption | 571850.5 | kWh/day | |

b) Methanation Unit

| Electricity consumption of methanation unit | | | Reference/ Notes |
|---|---|---|---|
| Higher heating value of methane | 0.0555 | GJ/kg | (Kassem et al., 2020b) |
| Methane production | 0.465 | kg/sec | |
| | 619181.90 | kWh/day | |

|  |  |  |  |
|---|---|---|---|
| Electricity consumption | 0.111 | kWh/kWh of $CH_4$ produced | (Guilera et al., 2021) |
|  | 68729.19 | kWh/day |  |

c) HTL Unit

| Electricity consumption of HTL unit |  |  | Reference/ Notes |
|---|---|---|---|
| Digestate flow rate | 34.291 | kg/sec |  |
| Total solid content | 3.75 | % | (Dereli et al., 2009; Markis et al., 2016) |
| Digestate dry flow rate | 1.286 | kg/sec |  |
|  | 4629 | kg/hour |  |
| Electricity consumption | 0.02 | kWh/kg-dry feed | (Snowden-Swan et al., 2017) |
|  | 2276.80 | kWh/day |  |
| Natural gas requirement for heating purposes | 0.0011 | GJ/kg-dry feedrate | (Snowden-Swan et al., 2017) |
|  | 40,838.5 | GJ/year |  |

Based on these in-depth material and energy balance analysis for each unit, a detailed assessment of the product recovery and electricity requirement was conducted. **Figure 4.12** provides a clear comparison of the product yields and energy demands for each case and equipment involved.

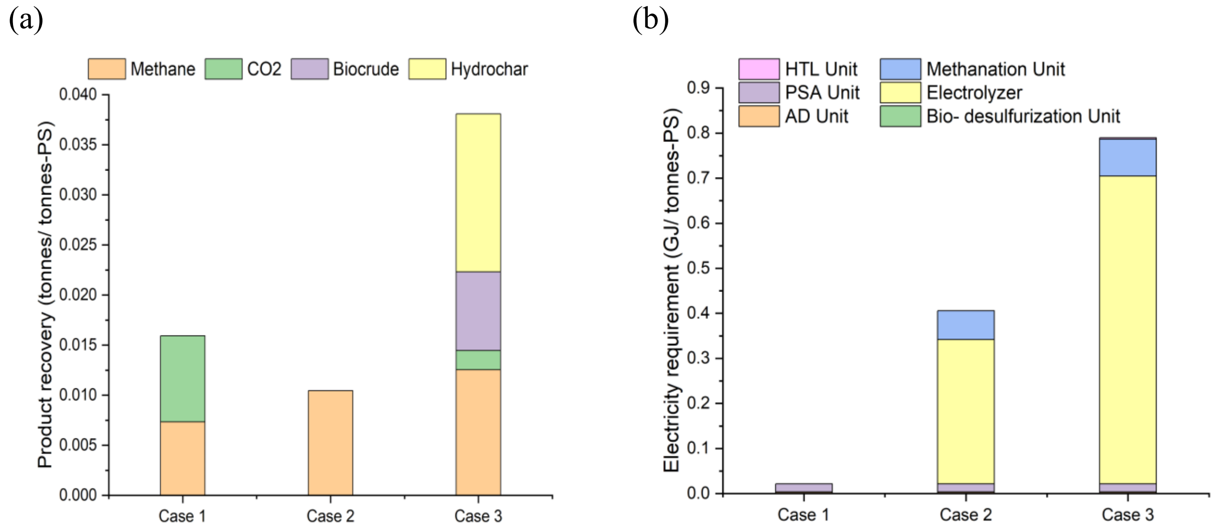

**Figure 4.12:** (a) Product recovery and (b) electricity requirement of three proposed configurations.

For Case 1 configuration, the integration of AD system and bio- desulfurization unit enhances the quality of the biogas produced. The $CO_2$ was further removed from biogas by the PSA unit. The produced biomethane is widely used for heating, electricity generation, and transportation purposes (Parvez & Ahammed, 2024). According to material balance calculations (**Figure 4.12 (a)**), for every tonne of sludge processed, 0.0073 tonnes of methane and 0.0086 tonnes of $CO_2$ were produced. Moreover, there is a noticeable difference in the formation of $CO_2$ and methane. The considerable amount of $CO_2$ emissions emphasizes the necessity of improving the process further in order to increase its sustainability.

The methanation unit was integrated to address the on-site $CO_2$ emissions, leading to the formation of Case 2 configuration setup. The methanation unit will improve the yield of methane by converting the $CO_2$ into methane. Moreover, this will lead to a reduction in on- site $CO_2$ emissions. In this configuration, $CO_2$ storage is not considered, assuming a 100 percent conversion of $CO_2$ to methane. A detailed material balance for Case 2 revealed a production rate of 0.0105 tonnes of methane per tonnes of PS fed into the system, which is higher than the rate reported in Case 1 (**Figure 4.12 (a)**).

In Case 3, a HTL system was incorporated in the Case 2 setup for the sustainable management of the digestate. The HTL process degrades the digestate at high temperature and pressure to produce valuable products like biocrude and hydrochar. The production of additional products will generate an additional revenue stream further enhancing the economic viability of the process. Biocrude produced could be upgraded to be utilized as a transportation fuel whereas hydrochar has a potential to be used as a soil amendment (Beims et al., 2020; Cabrera & Labatut, 2021; Ramzanipour et al., 2023). Moreover, the $CO_2$ generated during the process was fed as a feedstock in the methanation unit to produce methane. The quantitative assessment reveals that 0.0133 tonnes of methane, 0.0079 tonnes of biocrude, and 0.0158 tonnes of hydrochar are generated per tonne of sludge fed to AD-HTL system (**Figure 4.12 (a)**). Therefore, this strategic integration will maximize resource utilization and enhance the overall sustainability of the process (Thema et al., 2019). However, the HTL reactors require 40838.65 GJ of natural gas annually to maintain operating conditions. As a result, 0.0019 tonnes of $CO_2$ emissions were reported per tonne of sludge processed from the system. These metrics underscore the considerable potential of the HTL unit to improve the economic performance of the integrated system.

The operational efficiency of all equipment in proposed configurations was assessed by their electricity requirements (**Figure 4.12 (b)**). For Case 1, the AD unit consisting of an anaerobic digester, a feed pump, and a feed heat exchanger has the second highest share in the total energy consumption. The electricity consumption by bio-desulfurization unit is of minimal amount due to low energy demand by air blower and a pump. Furthermore, the PSA unit accounted for the largest portion (0.018 GJ/ tonnes-PS) of the electricity usage. The combined electricity consumption for these components in Case 1 was calculated to be 0.0217 GJ/tonnes of sludge processed by the system.

In Case 2, the addition of an electrolyzer and a methanation unit has significantly impacts the overall electricity profile of the integrated system. The total electricity consumption was evaluated to be 0.4060 GJ per tonne of PS fed to the system. This increasement in electricity requirement has highlighted the substantial electricity demand of the 0.320 GJ per tonne of sludge fed by the electrolyzer. The increment was due to the requirement of 9.076 kg of hydrogen per GJ of methane for the methanation unit and electricity requirement of 56.3 kWh to produce 1 kg of hydrogen. Additionally, the addition of a methanation unit requires 0.0645 GJ of electricity to process per tonne of PS fed to the system. However, the primary driver of the increased electricity consumption has been electrolyzer. Therefore, careful consideration is needed in the designing and operation of such systems.

For case 3, the integration of HTL unit has resulted in total electricity consumption of 0.790 GJ per tonne of PS processed into the AD- HTL configuration. The annual requirement of natural gas for HTL reactor was estimated to be 40,838.65 GJ to maintain 300°C for 60 minutes. Moreover, there is an increment in the production of $CO_2$ gases. This has increased electricity requirement of electrolyzer and methanation units to 0.683 GJ and 0.082 GJ per tonne of PS fed to the system, respectively. Moreover, the high energy requirement of the configuration highlights the necessity for efficient heat management and potential integration of energy recovery systems to mitigate operational costs. Thus, the comparative analysis of the three cases provides valuable insights for developing sustainable and economically attractive processes that contribute to the reduction of carbon emissions.

### *4.8.2 Capital costs, Operating costs, and Revenue for base case scenario*

**Figure 4.13** presents a detailed breakdown of the capital expenditure (CAPEX) for the three proposed configurations. The procurement and installation of all equipment, working capital to support initiate operations, and contingency funds for unforeseen expenses were added to estimate the CAPEX. In Case 1, the AD unit has emerged as the primary contributor to CAPEX with a share of 55.4% of the total capital investment. This significant share was due to the high costs of an anaerobic digester. The PSA unit contributed 15.8% to the total CAPEX. This concludes that the biogas upgrading technologies are relatively less capital-intensive. Moreover, contingency funds and working capital were the next largest contributors representing 14.5% and 13% of the total CAPEX, respectively. The bio-desulfurization unit had the lowest share of the CAPEX (1.2%), highlighting the cost-effectiveness of integrating biological treatment methods. The total CAPEX for the Case 1 scenario was estimated to be $21.94 million.

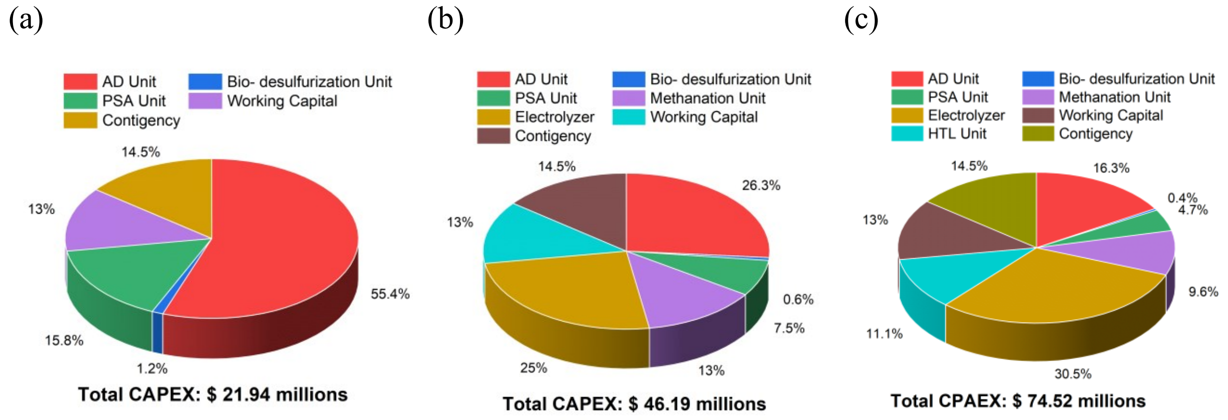

**Figure 4.13:** Break- down of the CAPEX for (a) Case 1, (b) Case 2, and (c) Case 3 configuration.

In Case 2, CAPEX increased to $46.19 million due to integration of a methanation unit and electrolyzer. Electrolyzer accounted for the second largest portion of CAPEX because of equipment expense of $856 per KW of energy utilized (Reksten et al., 2022). The contribution share of working capital and contingency funds were increased to 13 and 14.5 %, respectively. Moreover, the methanation unit also had the contribution of 13% to the total CAPEX. This significant amount highlights the capital requirement for its integration. Hence, the increment in the CAPEX of Case 2 is attributed to the advanced technology necessary for the efficient operation of these components.

Case 3 further escalates system complexity and capital expenditure by integrating a HTL unit, bringing the total CAPEX to $74.52 million. The integration of the HTL unit, which converts digestate into valuable byproducts, has a notable impact on the overall CAPEX distribution. The HTL unit, while not the most expensive, accounts for 11.1% of the total CAPEX, making it the fifth-largest cost factor. However, the introduction of the HTL unit increases the capital demand for the electrolyzer, as the carbon dioxide produced by the HTL process is converted into methane in the methanation unit thereby increasing hydrogen demand. This increment in hydrogen demand increases the electrolyzer from 11.16 MW (Case 2) to 23.83 MW. As a result, the electrolyzer becomes the highest CAPEX contributor at 30.5%, followed by the AD unit at 16.3%. The percentage shares of working capital and contingency funds remain consistent with those in Case 2. In addition, methanation, PSA, and bio-desulfurization unit made their contribution share keep a smooth trend in different configurations. The detailed breakdown of CAPEX underlines the strategic financial planning and resource allocation needed to obtain economic profitability and operational efficiency in reality. Besides, the costs of electrolyzer, methanation, and HTL units are expected to further decrease in forthcoming years with increased deployment.

**Figure 4.14** illustrates the annual breakdown of operational expenditure (OPEX) across the three proposed cases. OPEX includes transportation logistics, electricity consumption, water usage, carbon credits/taxes, and O&M expenditures. For the Case 1 configuration, the total annual OPEX was estimated to be \$2.06 million. The transportation costs had the largest contributing share of \$0.74 million per year. This significant contribution stems from the relatively low OPEX of the conventional AD plant with upgrading equipment, making sludge transportation the primary economic burden, thereby challenging its feasibility. The substantial carbon dioxide content in the biogas, which results in significant emissions post-PSA unit, incurs $CO_2$ taxes (as described in **section 4.7**), contributing \$0.63 million annually, making it the second-largest OPEX component. Electricity and O&M contribute similarly, each accounting for \$0.27 million annually, reflecting the lower energy consumption and maintenance requirements of the equipment. Water consumption contributes the least to OPEX annually. This is due to only usage in scrubbing of $H_2S$ in bio- desulphurization unit.

In the Case 2 configuration, the total annual OPEX increases to \$7.64 million. The integration of the methanation unit, which converts carbon dioxide into methane, eliminates on-site emissions, resulting in a carbon credit of \$0.14 million annually, reducing the OPEX from \$7.77 million to \$7.64 million. The most significant OPEX component is electricity. This amounts to \$6.10 million annually due to the high energy demand of the electrolyzer for hydrogen production. The addition of the methanation unit and electrolyzer also raises the annual O&M costs to \$0.75 million, surpassing transportation costs, which remain at \$0.74 million. Water consumption costs for this configuration are slightly higher, at \$0.18 million annually.

For Case 3, the annual OPEX rises to \$15.68 million per year. The integration of the HTL unit into the Case 2 configuration allows for the utilization of $CO_2$ in the methanation unit, with some $CO_2$ emissions resulting from natural gas use. However, these emissions are below the threshold. Hence, carbon credits are earned that reduce the OPEX from \$15.69 million to \$15.68 million. The increased $CO_2$ intake necessitates higher hydrogen production by the electrolyzer, driving the annual electricity costs up to \$11.95 million, the largest OPEX contributor. Therefore, electricity requirements need to be optimized to achieve operational efficiency and mitigate the financial impact. The incorporation of the HTL unit increases O&M costs to $2.79 million annually. However, water costs remain the lowest OPEX component.

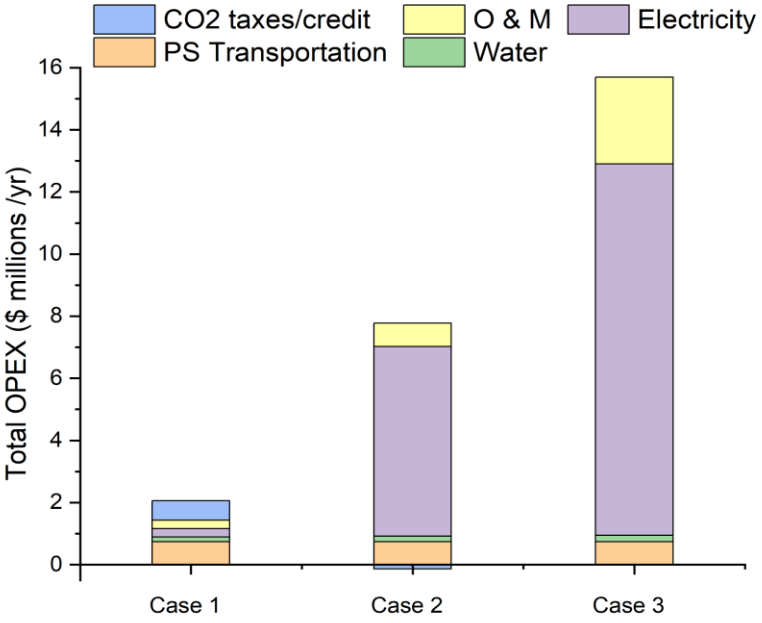

**Figure 4.14:** Break- down of the annual OPEX for all three proposed configurations.

The revenue generation across the three proposed configurations is presented in **Figure 4.15**. In Case 1, the methane quality is enhanced by PSA unit. This yielded an annual revenue of $4.92 million. Methane revenue in all three cases was calculated based on annual production and LCOE as described in **section 4.3**. For Case 2, the integration of the methanation unit enhances methane production. This integration resulted in a revenue generation of $13.67 million per year. The substantial revenue generation highlights the scalability of such integrated systems for broader industrial applications. Further. It bolsters the case for investment in waste-to-energy technologies. In the Case 3 configuration, total annual revenue was estimated to be $25.40 million every year. The contribution of biocrude, methane, and hydrochar accounts to be 59.6%, 35%, and 5.6% respectively. The selling prices of biocrude and hydrochar were taken from **table 4.2**. This generation of valuable by- products highlights the potential of diversified revenue stream in achieving the economic viability for the process.

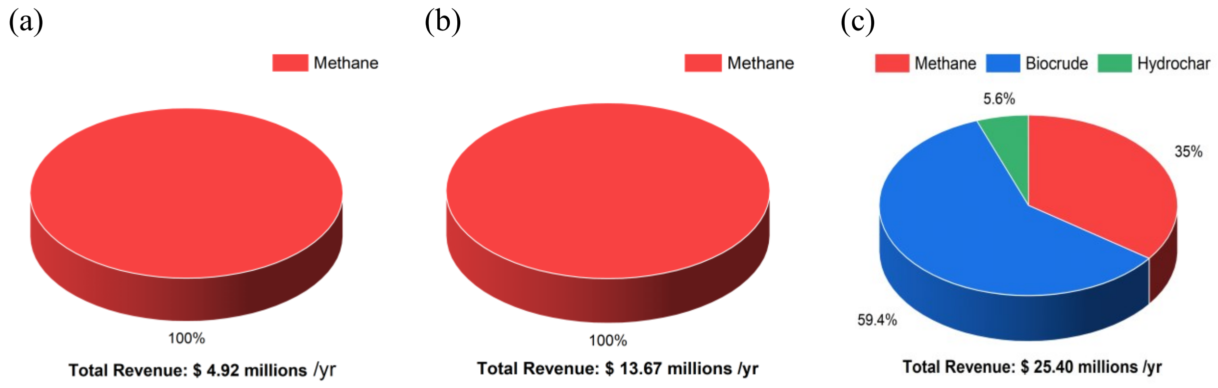

**Figure 4.15:** Break- down of the annual revenue generated from (a) Case 1, (b) Case 2, and (c) Case 3 configuration.

### *4.8.3 Levelized Cost of Energy (LCOE) for base case scenario*

The Levelized Cost of Energy (LCOE) accounts for the break- even price of methane at which methane must be sold for a project to cover its costs over its lifetime, including capital and operational expenditure. It is computed by fixing net present value (NPV) to be zero, demonstrating that the configuration will neither make profit nor loss money.

The contribution of electricity, non-energy OPEX, and CAPEX to the LCOE calculations for three cases is shown in **Figure 4.16**. To improve the quality of methane, an AD unit and a PSA unit were combined in Case 1. LCOE of methane was determined $ 11.47 per GJ, which is consistent with values found in previous studies (Kassem et al., 2020a; Kassem et al., 2020b; Huang & Fooladi, 2021). The global average cost of producing biomethane through biogas upgrading today is around USD 19/ MBtu and market selling price is in between $ 20-25/MBtu (IEA, 2020). The analysis reveals distinct contributions from various cost components. The fact that CAPEX constitutes the largest share of the LCOE at $5.97/GJ underscores the significant financial burden associated with the initial investment required to set up the AD system and PSA unit. This indicates equipment procurement, installation, and infrastructure costs had substantial amount. With a contribution of $4.77/GJ, non-energy OPEX is the second highest factor affecting the LCOE. This includes ongoing operational costs excluding electricity, such as maintenance, labor, insurance, and other routine expenses. The large contribution from non-energy OPEX in LCOE indicates that operational efficiency should be optimized as much as possible to better manage and minimize the recurring costs more effectively. The low relative contribution of the electricity cost of $0.73/GJ would suggest that energy consumption is not a major cost driver in this configuration. This supports the fact that the AD system with the PSA unit is relatively low intensity in using energy and, therefore, less sensitive to any fluctuations in electricity prices. On the other hand, another corollary of this would be that further reductions in the cost of electricity would have a limited additional impact on reducing the overall LCOE. While electricity costs are relatively low and thus less impactful on the LCOE, the system's capital and operational efficiency are critical areas where optimization can drive cost reductions and enhance the system's overall financial performance. Moreover, the dependance on the CAPEX indicates that there is a possibility of reducing the cost because of economies of scale. However, the digestate handling and storage cost was not included in case 1, which could increase the cost.

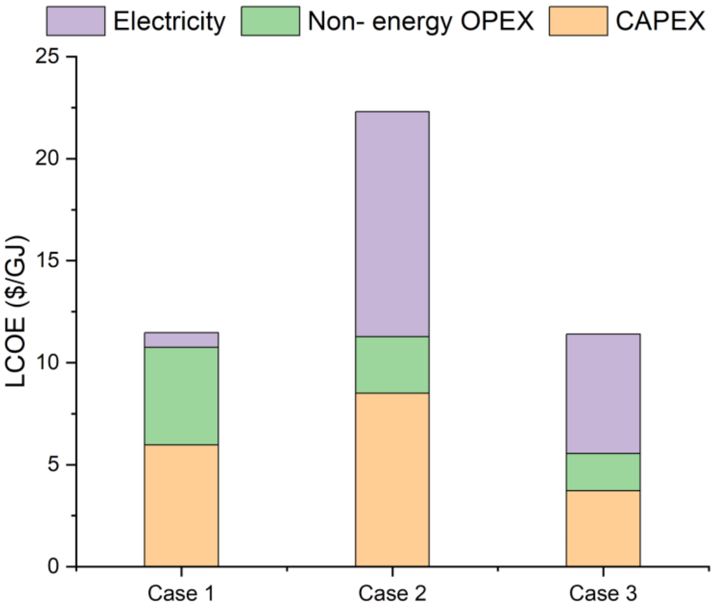

**Figure 4.16:** Breakdown of levelized cost of energy (LCOE) in $/GJ for all three proposed cases.

The LCOE for Case 2 was computed to be $22.31 per GJ which is higher than reported in Case 1. This additional cost is due to the increment in the size of electrolyzer and methanation unit. The electricity costs made the largest contribution to the LCOE that accounts for $11.03/GJ. The implication of this is twofold: first, it underscores that the process could only be feasible if low-carbon and low-cost electricity is available and that any fluctuations in electricity prices could put the process at risk. The second highest contribution of $ 8.50 per GJ to the LCOE comes from CAPEX. That points out to the high initial investment in the electrolyzer and methanation unit, which may be one of the huge financial challenges. In this respect, while integration increases methane production, it provides huge environmental benefits; still, there can be a barrier to initial capital burden implementation in markets with limited access to capital or higher financing costs. The non- energy OPEX had the lowest share of \$ 2.77 per GJ in LCOE. This means that ongoing non- electricity operational costs are less significant in the overall cost structure. Therefore, more efforts should be made to manage electricity costs and optimize capital investments rather than reducing operational expenses to enhance the economic viability of the system.

In Case 3, the LCOE was estimated at \$ 11.39/GJ with an added HTL unit. It is hence lower than Case 2 and closer to Case 1 regarding LCOE. This dramatic reduction in LCOE is basically because of extra revenue streams generated through biocrude and hydrochar productions at 59.4% and 5.6%, respectively, other than methane. These new revenue sources help to offset the capital and operational costs, which effectively lowers the LCOE. This highlights the benefits of multi-product systems in waste-to-energy configurations where financial burdens are distributed across various high-value outputs rather than relying solely on methane production. The electricity costs had the major share of contribution of \$5.85 per GJ in LCOE. This is due to the high electricity requirement of the electrolyzer. The integration of the HTL unit introduces additional $CO_2$ into the system, which is then processed by the methanation unit. This increase in flow of $CO_2$ requires increased production of hydrogen, which again increases the load on the electrolyzer. Besides this, the HTL unit itself is a very energy-intensive unit, which again raises the overall electricity requirement. This shows the cost of electricity to be the leading factor in this AD-HTL system. Hence, more emphasis should be directed to low-cost electricity or renewable sources. Correspondingly, the second highest contribution stands for CAPEX with a value of \$3.72/GJ. This is majorly because, for such a configuration, the electrolyzer would require very high costs, being the highest capital investment among other components. While the HTL unit is only the fifth highest in terms of direct CAPEX impact, it still contributes to the overall capital costs, albeit to a lesser extent. This indicates that although advanced technologies like the electrolyzer and HTL unit enhance the system's capability to produce additional valuable outputs like biocrude and hydrochar, they also introduce significant upfront costs. This underscores the importance of assessing the return on investment for such technologies and exploring ways to reduce capital expenditures through design optimization, technological advancements, or economies of scale. The lowest contributing factor to the LCOE was non-energy OPEX. Therefore, once the high initial capital and electricity costs are addressed, the system could operate efficiently with a lower additional financial burden, making it more sustainable in the long term.

### *4.8.4 Sensitivity Analysis*

The sensitivity analysis was carried out by changing a number of input parameters like PS feed rate, biogas yield, volatile content in PS, water price, electricity price, discount rate, transportation logistics, $CO_2$ taxes/credits, hydrochar yield and selling price, and biocrude yield and selling price to see the effects of these changes on the LCOE of methane to decide on the profitability of the system. These parameters were varied by ±50% to reflect the dynamic nature of both the market and technological development in the 20-year timeframe. This range accounts for the inherent uncertainty in cost estimates and scaling challenges associated with HTL technology, which, as an emerging technology, has not yet been implemented at full scale in the industry. Figure **4.17** depicts the sensitivity analysis of methane's LCOE for three cases.

For Case 1, which integrates an AD unit and a PSA unit, biogas yield and volatile content in PS are identified as the most significant factors affecting the LCOE, as evidenced by the wide range of LCOE values from \$9.6/GJ to over \$19.2/GJ (**Figure 4.17 (a)**). This underlines the high importance of optimization in biogas production and increasing volatile content in PS within the AD unit. Increasing biogas yield-from 562 to 843 L/ kg- VS fed-and volatile content-from 2.5 to 3.75%-significantly reduces the LCOE from \$ 11.5/ GJ to \$ 9.6/ GJ, demonstrating that increasing the effectiveness of the AD process could be highly economically beneficial. Given that biogas yield and volatile content are directly proportional, any enhancements in operational parameters or feedstock quality, such as co-digestion to increase volatile content, will boost biogas production and have a pronounced positive effect on reducing the LCOE. The discount rate is another major contributing factor, with variations from \$9.1/GJ to \$14.2/GJ observed in the plot. A higher discount rate increases the LCOE, reflecting the higher perceived risk and cost of capital, while a lower discount rate (best-case scenario) reduces the LCOE. This emphasizes the importance of financial structuring in project development. Lowering the cost of capital through favorable financing terms or incentives could substantially improve the economic viability of the process. Transportation cost and distance showed a variation in LCOE from \$10.6/GJ to \$12.3/GJ. Both factors exhibit a similar level of impact on the LCOE, indicating that as transportation costs increase, the LCOE correspondingly rises, though the effect is less pronounced than that of biogas yield and feed rate. This would mean that logistics play a vital role but are not the major cost drivers in this case. The efficient transportation logistics, with possible co-location of the AD unit near the feedstock source, might minimize such costs; however, their overall impact on the LCOE is relatively moderate. In Case 1, carbon dioxide is also produced as a by-product after the PSA unit, incurring $CO_2$ emission taxes. First, the findings show that $CO_2$ taxes take a smaller but not negligible part of the LCOE. It follows that the increase in $CO_2$ taxes could lead to a higher LCOE, though at less variation compared to other parameters such as biogas yield. The carbon tax rate in Canada is currently \$ 80/ tonnes however, it is supposed to increase to \$ 170/ tonne by 2030 (Dion & Linden-Fraser, 2024). Therefore, efforts should be made to mitigate these emissions, as $CO_2$ taxes could become a more critical consideration in future economic assessments. However, increasing feed rates did not affect the LCOE when using large enough plant size, considered in this work, at 1100000 tonnes PS per year. On the other hand, if the feed rate of PS is reduced, the LCOE increases to \$13.1/GJ. Hence, this would mean that scaling up the AD process may not be an appropriate strategy for reduction in LCOE. More emphasis should be given to optimization rather than mere scaling up.

(a)

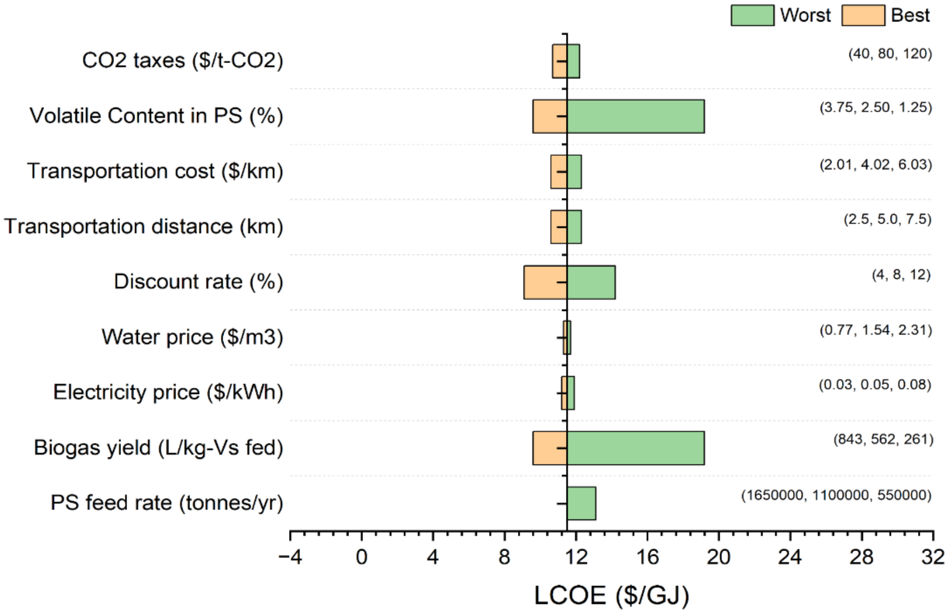

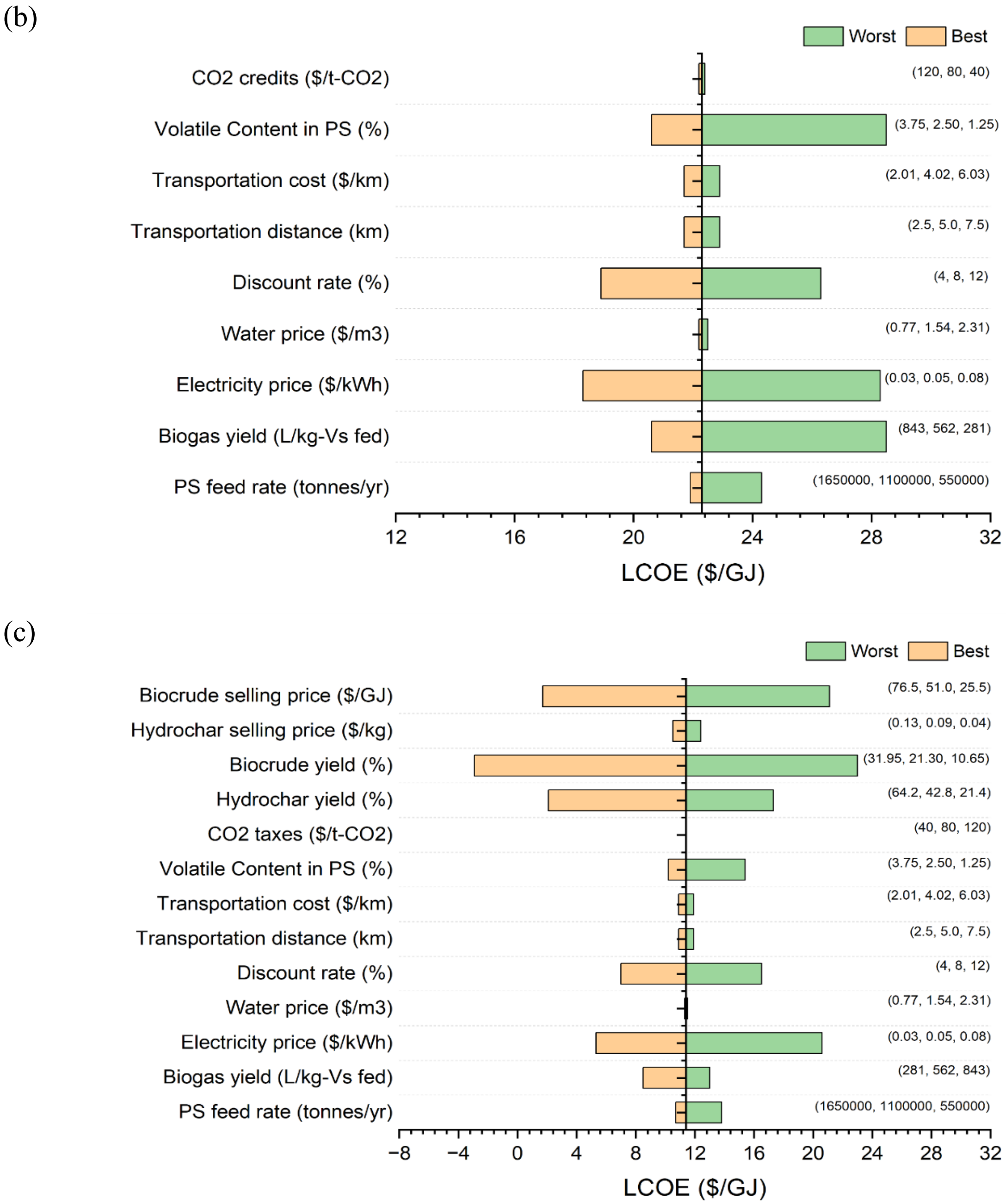

**Figure 4.17:** Sensitivity analysis to illustrate the impact of ±50% changes in input parameters on the LCOE of methane for the (a) Case 1, (b) Case 2, and (c) Case 3.

In Case 2, the LCOE of methane is very sensitive to the electricity price; within a wide range of from \$18.3/GJ to \$28.3/GJ, the electrolyzer requires a great deal of electricity. Hence, an inexpensive source of electricity supply or trying alternative renewable sources can be critical for reducing costs. The discount rate is the second most influential parameter, with LCOE fluctuations between \$18.9/GJ and \$26.3/GJ. A higher discount rate increases the LCOE, and vice versa. It then illustrates that advantageous financing terms or government incentives would be of major importance to raise the economic viability of the project. Quite significant effects are also shown in biogas yield and volatile content. In general, LCOE ranges between \$20.6/GJ and \$28.5/GJ. Strong influence from these parameters would suggest feedstock quality as a very critical parameter for the overall economics of the integrated process. By increasing the volatile content and improving biogas yield towards the best-case scenario, LCOE decreases noticeably. This fact can be a good indication that the optimization of PS feedstock for the purpose of enhancement of its volatile content could give high biogas yield and considerably lower methane production cost for making the overall process more economic. It points out the need to optimize anaerobic digestion, either through co-digestion or other improvements of feedstock for increasing volatile content, in ways that would maximize biogas production and lower the LCOE. The transportation cost per kilometer and the distance of transportation has a moderate impact on the LCOE, with recorded fluctuations in a range from \$21.7/GJ to \$22.9/GJ. While logistics are a factor, its effects are not as strong when compared to the price of electricity, volatile content, and yield of biogas. However, even optimization of transport logistics or co-location of facilities closer to feedstock sources could still present some cost benefits. The PS feed rate into the AD also exhibits a strong factor in LCOE. Where the feed rate is increased to the best-case scenario, the LCOE drops substantially, which would also suggest that scale-up of the process can achieve economies of scale. It indicates that the economic viability of the integrated system can be further improved by optimization of the PS feed rate, apart from improvement in the yield of biogas and its volatile content. The $CO_2$ credit gained on account of zero on-site emission since it is being utilized in methanation units and water price also have a very minor impact on LCOE, which has only minor variations. Even though water electrolysis uses 10 tonnes of $H_2O$ to make 1 tonne of $H_2$ due to low cost of water purification, it has little impact. More precisely, though, water availability should be considered in the design and commercialization of these plants. In this respect, efforts for reducing water consumption and enhancing carbon credits may bring environmental benefits; they do not lead to significant economic saving within this frame.

For Case 3, the sensitivity of biocrude yield and selling price of biocrude on LCOE is the highest, in the range from -\$2.9/GJ to \$23/GJ and \$1.7/GJ to \$21.1/GJ, respectively. The negative value of LCOE implies that revenues from biocrude can greatly offset the costs associated with methane production and hence the process can be viable under favorable conditions. Additionally, the rise in selling price from $51/ GJ to $76.50/ GJ decreases LCOE from $11.4/GJ to $1.7/GJ. This would mean that optimization of the quality of the produced biocrude and its yield will be crucial in attempts to improve the economics of the integrated system in general. Similarly, the hydrochar yield also had a similar impact on the LCOE of methane, with variations from $2.1/GJ to $17.3/GJ. In contrast, the change in selling price of hydrochar does not significantly impact the LCOE. Therefore, more efforts should be made to enhance hydrochar yield rather than improving its quality. The LCOE is still highly dependent on the electricity price, ranging from $5.3/GJ to $20.6/GJ. Access to low-price electricity or renewable energy for electricity generation is therefore a prerequisite to securing the overall performance of the economic system. Discount rate: As in Case 2, the impact of the discount rate is the same. LCOE also depends on biogas yield between $8.5/GJ and $13/GJ. Curiously, the higher the yields in biogas production, the higher the LCOE, which could indicate that although higher biogas yields generally try to promote the efficiency of a system, beyond a certain threshold, the costs outweigh the benefits accrued from the improved yields. Hence, an optimum yield point should be defined which may balance energy production with associated costs at a minimum level of LCOE and thereby improve the overall economic viability of the process. The LCOE ranges from $10.2/GJ to $15.4/GJ, hence moderately sensitive to volatile content in PS. This calls for optimization in feedstock quality to make the process more efficient, since higher volatile content will lead to better biogas production hence decreased production costs. Pre-treatment of PS is subjected to both volatile content and biogas yield optimization so that there can be an economic benefit. The PS feed rate has a similar, moderate effect on LCOE, ranging from $10.7/GJ to $13.8/GJ. As the feed rate increases towards the best-case rate, there are realizations of economies of scale whereby LCOE decreases, and process feasibility improves. Transportation logistics has a rather moderate impact on LCOE, trending within a variance from $10.9/GJ to $11.9/GJ. Water price also showed a minor impact on LCOE, with variations from $11.3/GJ to $11.5/GJ. $CO_2$ credits, gained in the Case 3 scenario as on-site emissions fall below the threshold value, show no impact on LCOE. Nonetheless, minimizing carbon emissions or capitalizing on $CO_2$ credits remains beneficial for the process's economic sustainability.

In conclusion, our study highlights that AD is a well- established commercialized technology to produce biomethane. However, there are some limitations to this technology, which includes low yield, $CO_2$ emissions, and disposal of digestate. Integrating a methanation unit to this process will increase the yield but the high electricity consumption makes the process economically challenging. Therefore, in order to improve the economic viability, the renewable energy sources to produce $H_2$ needs to be considered. However, handling and storage would still be an economic burden for this process. Hence, HTL unit was integrated with this process to address this issue. This integrated process has been thoroughly studied in this chapter. The valuable by- products produced can generate additional revenue which lowers down the biomethane production cost. However, further optimization in AD or HTL processes can significantly reduce the cost of biomethane production as seen in your sensitivity analysis.

### *4.8.5 Total Carbon dioxide emissions ($CO_2$) in base scenario*

This study does not conduct a full life-cycle assessment; however, $CO_2$ emissions on site, electricity-related emissions, and fugitive methane emissions were quantified using the methodologies in **Section 4.6**. These discrete emissions were summed to provide the overall GHG emissions for the study. In this regard, this present study has estimated the GHG emissions at process and energy sources as Scope 1 and Scope 2, respectively. **Figure 4.18** presents on-site $CO_2$, electricity-related, and fugitive methane emissions in the proposed cases. A grid carbon intensity was considered at 110 g CO2e/kWh, and a methane leakage rate of 2% taken into consideration for the analysis (C.E.R., 2024).

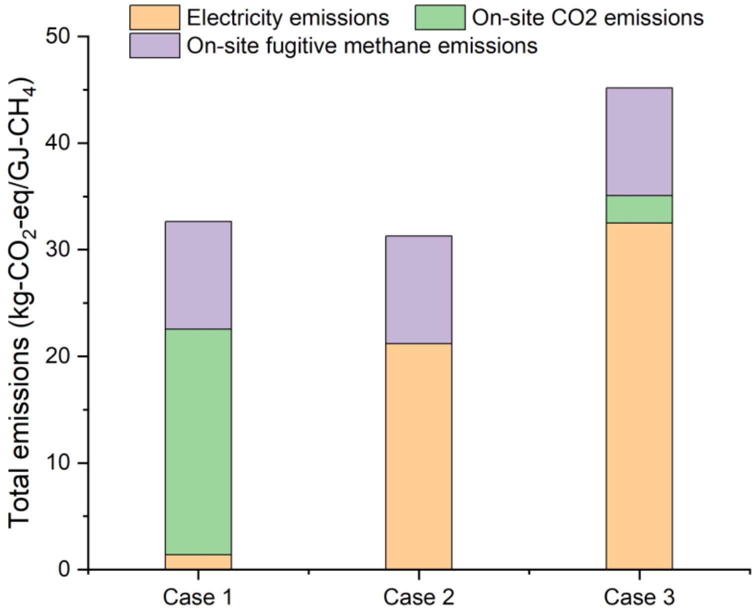

**Figure 4.18:** Net $CO_2$ emissions for all three configurations for base case scenario.

The calculations for the fugitive methane emissions in all cases were assumed to be 10.09 kg $CO_2$-eq/GJ-$CH_4$, based on a methane emission rate of 2% in the base case scenario (C.E.R., 2024). In Case 1, the $CO_2$ emissions are extremely high at about 21.14 kg $CO_2$-eq/GJ-$CH_4$ because of large-scale by-production of $CO_2$ after the PSA unit. However, the related electricity emissions in this case are negligible; thus, the total emission value amounts to 32.63 kg $CO_2$-eq/GJ-$CH_4$. In Case 2, adding a methanation unit and an electrolyzer decreases the total emission by a small margin to 31.29 kg $CO_2$-eq/GJ-$CH_4$ since on-site $CO_2$ emissions become zero. Nevertheless, the related electricity emissions increase significantly to 21.20 kg $CO_2$-eq/GJ-$CH_4$ due to the high energy demand of the electrolyzer. This increase justifies the application of energy-efficient processes or the implementation of renewable energy sources to reduce the impact that electricity-related emissions have on the project's overall environmental footprint. In Case 3, the addition of the HTL unit increases electricity-related emissions to 32.49 kg $CO_2$-eq/GJ-$CH_4$, driven by the expanded size of the electrolyzer due to increased energy requirements by the HTL unit. Furthermore, natural gas is used to keep the HTL reactor at operating temperature. This results in an on-site emission of 2.59 kg $CO_2$-eq/GJ-$CH_4$. Such higher emissions raise the suspicion that possibly there is a trade-off between the efficiency of the process and environmental impact, enhancing the need for optimization in energy use and alternative heating methods in order to make the system more viable.

**Figure 4.19** illustrates the impact of methane emission rates and grid carbon intensity on the total emissions across all three configurations. For Case 1, total emissions range from 24.30 to 39.00 kg $CO_2$-eq/GJ-$CH_4$. As the methane emission rate increases (moving up on the y-axis), there is a significant rise in total emissions. While higher emission factors from the generation-movements to the right on the x-axis-add to increasing the total amount of emissions, the role of methane emission rate is considerably larger. That would suggest that although reducing the emission factor is crucial, efforts toward reducing methane emissions would be more pivotal toward achieving better environmental benefits. This is within the range of 12.00 to 136.00 kg $CO_2$-eq/GJ-$CH_4$ in Case 2, and from 19.50 up to 200.00 kg $CO_2$-eq/GJ-$CH_4$ in Case 3. In the latter case, the factor of electricity generation becomes much more influential. This means that while methane emissions reduction is important, a focused approach on the reduction of the emission factor in the generation of electricity could have a more effective overall outcome in terms of emissions reduction for integrated AD-HTL routes.

(a)

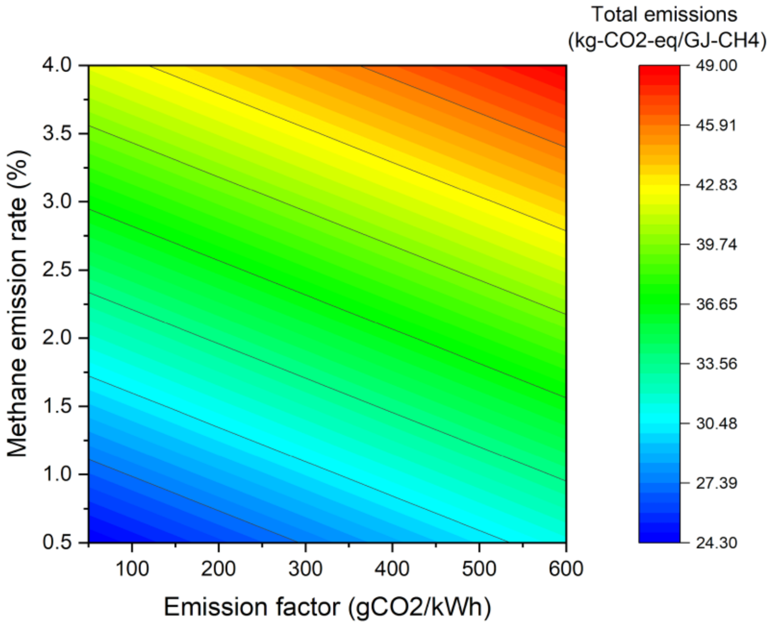

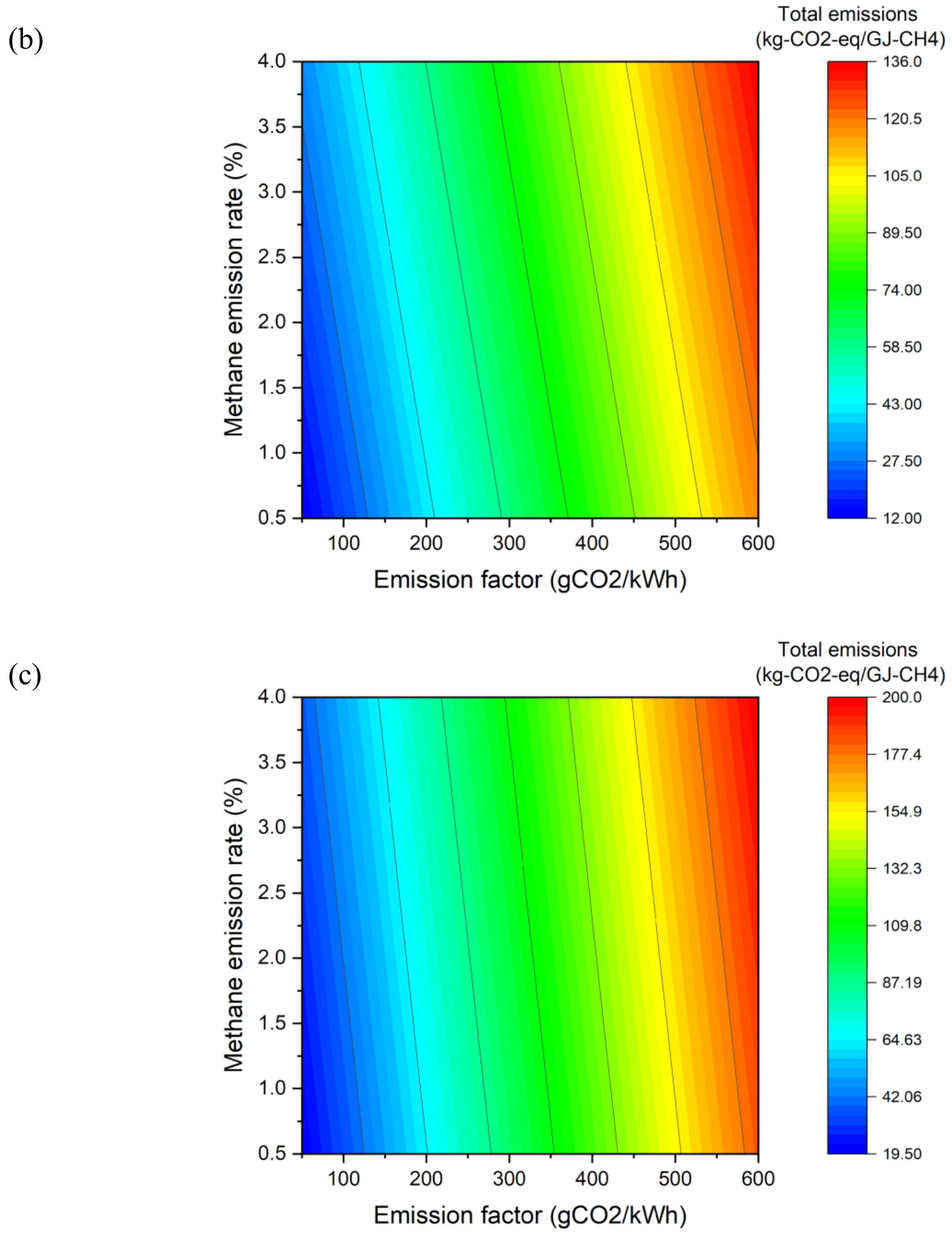

**Figure 4.19:** Effect of methane emission rate and emission factor on total emissions for (a) Case 1, (b) Case 2, and (c) Case 3.

## 4.9 Conclusion

The TEA performed in this study is essential to assess the feasibility, performance, and economic viability of the three system configurations proposed for processing 1.1 million tons per year of primary sludge. While the in-depth economic review through TEA provides a detailed view into the cost-effectiveness of each configuration, technological integrations underline the delicate balance of their impacts on operational efficiency, environmental sustainability, and revenue generation. Material and energy balance across these configurations indicates that while the incorporation of newer technologies, such as the methanation process and HTL unit, increases biomethane yield manifold and opens new revenue generation avenues, it also involves higher operational expenses due to increased electricity consumption and maintenance costs. This finding underlines the critical need for energy efficiency measures, as well as inclusion of energy recovery systems that could further enhance the economic viability of these advanced configurations. Among various configurations evaluated, the integrated AD-HTL system realized the lowest LCOE of $11.4/GJ, mainly because of the additional revenue contributed from biocrude and hydrochar production. This LCOE reduction underlines the need for diversified streams in order to economically enhance integrated systems of waste-to-energy. Sensitivity analysis, among others, affirms the view that the adoption of critical process parameters relating to yield from biogas and HTL efficiency can give the system a dramatic downward shift in LCOE and, therefore, calls for constant optimization and refinement of process parameters. The inclusion of energy-intensive components such as the electrolyzer and HTL unit also underlines the importance of electricity price to the overall viability of the system. This therefore calls for shifting of production towards renewable sources to drive down costs and enhance sustainability. The emissions analysis further amplifies this point by showing that there is a need to decrease the emission factor associated with the generation of electricity in order for economic goals to be in step with sustainability objectives. The future direction for studies should emphasize ways of optimizing the AD-HTL process towards better yield for biocrude and hydrochar through some co-digestion strategy in the anaerobic digestion system. Furthermore, the exploration of renewable energy source integration for reducing dependence on grid electricity is pursued, as is the adoption of more advanced emission reduction strategies, to make integrated AD-HTL systems highly sustainable and economical in the long term. This therefore calls for an in-depth life cycle assessment of the integrated system to ascertain the environmental viability of an integrated approach being holistic, as concerned with waste management and energy production.

# Chapter 5

# Conclusions and Recommendations

## 5.1 Conclusions

The objective of this work was comparing integrated systems, including Anaerobic Digestion and Hydrothermal Liquefaction, studying different sequences of these configurations: HTL followed by AD and vice versa, under different operating conditions for HTL in terms of temperature and residence time. In fact, the results show the fundamental role that integrated systems would play in optimizations of energy recovery and that there is ample room for improving efficiency in systems. Besides, the thesis allows for a detailed techno-economic analysis of a large-scale AD-HTL system by providing detailed performance targets required to attain economic feasibility in the sustainable management of sewage sludge.

This work investigates the recovery of energy from sewage sludge by two different sequencing configurations: AD followed by HTL and vice versa, under different HTL conditions of 250, 300, and 350 °C maintaining the retention time at 30 and 60 minutes, respectively. A comparison between the two configurations presents certain energy trade-offs between biocrude and biomethane generation. The result indicated that a sequence of HTL-AD gave higher recovery in the form of energy as biocrude due to the high content of fatty acids from the high lipid content in primary sludge. Contrasted to ADHTL, which gave a better recovery of biomethane due to the easily degradable nature of primary sludge with low nitrogen content. For HTL-AD, the recovery of energy varies within a wider range from 47.2% to 84.5%, while for AD-HTL, the recovery ranges between 57.2% and 77.3%. For HTL-AD, at 300 °C within 60 minutes, the maximum energy recovery was recorded, although recovery was higher in AD-HTL than with HTL-AD.

A techno-economic analysis study was conducted for an integrated AD- HTL system to identify key performance indicators to achieve economic viability for sewage sludge management. A processing capacity of 1.1 million tons of primary sludge annually was assessed for three different configurations. Our results concluded that the integration of AD and HTL process computed the lowest LCOE of $ 11.4/ GJ due to the generation of additional revenue from hydrochar and biocrude. Incorporation of methanation unit off- sets the on- site carbon dioxide emissions and contributed to annual revenue by generating additional methane. The capital cost of electrolyzer and electricity cost were the primary contributors to CAPEX and OPEX, respectively. Sensitivity analysis revealed that optimization of AD and HTL process could be beneficial to achieve economic profitability. Low electricity cost or integration of renewable energy source can provide economic viability to the integrated scheme and ensure long-term sustainability.

## 5.2 Recommendations

1. This study only considers primary sludge for the experimental study in energy recovery efficiency in sewage sludge management. A similar future study might extend into other types of sludge, such as secondary or even mixed sludge, to consider a wider perspective on energy efficacy of different types of sludge.
2. Full characterization of biocrudes produced from both integrated systems of HTL-AD and AD-HTL is recommended. This shall involve an analysis on the suitability of the various biocrudes for transportation fuels, together with estimations of the associated costs in upgrading such biocrude to fuel standards.
3. In this presented experimental study, electricity consumption by either the AD or HTL process is not taken into consideration. The future study should therefore accurately take into consideration energy balance to highlight net energy gain and overall efficiency of integrated systems.
4. The experiments were at a laboratory scale. Extrapolation of these processes to full-scale industrial level will raise a host of challenges-especially in the realm of reactor design, operation logistics, and efficiency of processes. This area of scalability needs further research for these technologies to be practically implemented.
5. Heavy metal presence in sludge and distribution between the products are not considered in the present work. In this direction, future research should clarify the role of heavy metal content on both the efficiency of AD and HTL and quality of by-products. This includes methods for recovery or removal, their regulatory and environmental relevance, and quantification of costs associated with heavy metals.

6. The TEA study in the present work was performed for AD-HTL configuration for primary sludge only. Further studies on different kinds of sludge are needed in order to draw a perspective on the economic performance of AD followed by HTL system for sewage sludge management.
7. The grid electricity was accounted as an electricity source for the TEA analysis. Future work should look for renewable energy sources to enhance process sustainability.
8. The TEA analysis does not incorporate the valorisation of aqueous phase generated from HTL process. Future research work should integrate the sustainable management of aqueous phase to achieve long-term sustainability.

# References

Aierzhati, A., Stablein, M. J., Wu, N. E., Kuo, C.-T., Si, B., Kang, X., & Zhang, Y. (2019). Experimental and model enhancement of food waste hydrothermal liquefaction with combined effects of biochemical composition and reaction conditions. *Bioresource Technology*, *284*, 139–147. https://doi.org/10.1016/j.biortech.2019.03.076

Akhtar, J., & Amin, N. A. (2011). A review on process conditions for optimum bio-oil yield in hydrothermal liquefaction of biomass. *Renewable and Sustainable Energy Reviews*, *15*(3), 1615–1624. https://doi.org/10.1016/j.rser.2010.11.054

Allegue, L. B., & Hinge, J. (2014). Biogas upgrading Evaluation of methods for H2S removal. *Danish technological institute*, *31*(December), 1-31.

Alonso-Vicario, A., Ochoa-Gómez, J. R., Gil-Río, S., Gómez-Jiménez-Aberasturi, O., Ramírez-López, C. A., Torrecilla-Soria, J., & Domínguez, A. (2010). Purification and upgrading of biogas by pressure swing adsorption on synthetic and natural zeolites. *Microporous and Mesoporous Materials*, *134*(1-3), 100-107.

Amigun, B., & Von Blottnitz, H. (2009). Capital cost prediction for biogas installations in Africa: Lang factor approach. *Environmental Progress & Sustainable Energy: An Official Publication of the American Institute of Chemical Engineers*, *28*(1), 134-142.

Anastasakis, K., Biller, P., Madsen, R., Glasius, M., & Johannsen, I. (2018). Continuous hydrothermal liquefaction of biomass in a novel pilot plant with heat recovery and hydraulic oscillation. *Energies*, *11*(10), 2695. https://doi.org/10.3390/en11102695

Angenent, L. T., Usack, J. G., Sun, T., Fink, C., Molitor, B., Labatut, R., Posmanik, R., Hörl, M., & Hafenbradl, D. (2022). Upgrading anaerobic digestion within the energy economy – the methane platform. *Resource Recovery from Water*, 141–158. https://doi.org/10.2166/9781780409566_0141

Angenent, L. T., Usack, J. G., Xu, J., Hafenbradl, D., Posmanik, R., & Tester, J. W. (2018). Integrating electrochemical, biological, physical, and thermochemical process units to expand the applicability of anaerobic digestion. *Bioresource Technology*, *247*, 1085–1094. https://doi.org/10.1016/j.biortech.2017.09.104

Anon, (2017). Lfgcost-web model user's manual.

Antar, M., Lyu, D., Nazari, M., Shah, A., Zhou, X., & Smith, D. L. (2021). Biomass for a sustainable bioeconomy: An overview of world biomass production and utilization. *Renewable and Sustainable Energy Reviews*, *139*, 110691. https://doi.org/10.1016/j.rser.2020.110691

Aui, A., & Wright, M. M. (2014). Life Cycle Cost Analysis of the Operations of Anaerobic Digesters in Iowa. *Iowa State University: Ames, IA, USA*.

Awasthi, M. K., Sarsaiya, S., Wainaina, S., Rajendran, K., Awasthi, S. K., Liu, T., Duan, Y., Jain, A., Sindhu, R., Binod, P., Pandey, A., Zhang, Z., & Taherzadeh, M. J. (2021). Techno-Economics and life-cycle assessment of biological and thermochemical treatment of bio-waste. *Renewable and Sustainable Energy Reviews*, *144*, 110837. https://doi.org/10.1016/j.rser.2021.110837

Badgett, A., Brauch, J., Thatte, A., Rubin, R., Skangos, C., Wang, X., ... & Ruth, M. (2024). *Updated Manufactured Cost Analysis for Proton Exchange Membrane Water Electrolyzers* (No. NREL/TP-6A20-87625). National Renewable Energy Laboratory (NREL), Golden, CO (United States).

Baloch, H. A., Nizamuddin, S., Siddiqui, M. T. H., Riaz, S., Jatoi, A. S., Dumbre, D. K., Mubarak, N. M., Srinivasan, M. P., & Griffin, G. J. (2018). Recent advances in production and upgrading of bio-oil from biomass: A critical overview. *Journal of Environmental Chemical Engineering*, *6*(4), 5101–5118. https://doi.org/10.1016/j.jece.2018.07.050

Barbarossa, V., & Vanga, G. (2011, October). Methanation of carbon dioxide. In *XXXIV Meeting of the Italian section of the Combustion Institute–Roma*.

Bartholomew, C. H. (2001). Mechanisms of catalyst deactivation. *Applied Catalysis A: General*, *212*(1-2), 17-60.

Bauer, F., Hulteberg, C., Persson, T., & Tamm, D. (2013). Biogas upgrading- Review of commercial technologies.

Becker, C. M., Marder, M., Junges, E., & Konrad, O. (2022). Technologies for biogas desulfurization - an overview of recent studies. *Renewable and Sustainable Energy Reviews*, *159*, 112205. https://doi.org/10.1016/j.rser.2022.112205

Beims, R. F., Hu, Y., Shui, H., & Xu, C. (Charles). (2020). Hydrothermal liquefaction of biomass to fuels and value-added chemicals: Products applications and challenges to develop large-scale operations. *Biomass and Bioenergy*, *135*, 105510. https://doi.org/10.1016/j.biombioe.2020.105510

Bellotti, D., Rivarolo, M., & Magistri, L. (2022). A comparative techno-economic and sensitivity analysis of Power-to-X processes from different energy sources. *Energy Conversion and Management*, *260*, 115565.

Beyene, H. D., Werkneh, A. A., & Ambaye, T. G. (2018). Current updates on waste to energy (WTE) Technologies: A Review. *Renewable Energy Focus*, *24*, 1–11. https://doi.org/10.1016/j.ref.2017.11.001

Borgschulte, A., Gallandat, N., Probst, B., Suter, R., Callini, E., Ferri, D., ... & Züttel, A. (2013). Sorption enhanced CO 2 methanation. *Physical Chemistry Chemical Physics*, *15*(24), 9620-9625.

Brooks, K. P., Hu, J., Zhu, H., & Kee, R. J. (2007). Methanation of carbon dioxide by hydrogen reduction using the Sabatier process in microchannel reactors. *Chemical Engineering Science*, *62*(4), 1161-1170.

Buttler, A., & Spliethoff, H. (2018). Current status of water electrolysis for energy storage, grid balancing and sector coupling via power-to-gas and power-to-liquids: A Review. *Renewable and Sustainable Energy Reviews*, *82*, 2440–2454. https://doi.org/10.1016/j.rser.2017.09.003

Buxbaum, M. (2013). Patent DE102011121930 A1.

Cabrera, D. V., & Labatut, R. A. (2021). Outlook and challenges for recovering energy and water from complex organic waste using hydrothermal liquefaction. *Sustainable Energy &amp; Fuels*, *5*(8), 2201–2227. https://doi.org/10.1039/d0se01857k

Cabrera, D. V., Barria, D. A., Camu, E., Celis, C., Tester, J. W., & Labatut, R. A. (2023). Enhancing energy recovery of wastewater treatment plants through hydrothermal liquefaction. *Environmental Science: Water Research &amp; Technology*, *9*(2), 474–488. https://doi.org/10.1039/d2ew00752e

Canada, E. and C. C. (2024). *Government of Canada*. Canada.ca. https://www.canada.ca/en/environment-climate-change/services/climate-change/greenhouse-gas-emissions/quantification-guidance/global-warming-potentials.html (Accessed on 17 August, 2024).

Canadian Council of Ministers of the Environment (2012). *Canada-wide approach for the management of wastewater biosolids*. https://ccme.ca/en/res/biosolids_cw_approach_e.pdf

Capson-Tojo, G., Rouez, M., Crest, M., Steyer, J.-P., Delgenès, J.-P., & Escudié, R. (2016). Food waste valorization via Anaerobic Processes: A Review. *Reviews in Environmental Science and Bio/Technology*, *15*(3), 499–547. https://doi.org/10.1007/s11157-016-9405-y

Carmo, M., Fritz, D. L., Mergel, J., & Stolten, D. (2013). A comprehensive review on PEM water electrolysis. *International journal of hydrogen energy*, *38*(12), 4901-4934.

Castello, D., Haider, M. S., & Rosendahl, L. A. (2019). Catalytic upgrading of hydrothermal liquefaction biocrudes: Different challenges for different feedstocks. *Renewable Energy*, *141*, 420–430. https://doi.org/10.1016/j.renene.2019.04.003

CEC. 2017. Characterization and Management of Food Loss and Waste in North America. Montreal, Canada: Commission for Environmental Cooperation. 48 pp.

C.E.R. (2024). *Canada energy regulator / Régie de l'énergie du Canada*. CER. https://www.cer-rec.gc.ca/en/data-analysis/energy-markets/provincial-territorial-energy-profiles/provincial-territorial-energy-profiles-canada.html, (Accessed on 17 August 2024).

Cervera-Mata, A., Lara, L., Fernández-Arteaga, A., Ángel Rufáin-Henares, J., & Delgado, G. (2021). Washed Hydrochar from spent coffee grounds: A second generation of coffee residues. evaluation as organic amendment. *Waste Management*, *120*, 322–329. https://doi.org/10.1016/j.wasman.2020.11.041

Chan, W. P., & Wang, J.-Y. (2018). Formation of synthetic sludge as a representative tool for thermochemical conversion modelling and performance analysis of Sewage Sludge – based on a TG-FTIR study. *Journal of Analytical and Applied Pyrolysis*, *133*, 97–106. https://doi.org/10.1016/j.jaap.2018.04.015

Chavan, D.; Arya, S.; Kumar, S. (2022). Open Dumping of Organic Waste: Associated Fire, Environmental Pollution and Health Hazards. *Advanced Organic Waste Management*, 15–31.

Cheikhwafa, J., Glińska, K., Torrens, E., & Bengoa, C. (2024). Effect of temperature on hydrothermal liquefaction of high lipids and carbohydrates content municipal primary sludge. *Heliyon*, *10*(3). https://doi.org/10.1016/j.heliyon.2024.e24731

Chen, H., Hao, S., Chen, Z., O-Thong, S., Fan, J., Clark, J., Luo, G., & Zhang, S. (2020a). Mesophilic and thermophilic anaerobic digestion of aqueous phase generated from hydrothermal liquefaction of Cornstalk: Molecular and Metabolic Insights. *Water Research*, *168*, 115199. https://doi.org/10.1016/j.watres.2019.115199

Chen, W.-T., Haque, Md. A., Lu, T., Aierzhati, A., & Reimonn, G. (2020b). A perspective on hydrothermal processing of Sewage Sludge. *Current Opinion in Environmental Science &amp; Health*, *14*, 63–73. https://doi.org/10.1016/j.coesh.2020.02.008

Chen, D., Wang, Y., Liu, Y., Cen, K., Cao, X., Ma, Z., & Li, Y. (2019a). Comparative study on the pyrolysis behaviors of rice straw under different washing pretreatments of water, acid solution, and aqueous phase bio-oil by using TG-FTIR and PY-GC/MS. *Fuel*, *252*, 1–9. https://doi.org/10.1016/j.fuel.2019.04.086

Chen, H., He, Z., Zhang, B., Feng, H., Kandasamy, S., & Wang, B. (2019b). Effects of the aqueous phase recycling on bio-oil yield in hydrothermal liquefaction of spirulina platensis, α-cellulose, and lignin. *Energy*, *179*, 1103–1113. https://doi.org/10.1016/j.energy.2019.04.184

Chen, H., Rao, Y., Cao, L., Shi, Y., Hao, S., Luo, G., & Zhang, S. (2019c). Hydrothermal conversion of sewage sludge: Focusing on the characterization of liquid products and their methane yields. *Chemical Engineering Journal*, *357*, 367–375. https://doi.org/10.1016/j.cej.2018.09.180

Chen, H., Wan, J., Chen, K., Luo, G., Fan, J., Clark, J., & Zhang, S. (2016). Biogas production from hydrothermal liquefaction wastewater (HTLWW): Focusing on the microbial communities as revealed by high-throughput sequencing of full-length 16S rrna genes. *Water Research*, *106*, 98–107. https://doi.org/10.1016/j.watres.2016.09.052

Chen, H., Zhang, C., Rao, Y., Jing, Y., Luo, G., & Zhang, S. (2017). Methane potentials of wastewater generated from hydrothermal liquefaction of rice straw: Focusing on the wastewater characteristics and microbial community compositions. *Biotechnology for Biofuels*, *10*(1). https://doi.org/10.1186/s13068-017-0830-0

Chen, K., Lyu, H., Hao, S., Luo, G., Zhang, S., & Chen, J. (2015). Separation of phenolic compounds with modified adsorption resin from aqueous phase products of hydrothermal liquefaction of Rice Straw. *Bioresource Technology*, *182*, 160–168. https://doi.org/10.1016/j.biortech.2015.01.124

Chen, W.-T., Zhang, Y., Zhang, J., Yu, G., Schideman, L. C., Zhang, P., & Minarick, M. (2014). Hydrothermal liquefaction of mixed-culture algal biomass from wastewater treatment system into bio-crude oil. *Bioresource Technology*, *152*, 130–139. https://doi.org/10.1016/j.biortech.2013.10.111

Chew, K. R., Leong, H. Y., Khoo, K. S., Vo, D.-V. N., Anjum, H., Chang, C.-K., & Show, P. L. (2021). Effects of anaerobic digestion of food waste on biogas production and environmental impacts: A Review. *Environmental Chemistry Letters*, *19*(4), 2921–2939. https://doi.org/10.1007/s10311-021-01220-z

Chiaberge, S., Leonardis, I., Fiorani, T., Bianchi, G., Cesti, P., Bosetti, A., Crucianelli, M., Reale, S., & De Angelis, F. (2013). Amides in bio-oil by hydrothermal liquefaction of organic wastes: A mass spectrometric study of the thermochemical reaction products of binary mixtures of amino acids and fatty acids. *Energy &amp; Fuels*, *27*(9), 5287–5297. https://doi.org/10.1021/ef4009983

Chiang, J. H., & Hopper, J. R. (1983). Kinetics of the hydrogenation of carbon dioxide over supported nickel. *Industrial & Engineering Chemistry Product Research and Development*, *22*(2), 225-228.

Chung, T.-S., Li, X., Ong, R. C., Ge, Q., Wang, H., & Han, G. (2012). Emerging forward osmosis (FO) technologies and challenges ahead for clean water and clean energy applications. *Current Opinion in Chemical Engineering*, *1*(3), 246–257. https://doi.org/10.1016/j.coche.2012.07.004

Cieślik, B. M., Namieśnik, J., & Konieczka, P. (2015). Review of Sewage Sludge Management: Standards, regulations and analytical methods. *Journal of Cleaner Production*, *90*, 1–15. https://doi.org/10.1016/j.jclepro.2014.11.031

*Consolidated federal laws of Canada* (2024, July 8)*, output-based pricing system regulations*. Output-Based Pricing System Regulations. https://laws-lois.justice.gc.ca/eng/regulations/SOR-2019-266/page-11.html#h-1185036

Crini, G., & Lichtfouse, E. (2018). Advantages and disadvantages of techniques used for wastewater treatment. *Environmental Chemistry Letters*, *17*(1), 145–155. https://doi.org/10.1007/s10311-018-0785-9

De Hullu, J., Maassen, J. I. W., Van Meel, P. A., Shazad, S., Vaessen, J. M. P., Bini, L., & Reijenga, J. C. (2008). Comparing different biogas upgrading techniques. *Eindhoven University of Technology, The Netherlands*.

Demirbas, A., Edris, G., & Alalayah, W. M. (2017). Sludge production from municipal wastewater treatment in Sewage Treatment Plant. *Energy Sources, Part A: Recovery, Utilization, and Environmental Effects*, *39*(10), 999–1006. https://doi.org/10.1080/15567036.2017.1283551

Dereli, R. K., Ersahin, M. E., Gomec, C. Y., Ozturk, I., & Ozdemir, O. (2009). Co-digestion of the organic fraction of municipal solid waste with primary sludge at a municipal wastewater treatment plant in Turkey. *Waste Management &amp; Research: The Journal for a Sustainable Circular Economy*, *28*(5), 404–410. https://doi.org/10.1177/0734242x09338227

Di Capua, F., Spasiano, D., Giordano, A., Adani, F., Fratino, U., Pirozzi, F., & Esposito, G. (2020). High-solid anaerobic digestion of sewage sludge: Challenges and opportunities. *Applied Energy*, *278*, 115608. https://doi.org/10.1016/j.apenergy.2020.115608

Dieguez-Alonso, A., Funke, A., Anca-Couce, A., Rombolà, A., Ojeda, G., Bachmann, J., & Behrendt, F. (2018). Towards biochar and Hydrochar Engineering—influence of process conditions on surface physical and chemical properties, thermal stability, nutrient availability, toxicity and wettability. *Energies*, *11*(3), 496. https://doi.org/10.3390/en11030496

Dimitriadis, A., & Bezergianni, S. (2017). Hydrothermal liquefaction of various biomass and waste feedstocks for biocrude production: A state of the art review. *Renewable and Sustainable Energy Reviews*, *68*, 113–125. https://doi.org/10.1016/j.rser.2016.09.120

Dion, J., & Linden-Fraser, R. (2024, May 7). *Industrial Carbon Pricing explained*. Canadian Climate Institute. https://climateinstitute.ca/large-emitter-trading-systems-explained/#:~:text=Let's%20assume%20the%20price%20of,have%20credits%20for)%20by%20%2480

Dodge, D. (2024). Macroeconomic Stabilization Policy in Canada. *Methods*.

Dovbeshko, G. (2000). FTIR spectroscopy studies of Nucleic Acid Damage. *Talanta*, *53*(1), 233–246. https://doi.org/10.1016/s0039-9140(00)00462-8

Duan, P., & Savage, P. E. (2010). Hydrothermal liquefaction of a microalga with heterogeneous catalysts. *Industrial &amp; Engineering Chemistry Research*, *50*(1), 52–61. https://doi.org/10.1021/ie100758s

Eboibi, B.E., Lewis, D. M., Ashman, P. J., & Chinnasamy, S. (2014). Effect of operating conditions on yield and quality of biocrude during hydrothermal liquefaction of halophytic microalga Tetraselmis sp.. *Bioresource Technology*, *170*, 20–29. https://doi.org/10.1016/j.biortech.2014.07.083

Eboibi, B. E., Lewis, D. M., Ashman, P. J., & Chinnasamy, S. (2015). Integrating anaerobic digestion and hydrothermal liquefaction for renewable energy production: An experimental investigation. *Environmental Progress &amp; Sustainable Energy*, *34*(6), 1662–1673. https://doi.org/10.1002/ep.12172

Elefsiniotis, P., & Oldham, W. K. (1994). Anaerobic acidogenesis of primary sludge: The role of solids retention time. *Biotechnology and Bioengineering*, *44*(1), 7–13. https://doi.org/10.1002/bit.260440103

Elliott, D. C., Biller, P., Ross, A. B., Schmidt, A. J., & Jones, S. B. (2015). Hydrothermal liquefaction of biomass: Developments from batch to continuous process. *Bioresource Technology*, *178*, 147–156. https://doi.org/10.1016/j.biortech.2014.09.132

Elliott, D. C., Hart, T. R., Schmidt, A. J., Neuenschwander, G. G., Rotness, L. J., Olarte, M. V., ... & Holladay, J. E. (2013). Process development for hydrothermal liquefaction of algae feedstocks in a continuous-flow reactor. *Algal research*, *2*(4), 445-454.

Fan, Y., Hornung, U., & Dahmen, N. (2022). Hydrothermal liquefaction of sewage sludge for biofuel application: A review on fundamentals, current challenges and strategies. *Biomass and Bioenergy*, *165*, 106570. https://doi.org/10.1016/j.biombioe.2022.106570

Fan, Q., Fu, P., Song, C., & Fan, Y. (2023). Valorization of waste biomass through hydrothermal liquefaction: A review with focus on linking hydrothermal factors to products characteristics. *Industrial Crops and Products*, *191*, 116017. https://doi.org/10.1016/j.indcrop.2022.116017

Fang, J., Zhan, L., Ok, Y. S., & Gao, B. (2018). Minireview of potential applications of hydrochar derived from hydrothermal carbonization of biomass. *Journal of Industrial and Engineering Chemistry*, *57*, 15–21. https://doi.org/10.1016/j.jiec.2017.08.026

Fang, Z., & Xu, C. C. (Eds.). (2014). *Near-critical and supercritical water and their applications for biorefineries* (Vol. 2). Springer.

Federation, W.E., APH Association, (2005). Standard Methods for the Examination of Water and Wastewater. American Public Health Association (APHA), Washington, DC, USA.

Francioso, O., Rodriguez-Estrada, M. T., Montecchio, D., Salomoni, C., Caputo, A., & Palenzona, D. (2010). Chemical characterization of municipal wastewater sludges produced by two-phase anaerobic digestion for biogas production. *Journal of Hazardous Materials*, *175*(1–3), 740–746. https://doi.org/10.1016/j.jhazmat.2009.10.071

Fregolente, L. G., dos Santos, J. V., Mazzati, F. S., Miguel, T. B., de C. Miguel, E., Moreira, A. B., Ferreira, O. P., & Bisinoti, M. C. (2021). Hydrochar from sugarcane industry by-products: Assessment of its potential use as a soil conditioner by germination and growth of maize. *Chemical and Biological Technologies in Agriculture*, *8*(1). https://doi.org/10.1186/s40538-021-00210-1

Fernandez, S., Srinivas, K., Schmidt, A. J., Swita, M. S., & Ahring, B. K. (2018). Anaerobic digestion of organic fraction from hydrothermal liquefied algae wastewater byproduct. *Bioresource Technology*, *247*, 250–258. https://doi.org/10.1016/j.biortech.2017.09.030

Forster-Carneiro, T., Pérez, M., & Romero, L. I. (2008). Influence of total solid and inoculum contents on performance of anaerobic reactors treating food waste. *Bioresource Technology*, *99*(15), 6994–7002. https://doi.org/10.1016/j.biortech.2008.01.018

Fuel Cells Bulletin (2019). Air Liquide to build 20 MW PEM electrolyser with Hydrogenics tech, Fuel Cells Bull. 2019 (2019) 9–9. https://doi.org/10.1016/s1464-2859(19)30108-7.

Gai, C., Zhang, Y., Chen, W.-T., Zhou, Y., Schideman, L., Zhang, P., Tommaso, G., Kuo, C.-T., & Dong, Y. (2015). Characterization of aqueous phase from the hydrothermal liquefaction of Chlorella Pyrenoidosa. *Bioresource Technology*, *184*, 328–335. https://doi.org/10.1016/j.biortech.2014.10.118

Gavrilescu, M., & Schiopu, A.-M. (2010). Municipal solid waste landfilling and treatment of resulting liquid effluents. *Environmental Engineering and Management Journal*, *9*(7), 993–1019. https://doi.org/10.30638/eemj.2010.133

Gerber Van Doren, L., Posmanik, R., Bicalho, F. A., Tester, J. W., & Sills, D. L. (2017). Prospects for energy recovery during hydrothermal and biological processing of waste biomass. *Bioresource Technology*, *225*, 67–74. https://doi.org/10.1016/j.biortech.2016.11.030

Ghadge, R., Nagwani, N., Saxena, N., Dasgupta, S., & Sapre, A. (2022). Design and scale-up challenges in hydrothermal liquefaction process for biocrude production and its upgradation. *Energy Conversion and Management: X*, *14*, 100223. https://doi.org/10.1016/j.ecmx.2022.100223

Görke, O., Pfeifer, P., & Schubert, K. (2005). Highly selective methanation by the use of a microchannel reactor. *Catalysis today*, *110*(1-2), 132-139.

Gotz, M. (2014). Methanisierung im Dreiphasen Reaktor, Karlsruhe Institute of Technology, Dissertation, Fakultat für Chemieingenieurwesen und Verfahrenstechnik. http://digbib.ubka.uni-karlsruhe.de/volltexte/ 1000044909

Götz, M., Bajohr, S., Graf, F., Reimert, R., & Kolb, T. (2013a). Einsatz eines Blasensäulenreaktors zur Methansynthese. *Chemie Ingenieur Technik (CIT)*, *85*(7).

Götz, M., Ortloff, F., Reimert, R., Basha, O., Morsi, B. I., & Kolb, T. (2013b). Evaluation of organic and ionic liquids for three-phase methanation and biogas purification processes. *Energy & Fuels*, *27*(8), 4705-4716.

Götz, M., Reimert, R., Bajohr, S., Schnetzer, H., Wimberg, J., & Schubert, T. J. (2015). Long-term thermal stability of selected ionic liquids in nitrogen and hydrogen atmosphere. *Thermochimica Acta*, *600*, 82-88.

Graf, F., Götz, M., Henel, M., Schaaf, T., & Tichler, R. (2014). Abschlussbericht: Techno-ökonomische Studie von Power-to-Gas-Konzepten. *DVGW Forschung–Deutscher Verein des Gas-und Wasserfaches eV Bonn*, 76-81.

Grande, C. A. (2011). Biogas upgrading by pressure swing adsorption. *Biofuel's Engineering Process Technology*, 65-84.

Grande, L., Pedroarena, I., Korili, S. A., & Gil, A. (2021). Hydrothermal liquefaction of biomass as one of the most promising alternatives for the synthesis of Advanced Liquid Biofuels: A Review. *Materials*, *14*(18), 5286. https://doi.org/10.3390/ma14185286

Gu, Y., Zhang, X., Deal, B., & Han, L. (2019). Biological Systems for treatment and valorization of wastewater generated from hydrothermal liquefaction of biomass and systems thinking: A Review. *Bioresource Technology*, *278*, 329–345. https://doi.org/10.1016/j.biortech.2019.01.127

Guan, L., Xu, H., & Huang, D. (2010). The investigation on states of water in different hydrophilic polymers by DSC and FTIR. *Journal of Polymer Research*, *18*(4), 681–689. https://doi.org/10.1007/s10965-010-9464-7

Guilera, J., Filipe, M., Montesó, A., Mallol, I., & Andreu, T. (2021). Carbon footprint of synthetic natural gas through biogas catalytic methanation. *Journal of Cleaner Production*, *287*, 125020.

Hao, S., Ren, S., Zhou, N., Chen, H., Usman, M., He, C., Shi, Q., Luo, G., & Zhang, S. (2020). Molecular composition of hydrothermal liquefaction wastewater from sewage sludge and its transformation during anaerobic digestion. *Journal of Hazardous Materials*, *383*, 121163. https://doi.org/10.1016/j.jhazmat.2019.121163

Hao, S., Zhu, X., Liu, Y., Qian, F., Fang, Z., Shi, Q., Zhang, S., Chen, J., & Ren, Z. J. (2018). Production temperature effects on the structure of Hydrochar-derived dissolved organic matter and associated toxicity. *Environmental Science &amp; Technology*, *52*(13), 7486–7495. https://doi.org/10.1021/acs.est.7b04983

Hao, B., Xu, D., Jiang, G., Sabri, T. A., Jing, Z., & Guo, Y. (2021). Chemical reactions in the hydrothermal liquefaction of biomass and in the catalytic hydrogenation upgrading of Biocrude. *Green Chemistry*, *23*(4), 1562–1583. https://doi.org/10.1039/d0gc02893b

Haosagul, S., Prommeenate, P., Hobbs, G., & Pisutpaisal, N. (2020a). Sulfide-oxidizing bacteria community in full-scale bioscrubber treating H2S in biogas from swine anaerobic digester. *Renewable Energy*, *150*, 973–980. https://doi.org/10.1016/j.renene.2019.11.139

Haosagul, S., Prommeenate, P., Hobbs, G., & Pisutpaisal, N. (2020b). Sulfur-oxidizing bacteria in full-scale biogas cleanup system of ethanol industry. *Renewable Energy*, *150*, 965–972. https://doi.org/10.1016/j.renene.2019.11.140

Herter, K., & Wayland, S. (2010). Residential response to critical-peak pricing of electricity: California evidence. *Energy*, *35*(4), 1561-1567.

Hu, Y., Gong, M., Feng, S., Xu, C. (Charles), & Bassi, A. (2019). A review of recent developments of pre-treatment technologies and hydrothermal liquefaction of microalgae for bio-crude oil production. *Renewable and Sustainable Energy Reviews*, *101*, 476–492. https://doi.org/10.1016/j.rser.2018.11.037

Huang, H., Yuan, X., Zhu, H., Li, H., Liu, Y., Wang, X., & Zeng, G. (2013). Comparative studies of thermochemical liquefaction characteristics of microalgae, lignocellulosic biomass and sewage sludge. *Energy*, *56*, 52–60. https://doi.org/10.1016/j.energy.2013.04.065

Huang, W., & Fooladi, H. (2021). Economic and environmental estimated assessment of power production from municipal solid waste using anaerobic digestion and landfill gas technologies. *Energy Reports*, *7*, 4460-4469.Inoue, S., Sawayama, S., Dote, Y., & Ogi, T. (1997). Behaviour of nitrogen during liquefaction of dewatered sewage sludge. *Biomass and Bioenergy*, *12*(6), 473–475. https://doi.org/10.1016/s0961-9534(97)00017-2

IEA (2019). *The future of hydrogen – analysis*. IEA. https://www.iea.org/reports/the-future-of-hydrogen (accessed on 12 August 2024).

IEA (2020). *Sustainable supply potential and costs – outlook for biogas and biomethane: Prospects for organic growth – analysis*. IEA. https://www.iea.org/reports/outlook-for-biogas-and-biomethane-prospects-for-organic-growth/sustainable-supply-potential-and-costs (accessed on 12 August 2024).

Islam, Md. A., Limon, Md. S., Romić, M., & Islam, Md. A. (2021). Hydrochar-based soil amendments for agriculture: A review of recent progress. *Arabian Journal of Geosciences*, *14*(2). https://doi.org/10.1007/s12517-020-06358-8

ISPT (2022). Next Level Solid Oxide Electrolysis: Upscaling potential and techno-economical evaluation for 3 industrial use cases, n.d. https://ispt.eu/media/20230508-FINAL-SOE-public-report-ISPT.pdf (accessed on 12 August 2024).

James, B. D., Baum, G. N., Perez, J., & Baum, K. N. (2009). *Technoeconomic analysis of photoelectrochemical (PEC) hydrogen production*. Directed Technologies, Inc., Arlington, VA (United States).

Janke, C., Duyar, M. S., Hoskins, M., & Farrauto, R. (2014). Catalytic and adsorption studies for the hydrogenation of CO2 to methane. *Applied Catalysis B: Environmental*, *152*, 184-191.

Janaszek, A., Silva, A. F., Jurišević, N., Kanuchova, M., Kozáková, Ľ., & Kowalik, R. (2024). The assessment of sewage sludge utilization in closed-loop economy from an environmental perspective. *Water*, *16*(3), 383. https://doi.org/10.3390/w16030383

Jasińska, A., Grosser, A., & Meers, E. (2023). Possibilities and limitations of anaerobic co-digestion of animal manure—A critical review. *Energies*, *16*(9), 3885. https://doi.org/10.3390/en16093885

Jena, U., Das, K. C., & Kastner, J. R. (2011). Effect of operating conditions of thermochemical liquefaction on Biocrude production from spirulina platensis. *Bioresource Technology*, *102*(10), 6221–6229. https://doi.org/10.1016/j.biortech.2011.02.057

Jenicek, P., Bartacek, J., Kutil, J., Zabranska, J., & Dohanyos, M. (2012). Potentials and limits of anaerobic digestion of sewage sludge: energy self-sufficient municipal wastewater treatment plant?. *Water science and technology*, *66*(6), 1277-1281.

Jones, S. B., Zhu, Y., Anderson, D. B., Hallen, R. T., Elliott, D. C., Schmidt, A. J., ... & Kinchin, C. (2014). *Process design and economics for the conversion of algal biomass to hydrocarbons: whole algae hydrothermal liquefaction and upgrading* (No. PNNL-23227). Pacific Northwest National Lab.(PNNL), Richland, WA (United States).

Jouny, M., Luc, W., & Jiao, F. (2018). General techno-economic analysis of CO2 electrolysis systems. *Industrial & Engineering Chemistry Research*, *57*(6), 2165-2177.

Kamali, M.; Gameiro, T.; Costa, M. E.; Capela, I. Anaerobic Digestion of Pulp and Paper Mill Wastes – an Overview of the Developments and Improvement Opportunities. *Chemical Engineering Journal* **2016**, *298*, 162–182.

Karatas, O., Khataee, A., & Kalderis, D. (2022). Recent progress on the phytotoxic effects of hydrochars and toxicity reduction approaches. *Chemosphere*, *298*, 134357. https://doi.org/10.1016/j.chemosphere.2022.134357

Kassem, N., Hockey, J., Lopez, C., Lardon, L., Angenent, L. T., & Tester, J. W. (2020a). Integrating anaerobic digestion, hydrothermal liquefaction, and biomethanation within a power-to-gas framework for Dairy Waste Management and grid decarbonization: A techno-economic assessment. *Sustainable Energy &amp; Fuels*, *4*(9), 4644–4661. https://doi.org/10.1039/d0se00608d

Kassem, N., Sills, D., Posmanik, R., Blair, C., & Tester, J. W. (2020b). Combining anaerobic digestion and hydrothermal liquefaction in the conversion of dairy waste into energy: A techno economic model for New York State. *Waste Management*, *103*, 228–239. https://doi.org/10.1016/j.wasman.2019.12.029

Khoshnevisan, B., Duan, N., Tsapekos, P., Awasthi, M. K., Liu, Z., Mohammadi, A., Angelidaki, I., Tsang, D. CW., Zhang, Z., Pan, J., Ma, L., Aghbashlo, M., Tabatabaei, M., & Liu, H. (2021). A critical review on livestock manure Biorefinery Technologies: Sustainability, challenges, and future perspectives. *Renewable and Sustainable Energy Reviews*, *135*, 110033. https://doi.org/10.1016/j.rser.2020.110033

Khoshnevisan, B., Tsapekos, P., Alfaro, N., Díaz, I., Fdz-Polanco, M., Rafiee, S., & Angelidaki, I. (2017). A review on prospects and challenges of biological h2s removal from biogas with focus on biotrickling filtration and microaerobic desulfurization. *Biofuel Research Journal*, *4*(4), 741–750. https://doi.org/10.18331/brj2017.4.4.6

Kiendl, I., Klemm, M., Clemens, A., & Herrman, A. (2014). Dilute gas methanation of synthesis gas from biomass gasification. *Fuel*, *123*, 211-217.

Kim, M., Ahn, Y.-H., & Speece, R. E. (2002). Comparative process stability and efficiency of anaerobic digestion; mesophilic vs. Thermophilic. *Water Research*, *36*(17), 4369–4385. https://doi.org/10.1016/s0043-1354(02)00147-1

Kiyasudeen S, K., Ibrahim, M. H., Quaik, S., & Ahmed Ismail, S. (2016). *Prospects of Organic Waste Management and the Significance of Earthworms*. https://doi.org/10.1007/978-3-319-24708-3

Knorr, D., Lukas, J., & Schoen, P. (2013). *Production of Advanced Biofuels via Liquefaction-Hydrothermal Liquefaction Reactor Design: April 5, 2013* (No. NREL/SR-5100-60462). National Renewable Energy Lab.(NREL), Golden, CO (United States).

Kopyscinski, J., Schildhauer, T. J., & Biollaz, S. M. (2010). Production of synthetic natural gas (SNG) from coal and dry biomass–A technology review from 1950 to 2009. *Fuel*, *89*(8), 1763-1783.

Kopyscinski, J., Schildhauer, T. J., & Biollaz, S. M. (2011). Methanation in a fluidized bed reactor with high initial CO partial pressure: Part I—Experimental investigation of hydrodynamics, mass transfer effects, and carbon deposition. *Chemical Engineering Science*, *66*(5), 924-934.

Krause, M. J., & Bronstein, K. E. (2024). Estimating national sludge generation and disposal from US drinking water and wastewater treatment plants. *Journal of Cleaner Production*, *453*, 142121. https://doi.org/10.1016/j.jclepro.2024.142121

Kumar, M., Olajire Oyedun, A., & Kumar, A. (2018). A review on the current status of various hydrothermal technologies on biomass feedstock. *Renewable and Sustainable Energy Reviews*, *81*, 1742–1770. https://doi.org/10.1016/j.rser.2017.05.270

Kumar, V., Chopra, A. K., & Kumar, A. (2017). A review on Sewage Sludge (Biosolids) A resource for sustainable agriculture. *Archives of Agriculture and Environmental Science*, *2*(4), 340–347. https://doi.org/10.26832/24566632.2017.020417

Leng, L., & Zhou, W. (2018). Chemical compositions and wastewater properties of aqueous phase (wastewater) produced from the hydrothermal treatment of wet biomass: A Review. *Energy Sources, Part A: Recovery, Utilization, and Environmental Effects*, *40*(22), 2648–2659. https://doi.org/10.1080/15567036.2018.1495780

Leng, L., Zhang, W., Leng, S., Chen, J., Yang, L., Li, H., Jiang, S., & Huang, H. (2020). Bioenergy recovery from wastewater produced by hydrothermal processing biomass: Progress, challenges, and opportunities. *Science of The Total Environment*, *748*, 142383. https://doi.org/10.1016/j.scitotenv.2020.142383

Li, C., Sun, J., Zou, H., & Cai, J. (2024). Experimental assessment on operation efficiency and output characteristics of an oil-free linear compressor in a refrigeration system under various parameters. *Applied Thermal Engineering*, *242*, 122453.

Li, R., Ma, Z., Yang, T., Li, B., Wei, L., & Sun, Y. (2018). Sub–supercritical liquefaction of municipal wet sewage sludge to produce bio-oil: Effect of different organic–water mixed solvents. *The Journal of Supercritical Fluids*, *138*, 115–123. https://doi.org/10.1016/j.supflu.2018.04.011

Li, R., Liu, D., Zhang, Y., Zhou, J., Tsang, Y. F., Liu, Z., Duan, N., & Zhang, Y. (2019). Improved methane production and energy recovery of post-hydrothermal liquefaction waste water via integration of zeolite adsorption and anaerobic digestion. *Science of The Total Environment*, *651*, 61–69. https://doi.org/10.1016/j.scitotenv.2018.09.175

Li, X., Hao, X., Abudula, A., & Guan, G. (2016). Nanostructured catalysts for electrochemical water splitting: Current State and prospects. *Journal of Materials Chemistry A*, *4*(31), 11973–12000. https://doi.org/10.1039/c6ta02334g

Li, Y., Hua, D., Xu, H., Jin, F., Zhao, Y., Chen, L., Zhao, B., Rosendahl, L. A., & Zhu, Z. (2022). Energy recovery from high ash-containing sewage sludge: Focusing on performance evaluation of bio-fuel production. *Science of The Total Environment*, *843*, 157083. https://doi.org/10.1016/j.scitotenv.2022.157083

Lievens, C., Mourant, D., He, M., Gunawan, R., Li, X., & Li, C.-Z. (2011). An FT-IR spectroscopic study of carbonyl functionalities in bio-oils. *Fuel*, *90*(11), 3417–3423. https://doi.org/10.1016/j.fuel.2011.06.001

Liu, Z., Chu, B., Zhai, X., Jin, Y., & Cheng, Y. (2012). Total methanation of syngas to synthetic natural gas over Ni catalyst in a micro-channel reactor. *Fuel*, *95*, 599-605.

Liu, Z., Grande, C. A., Li, P., Yu, J., & Rodrigues, A. E. (2011). Multi-bed vacuum pressure swing adsorption for carbon dioxide capture from flue gas. *Separation and Purification Technology*, *81*(3), 307-317.

Lytras, G., Lytras, C., Mathioudakis, D., Papadopoulou, K., & Lyberatos, G. (2020). Food waste valorization based on anaerobic digestion. *Waste and Biomass Valorization*, *12*(4), 1677–1697. https://doi.org/10.1007/s12649-020-01108-z

Maheshwary, A., Ambriano, J. R., Flaherty, J. J., & Subramanian, K. V. (2012). *U.S. Patent Application No. 12/846,532*.

Malins, K., Kampars, V., Brinks, J., Neibolte, I., Murnieks, R., & Kampare, R. (2015). Bio-oil from Thermo-Chemical Hydro-liquefaction of wet sewage sludge. *Bioresource Technology*, *187*, 23–29. https://doi.org/10.1016/j.biortech.2015.03.093

Mao, L., Tsui, T.-H., Zhang, J., Dai, Y., & Tong, Y. W. (2021). System integration of hydrothermal liquefaction and anaerobic digestion for wet biomass valorization: Biodegradability and Microbial Syntrophy. *Journal of Environmental Management*, *293*, 112981. https://doi.org/10.1016/j.jenvman.2021.112981

Markis, F., Baudez, J.-C., Parthasarathy, R., Slatter, P., & Eshtiaghi, N. (2016a). The apparent viscosity and yield stress of mixtures of primary and secondary sludge: Impact of volume fraction of secondary sludge and total solids concentration. *Chemical Engineering Journal*, *288*, 577–587. https://doi.org/10.1016/j.cej.2015.11.107

Mathanker, A., Das, S., Pudasainee, D., Khan, M., Kumar, A., & Gupta, R. (2021). A review of hydrothermal liquefaction of biomass for biofuels production with a special focus on the effect of process parameters, co-solvents, and extraction solvents. *Energies*, *14*(16), 4916. https://doi.org/10.3390/en14164916

Matute, G., Yusta, J. M., & Correas, L. C. (2019). Techno-economic modelling of water electrolysers in the range of several MW to provide grid services while generating hydrogen for different applications: A case study in Spain applied to mobility with FCEVs. *international journal of hydrogen energy*, *44*(33), 17431-17442.

Meegoda, J. N., Li, B., Patel, K., & Wang, L. B. (2018). A review of the processes, parameters, and optimization of anaerobic digestion. *International Journal of Environmental Research and Public Health*, *15*(10), 2224. https://doi.org/10.3390/ijerph15102224

Meister, M., Rezavand, M., Ebner, C., Pümpel, T., & Rauch, W. (2018). Mixing non-Newtonian flows in anaerobic digesters by impellers and pumped recirculation. *Advances in Engineering Software*, *115*, 194-203Minarick, M., Zhang, Y., Schideman, L., Wang, Z., Yu, G., Funk, T., & Barker, D. (2011). Product and economic analysis of direct liquefaction of swine manure. *BioEnergy Research*, *4*(4), 324–333. https://doi.org/10.1007/s12155-011-9157-z

Meng, F., Li, Z., Liu, J., Cui, X., & Zheng, H. (2015). Effect of promoter Ce on the structure and catalytic performance of Ni/Al2O3 catalyst for CO methanation in slurry-bed reactor. *Journal of Natural Gas Science and Engineering*, *23*, 250-258.

Mills, G. A., & Steffgen, F. W. (1974). Catalytic methanation. *Catalysis Reviews*, *8*(1), 159-210.

Mirmasoumi, S., Saray, R. K., & Ebrahimi, S. (2018). Evaluation of thermal pretreatment and digestion temperature rise in a biogas fueled combined cooling, heat, and power system using exergo-economic analysis. *Energy Conversion and Management*, *163*, 219-238.

Mishra, R. K., Kumar, V., Kumar, P., & Mohanty, K. (2022). Hydrothermal liquefaction of biomass for bio-crude production: A review on feedstocks, chemical compositions, operating parameters, reaction kinetics, techno-economic study, and Life Cycle Assessment. *Fuel*, *316*, 123377. https://doi.org/10.1016/j.fuel.2022.123377

Möller, K., & Müller, T. (2012). Effects of anaerobic digestion on digestate nutrient availability and crop growth: A Review. *Engineering in Life Sciences*, *12*(3), 242–257. https://doi.org/10.1002/elsc.201100085

Morales-Polo, C., del Mar Cledera-Castro, M., & Moratilla Soria, B. Y. (2018). Reviewing the anaerobic digestion of food waste: From waste generation and anaerobic process to its perspectives. *Applied Sciences*, *8*(10), 1804. https://doi.org/10.3390/app8101804

Motavaf, B., Capece, S. H., & Savage, P. E. (2021). Screening potential catalysts for the hydrothermal liquefaction of food waste. *Energy &amp; Fuels*, *35*(11), 9437–9449. https://doi.org/10.1021/acs.energyfuels.1c00672

Müller, K., Städter, M., Rachow, F., Hoffmannbeck, D., & Schmeißer, D. (2013). Sabatier-based CO 2-methanation by catalytic conversion. *Environmental Earth Sciences*, *70*, 3771-3778.

Nakason, K., Panyapinyopol, B., Kanokkantapong, V., Viriya-empikul, N., Kraithong, W., & Pavasant, P. (2018). Hydrothermal carbonization of unwanted biomass materials: Effect of process temperature and retention time on hydrochar and Liquid Fraction. *Journal of the Energy Institute*, *91*(5), 786–796. https://doi.org/10.1016/j.joei.2017.05.002

Neveux, N., Yuen, A. K. L., Jazrawi, C., Magnusson, M., Haynes, B. S., Masters, A. F., Montoya, A., Paul, N. A., Maschmeyer, T., & de Nys, R. (2014). Biocrude yield and productivity from the hydrothermal liquefaction of marine and freshwater green macroalgae. *Bioresource Technology*, *155*, 334–341. https://doi.org/10.1016/j.biortech.2013.12.083

Niknejad, P., Azizi, S. M., Hillier, K., Gupta, R., & Dhar, B. R. (2023). Biodegradability and transformation of biodegradable disposables in high-solids anaerobic digestion followed by hydrothermal liquefaction. *Resources, Conservation and Recycling*, *193*, 106979. https://doi.org/10.1016/j.resconrec.2023.106979

Nkoa, R. (2013). Agricultural benefits and environmental risks of soil fertilization with anaerobic digestates: A Review. *Agronomy for Sustainable Development*, *34*(2), 473–492. https://doi.org/10.1007/s13593-013-0196-z

Obeid, F., Chu Van, T., Brown, R., & Rainey, T. (2019). Nitrogen and sulphur in algal biocrude: A review of the HTL process, upgrading, engine performance and emissions. *Energy Conversion and Management*, *181*, 105–119. https://doi.org/10.1016/j.enconman.2018.11.054

O'Connor, J., Mickan, B. S., Rinklebe, J., Song, H., Siddique, K. H. M., Wang, H., Kirkham, M. B., & Bolan, N. S. (2022). Environmental implications, potential value, and future of food-waste anaerobic digestate management: A Review. *Journal of Environmental Management*, *318*, 115519. https://doi.org/10.1016/j.jenvman.2022.115519

O'Connor, S., Ehimen, E., Pillai, S. C., Black, A., Tormey, D., & Bartlett, J. (2021). Biogas production from small-scale anaerobic digestion plants on European farms. *Renewable and Sustainable Energy Reviews*, *139*, 110580. https://doi.org/10.1016/j.rser.2020.110580

OpenAI. (2023). *ChatGPT* (Mar 14 version) [Large language model]. https://chat.openai.com/chat

Okolie, J. A., Epelle, E. I., Tabat, M. E., Orivri, U., Amenaghawon, A. N., Okoye, P. U., & Gunes, B. (2022). Waste biomass valorization for the production of biofuels and value-added products: A Comprehensive Review of thermochemical, biological and Integrated Processes. *Process Safety and Environmental Protection*, *159*, 323–344. https://doi.org/10.1016/j.psep.2021.12.049

Palardy, O., Behnke, C., & Laurens, L. M. (2017). Fatty amide determination in neutral molecular fractions of green crude hydrothermal liquefaction oils from algal biomass. *Energy &amp; Fuels*, *31*(8), 8275–8282. https://doi.org/10.1021/acs.energyfuels.7b01175

Paul, T., Baskaran, D., Pakshirajan, K., Pugazhenthi, G., & Rajamanickam, R. (2021). Bio-oil production by hydrothermal liquefaction of Rhodococcus opacus biomass utilizing refinery wastewater: Biomass Valorization and process optimization. *Environmental Technology &amp; Innovation*, *21*, 101326. https://doi.org/10.1016/j.eti.2020.101326

Parvez, K., & Ahammed, M. M. (2024). Effect of composition on anaerobic digestion of organic fraction of municipal solid wastes: A Review. *Bioresource Technology Reports*, *25*, 101777. https://doi.org/10.1016/j.biteb.2024.101777

Pertl, A., Mostbauer, P., & Obersteiner, G. (2010). Climate balance of biogas upgrading systems. *Waste management*, *30*(1), 92-99.

Peterson, D., Vickers, J., & DeSantis, D. (2020). Hydrogen production cost from PEM electrolysis-2019. *DOE Hydrogen Fuel Cells Program Record*, *19009*.

Petrollese, M., & Cocco, D. (2020). Techno-economic assessment of hybrid CSP-biogas power plants. *Renewable Energy*, *155*, 420-431.

Piadeh, F., Offie, I., Behzadian, K., Rizzuto, J. P., Bywater, A., Córdoba-Pachón, J.-R., & Walker, M. (2024). A critical review for the impact of anaerobic digestion on the sustainable development goals. *Journal of Environmental Management*, *349*, 119458. https://doi.org/10.1016/j.jenvman.2023.119458

Pipitone, G., Zoppi, G., Bocchini, S., Rizzo, A. M., Chiaramonti, D., Pirone, R., & Bensaid, S. (2020). Aqueous phase reforming of the residual waters derived from lignin-rich hydrothermal liquefaction: Investigation of representative organic compounds and actual biorefinery streams. *Catalysis Today*, *345*, 237–250. https://doi.org/10.1016/j.cattod.2019.09.040

Pham, M., Schideman, L., Scott, J., Rajagopalan, N., & Plewa, M. J. (2013). Chemical and biological characterization of wastewater generated from hydrothermal liquefaction of *spirulina*. *Environmental Science &amp; Technology*, *47*(4), 2131–2138. https://doi.org/10.1021/es304532c

Ponnusamy, V. K., Nagappan, S., Bhosale, R. R., Lay, C.-H., Duc Nguyen, D., Pugazhendhi, A., Chang, S. W., & Kumar, G. (2020). Review on sustainable production of biochar through hydrothermal liquefaction: Physico-chemical properties and applications. *Bioresource Technology*, *310*, 123414. https://doi.org/10.1016/j.biortech.2020.123414

Posmanik, Roy, Labatut, R. A., Kim, A. H., Usack, J. G., Tester, J. W., & Angenent, L. T. (2017a). Coupling hydrothermal liquefaction and anaerobic digestion for energy valorization from model biomass feedstocks. *Bioresource Technology*, *233*, 134–143. https://doi.org/10.1016/j.biortech.2017.02.095

Posmanik, R., Martinez, C. M., Cantero-Tubilla, B., Cantero, D. A., Sills, D. L., Cocero, M. J., & Tester, J. W. (2017b). Acid and alkali catalyzed hydrothermal liquefaction of dairy manure digestate and food waste. *ACS Sustainable Chemistry &amp; Engineering*, *6*(2), 2724–2732. https://doi.org/10.1021/acssuschemeng.7b04359

Prestigiacomo, C., Proietto, F., Laudicina, V. A., Siragusa, A., Scialdone, O., & Galia, A. (2021). Catalytic hydrothermal liquefaction of municipal sludge assisted by formic acid for the production of next-generation fuels. *Energy*, *232*, 121086. https://doi.org/10.1016/j.energy.2021.121086

Qadir, M., Drechsel, P., Jiménez Cisneros, B., Kim, Y., Pramanik, A., Mehta, P., & Olaniyan, O. (2020). Global and regional potential of wastewater as a water, nutrient and energy source. *Natural Resources Forum*, *44*(1), 40–51. https://doi.org/10.1111/1477-8947.12187

Qian, L., Wang, S., & Savage, P. E. (2017). Hydrothermal liquefaction of sewage sludge under isothermal and fast conditions. *Bioresource Technology*, *232*, 27–34. https://doi.org/10.1016/j.biortech.2017.02.017

Quispe-Arpasi, D., de Souza, R., Stablein, M., Liu, Z., Duan, N., Lu, H., Zhang, Y., Oliveira, A. L., Ribeiro, R., & Tommaso, G. (2018). Anaerobic and photocatalytic treatments of post-hydrothermal liquefaction wastewater using H2O2. *Bioresource Technology Reports*, *3*, 247–255. https://doi.org/10.1016/j.biteb.2018.08.003

Ramirez, J., Brown, R., & Rainey, T. (2015). A review of hydrothermal liquefaction bio-crude properties and prospects for upgrading to transportation fuels. *Energies*, *8*(7), 6765–6794. https://doi.org/10.3390/en8076765

Ranganathan, P., & Savithri, S. (2019). Techno-economic analysis of microalgae-based liquid fuels production from wastewater via hydrothermal liquefaction and hydroprocessing. *Bioresource Technology*, *284*, 256–265. https://doi.org/10.1016/j.biortech.2019.03.087

Ranieri, E., Giuliano, S., & Ranieri, A. C. (2021). Energy consumption in anaerobic and aerobic based wastewater treatment plants in Italy. *Water Practice & Technology*, *16*(3), 851-863

Raposo, F., De la Rubia, M. A., Fernández-Cegrí, V., & Borja, R. (2012). Anaerobic digestion of solid organic substrates in batch mode: An overview relating to methane yields and experimental procedures. *Renewable and Sustainable Energy Reviews*, *16*(1), 861–877. https://doi.org/10.1016/j.rser.2011.09.008

Rege, S. U., Yang, R. T., Qian, K., & Buzanowski, M. A. (2001). Air-prepurification by pressure swing adsorption using single/layered beds. *Chemical engineering science*, *56*(8), 2745-2759.

Reksten, A. H., Thomassen, M. S., Møller-Holst, S., & Sundseth, K. (2022). Projecting the future cost of PEM and alkaline water electrolysers; a CAPEX model including electrolyser plant size and technology development. *International Journal of hydrogen energy*, *47*(90), 38106-38113.

Ren, S., Usman, M., Tsang, D. C., O-Thong, S., Angelidaki, I., Zhu, X., Zhang, S., & Luo, G. (2020). Hydrochar-facilitated anaerobic digestion: Evidence for direct interspecies electron transfer mediated through surface oxygen-containing functional groups. *Environmental Science &amp; Technology*, *54*(9), 5755–5766. https://doi.org/10.1021/acs.est.0c00112

Rezaee, M., Gitipour, S., & Sarrafzadeh, M.-H. (2020). Different Pathways to Integrate Anaerobic Digestion and Thermochemical Processes: Moving Toward the Circular Economy Concept. *Environmental Energy and Economic Research*, *4*(1), 57–67. https://doi.org/10.22097/eeer.2019.189193.1090

Rivas-Arrieta, M. J., Torri, C., Rombolà, A. G., & Biller, P. (2024). Hydrochar fractionation and composition in batch and continuous hydrothermal liquefaction. *Biomass and Bioenergy*, *183*, 107166. https://doi.org/10.1016/j.biombioe.2024.107166

Rönsch, S., & Ortwein, A. (2011). Methanation of synthetic gas–Fundamentals and process development. *Chemie Ingenieur Technik*, *83*(8), 1200-1208.

Rout, P. R., Goel, M., Pandey, D. S., Briggs, C., Sundramurthy, V. P., Halder, N., Mohanty, A., Mukherjee, S., & Varjani, S. (2023). Technological advancements in valorisation of industrial effluents employing hydrothermal liquefaction of biomass: Strategic Innovations, barriers and perspectives. *Environmental Pollution*, *316*, 120667. https://doi.org/10.1016/j.envpol.2022.120667

Samoraj, M., Mironiuk, M., Izydorczyk, G., Witek-Krowiak, A., Szopa, D., Moustakas, K., & Chojnacka, K. (2022). The challenges and perspectives for anaerobic digestion of animal waste and fertilizer application of the Digestate. *Chemosphere*, *295*, 133799. https://doi.org/10.1016/j.chemosphere.2022.133799

Sanaye, S., Khakpaay, N., & Chitsaz, A. (2020). Thermo-economic and environmental multi-objective optimization of a novel arranged biomass-fueled gas engine and backpressure steam turbine combined system for pulp and paper mills. *Sustainable Energy Technologies and Assessments*, *40*, 100778.

Sanaye, S., & Yazdani, M. (2022). Energy, Exergy, economic and environmental analysis of a running integrated anaerobic digester-combined heat and power system in a municipal wastewater treatment plant. *Energy Reports*, *8*, 9724–9741. https://doi.org/10.1016/j.egyr.2022.07.155

Santos, M. S., Grande, C. A., & Rodrigues, A. E. (2011). New cycle configuration to enhance performance of kinetic PSA processes. *Chemical Engineering Science*, *66*(8), 1590-1599.

Sawatdeenarunat, C., Surendra, K. C., Takara, D., Oechsner, H., & Khanal, S. K. (2015). Anaerobic digestion of lignocellulosic biomass: Challenges and opportunities. *Bioresource Technology*, *178*, 178–186. https://doi.org/10.1016/j.biortech.2014.09.103

Schaaf, T., Gruenig, J., Schuster, M., & Orth, A. (2014). Storage of Electrical Energy in a Gas Distribution System–Methanation of CO2-Containing Gases. *Chemie Ingenieur Technik*, *86*(4), 476-485.

Schmidt, O., Gambhir, A., Staffell, I., Hawkes, A., Nelson, J., & Few, S. (2017). Future cost and performance of water electrolysis: An expert elicitation study. *International Journal of Hydrogen Energy*, *42*(52), 30470–30492. https://doi.org/10.1016/j.ijhydene.2017.10.045

Seemann, M. C., Schildhauer, T. J., & Biollaz, S. M. (2010). Fluidized bed methanation of wood-derived producer gas for the production of synthetic natural gas. *Industrial & engineering chemistry research*, *49*(15), 7034-7038.

Shakya, R., Whelen, J., Adhikari, S., Mahadevan, R., & Neupane, S. (2015). Effect of temperature and NA2CO3 catalyst on hydrothermal liquefaction of algae. *Algal Research*, *12*, 80–90. https://doi.org/10.1016/j.algal.2015.08.006

Shakya, R., Adhikari, S., Mahadevan, R., Shanmugam, S. R., Nam, H., Hassan, E. B., & Dempster, T. A. (2017). Influence of biochemical composition during hydrothermal liquefaction of algae on product yields and fuel properties. *Bioresource Technology*, *243*, 1112–1120. https://doi.org/10.1016/j.biortech.2017.07.046

Shanmugam, S. R., Adhikari, S., Wang, Z., & Shakya, R. (2017). Treatment of aqueous phase of bio-oil by granular activated carbon and evaluation of biogas production. *Bioresource Technology*, *223*, 115–120. https://doi.org/10.1016/j.biortech.2016.10.008

Si, B., Li, J., Zhu, Z., Shen, M., Lu, J., Duan, N., Zhang, Y., Liao, Q., Huang, Y., & Liu, Z. (2018). Inhibitors degradation and microbial response during continuous anaerobic conversion of hydrothermal liquefaction wastewater. *Science of The Total Environment*, *630*, 1124–1132. https://doi.org/10.1016/j.scitotenv.2018.02.310

Si, B., Yang, L., Zhou, X., Watson, J., Tommaso, G., Chen, W.-T., Liao, Q., Duan, N., Liu, Z., & Zhang, Y. (2019). Anaerobic conversion of the hydrothermal liquefaction aqueous phase: Fate of organics and intensification with Granule Activated Carbon/Ozone Pretreatment. *Green Chemistry*, *21*(6), 1305–1318. https://doi.org/10.1039/c8gc02907e

Siddiqua, A., Hahladakis, J. N., & Al-Attiya, W. A. (2022). An overview of the environmental pollution and health effects associated with waste landfilling and open dumping. *Environmental Science and Pollution Research*, *29*(39), 58514–58536. https://doi.org/10.1007/s11356-022-21578-z

Sikosana, M. L., Sikhwivhilu, K., Moutloali, R., & Madyira, D. M. (2019). Municipal wastewater treatment technologies: A Review. *Procedia Manufacturing*, *35*, 1018–1024. https://doi.org/10.1016/j.promfg.2019.06.051

Silva Thomsen, L. B., Anastasakis, K., & Biller, P. (2022). Wet oxidation of aqueous phase from hydrothermal liquefaction of Sewage Sludge. *Water Research*, *209*, 117863. https://doi.org/10.1016/j.watres.2021.117863

Singh, R., Prakash, A., Dhiman, S. K., Balagurumurthy, B., Arora, A. K., Puri, S. K., & Bhaskar, T. (2014). Hydrothermal conversion of lignin to substituted phenols and aromatic ethers. *Bioresource Technology*, *165*, 319–322. https://doi.org/10.1016/j.biortech.2014.02.076

Snowden-Swan, L. J., Zhu, Y., Bearden, M. D., Seiple, T. E., Jones, S. B., Schmidt, A. J., ... & Elliott, D. C. (2017). *Conceptual biorefinery design and research targeted for 2022: hydrothermal liquefaction processing of wet waste to fuels* (No. PNNL-27186). Pacific Northwest National Lab.(PNNL), Richland, WA (United States).

Somers, M. H., Azman, S., Sigurnjak, I., Ghyselbrecht, K., Meers, E., Meesschaert, B., & Appels, L. (2018). Effect of digestate disintegration on anaerobic digestion of organic waste. *Bioresource Technology*, *268*, 568–576. https://doi.org/10.1016/j.biortech.2018.08.036

Spoorthi, G., Thakur, R. S., Kaistha, N., & Rao, D. P. (2011). Process intensification in PSA processes for upgrading synthetic landfill and lean natural gases. *Adsorption*, *17*, 121-133.

Sposob, M., Nam, J.-Y., Park, J.-G., Kim, T.-H., Hwang, Y., Jeong, S. M., & Yun, Y.-M. (2021). Starvation pretreatment enhances sulfidogenic operation of two-stage anaerobic digestion system for biogas production with low H2S content. *Journal of Cleaner Production*, *290*, 125166. https://doi.org/10.1016/j.jclepro.2020.125166

Sterner, M., & Stadler, I. (2014). *Energiespeicher-bedarf, Technologien, Integration*. Springer-Verlag.

Steward, D., Ramsden, T., & Zuboy, J. (2012). H2A central hydrogen production model, version 3 user guide (DRAFT). *National Renewable Energy Laboratory, USA*.

SundarRajan, P., Gopinath, K. P., Arun, J., GracePavithra, K., Adithya Joseph, A., & Manasa, S. (2021). Insights into valuing the aqueous phase derived from hydrothermal liquefaction. *Renewable and Sustainable Energy Reviews*, *144*, 111019. https://doi.org/10.1016/j.rser.2021.111019

SUZUKI, A., NAKAMURA, T., YOKOYAMA, S.-Y., OGI, T., & KOGUCHI, K. (1988). Conversion of sewage sludge to heavy oil by direct thermochemical liquefaction. *JOURNAL OF CHEMICAL ENGINEERING OF JAPAN*, *21*(3), 288–293. https://doi.org/10.1252/jcej.21.288

Tambone, F., Scaglia, B., D'Imporzano, G., Schievano, A., Orzi, V., Salati, S., & Adani, F. (2010). Assessing amendment and fertilizing properties of digestates from anaerobic digestion through a comparative study with digested sludge and compost. *Chemosphere*, *81*(5), 577–583. https://doi.org/10.1016/j.chemosphere.2010.08.034

Tan, E. C., & Lamers, P. (2021). Circular bioeconomy concepts—a perspective. *Frontiers in Sustainability*, *2*. https://doi.org/10.3389/frsus.2021.701509

Tatla, H. K., Ismail, S., Khan, M. A., Dhar, B. R., & Gupta, R. (2024). Coupling hydrothermal liquefaction and anaerobic digestion for waste biomass valorization: A review in context of circular economy. *Chemosphere*, *361*, 142419. https://doi.org/10.1016/j.chemosphere.2024.142419

Tesfamariam, E. H., Ogbazghi, Z. M., Annandale, J. G., & Gebrehiwot, Y. (2020). Cost–benefit analysis of municipal sludge as a low-grade nutrient source: A case study from South Africa. *Sustainability*, *12*(23), 9950.

Thema, M., Weidlich, T., Hörl, M., Bellack, A., Mörs, F., Hackl, F., Kohlmayer, M., Gleich, J., Stabenau, C., Trabold, T., Neubert, M., Ortloff, F., Brotsack, R., Schmack, D., Huber, H., Hafenbradl, D., Karl, J., & Sterner, M. (2019). Biological CO2-Methanation: An approach to standardization. *Energies*, *12*(9), 1670. https://doi.org/10.3390/en12091670

Tian, X., Richardson, R. E., Tester, J. W., Lozano, J. L., & You, F. (2020). Retrofitting Municipal Wastewater Treatment Facilities Toward a greener and circular economy by virtue of resource recovery: Techno-economic analysis and life cycle assessment. *ACS Sustainable Chemistry &amp; Engineering*, *8*(36), 13823–13837. https://doi.org/10.1021/acssuschemeng.0c05189

Tichý, R., Janssen, A., Grotenhuis, J. T. C., Lettinga, G., & Rulkens, W. H. (1994). Possibilities for using biologically-produced sulphur for cultivation of Thiobacilli with respect to bioleaching processes. *Bioresource Technology*, *48*(3), 221–227. https://doi.org/10.1016/0960-8524(94)90150-3

Toor, S. S., Rosendahl, L., Nielsen, M. P., Glasius, M., Rudolf, A., & Iversen, S. B. (2012). Continuous production of bio-oil by catalytic liquefaction from wet distiller's grain with solubles (WDGS) from bio-ethanol production. *Biomass and bioenergy*, *36*, 327-332.

Turton, R., Bailie, R. C., Whiting, W. B., & Shaeiwitz, J. A. (2008). *Analysis, synthesis and design of chemical processes*. Pearson Education.

*Understanding Global Warming Potentials*. US EPA. (2023). https://www.epa.gov/ghgemissions/understanding-global-warming-potentials

Urban, W., Lohmann, H., Girod, K., Dachs, G., & Zach, C. (2009). Beseitigung technischer, rechtlicher und ökonomischer Hemmnisse bei der Einspeisung biogener Gase in das Erdgasnetz zur Reduzierung klimarelevanter Emissionen durch Aufbau und Anwendung einer georeferenzierten Datenbank. Bd. 4: Technologien und Kosten der Biogasaufbereitung und Einspeisung in das Erdgasnetz. Ergänzte und aktualisierte Version 4.17.

Usman, M., Shi, Z., Ren, S., Ngo, H. H., Luo, G., & Zhang, S. (2020). Hydrochar promoted anaerobic digestion of hydrothermal liquefaction wastewater: Focusing on the organic degradation and microbial community. *Chemical Engineering Journal*, *399*, 125766. https://doi.org/10.1016/j.cej.2020.125766

Van Doren, L. G., Posmanik, R., Bicalho, F. A., Tester, J. W., & Sills, D. L. (2017). Prospects for energy recovery during hydrothermal and biological processing of waste biomass. *Bioresource technology*, *225*, 67-74.

Van Leeuwen, C., & Zauner, A. (2018). Innovative large-scale energy storage technologies and Power-to-Gas concepts after optimisation. *Report on the costs involved with PtG technologies and their potentials across the EU, University of Groningen*.

Vannice, M. A. (1976). The catalytic synthesis of hydrocarbons from carbon monoxide and hydrogen. *Catalysis Reviews—Science and Engineering*, *14*(1), 153-191.

Vardon, D. R., Sharma, B. K., Scott, J., Yu, G., Wang, Z., Schideman, L., Zhang, Y., & Strathmann, T. J. (2011). Chemical properties of biocrude oil from the hydrothermal liquefaction of spirulina algae, swine manure, and digested Anaerobic Sludge. *Bioresource Technology*, *102*(17), 8295–8303. https://doi.org/10.1016/j.biortech.2011.06.041

Walspurger, S., Elzinga, G. D., Dijkstra, J. W., Sarić, M., & Haije, W. G. (2014). Sorption enhanced methanation for substitute natural gas production: Experimental results and thermodynamic considerations. *Chemical Engineering Journal*, *242*, 379-386.

Wang, P., Sakhno, Y., Adhikari, S., Peng, H., Jaisi, D., Soneye, T., Higgins, B., & Wang, Q. (2021). Effect of ammonia removal and biochar detoxification on anaerobic digestion of aqueous phase from municipal sludge hydrothermal liquefaction. *Bioresource Technology*, *326*, 124730. https://doi.org/10.1016/j.biortech.2021.124730

Wang, X., Chen, T., Ge, Y., & Jia, Y. (2008). Studies on land application of sewage sludge and its limiting factors. *Journal of Hazardous Materials*, *160*(2–3), 554–558. https://doi.org/10.1016/j.jhazmat.2008.03.046

*Waste-to-energy 2050: Clean Technologies for Sustainable Waste Management*. ESWET (European Suppliers of Waste-to-Energy Technology). (2020, October 26). https://eswet.eu/documents/waste-to-energy-2050/

Watson, J., Lu, J., de Souza, R., Si, B., Zhang, Y., & Liu, Z. (2019). Effects of the extraction solvents in hydrothermal liquefaction processes: Biocrude oil quality and Energy Conversion Efficiency. *Energy*, *167*, 189–197. https://doi.org/10.1016/j.energy.2018.11.003

Watson, J., Wang, T., Si, B., Chen, W.-T., Aierzhati, A., & Zhang, Y. (2020). Valorization of hydrothermal liquefaction aqueous phase: Pathways towards commercial viability. *Progress in Energy and Combustion Science*, *77*, 100819. https://doi.org/10.1016/j.pecs.2019.100819

Wei, Y., Xu, D., Xu, M., Zheng, P., Fan, L., Leng, L., & Kapusta, K. (2024). Hydrothermal liquefaction of municipal sludge and its products applications. *Science of The Total Environment*, *908*, 168177. https://doi.org/10.1016/j.scitotenv.2023.168177

Xiu, S., Shahbazi, A., Wang, L., & W. Wallace, C. (2010). Supercritical ethanol liquefaction of swine manure for bio-oils production. *American Journal of Engineering and Applied Sciences*, *3*(2), 494–500. https://doi.org/10.3844/ajeassp.2010.494.500

Xu, D., Lin, G., Guo, S., Wang, S., Guo, Y., & Jing, Z. (2018a). Catalytic hydrothermal liquefaction of algae and upgrading of biocrude: A critical review. *Renewable and Sustainable Energy Reviews*, *97*, 103–118. https://doi.org/10.1016/j.rser.2018.08.042

Xu, F., Li, Y., Ge, X., Yang, L., & Li, Y. (2018b). Anaerobic digestion of food waste – challenges and opportunities. *Bioresource Technology*, *247*, 1047–1058. https://doi.org/10.1016/j.biortech.2017.09.020

Xu, Y.-H., & Li, M.-F. (2021). Hydrothermal liquefaction of lignocellulose for value-added products: Mechanism, parameter and production application. *Bioresource Technology*, *342*, 126035. https://doi.org/10.1016/j.biortech.2021.126035

Xu, Y., Wang, Y., Lu, J., Yuan, C., Zhang, L., & Liu, Z. (2022). Understand the antibacterial behavior and mechanism of hydrothermal wastewater. *Water Research*, *226*, 119318. https://doi.org/10.1016/j.watres.2022.119318

Yadav, G., Mishra, A., Ghosh, P., Sindhu, R., Vinayak, V., & Pugazhendhi, A. (2021). Technical, economic and environmental feasibility of Resource Recovery Technologies from wastewater. *Science of The Total Environment*, *796*, 149022. https://doi.org/10.1016/j.scitotenv.2021.149022

Yang, L., Si, B., Tan, X., Chu, H., Zhou, X., Zhang, Y., Zhang, Y., & Zhao, F. (2018). Integrated anaerobic digestion and algae cultivation for energy recovery and nutrient supply from post-hydrothermal liquefaction wastewater. *Bioresource Technology*, *266*, 349–356. https://doi.org/10.1016/j.biortech.2018.06.083

Yuan, X., Wang, J., Zeng, G., Huang, H., Pei, X., Li, H., Liu, Z., & Cong, M. (2011). Comparative studies of thermochemical liquefaction characteristics of microalgae using different organic solvents. *Energy*, *36*(11), 6406–6412. https://doi.org/10.1016/j.energy.2011.09.031

Zagklis, D. P., & Bampos, G. (2022). Tertiary Wastewater Treatment Technologies: A review of technical, economic, and life cycle aspects. *Processes*, *10*(11), 2304. https://doi.org/10.3390/pr10112304

Zeng, K., & Zhang, D. (2010). Recent progress in alkaline water electrolysis for hydrogen production and applications. *Progress in Energy and Combustion Science*, *36*(3), 307–326. https://doi.org/10.1016/j.pecs.2009.11.002

Zhang, J., Bai, Y., Zhang, Q., Wang, X., Zhang, T., Tan, Y., & Han, Y. (2014). Low-temperature methanation of syngas in slurry phase over Zr-doped Ni/γ-Al2O3 catalysts prepared using different methods. *Fuel*, *132*, 211-218.

Zhang, J., & Zhang, Y. (2014). Hydrothermal liquefaction of microalgae in an ethanol–water co-solvent to produce biocrude oil. *Energy &amp; Fuels*, *28*(8), 5178–5183. https://doi.org/10.1021/ef501040j

Zhang, C., Tang, X., Sheng, L., & Yang, X. (2016). Enhancing the performance of co-hydrothermal liquefaction for mixed algae strains by the Maillard reaction. *Green Chemistry*, *18*(8), 2542–2553. https://doi.org/10.1039/c5gc02953h

Zhang, S., Yang, X., Zhang, H., Chu, C., Zheng, K., Ju, M., & Liu, L. (2019a). Liquefaction of biomass and upgrading of bio-oil: A Review. *Molecules*, *24*(12), 2250. https://doi.org/10.3390/molecules24122250

Zhang, Y., Jiang, Q., Xie, W., Wang, Y., & Kang, J. (2019b). Effects of temperature, time and acidity of hydrothermal carbonization on the Hydrochar properties and nitrogen recovery from Corn Stover. *Biomass and Bioenergy*, *122*, 175–182. https://doi.org/10.1016/j.biombioe.2019.01.035

Zhang, X., Li, X., Li, R., & Wu, Y. (2020). Hydrothermal carbonization and liquefaction of sludge for harmless and resource purposes: A Review. *Energy &amp; Fuels*, *34*(11), 13268–13290. https://doi.org/10.1021/acs.energyfuels.0c02467

Zheng, J.-L., Zhu, M.-Q., & Wu, H. (2015). Alkaline hydrothermal liquefaction of swine carcasses to bio-oil. *Waste Management*, *43*, 230–238. https://doi.org/10.1016/j.wasman.2015.05.010

Zheng, M., Schideman, L. C., Tommaso, G., Chen, W.-T., Zhou, Y., Nair, K., Qian, W., Zhang, Y., & Wang, K. (2017). Anaerobic digestion of wastewater generated from the hydrothermal liquefaction of Spirulina: Toxicity Assessment and minimization. *Energy Conversion and Management*, *141*, 420–428. https://doi.org/10.1016/j.enconman.2016.10.034

Zhou, Y., Schideman, L., Zheng, M., Martin-Ryals, A., Li, P., Tommaso, G., & Zhang, Y. (2015). Anaerobic digestion of post-hydrothermal liquefaction wastewater for improved energy efficiency of hydrothermal bioenergy processes. *Water Science and Technology*, *72*(12), 2139–2147. https://doi.org/10.2166/wst.2015.435

Zhu, Z., Rosendahl, L., Toor, S. S., Yu, D., & Chen, G. (2015). Hydrothermal liquefaction of barley straw to bio-crude oil: Effects of reaction temperature and aqueous phase recirculation. *Applied Energy*, *137*, 183–192. https://doi.org/10.1016/j.apenergy.2014.10.005

Zhuo, Y., Yang, P., Zhou, M., Peng, D., & Han, Y. (2022). Low H2S content biogas biodesulfurization from high solid sludge anaerobic digestion using limited external aeration biotrickling filter: Effect of gas-liquid pattern on oxygen utilization performance. *Journal of Environmental Management*, *314*, 115084. https://doi.org/10.1016/j.jenvman.2022.115084

# Appendix

## *Supplementary Information for Chapter 3*

***Table S1**: Detailed Characteristics of the inoculum*

| | MC (wt. %) | TS (wt. %) | VS (wt. %) |
|---|---|---|---|
| Inoculum | 97.394 ± 0.02 | 2.606 ± 0.02 | 1.359 ± 0.01 |
| MC: moisture content; TS: total solids; VS: volatile solids. | | | |

***Table S2**: Major compounds identified in the biocrudes generated from the HTL of primary sludge and digestate.*

### Primary Sludge:

1. HTL Operating Conditions: 250°C: 30 & 60 min

| Peak | RT, min | Identified Compounds | Area% | |
|---|---|---|---|---|
| | | | 250°C & 30 min | 250°C & 60 min |
| 1 | 14.8 | n-Hexadecanoic acid | 36.506 | 35.137 |
| 2 | 16.3573 | Oleic anhydride | - | 7.969 |
| 3 | 16.3902 | Octadecanoic acid | 20.251 | 21.113 |
| 4 | 16.4073 | Octadecanoic acid, 2-(2-hydroxyethoxy)ethyl ester | 8.704 | - |
| 5 | 20.8319 | 2,6,10-Dodecatrien-1-ol, 3,7,11-trimethyl-, (E,E)- | 1.049 | - |
| 6 | 20.8424 | 2,6,10-Dodecatrien-1-ol, 3,7,11-trimethyl-, acetate, (E,E)- | 0.998 | 1.024 |
| 7 | 22.4569 | Cholestanol | - | 1.113 |

| | | | | |
|---|---|---|---|---|
| 8 | 22.4793 | 5-.beta.-cholestan-3.alpha.-ol, octanoate | 2.805 | 7.501 |
| 9 | 22.7659 | Cholest-5-en-3-ol, (3.alpha.)- | - | 2.347 |
| 10 | 22.7719 | Cholesteryl hydrogen succinate | 6.433 | - |
| 11 | 22.7982 | Cholesteryl benzoate | 1.113 | - |
| 12 | 22.8629 | Hexadecanoic acid, tetradecyl ester | 1.588 | - |
| 13 | 23.9792 | Hexadecanoic acid, octadecyl ester | 3.574 | 1.546 |
| 14 | 23.985 | Hexadecanoic acid, hexadecyl ester | 1.493 | 3.728 |

2. HTL Operating Conditions: 300°C: 30 & 60 min

| Peak | RT, min | Identified Compounds | Area% | |
|---|---|---|---|---|
| | | | 300°C & 30 min | 300°C & 60 min |
| 1 | 14.1469 | Hexadecanoic acid, methyl ester | 1.548 | - |
| 2 | 14.8 | n-Hexadecanoic acid | 37.735 | 38.71 |
| 3 | 16.3902 | Octadecanoic acid | 22.624 | 15.693 |
| 4 | 17.0993 | 1,7-Octanediol, 3,7-dimethyl- | - | 10.864 |
| 5 | 20.3295 | 5-.beta.-cholestan-3.alpha.-ol, propionate | 2.583 | 4.781 |
| 6 | 20.5178 | 3Beta-tosyloxy-5alpha-cholestane | 3.484 | - |
| 7 | 20.5389 | Cholest-2-ene, (5.alpha.)- | 2.965 | 5.147 |
| 8 | 20.6608 | Cholest-4-ene | 2.192 | 5.635 |
| 9 | 21.1186 | Cholest-5-en-3-ol (3.beta.)-, trifluoroacetate | 2.59 | - |

| | | | | |
|---|---|---|---|---|
| 10 | 21.5872 | Stigmastanol, 2-ethyl butyrate | 2.713 | - |

3. HTL Operating Conditions: 350°C: 30 & 60 min

| Peak | RT, min | Identified Compounds | Area% | |
|---|---|---|---|---|
| | | | 350°C & 30 min | 350°C & 60 min |
| 1 | 10.6873 | Cetene | 1.172 | - |
| 2 | 14.1469 | Hexadecanoic acid, methyl ester | - | 1.373 |
| 3 | 14.8 | n-Hexadecanoic acid | 52.808 | 52.031 |
| 4 | 16.3902 | Octadecanoic acid | 19.596 | 20.017 |
| 5 | 16.4073 | Octadecanoic acid, 2-(2-hydroxyethoxy)ethyl ester | 8.236 | 2.476 |
| 6 | 17.1027 | Hexadecanamide | - | 5.826 |
| 7 | 23.985 | Hexadecanoic acid, hexadecyl ester | - | 1.821 |

**Digestate:**

1. HTL Operating Conditions: 250°C: 30 & 60 min

| Peak | RT, min | Identified Compounds | Area% | |
|---|---|---|---|---|
| | | | 250°C & 30 min | 250°C & 60 min |
| 1 | 14.1469 | Hexadecanoic acid, methyl ester | 1.995 | - |
| 2 | 14.8 | n-Hexadecanoic acid | 16.65 | 18.213 |

| | | | | |
|---|---|---|---|---|
| 3 | 17.1027 | Hexadecanamide | 16.337 | 3.918 |
| 4 | 20.8319 | 2,6,10-Dodecatrien-1-ol, 3,7,11-trimethyl-, (E,E)- | 1.808 | - |
| 5 | 20.8424 | 2,6,10-Dodecatrien-1-ol, 3,7,11-trimethyl-, acetate, (E,E)- | - | 1.048 |
| 6 | 22.4179 | Cholestan-3-ol, (3.beta.,5.beta.)- | 7.708 | 11.181 |
| 7 | 22.4569 | Cholestanol | - | 5.079 |
| 8 | 22.7539 | Cholestane-3,5-diol, 5-acetate, (3.beta.,5.alpha.)- | 3.608 | 3.402 |
| 9 | 22.7659 | Cholest-5-en-3-ol, (3.alpha.)- | - | 0.88 |
| 10 | 22.7728 | Cholesterol | 3.344 | - |
| 11 | 23.5739 | Stigmastanol | 5.007 | 7.499 |
| 12 | 23.6008 | Cholestane, 3-ethoxy-, (3.beta.,5.alpha.)- | 2.741 | 3.374 |
| 13 | 23.6127 | Stigmastanol, butyrate | 2.771 | - |

2. HTL Operating Conditions: 300°C: 30 & 60 min

| Peak | RT, min | Identified Compounds | Area% | |
|---|---|---|---|---|
| | | | 300°C & 30 min | 300°C & 60 min |
| 1 | 14.8 | n-Hexadecanoic acid | 11.785 | 13.409 |
| 2 | 20.3295 | 5-.beta.-cholestan-3.alpha.-ol, propionate | 4.417 | 7.274 |
| 3 | 20.5178 | 3Beta-tosyloxy-5alpha-cholestane | 2.154 | - |
| 4 | 20.5389 | Cholest-2-ene, (5.alpha.)- | 4.24 | 4.836 |
| 5 | 20.6608 | Cholest-4-ene | 6.499 | 8.467 |

| | | | | |
|---|---|---|---|---|
| 6 | 21.5872 | Stigmastanol, 2-ethyl butyrate | - | 3.389 |
| 7 | 22.4001 | Ursodeoxycholic acid | - | 3.864 |
| 8 | 22.4179 | Cholestan-3-ol, (3.beta.,5.beta.)- | 2.347 | 8.105 |
| 9 | 22.4569 | Cholestanol | - | 2.103 |
| 10 | 22.9386 | 6-Methoxy-2,7,8-trimethyl-2-(4,8,12-trimethyl tetradecyl)chroman | 8.453 | - |
| 11 | 23.5739 | Stigmastanol | 6.843 | - |
| 12 | 23.6008 | Cholestane, 3-ethoxy-, (3.beta.,5.alpha.)- | 2.089 | - |
| 13 | 23.6127 | Stigmastanol, butyrate | 3.14 | - |

## 3. HTL Operating Conditions: 350°C: 30 & 60 min

| Peak | RT, min | Identified Compounds | Area% | |
|---|---|---|---|---|
| | | | 350°C & 30 min | 350°C & 60 min |
| 1 | 14.8 | n-Hexadecanoic acid | 9.362 | 19.594 |
| 2 | 20.3295 | 5-.beta.-cholestan-3.alpha.-ol, propionate | 3.139 | 2.966 |
| 3 | 20.5178 | 3Beta-tosyloxy-5alpha-cholestane | 1.802 | 3.54 |
| 4 | 20.5389 | Cholest-2-ene, (5.alpha.)- | 3.973 | 1.616 |
| 5 | 20.6608 | Cholest-4-ene | 9.159 | 1.815 |
| 6 | 20.6837 | Cholest-3-ene, (5.alpha.)- | - | 2.023 |
| 7 | 21.5872 | Stigmastanol, 2-ethyl butyrate | 9.529 | - |
| 8 | 21.5984 | Stigmastanol, isovalerate | 3.768 | - |

| | | | | |
|---|---|---|---|---|
| 9 | 21.7701 | Stigmastanol, acetate | 4.823 | - |
| 10 | 22.4179 | Cholestan-3-ol, (3.beta.,5.beta.)- | 8.895 | 4.698 |
| 11 | 22.4569 | Cholestanol | 6.243 | - |
| 12 | 22.687 | 17-(1,5-Dimethylhexyl)-10,13-dimethyl-2,3,4,5,8,9,10,11,12,13,14,15,16,17-tetradecahydro-1H-cyclopenta[a]phenanthren-4-ol | - | 3.994 |
| 13 | 22.7093 | Pregnan-20-one, 3,11-dihydroxy-17,21-[(methyl borylene)bis(oxy)]-, (3.alpha.,5.beta.,11.beta.)- | - | 1.268 |
| 14 | 22.7539 | Cholestane-3,5-diol, 5-acetate, (3.beta.,5.alpha.)- | - | 2.031 |
| 15 | 23.5739 | Stigmastanol | 1.857 | - |
| 16 | 23.6008 | Cholestane, 3-ethoxy-, (3.beta.,5.alpha.)- | 2.284 | - |
| 17 | 23.6122 | Cholest-4-en-3-one | - | 4.333 |

## FTIR Analysis:

***Table S3:*** *Summary of the literature used for identifying different function groups present in the feedstock, biocrude, HTL-AP, hydrochar, and digestate based on their wavenumber.*

| Wavelength (cm$^{-1}$) | Functional groups | Suggested compounds | Reference |
|---|---|---|---|
| 4000 - 3400 | Non-bonded O-H stretch | Water group in the aqueous phase | (Chen et al., 2019a) |

| | | | |
|---|---|---|---|
| 3400 - 3100 | O-H & N-H | Alcohols, acids, amides, and amines | (Chan & Wang, 2018; Chen et al., 2019b) |
| 3000 - 2800 | symmetric & asymmetric C-H stretching vibration | Saturated aliphatic groups | (Duan & Savage, 2010; Pipitone et al., 2020) |
| 2400 - 2100 | C≡C, −SCN, −NCS, & −N=C=O asymmetric stretch | Terminal alkyne (monosubstituted) or nitrogen multiple and cumulated double bond compounds | (Dovbeshko et al., 2000) |
| 1720 - 1700 | C=O stretch | Acids | (Vardon et al., 2011) |
| 1700 - 1680 | -C=N-, -C=O-, & -C=C- | Aromatic combination bands, quinone or conjugated ketone, and open-chain imino (-C=N-) compounds | (Yuan et al., 2011) |
| 1680 - 1615 | C=O stretching vibrations & weaker bending of the N-H group | Unsaturated ketones, aldehydes, amides and amino acids | (Lievens et al., 2011; Vardon et al., 2011; Xiu et al., 2010) |
| 1615–1500 | Aromatic C=C ring breathing vibrations | Aromatics with various substitutions | (Lievens et al., 2011) |

| | | | |
|---|---|---|---|
| 1470 - 1350 | C-H deformations | Alkanes and alkenes | (Xiu et al., 2010) |
| 1300 - 950 | C=O & O-H stretching | Alcohol, ester, or ether, silicate ions, simple heteroatomic oxycompounds, and inorganic compounds | (Francioso et al., 2010; Xiu et al., 2010) |
| 900 - 430 | -C=C- | Aromatic compounds and inorganic ions vibrations | (Chen et al., 2019b) |

***Figure S1:*** *FTIR spectra of biocrude samples from both integrated schemes.*

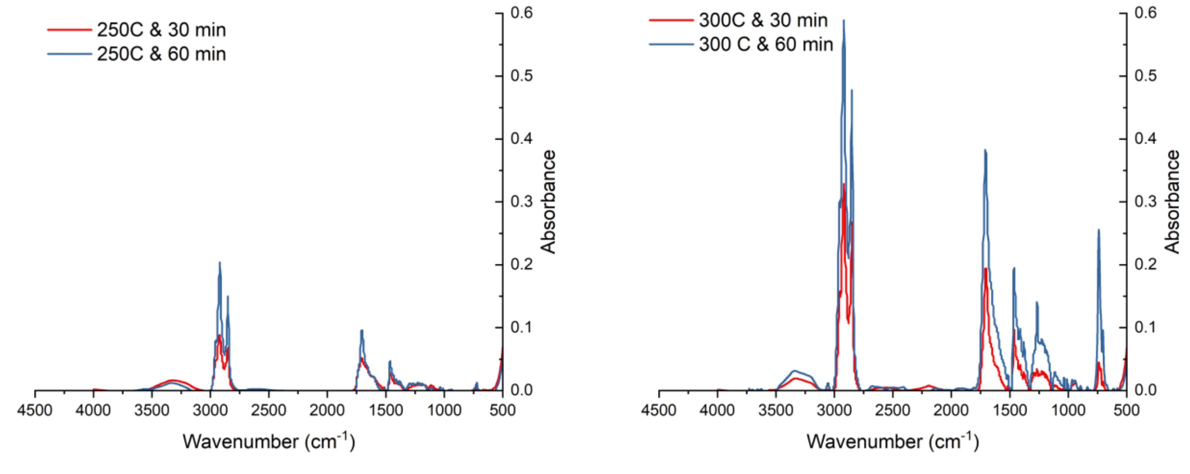

(a)

(b)

(c)

(d)

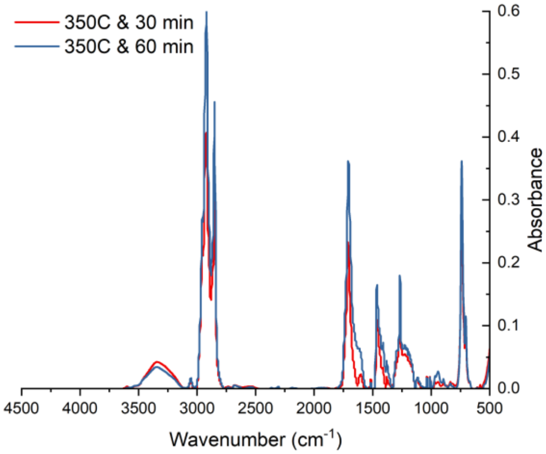
350C & 30 min
350C & 60 min
Absorbance
0.0
0.1
0.2
0.3
0.4
0.5
0.6
Wavenumber (cm$^{-1}$)
4500
4000
3500
3000
2500
2000
1500
1000
500

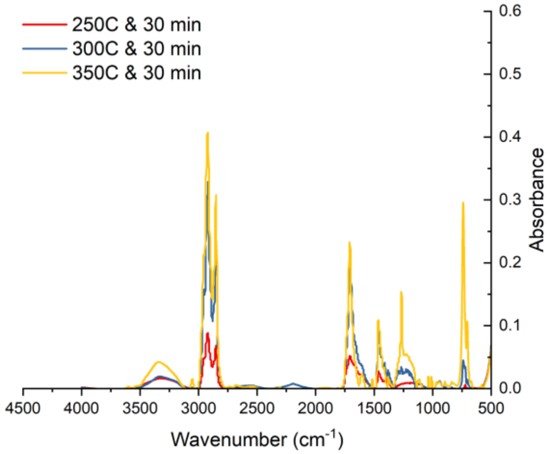
250C & 30 min
300C & 30 min
350C & 30 min
Absorbance
0.0
0.1
0.2
0.3
0.4
0.5
0.6
Wavenumber (cm$^{-1}$)
4500
4000
3500
3000
2500
2000
1500
1000
500

(e)

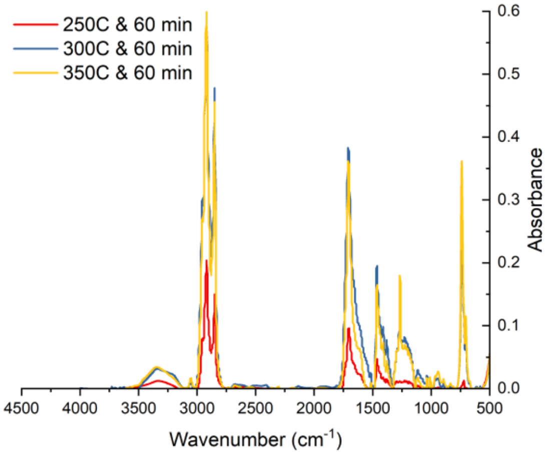
250C & 60 min
300C & 60 min
350C & 60 min
Absorbance
0.0
0.1
0.2
0.3
0.4
0.5
0.6
Wavenumber (cm$^{-1}$)
4500
4000
3500
3000
2500
2000
1500
1000
500

(f)

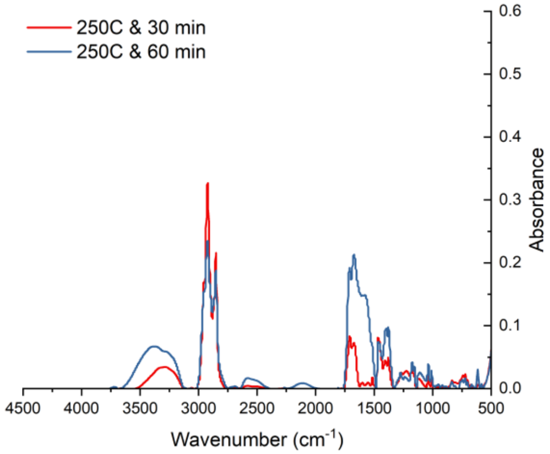
250C & 30 min
250C & 60 min
Absorbance
0.0
0.1
0.2
0.3
0.4
0.5
0.6
Wavenumber (cm$^{-1}$)
4500
4000
3500
3000
2500
2000
1500
1000
500

(g)

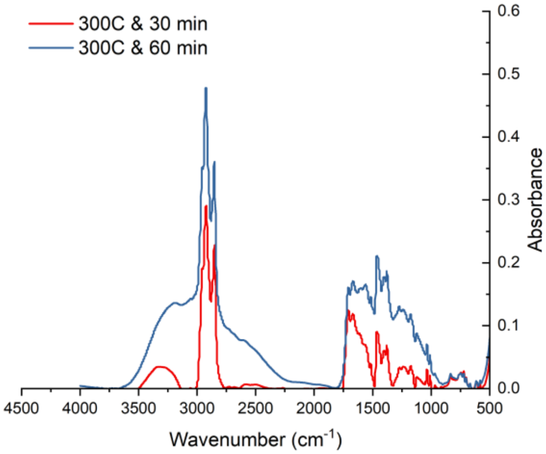
300C & 30 min
300C & 60 min
Absorbance
0.0
0.1
0.2
0.3
0.4
0.5
0.6
Wavenumber (cm$^{-1}$)
4500
4000
3500
3000
2500
2000
1500
1000
500

(h)

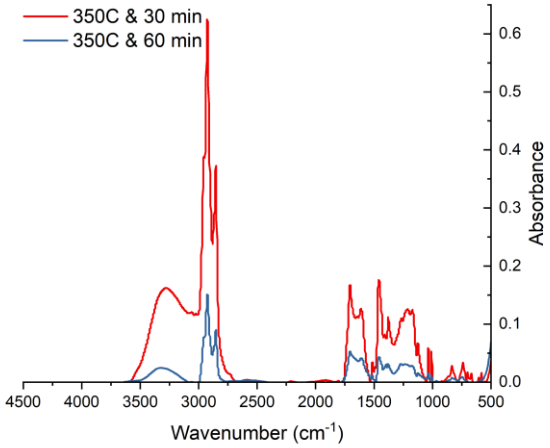
350C & 30 min
350C & 60 min
Absorbance
0.0
0.1
0.2
0.3
0.4
0.5
0.6
Wavenumber (cm$^{-1}$)
4500
4000
3500
3000
2500
2000
1500
1000
500

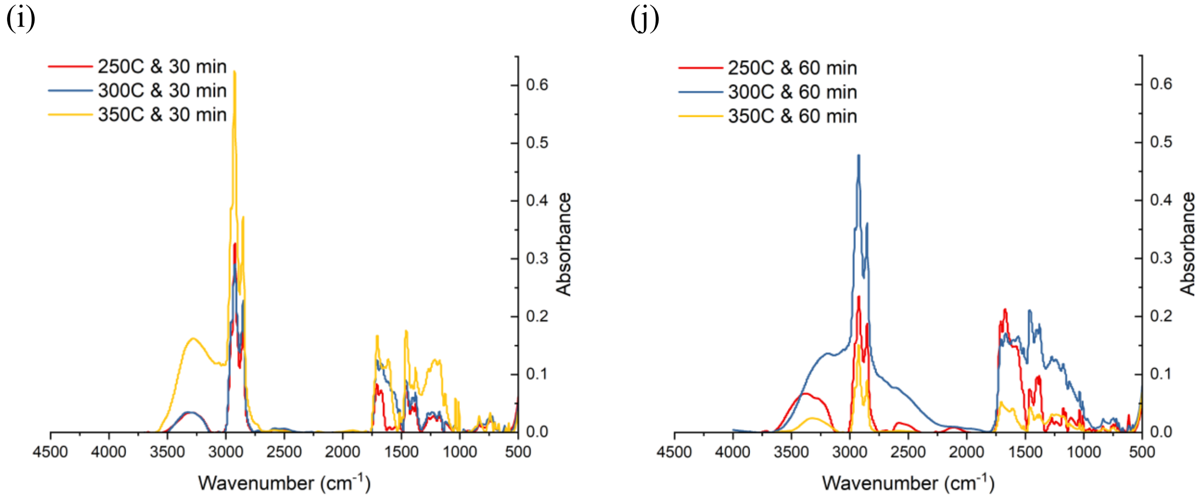

**Figure S1:** FTIR spectra of the biocrude resulting from different HTL operating conditions of: (a) 250°C for 30 & 60 min, (b) 300°C for 30 & 60 min, (c) 350°C for 30 & 60 min, (d) 250, 300 & 350°C for 30 min, & (e) 250, 300 & 350°C for 60 min of Scheme 1 and (f) 250°C for 30 & 60 min, (g) 300°C for 30 & 60 min, (h) 350°C for 30 & 60 min, (i) 250, 300 & 350°C for 30 min, & (j) 250, 300 & 350°C for 60 min of Scheme 2.

***Figure S2:*** *FTIR spectra of HTL-AP samples from both integrated schemes.*

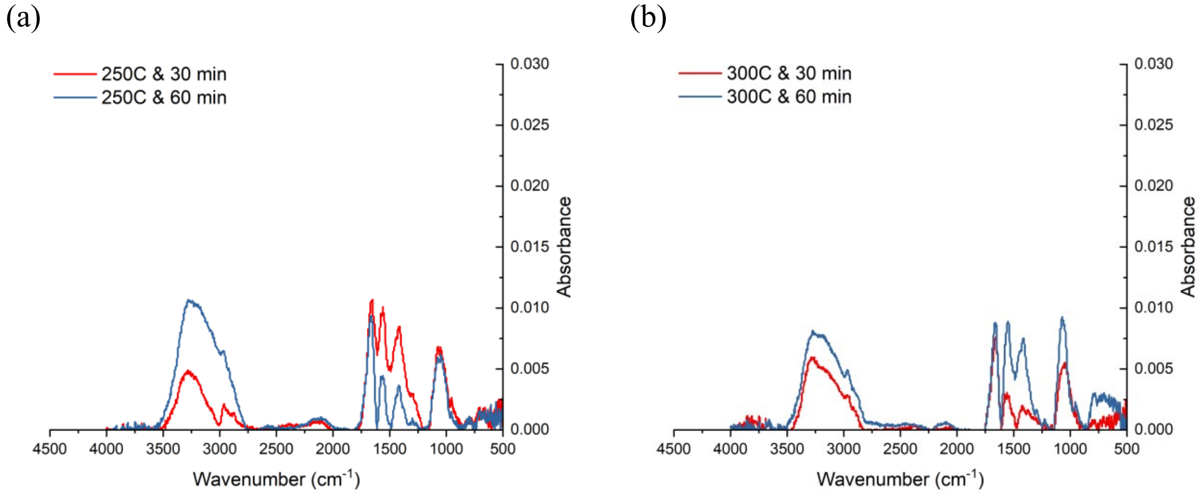

(c)

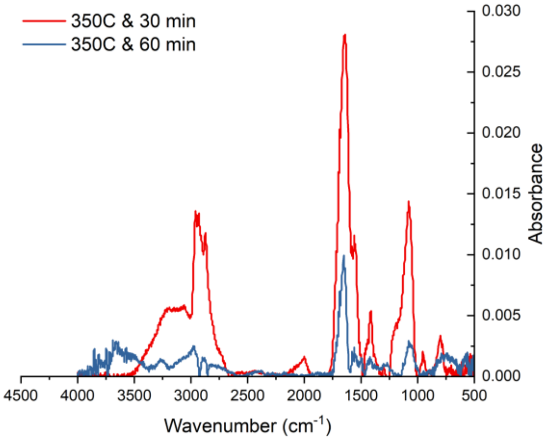
350C & 30 min
350C & 60 min
0.030
0.025
0.020
0.015
0.010
0.005
0.000
Absorbance
4500
4000
3500
3000
2500
2000
1500
1000
500
Wavenumber (cm$^{-1}$)

(d)

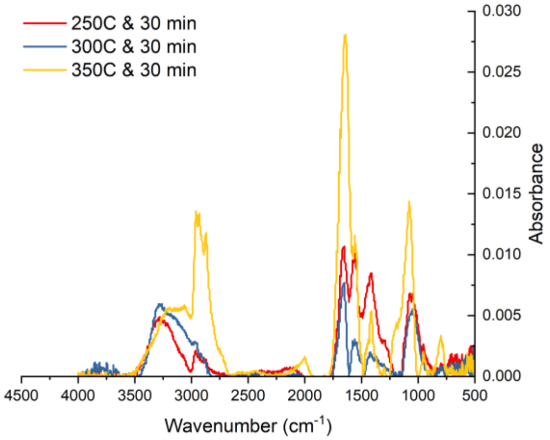
250C & 30 min
300C & 30 min
350C & 30 min
0.030
0.025
0.020
0.015
0.010
0.005
0.000
Absorbance
4500
4000
3500
3000
2500
2000
1500
1000
500
Wavenumber (cm$^{-1}$)

(e)

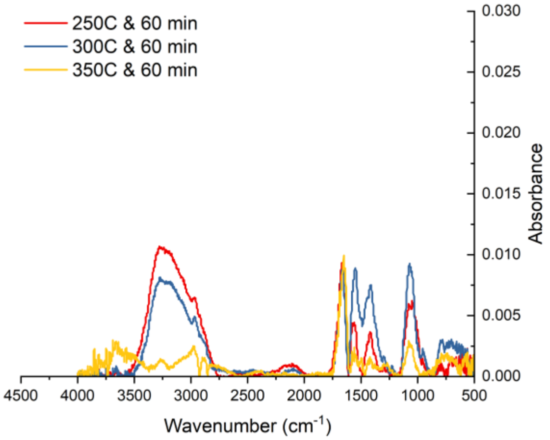
250C & 60 min
300C & 60 min
350C & 60 min
0.030
0.025
0.020
0.015
0.010
0.005
0.000
Absorbance
4500
4000
3500
3000
2500
2000
1500
1000
500
Wavenumber (cm$^{-1}$)

(f)

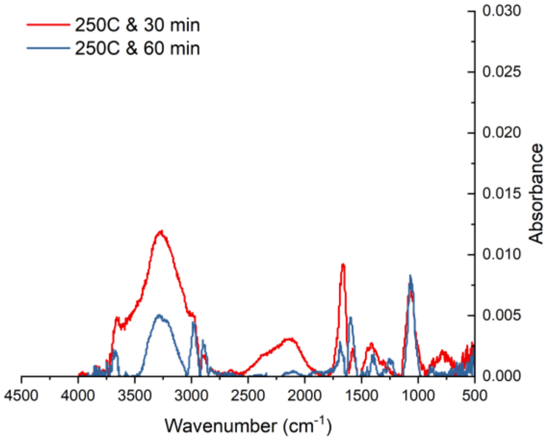
250C & 30 min
250C & 60 min
0.030
0.025
0.020
0.015
0.010
0.005
0.000
Absorbance
4500
4000
3500
3000
2500
2000
1500
1000
500
Wavenumber (cm$^{-1}$)

(g)

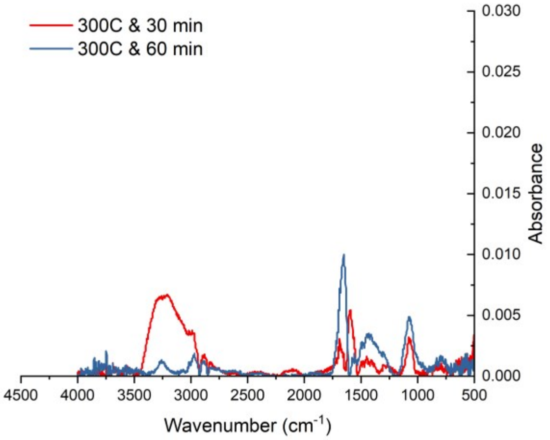
300C & 30 min
300C & 60 min
0.030
0.025
0.020
0.015
0.010
0.005
0.000
Absorbance
4500
4000
3500
3000
2500
2000
1500
1000
500
Wavenumber (cm$^{-1}$)

(h)

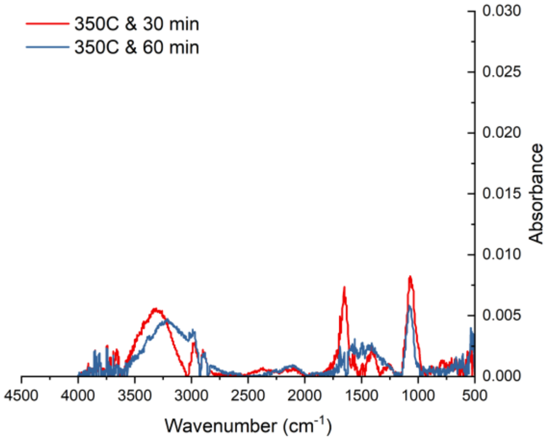
350C & 30 min
350C & 60 min
0.030
0.025
0.020
0.015
0.010
0.005
0.000
Absorbance
4500
4000
3500
3000
2500
2000
1500
1000
500
Wavenumber (cm$^{-1}$)

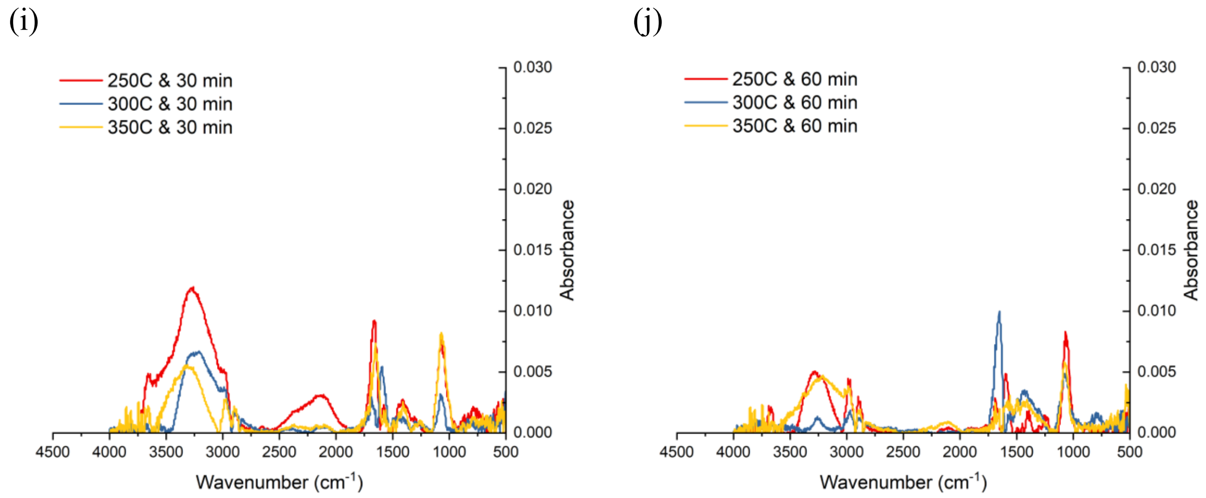

**Figure S2:** FTIR spectra of the HTL-AP resulting from different HTL operating conditions of: (a) 250°C for 30 & 60 min, (b) 300°C for 30 & 60 min, (c) 350°C for 30 & 60 min, (d) 250, 300 & 350°C for 30 min, & (e) 250, 300 & 350°C for 60 min of Scheme 1 and (f) 250°C for 30 & 60 min, (g) 300°C for 30 & 60 min, (h) 350°C for 30 & 60 min, (i) 250, 300 & 350°C for 30 min, & (j) 250, 300 & 350°C for 60 min of Scheme 2.

***Figure S3:*** *FTIR spectra of hydrochar samples from both integrated schemes.*

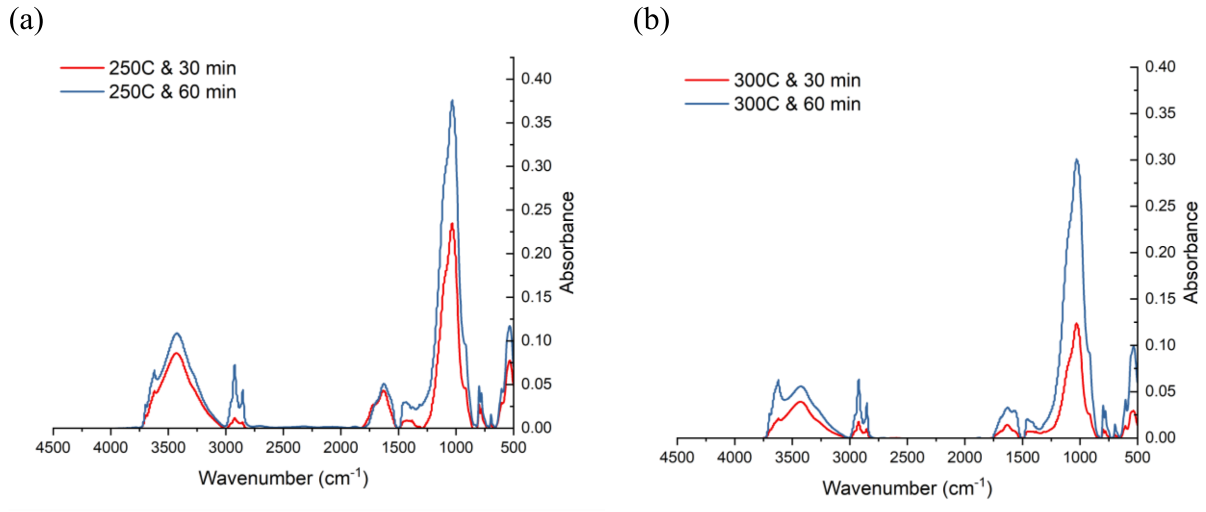

(c)

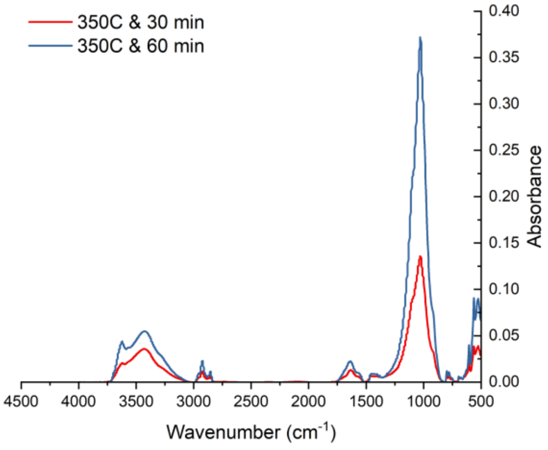
350C & 30 min
350C & 60 min
Absorbance
0.40
0.35
0.30
0.25
0.20
0.15
0.10
0.05
0.00
4500
4000
3500
3000
2500
2000
1500
1000
500
Wavenumber (cm$^{-1}$)

(d)

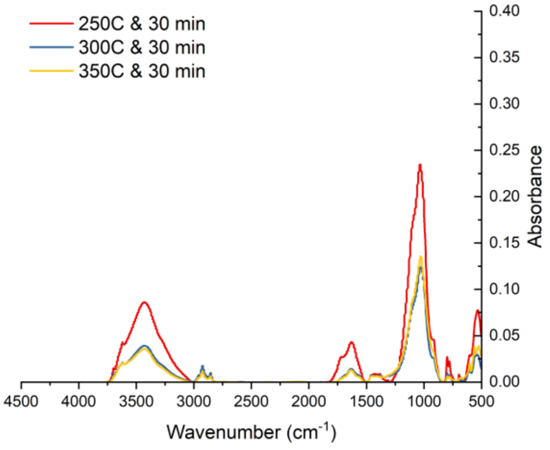
250C & 30 min
300C & 30 min
350C & 30 min
Absorbance
0.40
0.35
0.30
0.25
0.20
0.15
0.10
0.05
0.00
4500
4000
3500
3000
2500
2000
1500
1000
500
Wavenumber (cm$^{-1}$)

(e)

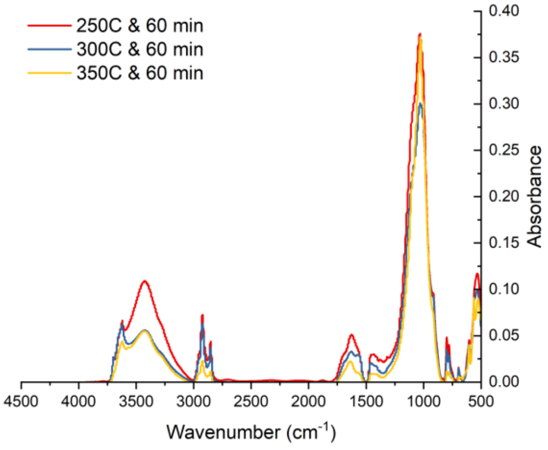
250C & 60 min
300C & 60 min
350C & 60 min
Absorbance
0.40
0.35
0.30
0.25
0.20
0.15
0.10
0.05
0.00
4500
4000
3500
3000
2500
2000
1500
1000
500
Wavenumber (cm$^{-1}$)

(f)

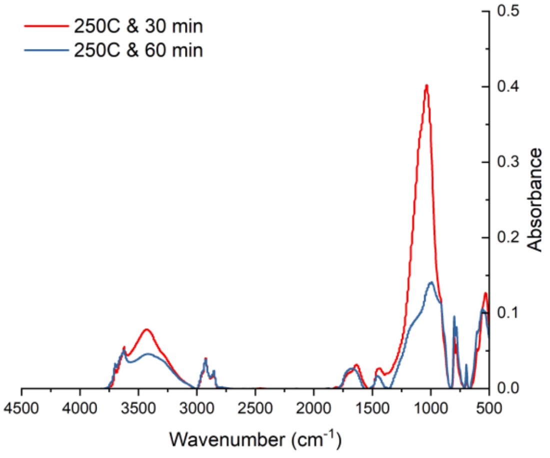
250C & 30 min
250C & 60 min
Absorbance
0.5
0.4
0.3
0.2
0.1
0.0
4500
4000
3500
3000
2500
2000
1500
1000
500
Wavenumber (cm$^{-1}$)

(g)

(h)

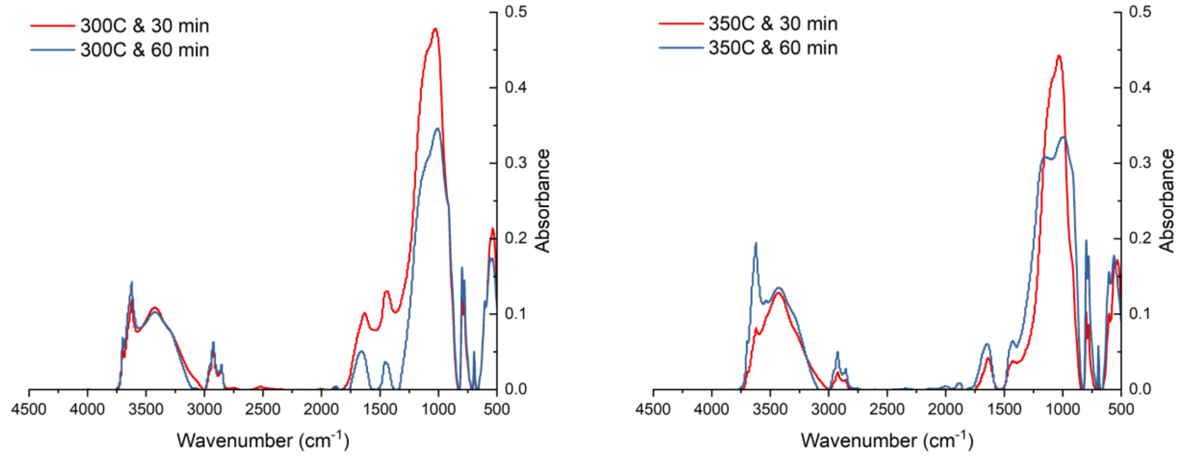

(i)

(j)

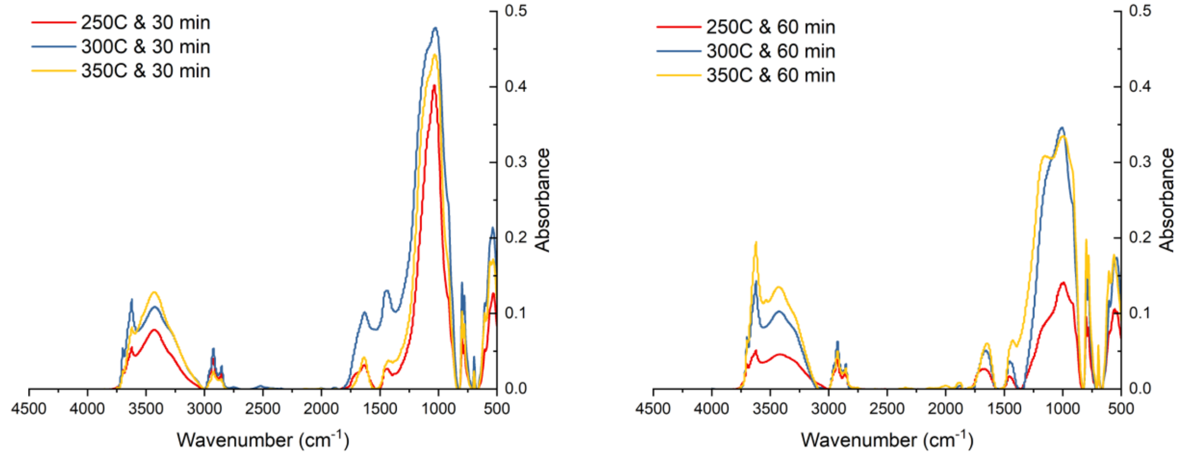

**Figure S3:** FTIR spectra of the hydrochar resulting from different HTL operating conditions of: (a) 250°C for 30 & 60 min, (b) 300°C for 30 & 60 min, (c) 350°C for 30 & 60 min, (d) 250, 300 & 350°C for 30 min, & (e) 250, 300 & 350°C for 60 min of Scheme 1 and (f) 250°C for 30 & 60 min, (g) 300°C for 30 & 60 min, (h) 350°C for 30 & 60 min, (i) 250, 300 & 350°C for 30 min, & (j) 250, 300 & 350°C for 60 min of Scheme 2.

***Figure S4:*** *FTIR spectra of digestate samples from both integrated schemes.*

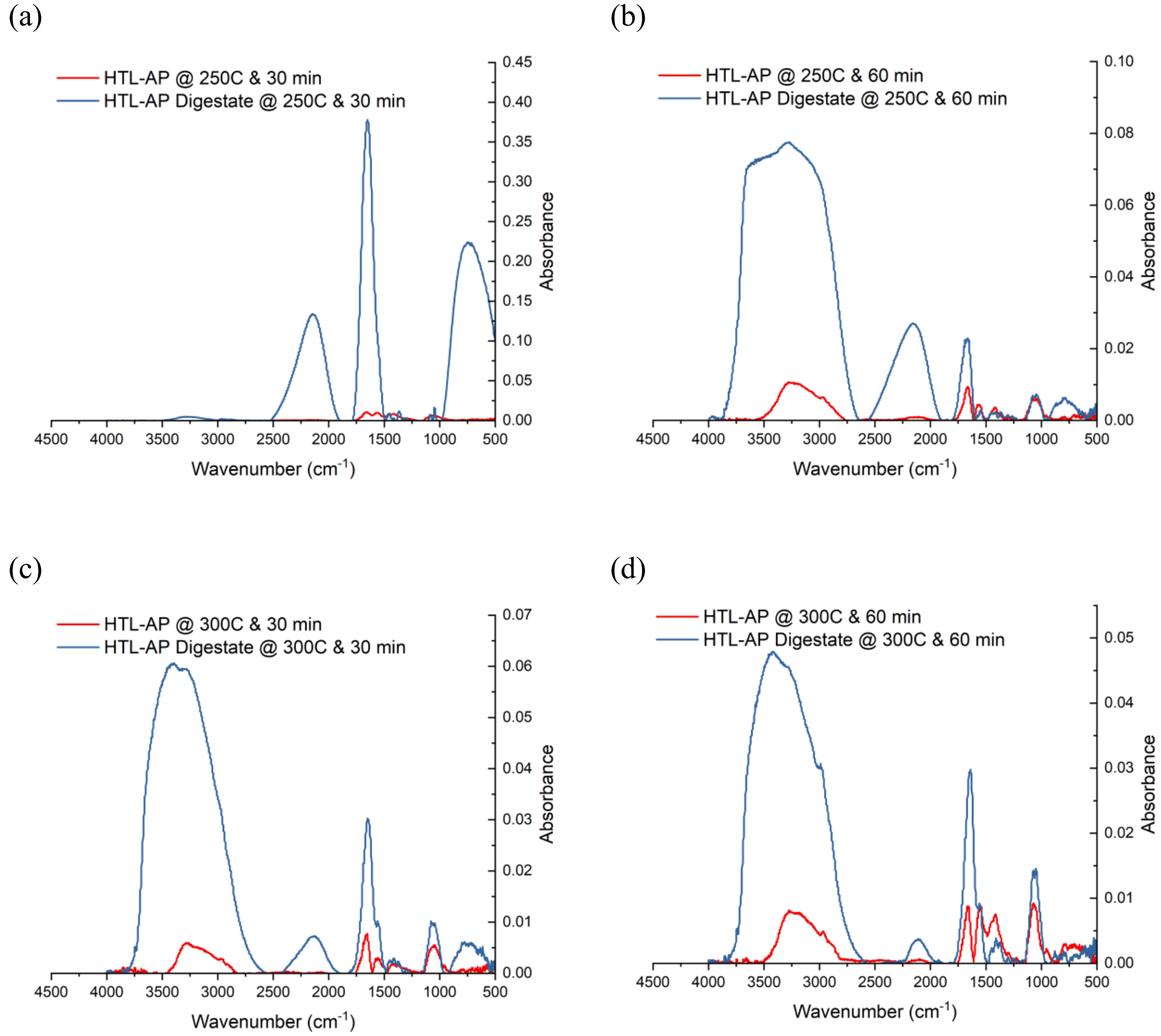

(e)

(f)

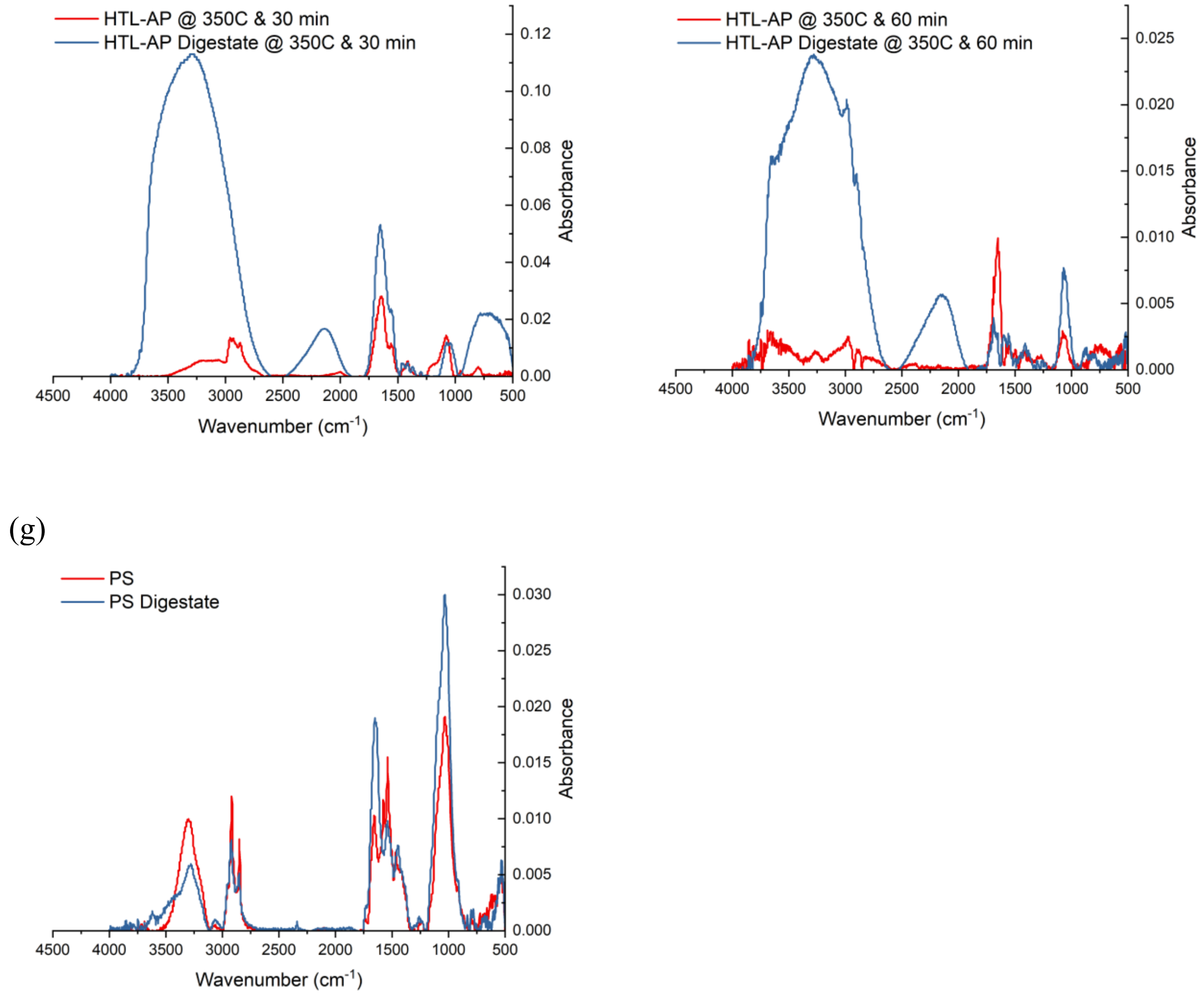

**Figure S4:** FTIR spectra of the different feedstock and resulting digestate: (a) HTL-AP generated at 250°C for 30 min, (b) HTL-AP generated at 250°C for 60 min, (c) HTL-AP generated at 300°C for 30 min, (d) HTL-AP generated at 300°C for 60 min, (e) HTL-AP generated at 350°C for 30 min, & (f) HTL-AP generated at 350°C for 60 min of Scheme 1 and (g) primary sludge of Scheme 2.

***Table S4:*** *Elemental analysis of feedstock and resulting hydrochar obtained from various HTL operating conditions from both schemes.*

| HTL Operating Conditions | Elemental Analysis (wt. %, dry basis) | | | | | | HHV (MJ/kg) |
|---|---|---|---|---|---|---|---|
| | N | C | H | S | O | Ash content | |
| Scheme 1 (HTL followed by AD) | | | | | | | |
| PS | 3.48 ± 0.09 | 36.51 ± 1.25 | 5.16 ± 0.20 | 0.56 ± 0.01 | 20.96 ± 1.55 | 33.3 ± 0.11 | 16.02 ± 0.99 |
| 250°C & 30 min | 1.04 ± 0.04 | 15.04 ± 1.38 | 1.76 ± 0.17 | 0.21 ± 0.01 | 14.20 ± 1.58 | 67.8 ± 0.19 | 5.1 ± 0.99 |
| 250°C & 60 min | 1.17 ± 0.01 | 17.44 ± 0.11 | 2.17 ± 0.02 | 0.25 ± 0.01 | 9.33 ± 0.13 | 69.6 ± 0.22 | 7.4 ± 0.08 |
| 300°C & 30 min | 0.95 ± 0.04 | 12.59 ± 0.16 | 1.77 ± 0.04 | 0.25 ± 0.01 | 6.44 ± 0.25 | 78.0 ± 0.15 | 5.6 ± 0.16 |
| 300°C & 60 min | 1.0 ± 0.09 | 13.25 ± 0.67 | 1.87 ± 0.09 | 0.26 ± 0.05 | 5.11 ± 0.89 | 78.5 ± 0.14 | 6.3 ± 0.52 |
| 350°C & 30 min | 0.84 ± 0.01 | 8.63 ± 0.01 | 1.33 ± 0.01 | 0.24 ± 0.01 | 3.18 ± 0.01 | 85.8 ± 0.27 | 4.3 ± 0.01 |
| 350°C & 60 min | 0.92 ± 0.01 | 8.49 ± 0.08 | 1.35 ± 0.01 | 0.24 ± 0.01 | 4.03 ± 0.12 | 85.0 ± 0.33 | 4.1 ± 0.07 |
| Scheme 2 (AD followed by HTL) | | | | | | | |
| Digestate | 3.40 ± 0.05 | 27.8 ± 0.57 | 3.80 ± 0.10 | 0.75 ± 0.05 | 14.48 ± 0.62 | 49.8 ± 0.30 | 12.2 ± 0.44 |
| 250°C & 30 min | 0.89 ± 0.02 | 11.77 ± 0.82 | 1.52 ± 0.05 | 0.21 ± 0.04 | 2.25 ± 0.86 | 83.4 ± 0.15 | 5.8 ± 0.50 |

| | | | | | | | |
|---|---|---|---|---|---|---|---|
| 250°C & 60 min | 1.08 ± 0.01 | 11.98 ± 0.01 | 1.54 ± 0.01 | 0.36 ± 0.06 | 5.33 ± 0.06 | 79.7 ± 0.09 | 5.3 ± 0.02 |
| 300°C & 30 min | 0.92 ± 0.01 | 8.72 ± 0.05 | 1.20 ± 0.03 | 0.36 ± 0.02 | 5.13 ± 0.05 | 83.7 ± 0.01 | 3.8 ± 0.01 |
| 300°C & 60 min | 0.88 ± 0.01 | 8.42 ± 0.07 | 1.19 ± 0.01 | 0.30 ± 0.02 | 4.47 ± 0.09 | 84.7 ± 0.02 | 3.8 ± 0.05 |
| 350°C & 30 min | 0.62 ± 0.01 | 5.43 ± 0.10 | 0.84 ± 0.01 | 0.21 ± 0.01 | 2.69 ± 0.12 | 90.2 ± 0.05 | 2.6 ± 0.07 |
| 350°C & 60 min | 0.55 ± 0.01 | 4.93 ± 0.01 | 0.80 ± 0.02 | 0.19 ± 0.03 | 3.64 ± 0.06 | 89.9 ± 0.02 | 2.2 ± 0.04 |
| HTL: hydrothermal liquefaction; HHV: higher heating value; PS: primary sludge. | | | | | | | |